Task-driven Data Fusion for Additive Manufacturing

Fu Hu

School of Engineering
Cardiff University

A thesis submitted to Cardiff University
for the degree of Doctor of Philosophy

November 2023

Acknowledgements

This thesis documents my years of effort and perseverance in research. It's been tough and challenging to conduct research during the years of the COVID-19 pandemic. However, passion and dedication keep driving me to push forward my research work.

First and foremost, I would express my sincere gratitude to my main supervisor Prof. Ying Liu for his knowledge, encouragement, dedication, and support during these years. Under his supervision and guidance, I have learned how to think critically, conduct research rigorously, and write academically. His enthusiasm and mentality towards research have much inspired me, making me brave and strong when facing challenges. Prof. Liu has also provided me with opportunities to engage in exchanges with international research institutions, universities, and industrial companies. I believe that the experiences of living and studying at Cardiff University will become one of the most unforgettable days in my life.

I would also like to thank my co-supervisor, Dr. Xianfang Sun, sincerely. His academic guidance and support have always been helpful. Many thanks to my senior and junior colleagues in the research group, especially Dr. Jian Qin, Dr. Chong Chen, and Dr. Zheyuan Chen for their assistance and encouragement not only in studying but in my personal life. I am also grateful for the help and assistance from my research collaborators, Dr. Shuai Ma and Dr. Jun Song. Many thanks to the guidance and domain knowledge support from Dr. Paul Witherell, Prof. Charlie C.L. Wang, and Prof. David W. Rosen. Additionally, I am thankful to Hubei Zhican Internet Technology Co. Ltd and CEO Mrs. Hong Fang, for their financial support of my PhD research. I also want to express my gratitude to the people who have helped me but are not mentioned above.

Finally, I want to thank my family. I will never forget the support and encouragement, both physically and emotionally, from my family who has always been at my side and

accompanied me through every milestone in my life. Many thanks to my girlfriend, Zhiyan Li, who is brave and kind. Her accompany, encouragement, and understanding helped me get through hard times. They are the lighthouse in my life, lighting up the way and guiding me through storms and darkness.

Abstract

Additive manufacturing (AM) is a critical technology for the next industrial revolution, offering the prospect of mass customization, flexible production, and on-demand manufacturing. However, difficulties in understanding underlying mechanisms and identifying latent factors that influence AM processes build up barriers to in-depth research and hinder its widespread adoption in industries. Recent advancements in data sensing and collection technologies have enabled capturing extensive data from AM production for analytics to improve process reliability and part quality. However, modelling the complex relationships between the manufacturing process and its outcomes is challenging due to the multi-physics nature of AM processes. The critical information of AM production is embedded within multi-source, multi-dimensional, and multi-modal heterogeneous data, leading to difficulties when jointly analysing. Therefore, how to bridge the gap between the multi-physics interactions and their outcomes through heterogeneous data analytics becomes a crucial research challenge. Data fusion strategies and techniques can effectively leverage multi-faceted information. Since AM tasks can have various requirements, the corresponding fusion techniques should be task-specific. Hence, this thesis will focus on how to deal with task-driven data fusion for AM.

To address the challenges stated above, a comprehensive task-driven data fusion framework and methodology are proposed to provide systematic guidelines to identify, collect, characterise, and fuse AM data for supporting decision-making activities. In this framework, AM data is classified into three major categories, process-input data, process-generated data, and validation data. The proposed methodology consists of three steps, including the identification of data analytics types, data required for tasks, acquisition, and characterization, and task-driven data fusion techniques. To implement the framework and methodology, critical strategies for multi-source and multi-hierarchy data fusion, and Cloud-edge fusion, are introduced and the detailed approaches are described in the following chapters.

One of the major challenges in AM data fusion is that the multi-source data normally has various dimensions, involving nested hierarchies. To fuse this data for analytics, a

hybrid deep learning (DL) model called M-CNN-LSTM is developed. In general, two levels of data and information are focused on, layer level and build level. In the proposed hybrid model, the CNN part is used to extract features from layer-wise images of sliced 3D models, and the LSTM is used to process the layer-level data concatenated with convolutional features for time-series modelling. The build-level information is used as input into a separate neural network and merged with the CNN-LSTM for final predictions. An experimental study on an energy consumption prediction task was conducted where the results demonstrated the merits of the proposed approach.

In many AM tasks at the initial stage, it is usually time-consuming and costly to acquire sufficient data for training DL-based models. Additionally, these models are hard to make fast inferences during production. Hence, a Cloud-edge fusion paradigm based on transfer learning and knowledge distillation (KD)-enabled incremental learning is proposed to tackle the challenges. The proposed methodology consists of three main steps, including (1) transfer learning for feature extraction, (2) base model building via deep mutual learning (DML) and model ensemble, and (3) multi-stage KD-enabled incremental learning. The 3-step method is developed to transfer knowledge from the ensemble model to the compressed model and learn new knowledge incrementally from newly collected data. After each incremental learning in the Cloud platform, the compressed model will be updated to the edge devices for making inferences on the incoming new data. An experimental study on the AM energy consumption prediction task was carried out for demonstration.

Under the proposed task-driven data fusion framework and methodology, case studies focusing on three different AM tasks, (1) mechanical property prediction of additively manufactured lattice structures (LS), (2) porosity defects classification of parts, and (3) investigating the effect of the remelting process on part density, were carried out for demonstration. Experimental results were presented and discussed, revealing the feasibility and effectiveness of the proposed framework and approaches. This research aims to pave the way for leveraging AM data with various sources and modalities to support decision-making for AM tasks using data fusion and advanced data analytics techniques. The feasibility and effectiveness of the developed fusion strategies and methods demonstrate their potential to facilitate the AM industry, making it more adaptable and responsive to the dynamic demands of modern manufacturing.

Research Achievements

Journal papers:

1. **Hu, F.**, Liu, Y., Li, Y., Ma, S., Qin, J., Song, J., Sun, X. and Tang, Q., 2023. *Task-driven data fusion for additive manufacturing: framework, approaches, and case studies*. Journal of Industrial Information Integration, p.100484. 10.1016/j.jii.2023.100484 **(Impact factor: 15.7)**

2. Qin, J., **Hu, F.**, Liu, Y., Witherell, P., Wang, C.C., Rosen, D.W., Simpson, T.W., Lu, Y. and Tang, Q., 2022. *Research and application of machine learning for additive manufacturing*. Additive Manufacturing, 52, p.102691. 10.1016/j.addma.2022.102691 **(Co-first author, Impact factor: 11.632, Highly cited paper)**

3. Li, Y., **Hu, F.**, Liu, Y., Ryan, M. and Wang, R., 2023. *A hybrid model compression approach via knowledge distillation for predicting energy consumption in additive manufacturing*. International Journal of Production Research 61(13), pp.1-23. 10.1080/00207543.2022.2160501 **(Impact factor: 9.018)**

Conference papers:

1. **Hu, F.**, Qin, J., Li, Y., Liu, Y. and Sun, X., 2021. *Deep fusion for energy consumption prediction in additive manufacturing*. Procedia CIRP, 104, pp.1878-1883. 10.1016/j.procir.2021.11.317

2. **Hu, F.**, Liu, Y., Qin, J., Sun, X. and Witherell, P., 2020, August. *Feature-level data fusion for energy consumption analytics in additive manufacturing*. In 2020 IEEE 16th International Conference on Automation Science and Engineering (CASE), pp. 612-617. IEEE. 10.1109/CASE48305.2020.9216947

3. Li, Y., **Hu, F.**, Ryan, M., Wang, R. and Liu, Y., 2022. Knowledge distillation for energy consumption prediction in additive manufacturing. IFAC-PapersOnLine, 55(2), pp.390-395. 10.1016/j.ifacol.2022.04.225

4. Wan, Y., Chen, Z., **Hu, F.**, Liu, Y., Packianather, M. and Wang, R., 2022. Exploiting knowledge graph for multi-faceted conceptual modelling using GCN. Procedia Computer Science, 200, pp.1174-1183. 10.1016/j.procs.2022.01.317

5. You, Y., Chen, C., **Hu, F.**, Liu, Y. and Ji, Z., 2022. Advances of digital twins for predictive maintenance. Procedia computer science, 200, pp.1471-1480. 10.1016/j.procs.2022.01.348

Table of Contents

Acknowledgements ..... **i**

Abstract ..... **iii**

Research Achievements ..... **v**

Table of Contents ..... **vii**

List of Tables ..... **xii**

List of Figures ..... **xiii**

List of Symbols ..... **xvii**

List of Abbreviation ..... **xxi**

Chapter 1 Introduction **1**

1.1 Background 1
1.2 Motivations 4
1.3 Research Questions and Objectives 7
1.4 Thesis Outline 8

Chapter 2 Literature Review **11**

2.1 Introduction 11
2.2 AM Systems 11
2.2.1 Popular AM Technologies 11
2.2.2 Data Generation of the AM Process 15
2.3 Data Fusion Technologies 17
2.3.1 Categories of Data Fusion Strategy 18
2.3.2 Prevailing Data Fusion Techniques 22
2.3.3 The Applications of Data Fusion in the AM Industry 27
2.4 Advanced Data Analytics for AM 33

2.4.1 Prevailing ML Algorithms 34
2.4.2 Research and Applications of ML in AM 39
2.4.2.1 ML for DfAM 39
2.4.2.2 ML on Material Analytics for AM 44
2.4.2.3 Defect Detection and In-Situ Monitoring for AM based on ML .. 46
2.4.2.4 ML for Process Modelling and Control in AM 51
2.4.2.5 ML on AM Sustainability 58
2.5 Summary 62

Chapter 3 Framework and Methodology of Task-driven Data Fusion for AM ……...65

3.1 Introduction 65
3.2 Definition of Task-driven 66
3.3 Categories of AM data 67
3.3.1 Process-input Data 67
3.3.2 Process-generated Data 68
3.3.3 Validation Data 68
3.4 Task-driven Data Fusion Framework and Approaches 69
3.4.1 Identification of Task-driven Data Analytics 71
3.4.2 Data Required for Tasks, Acquisition, and Characterization 72
3.4.2.1 Data Required for Tasks 72
3.4.2.2 Data Acquisition and Characterisation 73
3.4.3 Task-driven Data Fusion Techniques 75
3.4.3.1 Multi-source and Multi-hierarchy Data Fusion 78
3.4.3.2 Cloud-edge Fusion 79
3.5 Summary 81

Chapter 4 Multi-source and Multi-hierarchy Data Fusion for AM Using Deep Learning……...82

4.1 Introduction 82
4.2 Methodology 84

4.2.1 Convolutional Feature Extraction of CAD models..... 86
4.2.2 Time-series Modelling based on LSTM..... 89
4.2.3 Fusion of Multi-source and Multi-hierarchy Information based on M-CNN-LSTM 91
4.3 Energy Consumption Prediction for AM 94
4.4 Experimental Setup 95
4.4.1 Data Acquisition and Preparation 95
4.4.2 Evaluation Metrics 98
4.4.3 Experiment 1: Analytics of the Impacts of Design Features on Energy Consumption 98
4.4.4 Experiment 2: Energy Consumption Prediction Based on M-CNN-LSTM ……..103
4.5 Discussion 108
4.6 Summary 110

Chapter 5 Cloud-edge Fusion for AM based on Knowledge Distillation-enabled Incremental Learning..... 112

5.1 Introduction 112
5.2 Methodology 115
5.2.1 Base Model Building via Transfer Learning and DML..... 118
5.2.2 Knowledge Transfer and Model Compression based on KD..... 124
5.2.3 Cloud-edge Fusion through KD-enabled Incremental Learning..... 127
5.3 Multi-stage KD-enabled Incremental Learning for AM Energy Consumption Prediction 131
5.4 Experimental Setup 131
5.4.1 Evaluation Metrics 132
5.4.2 Experiment 1: Transfer Learning Combined with FEI-FEO Strategy . 132
5.4.3 Experiment 2: With DML or Without DML..... 136
5.4.4 Experiment 3: Multi-stage KD-enabled Incremental Learning..... 138
5.5 Discussion 141
5.6 Summary 143

Chapter 6 Case Studies 145

6.1 Introduction 145

6.2 Case Study 1: Mechanical Property Prediction of AM Produced LS 148

6.2.1 Background 148

6.2.2 Data Description 149

6.2.3 Data Fusion for Mechanical Properties Prediction based on ML Models 150

6.2.4 Evaluation Metrics 154

6.2.5 Experimental Results 154

6.3 Case Study 2: Porosity Defects Classification of Parts 156

6.3.1 Background 156

6.3.2 Data Description 157

6.3.3 Data Fusion for Porosity Defects Classification based on ML Models 158

6.3.4 Evaluation Metrics 160

6.3.5 Experimental Results 161

6.4 Case Study 3: Investigating the Effect of the Remelting Process on Part Density 165

6.4.1 Background 165

6.4.2 Data Description 165

6.4.3 Data Fusion for Identifying the Relationship between Remelt Process and Part Density 166

6.4.4 Analytics Results 168

6.5 Discussion 170

6.5.1 Data Considered in Analytics 170

6.5.2 With Fusion and Without Fusion 171

6.5.3 Optimization between Performance and Task Requirements 172

6.6 Summary 172

Chapter 7 Achievements and Conclusions 174

7.1 Achievements 174

7.2 Limitations 177
7.3 Future Works 178
7.4 Conclusions 179

References 181

Appendix A. Advanced Data Analytics Technologies 200

A1 Machine learning 200

Appendix B. Datasets used in this Thesis 203

B1 Extracted build-level design features dataset 203

B2 Statistical features of detected pores (Selected region) 210

List of Tables

Table 2.1 Categories of AM processes and representative technologies 14

Table 2.2 The studies of applying data fusion strategies for tackling AM issues in recent 5 years..... 31

Table 2.3 Mechanical property-related factors of AM-produced LS in the literature 55

Table 2.4 AM energy consumption-related factors in the literature 61

Table 3.1 An example of the data generated during an AM process 74

Table 4.1 Material information collected from the support company material sheet 97

Table 4.2 Description of the process parameters recorded in the Job file 97

Table 4.3 The extracted design features of CAD models 100

Table 5.1 The Pseudo-code of the DML on three base models for regression tasks 122

Table 5.2 The Pseudo-code of the two-stage KD-enabled incremental learning..... 130

Table 5.3 Performances of models in experiment 1 135

Table 5.4 Detailed information of the models..... 141

Table 6.1 The details of applying the proposed task-driven data fusion framework and methodology for the case studies 146

Table 6.2 The input features for mechanical properties prediction..... 151

List of Figures

Figure 2.1 Data generation process of an AM system 16

Figure 2.2 Illustration of the data fusion process based on abstraction levels 21

Figure 2.3 Illustration of Dasarathy's data fusion model 22

Figure 2.4 Illustration of the structure of an FCNN 37

Figure 2.5 An example of the convolution operation in CNN 39

Figure 3.1 The proposed task-driven data fusion framework for AM 70

Figure 3.2 Illustration of the 3-step methodology for identifying, collecting, characterising, and fusing data for AM data analytics 71

Figure 3.3 The connections between different types of data analytics 73

Figure 3.4 The flowchart of the task-driven data fusion 77

Figure 4.1 The flow chart of the proposed approach based on M-CNN-LSTM 85

Figure 4.2 The illustration of the CNN architecture without the fully connected layer 87

Figure 4.3 The illustration of the convolutional feature extraction process of CAD models 87

Figure 4.4 The schematic diagram of the LSTM structure and an LSTM cell 90

Figure 4.5 Fusion of the multi-source and multi-hierarchy information in the merged LSTM 93

Figure 4.6 Examples of CAD models in the SLS production 96

Figure 4.7 The flow chart for the analytics of the impacts of design features on energy consumption 99

Figure 4.8 The PCC between design features and unit energy consumption 102

Figure 4.9 Feature importance ranking based on information gain 103

Figure 4.10 An example of transforming the CAD model to sliced layer-wise images for analysis 104

Figure 4.11 The illustration of the feature extraction process of layer-wise images of sliced CAD models..... 104

Figure 4.12 Energy consumption prediction based on the proposed M-CNN-LSTM model with different fusion strategies 105

Figure 4.13 The performances of different prediction models..... 106

Figure 4.14 The comparisons of performances between different fusion techniques 107

Figure 5.1 Illustration of the proposed methodology 116

Figure 5.2 Illustration of the Cloud-edge fusion paradigm 117

Figure 5.3 Illustration of the employed feature-based transfer learning approach for feature extraction..... 119

Figure 5.4 The illustration of DML for regression tasks on three base models..... 123

Figure 5.5 The schematic diagram of KD in the classic teacher-student architecture 125

Figure 5.6 The schematic diagram of KD between the ensemble teacher model and student model 126

Figure 5.7 The proposed Cloud-edge fusion approach through multi-stage KD-enabled incremental learning..... 129

Figure 5.8 The transfer learning combined with FEI-FEO strategy for energy consumption prediction via DML 133

Figure 5.9 The RMSE results of models trained via different strategies 137

Figure 5.10 The MAE results of models trained via different strategies 137

Figure 5.11 Multi-stage KD-enabled incremental learning for AM energy consumption prediction..... 138

Figure 5.12 The RMSE of student models trained with and without KD_IL strategy 140

Figure 5.13 The MAE of student models trained with and without KD_IL strategy 140

Figure 6.1 The examples of LS in the case study 149

Figure 6.2 The proposed fusion method for mechanical properties prediction of LS 151

Figure 6.3 Examples of voxelization of LS with 100*100*100 resolution 152

Figure 6.4 Obtaining the entropy vector of LS units based on the entropy of 20 subspaces 153

Figure 6.5 The performances of different prediction models for elastic modulus prediction 155

Figure 6.6 The performances of different prediction models for yield strength prediction 155

Figure 6.7 Examples of LOM images for porosity detection in the dataset 157

Figure 6.8 Examples of binarized LOM images in the dataset 158

Figure 6.9 Illustration of the proposed approach for classifying porosity defects of the cross-section of cubes 159

Figure 6.10 The SSE of different numbers of clusters 162

Figure 6.11 The silhouette scores of different numbers of clusters 162

Figure 6.12 Typical porosity defect images for each cluster 163

Figure 6.13 The classification results of different ML algorithms 164

Figure 6.14 The classification results of different ML algorithms after implementing FEI-FEO strategy on extracted features 164

Figure 6.15 Schematic diagram of the remelting process 166

Figure 6.16 Data fusion for identifying the relationship between the remelting process and part density level..... 167

Figure 6.17 PCC between remelting process parameters and part density 168

Figure 6.18 The accuracy for classifying part density levels of different models ... 169

Figure 6.19 The feature importance ranking of remelting process parameters..... 170

List of Symbols

A : Feature A in the tree-based algorithm

A_K : The matrix in Kalman filter

A_l : The area of the printed layer

$\boldsymbol{b}$: The bias in neural network

$\boldsymbol{B}_F$: The bias of the FCNN

Bu_k : The control input in Kalman filter

c_t : The memory cell that stores the observed information up to the time step t

D_m : Material density

D_{KL} : The Kullback Leibler divergence

D_{MSE} : The distance between predictions measured by MSE

E_l : The total energy consumed for each printed layer

E_u : The unit energy consumption

E_T : The total energy consumed for the whole build

E_{uT} : The unit energy consumption of the whole printed build

$f_{LSTM}(\ )$: The LSTM model

$f_{\mathrm{ReLU}}(\ )$: The activation function of rectified linear unit

f_N : The activation function in the FCNN

f_t: The forget gate at time t

f_{bj} : The techniques used for processing the jth build-level data

f_{li} : The techniques used for processing the ith layer-level data

F_C : The analytics model trained in the Cloud platform

F_E : The initially designed target analytics model at edge

$F_E^{'}$: The final analytics model at edge

$Gain$ ( ) : The information gain

h_t : The hidden state at time step t

H_l : Layer thickness

$H(D)$: The entropy of dataset D

i_t : The input gate at time step t

K_k : The Kalman gain

$Loss$ ( ) : The loss function

$Loss_{student}$: The loss function for the student model

$Loss_{distill}$: The loss function for the knowledge distillation

$Loss_A$: The loss function for the actual label

$Loss_{soft}$: The loss function for the soft label

$Loss_{hard}$: The loss function for the hard label

$Loss_{latter}$: The loss function for the latter student model

M_T : The weight of the whole printed build

N_b : The output of neurons where the build-level information are processed

o_t : The output gate at time step t

P_i : The proportion of the object i

$P_{k|k}$: The updated error covariance in Kalman filter at time k

$p_j^m(x_i)$: The probability of class m for x_i in the jth neural network

q_i : The weighted averaging soft label

Q : The process noise covariance in Kalman filter

r_{XY} : The correlation coefficient between variables X and Y

R^2 : The coefficient of determination

s_i^m : The output of the softmax layer in the neural network

S_k : The processed inputs of neurons before the activation function of the FCNN

Softmax ( ): The softmax function

$tree_m$ ( ) : The base decision tree model

T_m ( ) : The LGBM model

$\boldsymbol{U}$: Learnable parameters in neural networks

v_i : The given actual value in the knowledge distillation

$\hat{v}_{si}$: The predicted value of the student model

$\hat{v}_{Ei}$: The predicted value of the teacher ensemble

V : The target value of task

V_C : The estimated target value at the Cloud

$V_E^{'}$: The estimated target value at the edge

V_b : The target value at the build-level

V_l : The target value at the layer-level

$\boldsymbol{w}_n$: The weights in neural networks

w_i : The weight assigned to the ith base model for ensemble

$\boldsymbol{W}$: Learnable parameters in neural networks

$\boldsymbol{W}_F$: The weight matrix of the FCNN

$\hat{x}_{k|k-1}$: The predicted state at time k based on the information up to time k-1

$\overline{x}$: The mean value of variable x

$x_{li}(t)$: The ith time-series measurement data at layer-level at time t

x_{bj} : The jth build-level data

$X_{(l+b)}$: The concatenated feature vectors in the layer

$\overline{y}$: The mean value of outputs

$\hat{y}_i$: The ith predicted value

y_b : The output of each neuron in the LSTM

Y_{final} : The final output of the M-CNN-LSTM

z_k : The observation at time k in Kalman filter

$\boldsymbol{Z}$: The given input with k variables

α : The weight for training loss

β : The weight for training loss

γ : The weight for training loss

θ_1 : Base neural network one

θ_2 : Base neural network two

θ_3 : Base neural network three

θ_i : The ith base model

θ_E : The initial model parameter

$\theta_E^{'}$: The fine-tuned parameters by knowledge transfer

List of Abbreviation

AM: Additive manufacturing

AE: Acoustic emission

ANN: Artificial neural network

AI: Artificial intelligence

BJ: Binder jetting

BNN: Bayesian neural network

CAD: Computer-aided design

CFD: Computational fluid dynamics

CLSM: Confocal laser scanning microscopy

CNN: Convolutional neural network

CPS: Cyber-physical system

CPPS: Cyber-physical production system

DAI-DAO: Data in-Data out

DAI-FEO: Data in-Feature out

DEI-DEO: Decision in-Decision out

DED: Directed energy deposition

DL: Deep learning

DML: Deep mutual learning

DBN: Deep belief network

DBSCAN: Density-based spatial clustering of applications with noise

DCNN: Deep convolutional neural network

DfAM: Design for AM

DOD: Drop on demand

DLP: Digital light processing

DT: Decision tree

EBM: Electron beam melting

EFB: Exclusive feature bundling

FCNN: Fully connected neural network

FDM: Fused deposition modelling

FEI-FEO: Feature in-Feature out

FEI-DEO: Feature in-Decision out

FEA: Finite element analysis

FV: Focus variation

GAN: Generative adversarial network

GCN: Graph convolutional network

GBDT: Gradient boosting decision tree

GP: Gaussian process

GOSS: Gradient-based one-side sampling

ICT: Information and communication technology

IoT: Internet of things

IIoT: Industrial Internet of things

k-NN: *k* nearest neighbours

k-SVD: *k*-means singular value decomposition

KD: Knowledge distillation

KPCA: Kernel PCA

KL: Kullback Leibler

LS: Lattice structure

LCA: Life cycle assessment

LSTM: Long-short-term memory

LGBM: Light gradient boosting machine

LRCN: Long-term recurrent convolutional network

LLE: Locally linear embedding

LPP: Locality preserving projections

LMD: Laser metal deposition

LOM: Light optical microscopy

LDA: Linear discriminant analysis

ML: Machine learning

M-CNN-LSTM: Merged-CNN-LSTM

ME: Material extrusion

MJ: Material jetting

MAE: Mean absolute error

MsCNN: Multi-scale CNN

NNS: Near-net-shape

NIR: Near-infrared

PBF: Powder bed fusion

PCA: Principal component analysis

PCC: Pearson correlation coefficient

PS: Process-structure

PSP: Process-structure-property

PPP: Process-property-performance

RFs: Random forests

RL: Reinforcement learning

RBF: Radial basis function

RNN: Recurrent neural network

RMSE: Root mean square error

SSE: Sum of squared errors

SLS: Selective laser sintering

SLM: Selective laser melting

SLA: Stereolithography

SL: Sheet lamination

SVM: Support vector machine

SAE: Sparse auto-encoders

SVDD: Support vector data description

SIFT: Scale-invariant feature transform

t-SNE: *t*-distributed stochastic neighbour embedding

UAM: Ultrasonic AM

UV: Ultraviolet

USD: United States dollars

VP: Vat photopolymerization

VAE: Variational autoencoders

XCT: X-ray computed tomography

Chapter 1 Introduction

1.1 Background

Additive manufacturing (AM), also known as rapid prototyping, 3D printing, and freeform fabrication, is capable of depositing, joining or solidifying materials to construct physical objects from computer-aided design (CAD) models (Gibson et al., 2021b). Compared with conventional manufacturing methodologies, such as subtractive manufacturing and formative manufacturing, AM systems show higher efficiency and flexibility within the high-yield production and offer a new perspective for the design and processing of both parts and materials. Due to its unique production paradigm and advantages, AM technologies have been increasingly used for mass customization, and production of any type of open-source designs in the field of agriculture, healthcare, automotive industry, and aerospace industries (Keleş et al., 2017, Shahrubudin et al., 2019). As one of the key technologies driving the shift to Industry 4.0, the global market of AM reached a size of 13.84 billion USD (United States dollars) in 2021 and it is estimated to achieve a compound annual growth rate of 20.8% from 2022 to 2030 (GrandViewResearch, 2022). AM also offers significant economic benefits since it is considered a type of sustainable technology that supports reusing and recycling materials to reduce waste generation (Ferreira et al., 2021). Although AM has bright prospects for industrial applications, it has not yet been widely used in large-scale industrial production. This is due to a number of challenges stemming from not only the complexity of manufacturing systems but the demand for increasingly complex and high-quality products, in terms of design principles,

standardization and quality control. AM process is well-known as a highly complex system including various technologies that combines material science, mechanics, optics, and electronics with computer science. As a result, the quality of produced parts is affected by numerous factors, such as material properties, processing parameters, process stability, and working conditions. This leads to the crucial challenges that prevent the wide-spread adoption of AM in manufacturing industries.

With the fast development of the Industrial Internet of Things (IIoT), artificial intelligence (AI), and cyber-physical systems (CPS) towards the upcoming era of Industry 4.0, advanced data analytics play an important role in decision-making activities for improving product quality, process stability and repeatability, and sustainability. IIoT is the subset of the Internet of Things (IoT) that specifically focuses on the industry area, operating by collecting, managing, communicating, and analyzing data from various sources within the industrial environment (Qin et al., 2021). It involves the deployment of internet-connected machinery and devices to improve the efficiency and effectiveness of industrial processes. IIoT technologies have been increasingly used in the field of manufacturing, transportation, agriculture, logistics, and energy for environment monitoring, automation, and system performance optimization (Malik et al., 2021). AI refers to the simulation of the problem-solving and decision-making capabilities of humans by machines. It belongs to the intersection of computer science and cognitive science and involves tasks such as image recognition, voice recognition, understanding natural languages, and target tracking (Ertel, 2018).

AI has become one of the most crucial technologies in Industry 4.0, significantly facilitating and improving the decision-making processes in the field of manufacturing, agriculture, transportation and logistics, and so on. Machine learning (ML) technologies are the most advanced and prevailing data analytics tools to achieve AI. CPS is the system of collaborating computational elements controlling physical entities. It integrates computation, networking, and physical processes (Dafflon et al., 2021). By utilizing advanced communication and computation technologies (e.g., IIoT and AI), CPS enables adaptation, reconfiguration, and improvement of stability,

reliability, efficiency, and robustness of physical systems. In recent years, CPS has emerged across various industries and deployed in modern technological systems, including smart grids, real-time control of flight systems, autonomous automobile systems, and robot control systems (Lun et al., 2019, Jha et al., 2021). As CPS is promising to greatly enhance the efficiency and quality of AM production, researchers have made great efforts to incorporate CPS or cyber-enabled platforms into AM systems that aim to achieve real-time monitoring and control, process optimization, remote operation, and predictive maintenance (Malik et al., 2023, Gupta et al., 2020). To achieve this, significant research and practical solutions are required to overcome several crucial challenges. For instance, data management and analytics. In AM systems, a large amount of data will generate during the AM production which needs to be effectively managed, processed, stored, and analysed. Robust data analytics capabilities are required. Also, the monitoring and control of AM processes usually operate in real-time or near-real-time where considerable computing resources and efficient analytics models are essential.

Benefiting from the data-intensive environment and rapid development of high-performance computing, research methodologies across science and engineering have witnessed a shift to data-driven and informatics approaches (Wang et al., 2022). As a result, AI, especially ML, has considerably aided and improved the decision-making processes in the manufacturing industry. The integration of advanced data sensing and collection technologies in AM systems has enabled exponential growth of data, providing unprecedented opportunities for understanding the nature of AM processes and uncovering hidden knowledge (Khosravani et al., 2022). Since it is difficult to model the mathematical relations of underlying AM processes, data-driven modelling based on ML technologies is emerging as an effective method to tackle challenging AM issues. The number of research studies on using ML in AM has been increasing sharply since 2020 (Jiang, 2023), and the trend will continue for the next few years due to the increasing amount of available data and the fast development of ML algorithms. However, with the emergence of new sensing technologies and algorithms, it becomes rather difficult for researchers and AM engineers to simply put the data into

ML models to get the results especially when dealing with new AM issues or tasks. The collected data becomes more diverse which normally has different sources, types, scales, and dimensions. Moreover, some researchers raise the concerns that the quality of AM data is rarely paid attention to. Also, it's hard to understand and trust the practical deployment of AI models as it's normally black-box models (Arrieta et al., 2020). Therefore, here comes the question, how should the AM data be leveraged?

Data fusion is defined as a framework (Cocchi, 2019), fit by an ensemble of tools, for the joint analysis of data from multiple sources or modalities to uncover information not recoverable by individual ones. Since data-driven modelling methods have risen to play an important role in academia and industry, data fusion strategies are increasingly adopted for data analytics. It has been widely employed in environment monitoring (Himeur et al., 2022), movement identification (Sbargoud et al., 2019, Lamsellak et al., 2022), and fault diagnosis (Wang et al., 2021a). As is known, AM process is a data generation process starting from the initial order to the product delivery and it includes six essential stages (Convert, Locate and orient, Adding support structure, Slice, Build, and Post-process) (Wang and Alexander, 2016, Qin et al., 2018a). The collected data is normally from different sources and can have various modalities. Also, this data is rarely independent and contains information related to product quality, process stability, and system efficiency. Therefore, leveraging data fusion techniques for AM data analytics to improve the decision-making process has become one of the most crucial research targets in the era of Industry 4.0.

1.2 Motivations

As one of the most crucial technologies in the era of Industry 4.0, AM is promising to take a dominant position in the manufacturing sector. Its unique production paradigm offers a range of advantages over traditional manufacturing methods. However, critical challenges limit the broader applications of AM in the industry. For example, one of the major challenges is to ensure consistent quality of products especially when producing customized complex geometries or when using the same AM process but different machines (Vafadar et al., 2021). Also, the size limitations and production

speed make it less suitable for large industrial parts. The range of materials available for AM is more limited than those for traditional manufacturing. Moreover, the lack of standardized procedures and certifications in nowadays AM industry are the major concerns in the application scenario where part reliability and reproducibility are critical (e.g., aerospace, healthcare) (Chen et al., 2022). Therefore, how to improve product quality, process stability, and reproducibility become crucial research targets. The complexity of AM systems leads to the challenge that it is difficult to model the mathematical relations of the underlying AM process because the correlated factors are from various heterogeneous perspectives and different process stages. High-fidelity physical-based models are generally too complicated considering the in-process uncertainties of the AM process, which demand significant computational resources. Additionally, it is challenging to integrate AM digital models, pertinent to various phenomena, at multiple scales into one unified framework (Smith et al., 2016b, Qin et al., 2022b).

Data-driven modelling methods have proven to be effective in tackling challenging AM issues in recent years especially when advanced sensing and communicating technologies emerge. As manufacturing data continues to grow exponentially, data-driven intelligence with advanced analytics transforms unprecedented volumes of data into actionable and insightful information for smart manufacturing (Wang et al., 2018a). More and more critical information can be captured and analysed based on ML technologies for hidden knowledge discovery and building highly complex relationships in digital manufacturing systems (Wang et al., 2020a). Data analytics using ML technologies have largely improved the decision-making process in AM research, such as part design, shape deviation control, defect detection, process modelling and control, and sustainability. However, as using ML technologies to address AM issues involves multidisciplinary knowledge, it is normally hard for AM engineers and experts to find out what issues can be tackled by ML and select appropriate algorithms at the beginning of the research. More importantly, since the final product is affected by various factors in AM production, the collected data and

information is from different sources at different process stages, which should be integrated or fused for analysing (Tian et al., 2021b).

Data fusion strategies have been increasingly adopted to improve the performance of the corresponding decision-making process in the manufacturing industry. However, the collected multi-source data is normally heterogeneous and usually involves various structures, types, modalities, and dimensions. This heterogeneous data is difficult to be jointly analysed and cannot simply be used as input to be fed into conventional fusion models. Hence, in what way to fuse the AM data for analytics and how to leverage it to help decision-making activities become critical research topics (Qin et al., 2022b). Deep learning (DL), as a subset of ML techniques, is particularly powerful in handling large and complex datasets, being capable of learning hidden knowledge automatically from raw data. Its strong scalability and versatility make it a powerful fusion model and has demonstrated outstanding performance in various applications for smart manufacturing or intelligent manufacturing in recent years (Lee et al., 2020a). The variant DL models, such as convolutional neural networks (CNN), are also capable of handling data with different structures and dimensions.

With the rise of data-driven intelligence in AM, several main concerns are raised by both industry and academia. For instance, data quality and reliability can affect results significantly. Poor quality and unnecessary data can lead to inaccuracy and jeopardize the performance of analytic models. Also, for some specific AM tasks, acquiring an adequate amount of data for training ML models is rather costly and time-consuming (e.g., X-ray computed tomography (XCT)) (Zhang et al., 2022b). In some scenarios, the decisions made by data-driven models are challenging to be understood and interpreted (Guo et al., 2022). Moreover, for different applications of AM-produced products, the requirements in terms of quality, cost, and other specific indicators can be various. A general-purpose analytic model might be capable of handling a series of similar AM tasks but it wouldn’t necessarily have decent performances on the task with specific requirements. Therefore, the analytic models for a specific AM task or objective should be designed to consider the specific requirements to achieve desired performance.

1.3 Research Questions and Objectives

Following the background and motivations, this research aims to investigate how to effectively leverage data fusion techniques to fuse multi-source and multi-dimensional heterogeneous data, and knowledge for data analytics to support decision-making activities in AM, thus to bridge the gap between the multi-physics interactions of the complex AM manufacturing process and resultant outcomes. The following research questions have been formulated to achieve this goal:

1. *With the development of emerging technologies such as IIoT, CPPS, and DL, the AM industry has shifted to a data-intensive environment. In this case, what is an appropriate data fusion framework for AM with the full exploitation of these resources to support decision-making activities?*

2. *The data generated from an AM system often covers a wide range of spatial and temporal scales and is normally from different sources, leading to critical challenges for joint analysis of this multi-source and multi-hierarchy data. In addition, traditional methods for analysis of part geometries normally use hand-crafted features which are hard to describe complex geometries precisely and usually cannot reflect the sequential patterns. Therefore, how to analyse and integrate geometric features with other related information of different hierarchies to obtain target values of AM tasks?*

3. *At the initial stage of some AM tasks, it usually cannot provide a sufficient amount of data samples for building reliable and robust ML-based models due to the constraints of time and expenses. Also, most of these models cannot make fast inferencing while the main requirement of some AM tasks is fast response. In this context, what strategy can be applied to address these challenges? How to leverage the new incoming data and enable the analytics model to make fast inferences?*

With the identification of the research questions, the research objectives following these research questions are listed below:

1. *To propose a data fusion framework for data analytics in AM that can provide a guideline and systematic way to support decision-making activities of AM tasks.*

2. *To propose a multi-source and multi-hierarchy data fusion method for AM tasks. The method can fuse geometric features with other task-related information of different hierarchies.*

3. *To propose a strategy and methodology for building the analytics model for the AM tasks that not only continuously improves model performance but also enables fast inferences.*

4. *To apply the proposed data fusion framework for tackling different AM tasks to demonstrate its feasibility and effectiveness.*

The details of this research will be presented in Chapters 3, 4, 5, and 6.

1.4 Thesis Outline

In **Chapter 1**, a broader context and background are provided as to the motivation and significance of this research.

Chapter 2 presents a detailed review of the existing technologies and literature on related topics, which is divided into three main parts, including (1) an overview of AM technologies and representative processes with the general AM data generation process; (2) data fusion categories and technologies, and their applications in the AM industry; (3) prevailing technologies of advanced data analytics, and research and application of ML for AM tasks.

In **Chapter 3**, a task-driven data fusion framework and methodology are proposed to provide a systematic way to identify, collect, characterise, and fuse the data for

supporting decision-making activities in AM. The proposed methodology consists of three steps, including (1) identification of task-driven data analytics, (2) data required for tasks, acquisition, and characterization, and (3) task-driven data fusion techniques. The task-driven data fusion techniques provide guidelines on how to fuse multi-source heterogeneous data and information from different system levels.

Chapter 4 presents a multi-source and multi-hierarchy data fusion approach based on the developed M-CNN-LSTM model, which can analyse geometric data in sequential patterns and fuse it with other task-related information from different hierarchies. In this approach, the CNN part extracts features from layer-wise images of sliced 3D models, while the LSTM part models time-series data by combining layer-level data with convolutional features. The build-level information is used as input into a separate neural network and merged with the CNN-LSTM in the fully connected neural network for obtaining the final target value. A case study was carried out on an energy consumption prediction task where the experimental results using real-world data revealed the effectiveness of the proposed approach.

Considering the challenging issues in some AM tasks that (1) lack sufficient data samples for training reliable and robust ML models at the initial stage, and (2) the AM tasks require fast inferencing, **Chapter 5** aims to introduce a Cloud-edge fusion strategy and methodology based on transfer learning and multi-stage KD-enabled incremental learning. The proposed methodology consists of three main steps, including (1) transfer learning for feature extraction, (2) base model building via DML and model ensemble, and (3) multi-stage KD-enabled incremental learning. As part of the base model training, the transferred pre-trained CNN model (on similar or related tasks) extracts features from images and concatenates them with task-related information. DML strategy is employed to train three neural network-based base models, which are then fused into an ensemble model. By implementing the multi-stage KD-enabled incremental learning method, knowledge is transferred from the ensemble model to the compressed student model while new knowledge is acquired incrementally when new data is collected. The experimental results from an AM

energy consumption prediction task demonstrated the feasibility and effectiveness of the proposed methodology.

In **Chapter 6**, three case studies were carried out to demonstrate the applications of the proposed task-driven data fusion framework and methodology for different AM tasks, including (1) mechanical property prediction based on of additively manufactured LS, (2) porosity defects classification of parts, and (3) investigating the effect of the remelting process on part density. Different strategies and approaches were proposed to tackling these AM tasks with different considerations. Finally, the strategies and approaches are discussed in depth and presented.

Chapter 7 concludes the thesis, providing a summary of its achievements. The limitations and future work of this research are also discussed and presented. As a final note, the main contributions to advanced data analytics for AM resulting from this research are summarised.

Chapter 2 Literature Review

2.1 Introduction

This chapter consists of three main sections that review state-of-the-art AM technologies, data fusion technologies and their applications in the manufacturing industry, and applications of advanced data analytics in AM. The categories of AM processes, popular AM technologies within each category, and the data and information generated during AM production were introduced in Section 2.2. Several prevailing data fusion architectures, techniques, and their recent applications in the manufacturing industry were reviewed in Section 2.3. In Section 2.4, prevailing ML technologies were introduced, followed by the review of research and studies that applied ML to tackle AM issues. Section 2.5 summarises this chapter.

2.2 AM Systems

2.2.1 Popular AM Technologies

The first commercial AM system recognizably emerged in 1987 with stereolithography by 3D Systems (Wohlers and Gornet, 2014). Since then, AM has become one of the most crucial manufacturing solutions across various industries, such as automobile (Sarvankar and Yewale, 2019), aerospace (Kamal and Rizza, 2019), and construction (Paolini et al., 2019). There are currently seven AM process categories, published in the Standard Terminology for Additive Manufacturing Technologies, which are binder jetting (BJ), directed energy deposition (DED), material extrusion (ME), material jetting (MJ), powder bed fusion (PBF), sheet lamination (SL) and vat

photopolymerization (VP) (ISO/ASTM, 2016). Table 2.1 shows the details of these AM process categories. These seven categories focus on the single-step process, and for the multi-step AM process, the system combines two or more AM processes (Quan et al., 2015).

1) **Binder Jetting:** BJ process is one of the earliest AM processes developed for polymer powder-based material. An inkjet print head is used to spray the liquid binder onto the polymer powder. The powder material is solidified crossing the section of the produced part layer by layer by the chemical reaction bonding at a reasonable speed (Gokuldoss et al., 2017).
2) **Material Extrusion:** ME process is currently the most prevailing AM process in the market. The materials of extrusion-based AM systems are normally forced out in a semisolid state via a nozzle where constant pressure is applied. Then the extruded materials solidify and bond to the previous extruded materials to form a solid structure (Park et al., 2014). Fused deposition modelling (FDM) is the commonly used ME process.
3) **Direct Energy Deposition:** DED processes utilize focused energy, such as a laser beam, electron beam, or plasma arc, to melt and fuse simultaneously the substrate and the material that is being deposited into the substrate's melt pool to construct parts (Gibson et al., 2021a). Powder-based and wire-based materials can be used for DED processes (Shim et al., 2016). Representative DED technologies include wire arc AM (WAAM) and electron beam AM (EBAM). WAAM uses an electric arc to melt metal wire for depositing materials layer by layer. This technology is a variation of traditional welding techniques. EBAM uses an electron-beam gun to melt metal materials for depositing through a wire feedstock.
4) **Material Jetting:** MJ is another fast AM process, which uses ultraviolet (UV) light as the main power to solid-liquid photopolymer droplets. The droplets are controlled by the voltage signal. Through the print head, the liquid or melted material is jetted onto the produced part surface (Udroiu et al., 2019). Drop on demand (DOD) is one of the most popular MJ technology. DOD releases droplets when necessary instead of continuous lines and is normally used for

viscous liquid materials.

5) **Powder Bed Fusion:** PBF processes consist of thin layers of fine powders, which are spread and closely packed on a platform. One or two thermal sources are employed in the systems to melt and fuse material powder particles in each layer. Selective laser sintering (SLS), selective laser melting (SLM), and powder-based electron beam melting (EBM) are the commonly used PBF technologies (Ngo et al., 2018). SLS technology uses lasers to sinter powder materials while EBM technology uses an electron gun to generate a high-velocity electron beam to melt and fuse materials. SLS commonly uses powder materials such as polymers, ceramics, or meta powders with lower melting points. SLM and EBM are normally used for metals with higher melting points.

6) **Sheet Lamination:** Two AM technologies are commonly classified into the class of SL processes, ultrasonic additive manufacturing (UAM) and laminated object manufacturing. The sheets of the material are bonded together as part based on the fusion resource, like ultrasonic (Bhatt et al., 2019). Continuous sheets of materials (normally plastic or paper) are fused or laminated by heat and pressure in the LOM technology.

7) **Vat Photopolymerization:** VP processes mainly use ultraviolet (UV) to cure or harden materials such as photopolymers, liquids, and resins for building products. These processes are capable of manufacturing large parts with submillimetre details and are widely applied in the coating and printing industry (Chartrain et al., 2018). The popular VP technologies include stereolithography (SLA) and digital light processing (DLP). The most commonly used materials for VP processes are resins.

Table 2.1 Categories of AM processes and representative technologies

AM process	Working principle	Material	Material feedstock	State of fusion	Representative technology
BJ	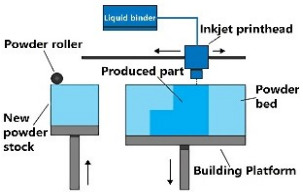	Polymer	Liquid	Chemical reaction bonding	BJ
ME	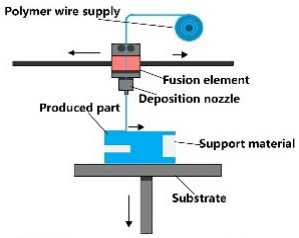	Polymer	Filament	Thermal reaction bonding	FDM
DED	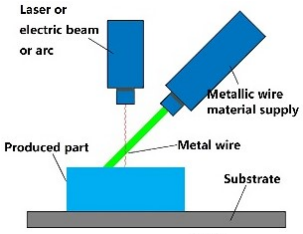	Metallic	Filament/ powder	Melted state: (electric beam/arc /laser)	WAAM, EBAM
MJ	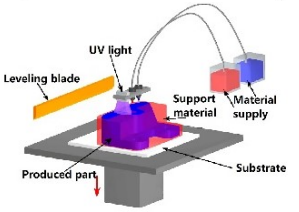	Polymer	Liquid	Chemical/ thermal reaction bonding	DOD
PBF	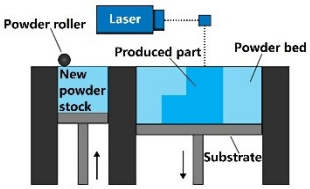	Polymer/ metallic/ ceramic	Powder	Melted state/ laser/ solid-state	SLS, SLM
SL	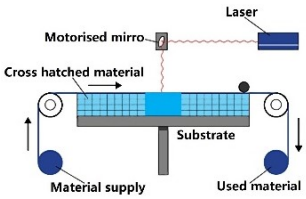	Polymer/ metallic	Sheet	Solid state: (ultrasound)/ chemical reaction bonding	UAM
VP	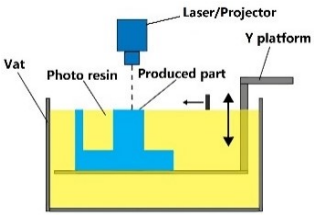	Polymer	Liquid	Chemical reaction bonding	DLP, SLA

Different AM technologies have their unique advantages and limitations. When dealing with different materials, manufacturing requirements, and considerations for resource efficiency, industries will select the technologies based on specific AM task requirements and application scenarios. FDM is the most commonly used AM technology, especially for personal and low-cost applications while SLM and EBM are typically used for certain aerospace and medical applications. DED is more often used for repair work or adding materials to existing components. AM is able to offer enhanced performance, such as for parts with complex and customized geometries that are either difficult or expensive to produce using traditional manufacturing methods. For example, lattice structures (LS) can only be produced by AM and are typically used in end-use products (Chen et al., 2021a), such as components in the aerospace industry. In the medical industry, with the increasing demand for personalization, AM has received widespread attention as it can provide customized products for patients.

According to the Wohlers Report (Wohlers, 2022), PBF systems tend to be increasingly adopted for end-use parts production than VP. Considerable growth has been witnessed in the use of polymer powder for custom products and series production in 2021, which increased by 43.3 % to make photopolymers the most commonly used AM material. AM also enables manufacturers to minimize inventory levels by combining components and utilizing on-demand production, thereby decreasing the requirements for storage and warehousing. AM is believed to be widely used for manufacturing end-use and customized parts in the near future. Hence, how to enhance the quality of the final produced parts, improve the stability of the process, and ensure the repeatability of the process become the most critical research targets.

2.2.2 Data Generation of the AM Process

This section will introduce the data generation of a standard AM process. The advancement of sensing and storage technologies has led to the data-intensive environment of AM systems where a large amount of production information can be captured, stored, and leveraged. Normally, AM data is continuously generated from the part design phase to the final part validation phase, the attributes of which involve

various types, structures and dimensions. Different studies characterise AM data from different perspectives with different purposes in terms of the temporal dimension, spatial dimension, and functions of the process. Figure 2.1 illustrates the data generation and collection of a standard AM process.

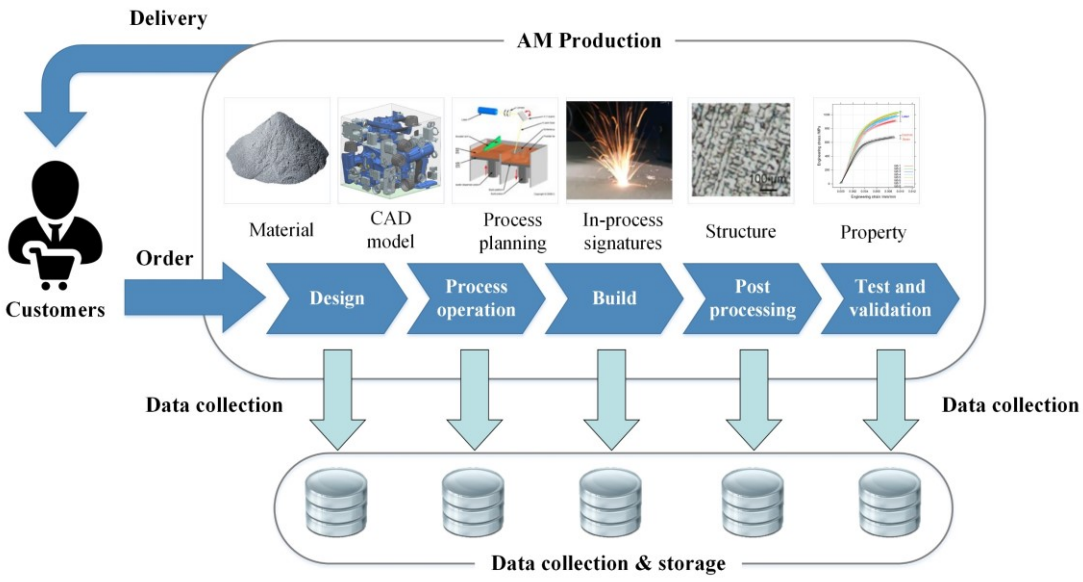

Figure 2.1 Data generation process of an AM system

Sayyeda et al., (Razvi et al., 2019) characterised AM data from three perspectives, including volume, velocity, and variety. From the volume perspective, terabytes (TB) size of monitoring data and CT scan data can be generated for each build. The velocity of data depends on the sampling rates of sensors and machine log frequencies. For the variety aspect, various data types are generated per build, such as sensor signals, machine logs, images, CAD models, CT scan data, thermal videos, etc. Qin et al., (Qin et al., 2018a) defined the data generated from AM production as multi-source data, including four main sources, process operation data, working environment data, design-relevant data, and material condition data. Process operation data is the data generated by process operating, including parameter setting. The working environment data represents the data generated during the AM production. It can be collected from monitoring systems where chamber temperature, gas rates, and multi-sensor signals can be captured. The authors classified part design, material design, and part location

and orientation data into design-relevant data. In material condition data, information such as material density, melting point, and humidity is included.

Hyunseop et al., (Park et al., 2019) defined 6 types of AM data, including material properties, design parameters, process parameters, process signatures, part properties, and product performance. For example, in material properties, information on material chemistry and powder size distribution is included. To systematically manage and analyse the data generated from design to final product, the end-to-end digital spectrum of AM was categorized by Kim et al., (Kim et al., 2015) into 8 phases. The first phase is the part geometry which deals with the information created during part design. Materials are also selected in phase 1. The second phase and third phases are defined as tessellated data and tessellated 3D models respectively where usable geometries are created from raw data. Followed by the fourth phase build file, the fifth phase machine data, the sixth phase fabricated part, seventh phase finished part, and eighth phase validated part. Information of post-processing and mechanical testing on the fabricated parts are included in phases 7 and 8 respectively. Particularly targeted at the metal powder bed fusion process, the study (Witherell, 2018) also mentioned data categories which are separated into 3 subsections, feedstock materials, and in-situ and ex-situ measurements. For this thesis, more details of the data generated during AM production in terms of data categories, types, and stages of generation are presented in Section 3.

2.3 Data Fusion Technologies

In general, the terms "data fusion" and "information fusion" are typically used as synonyms while there are still slight differences under some specific contexts (Castanedo, 2013). When it comes to the raw data especially obtained from multiple sensors, the term "data fusion" is normally used. The term "information fusion" is adopted to define the fusion of already refined or processed data, which implies a higher semantic level than the "data fusion". But in general contexts, these two terms mean the same thing and can be used interchangeably. Decision fusion, data integration, data aggregation, and data combination are commonly used terms that are

associated with data fusion. There are several versions of the definition of the term "data fusion". They have some differences due to the limitations of their eras but the core concepts expressed in these definitions are consistent. A widely accepted definition of data fusion is provided by the Joint Directors of Laboratories workshop (White, 1991): "A multi-level process dealing with the association, correlation, combination of data and information from single and multiple sources to achieve refined position, identify estimates and complete timely assessments of situations, threats and their significance.". Another widely-used definition of data fusion is that data fusion is defined as a framework, fit by an ensemble of tools, for the joint analysis of data from multiple sources or modalities that allows achieving information or knowledge not recoverable by the individual ones (Cocchi, 2019). Data fusion technologies have been widely implemented for fusing data in multisensory environments to achieve higher reliability and accuracy of estimation. With the advancement of sensing technologies, an exponential growth of data with different modalities, types, and dimensions can be obtained and captured. Data fusion technologies are also applied to various domains, such as manufacturing industries, robotics, healthcare, earth observation (Salcedo-Sanz et al., 2020), and so on. The following paragraphs will introduce the detailed categories of data fusion strategies, prevailing techniques, and their typical applications in the manufacturing domain.

2.3.1 Categories of Data Fusion Strategy

Data fusion is a multidisciplinary domain that involves various fields, making it hard to define a clear and rigid classification for their techniques (Castanedo, 2013). These techniques can be broadly classified into different categories in terms of abstraction level, relations between data sources, and type of architecture. The widely adopted and the most prevailing taxonomy for data fusion is based on the abstraction level, which is low-level, mid-level, and high-level. In some literature, the levels are also known as data-level, feature-level, and decision-level.

Data fusion at low-level (also known as data-level, sensor-level, or observational level) refers to the fusion or integration of raw data directly without any significant

processing or feature extraction process. Low-level data fusion can be accomplished through various approaches that either operate directly on multiple data blocks, joined or coupled, by decomposition (e.g., multiblock, multiset, tensor, and coupled matrix-tensor factorization), or by simply concatenating the different data blocks (Cocchi, 2019). low-level data fusion can enhance the quality of raw data by reducing redundancy and noise either for further processing steps or directly obtaining the modelling results. The characteristic of low-level fusion is that the data is modelled for either exploratory or predictive objectives after the fusion process. The main advantage of implementing low-level data fusion is the possibility to interpret the results of fusion as it directly operates on the original variables from each data block. Additionally, it is more efficient in terms of computational resources. A major drawback of low-level fusion is that the number of observations in datasets is typically much smaller than the number of variables. Low-level data fusion is commonly applied to real-time processing for sensor fusion in robotics, the automotive industry, and aerospace and defence.

Mid-level data fusion, also known as feature-level data fusion, refers to the fusion of refined or processed data rather than directly combing raw data, in which features are obtained from multiple data sources. Feature vectors are extracted from data blocks by using decomposition techniques or variable selection methods before the fusion occurs. Then, these features are used as input in the integration for further analysis or decision-making process, such as producing the desired outcomes (e.g., predictions). Hence, dimensionality reduction contributes to the main advantage of mid-level data fusion, making the subsequent processing more efficient. Also, noninformative variables can be removed in the feature reduction process, leading to better performance in the final modelling. For model interpretation in mid-level fusion, interpreting the model in terms of the original variables becomes straightforward if variable selection is employed initially. However, if not, it needs to trace back the importance of each feature in the final model to its corresponding pattern among the original variables. Typical applications of mid-level data fusion are natural language processing, medical imaging, and financial market analysis.

High-level data fusion, also known as decision-level data fusion, implies the fusion of decisions, outcomes, or interpretations that are obtained from the modelling results of each data block. High-level data fusion focuses on the final results, such as correctly classifying samples or identifying targets, where the significance of each data block and its original variables is not investigated. The main objective of high-level data fusion is to improve the performance of the final model by various approaches, such as weighted decision, Bayesian inference, and fuzzy set theory. By integrating decisions from multiple sources to reduce overall uncertainty, the final result is normally more reliable and robust. The computational complexity involved in the high-level fusion process is largely reduced as it simply tackles processed information. However, the major drawbacks of high-level data fusion are the difficulties in error tracing and the loss of detailed information from the original data sources. Since high-level fusion deals with processed decisions rather than raw data, the granular details from the original variables are not provided, making it challenging to trace back the fused decisions to the original variables. Additionally, potentially informative patterns in the raw data might be overlooked in earlier data processing stages, leading to less accurate decisions. It is also difficult to deal with the scenarios when multiple sources generate conflicting results.

Different levels (i.e., low, mid, and high) of the data fusion process are illustrated in Figure 2.2. In the figure, X_1-X_n, F_1-F_n, and D_1-D_n represent the original variables, extracted features, and obtained decisions from datasets respectively. The solid lines with arrows indicate the low-level data fusion process where the fusion is directly implemented on original variables (raw data) for further generating model outcomes. The dashed lines with arrows indicate the mid-level data fusion process where features are first extracted before fusion. High-level data fusion is represented by the dotted lines with arrows where initial modelling results are obtained based on the original variables or extracted features and then used as input in the fusion for producing the final model outcome.

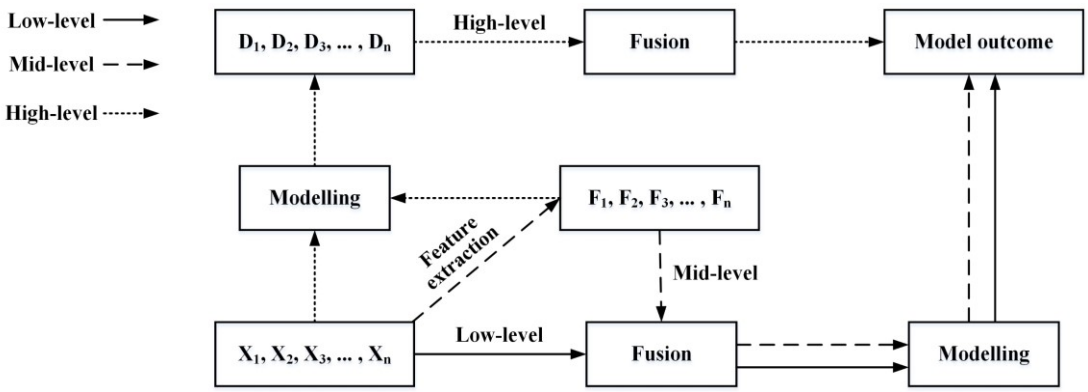

Figure 2.2 Illustration of the data fusion process based on abstraction levels

Another widely adopted classification system for data fusion is Dasarathy's classification (Dasarathy, 1997) which is composed of five categories, including data in-data out, data in-feature out, feature in-feature out, feature in-decision out, and decision in-decision out. This classification is the specification of the abstraction level for the input and output. For example, data fusion at the data in-data out fusion level is conducted immediately after the data is collected from multiple sources or sensors. At the feature in-decision out level, a set of features is used as input to provide a set of decisions as output. The Dasarathy's data fusion model is illustrated in Figure 2.3. Besides the classification based on abstraction level, data fusion can also be classified based on the type of architecture, including centralised architecture, decentralised architecture, distributed architecture, and hierarchical architecture. In the centralised architecture, all data and information from multiple sources are sent to a central processor, node, or unit where the fusion occurs. The centralised data fusion system is generally easy to design, implement, and manage. However, the major drawbacks of centralised data fusion are the latency of transmitting data to the central processor and bandwidth limitations. In the decentralised architecture, this architecture contains a network of nodes where each node can fuse its local information and the information received from its peers.

This type of fusion architecture can easily adapt to an increased number of data sources and offer benefits in terms of efficiency, leading to real-time processing. Data fusion

in distributed architecture refers to the data and information that are processed at each node independently before being sent to the fusion node. In other words, some level of fusion can be implemented on its local information at each node and this processed information (e.g., local estimation) is used as input in the final fusion node to provide global outcomes. It offers benefits in terms of scalability, efficiency, and flexibility but comes with complexity. The combination of decentralised and distributed nodes for data fusion is considered as a hierarchical architecture where the fusion is performed at different levels in the hierarchy.

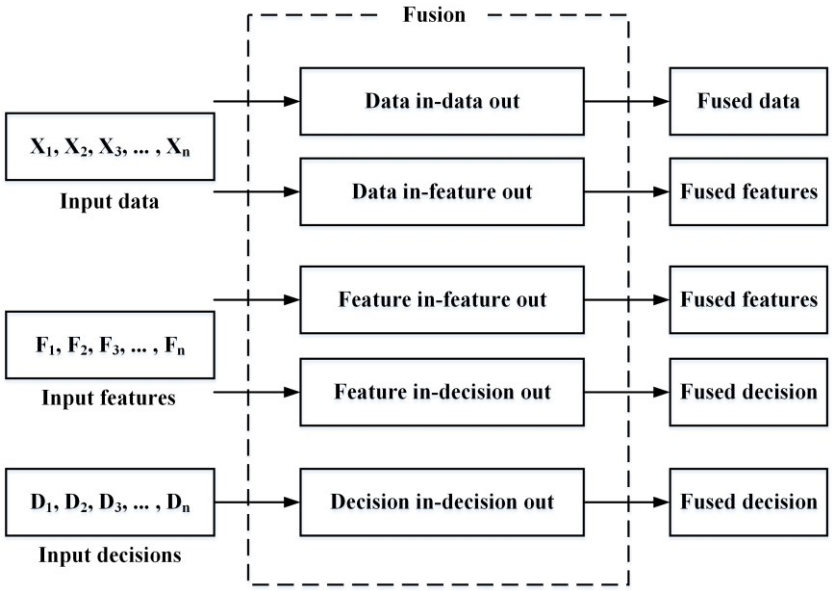

Figure 2.3 Illustration of Dasarathy's data fusion model

2.3.2 Prevailing Data Fusion Techniques

Data fusion techniques have gained prominence due to their effectiveness across various application domains. These techniques can often be categorized based on the abstraction level at which fusion occurs—low-level, mid-level, and high-level. They can also be assigned into different categories according to their underlying methodologies. The following paragraphs introduce some of the prevailing data fusion techniques with their detailed principles.

- **Kalman Filter**

Kalman filter is a widely used and powerful algorithm for state estimation of dynamic systems from a series of observations with noise. It was developed by R. E. Kalman in 1960 (Kalman, 1960) and quicky became popular in the field of optimal estimation as it offers real-time operation, low computational cost, and robustness to noise. Due to the merits of Kalman filter and its variants (e.g., Extended Kalman filter), it has been extensively applied in target tracking, multi-sensor fusion, robotics, and especially in the current hot research fields, such as pattern recognition and image segmentation. The Kalman filter operates on the principle of recursively updating the estimated state of a system by two operations, prediction and update. In the prediction step, it generates an estimate of the current state along with the uncertainty of this estimate based on the system dynamics model. In the update step, it refines this prediction by incorporating a new measurement, weighting it by the respective uncertainty of the prediction and measurement. The following equations are used to describe the Kalman filter for a linear system.

Prediction step:

$$\hat{x}_{k|k-1} = A_K \hat{x}_{k-1|k-1} + Bu_k \tag{2.1}$$

$$P_{k|k-1} = A_K P_{k-1|k-1} A_K^T + Q \tag{2.2}$$

Equations (2.1) ~ (2.2) represent the prediction step of Kalman filter, where $\hat{x}_{k|k-1}$ is the predicted state at time *k* based on all information up to time *k-1*. $\hat{x}_{k-1|k-1}$ is the estimated state at time *k-1*. $P_{k|k-1}$ denotes the error covariance and $P_{k-1|k-1}$ is the estimated error covariance at time *k-1*. Bu_k and Q represent the control input and process noise covariance respectively.

Update step:

$$K_k = P_{k|k-1} H^T (HP_{k|k-1} H^T + R)^{-1} \tag{2.3}$$

$$\hat{x}_{k|k} = \hat{x}_{k|k-1} + K_k(z_k - H\hat{x}_{k|k-1}) \tag{2.4}$$

$$P_{k|k} = (I - K_k H)P_{k|k-1} \tag{2.5}$$

Equations (2.3) ~ (2.5) represent the update step of Kalman filter, where K_k is the Kalman gain, H is the observation matrix, and R is the measurement noise covariance. $\hat{x}_{k|k}$ and $P_{k|k}$ is the updated state estimate and error covariance respectively. z_k is the observation at time k.

- **Principal Component Analysis**

Principal component analysis (PCA) is a widely used dimensionality reduction method and commonly used in the field of data mining, image analysis, finance, and many other fields where high-dimensional data needs to be processed. The aim of PCA is to transform the original variables into a new set of uncorrelated variables (i.e., principal components) that keep most of the variance in the dataset. These principal components are the eigenvectors of the covariance matrix of the original dataset. The following equations explain the underlying mathematics of PCA.

$$Cov(X_p)x_p = \lambda x_p \tag{2.6}$$

$$Y_p = X_p * W_p \tag{2.7}$$

In equations (2.6) ~ (2.7), X_p is a data matrix with m samples and n variables, $Cov(X_p)$ is the covariance matrix of X_p. x_p and λ are the eigenvector and eigenvalue respectively. Y_p is the transformed dataset by projecting X_p onto the selected eigenvectors where W_p is the matrix formed by the selected eigenvectors.

- **Locally Linear Embedding**

Locally linear embedding (LLE) is a nonlinear dimensionality reduction technique for embedding high-dimensional data into a lower-dimensional space. It aims to preserve local neighborhood relationships in the data when embedding it to a lower dimensional space. LLE assumes the high-dimensional data lies on a manifold that can be

characterized by linear relationships locally and its objective is to find out the underlying manifold structure. LLE operates by computing the nearest neighbors for each data point and then captures the local geometric structure by calculating linear coefficients that reconstruct each data point from its nearest neighbors. The following equations describe the LLE algorithm.

$$\varepsilon(L) = \sum_i \left| x_i - \sum_j l_{ij} x_j \right|^2 \tag{2.8}$$

$$\phi(Y) = \sum_i \left| y_i - \sum_j L_{ij} y_j \right|^2 \tag{2.9}$$

Equation (2.8) represents the reconstruction with linear weights, where l_{ij} is the weights that linearly reconstruct data point x_{ij} from its k nearest neighbors x_j. It aims to minimize the reconstruction error and it is subject to the constraints $l_{ij} = 0$ if x_j does not belong to the neighbors of x_i and $\sum_j l_{ij} = 1$. Equation (2.9) is used to compute the lower-dimensional embedding, where y_i and y_j are the lower-dimensional representations of x_i and x_j respectively. The objective of the equation is to minimize $\phi(Y)$ and to keep Y centered at the same time. LLE focuses on preserving local relationships and is useful for capturing structures from complex high-dimensional data. However, it inevitably suffers from high computational costs and it is hard to handle very high-dimensional data.

- **Majority Voting, Boosting, and Stacking**

Majority voting, boosting, and stacking techniques are typical high-level data fusion methods that aim to fuse decisions to obtain the final outcome. Majority voting is a simple ensemble technique to combine the decision outputs from multiple base models. Take classification as an example, in majority voting, it needs to train multiple base models on the same datasets and use each model to predict the class label of a new instance. Then count the number of votes for each class label and the one that receives the majority of votes is selected as the final classification. Majority voting performs

well when the base models make independent errors. It reduces variance without increasing bias. However, it performs badly if the classifiers make the same errors.

For boosting techniques, the core idea is to combine multiple weak classifiers into a strong classifier by weighting their outputs based on their performance. Base models are trained sequentially that try to correct the errors made by their predecessors. The weak model is added to the ensemble of models. The final model is acquired by a weighted sum or vote of weak base models. Boosting algorithms are normally effective in dealing with imbalanced data but have relatively high computational costs. Popular boosting algorithms are adaptive boosting and gradient boosting.

Stacking techniques are also ensemble techniques that combine multiple base models through a meta-model. In stacking, the outputs of each base model are used as input into the meta-model for the final prediction. The datasets used for training are normally divided into two subsets of which one subset is for training base models and the other subset is used for the trained base models to generate predictions. These predictions are used as inputs to train the meta-model where the original labels are used as targets. The meta model leans how to best combine the outputs from the base models to improve the accuracy of the final prediction. Stacking techniques can largely leverage the strengths of each base model to produce a more robust model. However, it also increases the computational complexity and may lead to overfitting problems.

- **ML Technologies**

With the increasing demand of multi-source, multi-dimensional, and multi-modal data fusion for real-world applications, conventional data fusion techniques are hard to handle the heterogeneous data effectively. As introduced previously, ML technologies have strong abilities of learning hidden patterns within the data, modelling highly complex relationships, and merging data with various modalities and dimensions at different abstraction levels. Therefore, ML technologies have become the most prevailing and effective data fusion methods in recent years. Also, for some ML algorithms, their underlying methodologies are based on data fusion techniques (e.g.,

boosting). ML offers a wide range of techniques and approaches that can largely improve the effectiveness of data fusion in various domains.

For low-level data fusion, unsupervised ML techniques, such as *k*-Means clustering or autoencoders can be used to reduce dimensionality and dig out essential information from raw data. In mid-level data fusion, techniques such as neural networks or *t*-distributed stochastic neighbor embedding (*t*-SNE) can be used to transform features into different spaces to make fusion more effective. Neural networks are widely used for fusing data at different levels, fusing data into different layers, and merging features at intermediate layers. Multiple ML models can also be combined by using ensemble techniques (e.g., majority voting, boosting, and stacking) to obtain final decisions. The details of some prevailing ML techniques are introduced in Section 2.4.

2.3.3 The Applications of Data Fusion in the AM Industry

In recent years, benefiting from advanced sensing and IoT technologies, data fusion techniques have been increasingly applied in manufacturing industries, such as the aerospace industry, automotive industry, and additive manufacturing industry (Diez-Olivan et al., 2019, Kong et al., 2020, Cai et al., 2017). It is common for real-world manufacturing data to be massive, heterogeneous, and contain noise, which makes it difficult to combine data from multiple sources for joint analysis. In AM, researchers have explored using data fusion strategies and techniques for regression and classification tasks, such as process monitoring and defect detection, mechanical property prediction, and surface roughness prediction, which obtained considerable performances (Kim et al., 2018, Montazeri et al., 2019, Bastani et al., 2016, Li et al., 2019, Hu et al., 2021).

Due to the diversity and complexity of interactions during the AM process, process monitoring and defect detection are the most common application scenarios of data fusion techniques. A fault diagnosis approach for fused deposition modelling FDM process states by using sensor data fusion was proposed by Kim et al. (Kim et al., 2018). In this work, to classify process states, accelerometer and acoustic emission

signals were collected in real-time from healthy and faulty states where features were extracted from raw signals. Then these features were used as inputs in the SVM model for process state classification.

Zhang et al. (Zhang et al., 2022a) introduced a registering and fusion method for in-situ monitoring of the LPBF process based on sensor data. The signatures of melt pools were obtained from a coaxial high-speed camera and the spatial information of melt pools was collected by an off-axis camera system. Through perspective transformation and multi-thresholding filtering, the processed images were analysed by CNN where the spatial distribution of melt pools was retrieved and finally registered in both global and local coordinates systems. An LSTM neural network was used to fuse the melt pool signatures for predicting layer surface topography.

Gaikwad et al. (Gaikwad et al., 2022) also adopted data fusion strategies for flaw detection in the LPBF process where multiple process phenomena of melt pools were captured by video cameras and a temperature field imaging system. Key signatures of melt pools were extracted and used as inputs in ML models for detecting laser defocusing and predicting porosity levels. Deep learning algorithms are prevailing approaches for fusing data to obtain desired outputs and have been increasingly applied in AM systems, such as CNN and long-term recurrent convolutional networks (LRCN) for in-situ porosity detection based on multiple sensor data from melt pools (Tian et al., 2021a), LSTM for tensile strength prediction based on in-process signatures and static factors (Zhang et al., 2019d), and CNN-LSTM for energy consumption prediction based on CAD models and process parameters (Hu et al., 2021).

In the study (Zhang et al., 2019d), the tensile strength of the parts manufactured by the FDM process was predicted based on the in-process signatures and static factors. Multiple sensors were employed to capture in-process signatures and interactions between layers. These signatures were then fused with static factors (e.g., material properties) for tensile strength prediction based on the LSTM model. In addition to the strategies of fusing features in models for obtaining desired outputs, decision fusion is also considered in AM studies. For example, Li et al. (Li et al., 2019) introduced an

approach for surface roughness prediction of the products produced by the FDM process based on ensemble learning. In this work, real-time sensor signals were collected from different sensors, including accelerometers, thermocouples, and infrared sensors. Time and frequency-domain features were extracted from sensor signals and used as inputs in different ML algorithms for training. An ensemble learning model was introduced to fuse the decision outputs from those base ML models for final surface roughness prediction. The experimental results show that the developed ensemble model outperformed the individual base models.

Apart from multi-sensor signal fusion, fusion strategies and techniques are considered significant when dealing with heterogeneous data. Data with different dimensions, such as images and geometries, is commonly generated in AM systems but is difficult to be analysed precisely and integrated properly. Chen et al. (Chen et al., 2021b) used in-situ point clouds to represent the geometries of the surface for defect identification in the DED process. In this work, the point cloud data was clustered by the density-based spatial clustering of applications with noise (DBSCAN) algorithm for separating the regions that potentially have defects (4 surface classes were obtained). Then the key features of the clustered point cloud were extracted and used as input into different ML algorithms for defect classification.

Differently, Ma et al. (Ma et al., 2022) calculated the entropy of geometries to represent the solid and empty information of complex lattice structures. The entropy was fused with other parameters in the SVM model for final mechanical property prediction. To fuse multi-dimensional data for the DED process control (Vandone et al., 2018), Vandone et al. proposed a data-driven approach for process modelling where the data collected from online and offline, including machine parameter settings, images of melt pools, sensor signals, 3D scan of geometries, were combined to estimate the performance of the developed process model.

Data fusion techniques are also applied to refine data and improve the quality of data in AM research. For example, to enhance the quality of the reconstructed surface

topography of the parts produced by the DED process, Zou et al. (Zou et al., 2022) proposed two data fusion methods, competitive data fusion and cooperative data integration. The confocal laser scanning microscopy (CLSM) and focus variation microscopy (FV) were used to acquire surface topography data. The CLSM was good at retaining the large shape features while FV was better in resolving small features. Therefore, the competitive data fusion method was used to integrate the advantages of CLSM and FV while cooperative data integration was aiming at including both the global and local details in a representation.

Based on previous studies above, data fusion technologies are beneficial in reducing dimensionality, refining data, and improving model performance, especially when dealing with multi-source and multi-dimensional data. Studies that adopted data fusion techniques for tackling AM issues in the past 5 years are summarised in Table 2.2. It can be seen from Table 2 that most studies employed ML-based techniques for data fusion to obtain desired outputs, especially in classification and regression tasks. In addition, considering the nature of collected data, LSTM algorithms are frequently employed for tackling sensor signals and CNN-based algorithms are typically adopted for processing image data. Clustering techniques are used in some studies when dealing with the feature or data refinement task, such as (Qin et al., 2018a, Chen et al., 2021b). A few studies (Zou et al., 2022, Lin et al., 2019) dealt with the data scale and spatial issues in AM.

Owing to the advancement of data collecting and analysis technologies, data-driven methods and ML techniques have been increasingly employed to tackle AM issues. However, it lacks a systematic approach to identify what data should be collected for data analytics to support decision-making activities. This collected data is normally from different sources and has different dimensions, modalities, and structures, which is difficult to be jointly analysed. In addition, in what way to effectively uncover the hidden knowledge inside the data remains a challenging issue.

Table 2.2 The studies of applying data fusion strategies for tackling AM issues in recent 5 years

Existing studies	AM process	AM tasks	Data used in the study	Data fusion method
(Kim et al., 2018)	ME	In-situ process state diagnosis	Multi-sensor signals	SVM
(Li et al., 2019)	ME	Surface roughness prediction	Multi-sensor signals, surface roughness	SVM, RFs, ANN, Ridge regression
(Zhang et al., 2019d)	ME	Tensile strength prediction	Material properties, process parameters, sensor signals	LSTM
(Zhang et al., 2019e)	ME	Dynamic condition monitoring for 3D printer states	Multi-sensor signals	Sparse auto-encoders (SAE), LSTM
(Lin et al., 2019)	ME	Online monitoring of overfill and underfill defects in the ME process	3D CAD models, 3D point cloud data	Scale-invariant feature transform
(Xu et al., 2022)	ME	Real-time in situ process defect detection	Acoustic emission, 3D point cloud data	SVM, Naïve Bayes, decision tree
(Vandone et al., 2018)	DED	Process control for improving part quality	Sensor signals, melt pool images, 3D geometries, process parameters	Statistical process models
(Chen et al., 2021b)	DED	Automatic rapid surface defect detection	3D surface shapes	DBSCAN, *k*-NN

(Grasso et al., 2018)	DED	Automatic process monitoring	Multi-sensor signals	Support vector data description (SVDD)
(Zou et al., 2022)	DED	Improving the quality of the reconstructed surface tomography	3D surface tomographic data	Cooperative fusion, competitive fusion
(Qin et al., 2018a)	PBF	Energy consumption prediction for the selective laser sintering (SLS) process	3D CAD models, Multi-sensor signals, process parameters	*k*-means, ANN
(Tian et al., 2021a)	PBF	In situ porosity detection	Thermal images, pyrometer images, 3D X-ray CT scan data,	CNN, LRCN
(Gaikwad et al., 2022)	PBF	Process monitoring for porosity-related flaws	Melt pool images, thermal signals, 3D X-ray CT scan data	*k*-means, CNN
(Harbig et al., 2022)	PBF	Determine melt pool anomalies in Metal PBF process	Multi-sensor signals	Threshold filters

2.4 Advanced Data Analytics for AM

Data analytics is increasingly crucial to help engineers or technicians make decisions for tackling critical issues such as energy efficiency improvement, product quality enhancement, and waste reduction, in manufacturing industries. To achieve specific objectives for AM production, it is essential to identify what tasks are involved and then what data analytics activities should be required. These steps are normally done by experienced AM engineers and data scientists (Park et al., 2021). For example, to reduce the porosity of the manufactured parts, tasks such as process parameter optimisation or in-situ monitoring can be involved. In this case, the goal of data analytics is to infer where the porosities possibly form based on the collected information (e.g., process parameters, sensor signals, etc) and provide actionable insights for decision-makers. Identifying data analytics activities for tackling AM tasks is hard as it lacks systematic methods specifically for AM. Some researchers have made efforts to explore this.

Hyunseop et al., (Park et al., 2019) introduced a five-tier taxonomy, i.e., “Value Tier”, “Decision-Making Tier”, “Data Analytics Tier”, “Data Tier”, and “Data-Source Tier”, to identify and prioritize data analytics opportunities in AM. In this classification, the target values are defined in the “Value Tier” in terms of quality, cost, and delivery. The decision-making activities for data analytics are obtained from the “Decision-Making Tier” by using the integration definition for function modelling (IDEF0) (Technology, 1993) where the activities are defined by function models or ICOMs (input (I), control (C), output (O), mechanism (M)). Based on the predefined values and decision-making activities, the decision-making objectives can be represented by using the statement “Improving + [value] + when + [decision-making activity]”. Accordingly, the potential data analytics problems corresponding to the objectives are identified in “Data Analytics Tier”. As an extension of this study, a data analytics opportunity knowledge (DOKB) base was developed in (Park et al., 2021) where AM activity-specific data analytics tasks were defined by experts.

Typically, data analytics problems are classified into 4 types (Muneeswaran et al., 2021, Kühn et al., 2018), descriptive analytics, diagnostic analytics, predictive analytics, and prescriptive analytics. Each type of analytics answers different types of questions. Descriptive analytics answers the questions of what happened. Diagnostic analytics is for answering why it happened. Predictive analytics is to figure out what and when will happen. Prescriptive analytics aims to answer the question of what strategies should be applied. The explosive availability of data in AM industries has motivated the transformation from traditional analysis methods to advanced data analytics for decision-making. The past decade has witnessed the rise of the adoption of ML technologies for smart manufacturing. As powerful data analytics tools for processing, interpreting, and leveraging data, ML technologies have played a central role in supporting decision-making for tackling AM issues in recent years (Ding et al., 2021, Li et al., 2022, Kumar and Tripathi, 2018).

2.4.1 Prevailing ML Algorithms

As introduced in the previous sections, ML algorithms have risen to play an important role in advanced data analytics for a wide range of fields. The rapid development of computer hardware has led to significant enhancement of computational capabilities that make it possible for various complex and data-intensive applications. As a result, neural network-based algorithms, especially DL techniques, become the mainstream for data fusion, modelling non-linear systems, and decision support in various AI applications. The following paragraphs introduce several prevailing ML technologies.

- **Support Vector Machine**

SVM (Cortes and Vapnik, 1995) is a widely applied supervised ML algorithm that mainly tackles classification and regression tasks. Although it was developed more than a decade ago, it still outperforms many conventional ML algorithms in a variety of applications. The core idea of SVM is to find out the optimal hyperplane in an n-dimensional space (n is the number of variables) that can maximize the margin between classes (i.e., the maximum distance between data points of classes). Support vectors are the data points that lie closest to the hyperplane and are essential elements

of data to define the position of the hyperplane. In addition, SVM uses kernels to transform the original feature space into a higher-dimensional space where data possibly becomes separable. The most commonly used kernels are Linear kernel, polynomial kernel, and radial basis function (RBF) kernel. The following equations are the mathematical foundations of these prevailing kernels.

Linear kernel: $$Kernel(x, y) = x \bullet y \tag{2.10}$$

Polynomial kernel: $$Kernel(x, y) = (x \bullet y + c)^d \tag{2.11}$$

RBF kernel: $$Kernel(x, y) = \exp(-\gamma_s \| x - y \|^2) \tag{2.12}$$

In equations (2.10) ~ (2.12), x and y are vectors, and c, d, and γ_s are parameters that need to be set. SVM is normally effective in tackling high-dimensional data but its performance is sensitive to the kernel selected. Choosing the wrong kernel functions will lead to overfitting or underfitting problems.

- **Light Gradient Boosting Machine**

Light Gradient Boosting Machine (LGBM) is a decision tree-based algorithm and was developed in 2017 (Ke et al., 2017). It is a promotion framework using ensemble techniques that strengthens weak learners into strong ones and mainly tackles classification and prediction tasks. LGBM adopts a histogram-based decision tree algorithm and leaf-wise leaf growth strategy with a depth restriction, largely reducing the storage and computational costs while simultaneously ensuring high accuracy. The split points are determined by calculating variance gain in LGBM which adopts gradient-based one-side sampling (GOSS). GOSS keeps the instances with large gradients and performs random sampling on the instances with small gradients. Additionally, by converting features to a multi-dimensional one-hot feature for tackling sparse features, LGBM employs an exclusive feature bundling (EFB) algorithm to avoid additional computational and memory costs. As LGBM is an ensemble model, the final model can be obtained through a weighted combination of base decision trees. The basic gradient boosting decision tree (GBDT) can be

represented by the following equations of which the objective is to minimize the loss function *Loss* (y, $T(x)$).

$$T = \arg\min_{T} E_{xy}\left[Loss(y, T(x))\right] \tag{2.13}$$

x and y represent the data instance and the target to be predicted respectively, and $T(x)$ is the estimated function. The loss function is minimized by the iteration in line search:

$$T_m(x) = T_{m-1}(x) + \gamma_m tree_m(x) \tag{2.14}$$

$$\gamma_m = \arg\min_{\gamma} \sum_{i=1}^{n} Loss(y_i, T_{m-1}(x_i) + \gamma_0 tree_m(x_i)) \tag{2.15}$$

In equations (2.14) ~ (2.15), $tree_{\mathrm{m}}(x)$ represents the base decision tree, and m is the iteration number. The final LGBM model $T_m(x)$ can be obtained through a weighted combination of decision trees, described by equation (2.16).

$$T_M(x) = \sum_{m=1}^{M} \gamma_m tree_m(x) \tag{2.16}$$

LGBM is capable of distributed and parallel learning and is normally faster than gradient-boosting-based models. It is computationally efficient in dealing with large datasets.

- **Fully Connected Neural Network**

The fully connected neural network (FCNN), also known as multi-layer perceptron (MLP), is a basic type of neural network and is the most commonly used model for classification and regression tasks in a wide range of domains. FCNN consists of three kinds of layers, input layer, hidden layer, and output layer, where each neuron in a layer is connected to every neuron in the adjacent layers. The structure of an FCNN is illustrated in Figure 2.4.

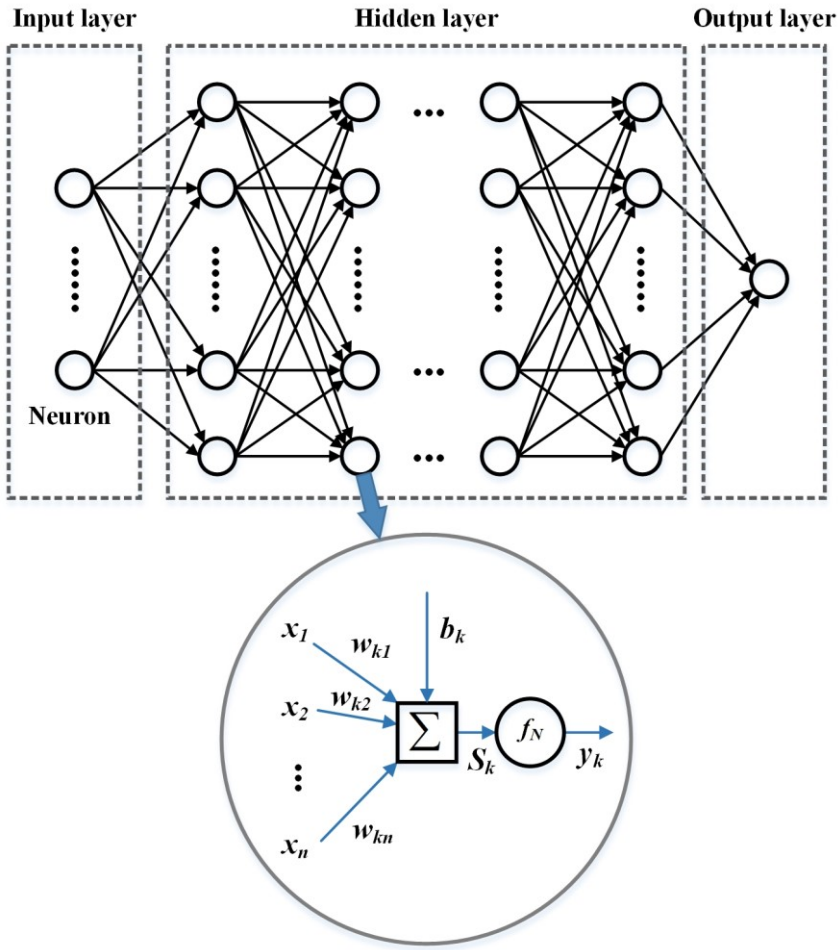

Figure 2.4 Illustration of the structure of an FCNN

The input layer is used to process the input datasets and the number of its neurons is equal to the number of variables in the datasets. In the hidden layer, the number of layers can be one or multiple layers where each neuron is connected to the neurons in the previous and next layers. With the increasing of hidden layers and neurons, the whole neural network becomes more complex and normally has stronger capability for modelling highly complicated non-linear relationships. A deeper neural network often means a more powerful model. In the output layer, the number of neurons equals the number of classes for classification tasks or one for regression tasks. In layers of an FCNN, each neuron is a computational unit, shown in Figure 2.4, and it treats the outputs of the neurons from the previous layer as input x_n which will be multiplied by the weights w_{kn} and then added with a bias b_k. The equation is presented below:

$$S_k = \sum_{i=1}^{n} w_{kn} * x_n + b_k \tag{2.17}$$

The S_k is processed through the activation function f_N to get the output y_k. During the training process, a backpropagation approach is adopted to adjust the weights and biases of neurons in the FCNN to minimize the error between the final output and the actual target value. This process normally requires considerable computational power and costs a relatively long training time. FCNN has proven to be effective in modelling complex systems especially when the amount of training data is adequate. However, being computationally expensive is always a drawback when implementing the FCNN with deep structures.

- **Convolutional Neural Network**

CNN is a type of DL technique to deal with the data with grid patterns (e.g., image). It is able to automatically learn the spatial hierarchies of features by several building blocks (Yamashita et al., 2018), including convolution layers, pooling layers, and fully connected layers. In the vision of computers, an image is treated as an array of numbers. In a typical CNN architecture, convolutional layers aim to extract and learn the highly representative features from input images. A kernel is applied across the input image matrix where an element-wise product between each element of the kernel and the input matrix is calculated to obtain the output feature map, shown in Figure 2.5. In this figure, the kernel size is 3×3 and the stride value is 1. After the convolution operation, the output is passed through a nonlinear activation function to the pooling layer for dimensionality reduction. The pooling layers offer down sampling functions such as max pooling and average pooling to reduce the dimensionalities of the feature map received from the previous convolution layer. Max pooling uses the maximum values from the given grids to serve as the output, while average pooling uses the mean values of the grids as the output. Normally, a typical CNN architecture consists of more than one convolution layer and pooling layer. After several convolution and pooling operations, the extracted features are flattened and used as input into a fully connected layer for further processing.

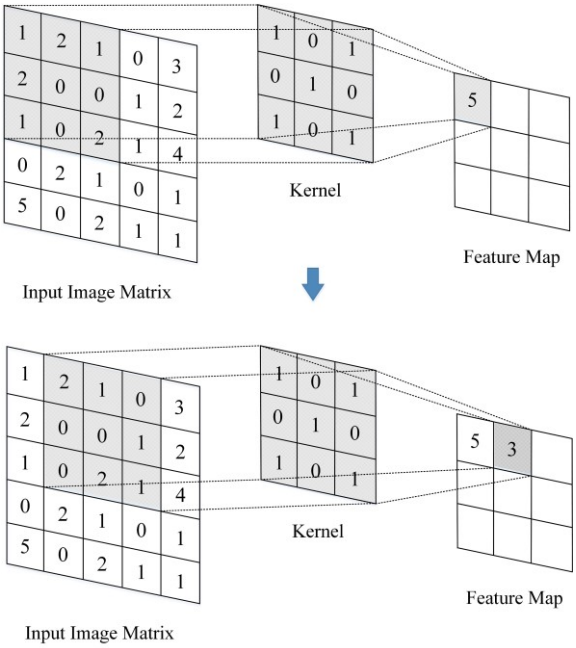

Figure 2.5 An example of the convolution operation in CNN

CNN has become the most prevailing algorithm in the field of computer vision where several well-known variants were designed and developed, such as ResNet-50 (Xie et al., 2017), VGG-16 (Simonyan and Zisserman, 2014), FaceNet (Schroff et al., 2015), ShuffleNet (Zhang et al., 2018a), and so on.

2.4.2 Research and Applications of ML in AM

2.4.2.1 ML for DfAM

AM has provided opportunities for innovative designs and advances in product performance, in terms of geometric freedom and highly integrated structures (Kumke et al., 2016). DfAM has been proposed as a way to provide AM design professionals with a wide range of design and analysis tools for complex part structures and AM processes. Typically, DfAM includes two main research topics, part design and design optimization (Thompson et al., 2016). For part design, AM creates free forms and customized geometries, enabling the creation of complex internal features to increase functionality and improve the performance of target parts, which provides designers with huge design space. For design optimization, AM part designers need to determine

production path strategies, part locations, build orientations, and support structures for improving the quality of final printed products. Due to the advances of artificial intelligence and available data, ML technologies have been increasingly applied to DfAM in recent years (Jiang et al., 2020a).

- **Part Design**

At the conceptual design phase, most AM designers select appropriate design features based on their knowledge and experience. However, there is a lack of systematic and intelligent techniques to assist AM professionals in exploring AM-enabled design space (Yao et al., 2017, Hsiao and Tsai, 2005). Hence, Yao, et al. (Yao et al., 2017) introduced a hybrid ML approach for design features recommendation at the conceptual design phase in AM. In the paper, the authors classified the functionality-centric design knowledge inherent in AM design features and target components into 'loadings', 'objectives', and 'properties', which were coded with numerical digits and saved in database files. Then hierarchical clustering was carried out on the coded design knowledge to reveal the relationships among design features and target components, resulting in a dendrogram. Previous industrial application examples with their design features implementation were simplified as a binary classification problem (implemented design features denote as '+1', otherwise '-1') and trained by an SVM classifier. The trained SVM model was used to refine the hierarchical clustering results by an SVM-based progressive dendrogram cutting process, which aims at identifying the final sub-cluster containing the recommended AM design features.

Andrew and Markus (Lew and Buehler, 2021) introduced a method that uses variational autoencoders (VAE) and ML techniques for the compliance optimization of cantilever design. In this work, the cantilever structures were encoded into a 2D latent space by VAE and the LSTM was adopted to learn the latent space trajectories that correspond to the topology optimization process. A framework of using neural networks for the analysis and design of micro-lattice architectures in AM was introduced by Nathaniel (Després et al., 2020). In this study, to obtain training datasets, the authors used a compact genetic algorithm to generate micro-lattice structures of

which the corresponding mechanical properties were obtained by finite-element analysis (FEA). The graph convolutional networks (GCN) with an asymmetric auto-encoder was adopted and trained by the graph representation of the generated micro-lattices.

Another example of applying neural networks is that Jonnel et al., (Alejandrino et al., 2020) used ANN for geometry corrections of the designed lattice infill patterns in FDM systems. In this work, the 3D coordinates of the designed infill structures were used as the input of the ANN model, while the symmetrical deviation surface coordinates were the output. After training, the model was implemented into the STL file for geometric corrections.

Considering the manufacturability of AM process, Tang et al., (Tang et al., 2017b) proposed a strategy for lattice structure design and optimization to ensure product quality. To represent the design space of lattice structures, the concept of "physical entity" was introduced to include the design information (geometrical information and material information) for each design stage. Then, the lattice unit cell model was defined and proposed to represent the topology of the elements inside lattice structures. The authors used the concept of "manufacturable element" to include the geometry, material, and process information of a lattice strut. ANN was used to bridge the relationship between manufacturability and geometrical data. Integrating the physical and domain knowledge in ML algorithms has been proven to improve ML performance significantly (Karniadakis et al., 2021).

Hyunwoong et al., (Ko et al., 2021) introduced a methodology for bridging the gap between multi-discipline designs and AM capabilities based on knowledge graph ML. In this work, the framework of the proposed method consists of 4 main modules, including 1) AM prior knowledge structuration, 2) transformation of knowledge to DfAM ontology, 3) extraction of knowledge from AM data using ML, 4) design rules transformation. The design fundamentals, principles, and rules were obtained by formalizing unstructured AM prior knowledge into structured knowledge and

extracting knowledge from AM data based on ML algorithms. Then, these designs' knowledge was encoded into ontologies with knowledge graphs. Finally, the design rules were constructed by reasoning with prior knowledge and newly discovered knowledge.

- **Design Optimisation**

To obtain the required production quality, design optimization is a critical step before the AM process begins (Zhang et al., 2019f). Many crucial elements and parameters are defined in this step. For instance, the determination of build orientation and direction significantly affects process and fabrication attributes (Ahsan et al., 2016). In Ref (Zhang et al., 2019f), the authors applied *k*-means clustering with Davies–Bouldin Criterion cluster measuring on surface models to generate alternative build orientations in a computationally efficient way. The *k*-means clustering method was adopted to decompose STL models into *k*-facet clusters where the number of clusters was determined by the Davies–Bouldin Criterion. The central normal vectors of each facet normal cluster were used as alternative build orientations where the optimal orientation was ultimately obtained by a statistical evaluation process.

To prevent unsightly surface damage of fine surface details when removing support structures, a perceptual model of preference in the printing direction of AM was proposed by Zhang, et al. (Zhang et al., 2015). Zhang, et al. developed a perceptual model to determine the preference of printing orientation in terms of area of support, visual saliency, preferred viewpoint, and smoothness preservation. To find the minimum amount of support structures for successfully fabricating a model, Huang et al. (Huang et al., 2019) developed a support detection approach based on a surfel convolutional neural network (surface element - CNN) in AM. In this method, the surfel is the sampling point on the surface with normal information, defined through the layered depth-normal image (LDNI) (Wang et al., 2010) sampling method. The LDNI stores an array of rays that are shot to intersect with the CAD model, where the depth and normal values of intersection points on the rays are included. Based on

LDNI sampling, local surfel images with ground-truth support regions were obtained and fed into the CNN model for classification.

AM has been increasingly employed for printing composite material parts. However, the fibre size, volume fraction, and direction are important in determining the properties of the printed part. Kaushik et al. (Yanamandra et al., 2020) introduced a method for reversing additively manufactured composite parts by toolpath reconstruction of the printing process using the LSTM network. In this method, the CT-scan images of fibre orientation at each layer were sequentially fed into the LSTM model for predicting the orientation angle of fibres. Then the G-code can be generated based on the fibre orientation and measured layer thickness.

- **Shape Deviation**

Due to the functionality and manufacturing requirements, shape accuracy measurement is essential and critical in DfAM, aiming to reduce the geometrical deviations of the final products (Zhu et al., 2018). The geometrical inaccuracies of the produced products pose significant challenges to the predictive modelling of shape deviations and developing error compensation strategies for AM. Several researchers have explored that ML models are used for tackling geometrical accuracy-relevant issues, such as shape deviation prediction (Zhu et al., 2018, Huang et al., 2020, Ferreira et al., 2019, Rong-Ji et al., 2009, Lee et al., 2001, Vosniakos et al., 2007, Li et al., 2018, Wacker et al., 2021), classifying and quantifying geometrical accuracy (Khanzadeh et al., 2018b, Samie Tootooni et al., 2017), and deviation compensation (Shen et al., 2019). In studies (Rong-Ji et al., 2009, Lee et al., 2001, Vosniakos et al., 2007, Li et al., 2018), ANN was adopted to model the relationship between process parameters and geometry-related errors in different AM processes.

Zhu et al. (Zhu et al., 2018) proposed an ML-based method to model in-plane deviation and random local variants in AM. A mathematical relationship between the designed shape and the final shape was constructed from a transformation perspective, aiming at capturing the global trend of shape deviations. Due to unexplained variations with

complex patterns, a multi-task Gaussian process (GP) learning algorithm was adopted to learn from the unexplained deviation data and model the local deviation. An automated geometric shape deviation modelling approach based on Bayesian neural networks (BNN) and transfer learning techniques for different shapes and AM processes was proposed by Ferreira et al. (Ferreira et al., 2019). In this approach, the geometry shapes are defined under the polar coordinate representation, where each point on a product is identified by an angle θ. The in-plane and out-of-plane deviations of different shapes and processes are represented by statistical models. A baseline BNN for modelling shape deviation was first built by training on a small number of product samples under a specific AM process. Then transfer learning techniques were employed to transfer the baseline model to new shapes and processes.

Tootooni et al., (Samie Tootooni et al., 2017) introduced a method to classify the dimensional variation of AM-produced products based on spectral graph theory and ML techniques. This work extracted the spectral graph Laplacian eigenvalues from the 3D point cloud data of the manufactured parts and used them as features in ML models for classification. For shape deviation compensation, Shen et al. (Shen et al., 2019) introduced a framework for AM using CNN. In this framework, the 3D model was encoded as a binary probabilistic distribution in 3D space and fed into the CNN model for capturing deformation features. An inverse function network was trained to obtain the compensated model.

2.4.2.2 ML on Material Analytics for AM

A variety of materials, such as metals, ceramics, plastics, and their combinations are used for AM applications and the development of new materials is in progress (Singh et al., 2017). Using different materials for producing products can result in different performances and properties. A significant amount of data can be generated from material property and conditions. It is essential to analyse and understand the relationships among material chemistry, material characteristics, and final part performances based on the material data. The powder property is one of the key elements that affect the build process and final part quality in powder-based AM

(Poorganji et al., 2020). During the printing process, the interaction and consolidation between powder particles are complicated where high-quality powders are required to ensure the process reliability and final part property. Thus, qualifying powder materials is critical, and some researchers have made efforts to measure and analyse powder materials by using ML technologies.

Powder characterization is important for evaluating the quality of powder materials in AM, where computer vision and ML technologies have been applied for autonomous characterization (DeCost et al., 2017, DeCost and Holm, 2017). DeCost, et al. (DeCost and Holm, 2017) introduced a method that used key-point-based computer vision for quantitatively characterizing powder materials. In this study, eight powders that only differed in their particle size distribution were considered. The study employed a computer graphics suite, called Blender, to generate synthetic powder micrographs. A bag of visual words image representation was adopted for characterizing the synthetic powder micrographs, where the images were represented by key-point features and organized into a visual dictionary. Then the difference between Gaussians and Harris-LaPlace interest point detectors was used to select critical key-point features. The regions surrounding the key-point features were characterized by applying scale-invariant feature transform (SIFT). Finally, the SVM was used for the particle size classification.

Vrábel et al. (Vrábel et al., 2019) also adopted SVM to classify Al alloy powder materials for the SLM process. In this work, Vrábel et al. used the laser-induced breakdown spectroscopy technique to obtain spectra from the powder materials. Then the spectra were processed through unit vector normalization and PCA. The PCA model was applied to reduce dimensionality and remove noise data, where four principal components (PCs) were obtained. These PCs were fed into the SVM model for material classification. Richard et al., (Valente et al., 2020) used the decision trees (DT) algorithm to classify powder flowability based on particle-level physical property measurements in cold spray AM.

Currently, ML technologies are generally used for classification tasks for powder material analysis. There still needs further exploration and research to achieve the potential of leveraging ML for material analytics in AM, such as analysing material composition for alloy development and modelling the relationship among material chemistry, material properties, and final part performances.

2.4.2.3 Defect Detection and In-Situ Monitoring for AM based on ML

Lack of quality assurance in AM-produced parts is one of the key technological barriers that prevent manufacturers from adopting AM technologies, especially for high-value applications where component failure cannot be tolerated (Everton et al., 2016). Due to different material supplies and working principles of different AM processes, the defects or quality issues can be various. For instance, the issues of porosity, lack-of-fusion, balling, crack are critical in the powder-based processes (Zhang et al., 2017a, Taheri et al., 2017, Everton et al., 2016) and the geometry deviation (Lee et al., 2014), shape shrinkage (Wang et al., 2016), and surface roughness (Ahn et al., 2009, Xia et al., 2021, Gerdes et al., 2021) in FDM processes have been focused by many relevant research groups. Only when these defect issues are detected synchronously and accurately during the AM process, the real-time control strategies can be realized. ML technologies have been increasingly used for in situ monitoring in AM systems (Bisheh et al., 2021, Bugatti and Colosimo, 2021). The ML models are trained by different types of data which are classified into three categories, including 1D data (e.g., spectra), 2D data (e.g., images), and 3D data (e.g., tomography) (Qi et al., 2019a). Each strategy developed in existing studies has pros and cons. In general, two main types of strategies, image-based and sensor signal-based, are adopted for defect detection and in situ monitoring in AM. Strategies that leverage 3D point cloud data with ML models have also been explored in recent studies (Li et al., 2021a, Chen et al., 2021b).

- **Image-based Approach**

Zhang et al. (Zhang et al., 2018b) developed a vision system with a high-speed camera to capture sequential images for PBF process monitoring. Their research focused on

detecting the information of melt pool, plume, and spatter. Features of these objects were extracted based on the understanding of the physical mechanisms. These features were then selected by PCA before being used as inputs for SVM classification. CNN-based defect detection and monitoring methods are developed in Ref (Caggiano et al., 2019, Scime and Beuth, 2018, Zhang et al., 2019b, Zhang et al., 2019g, Angelone et al., 2020, Baumgartl et al., 2020, Khan et al., 2021, Davtalab et al., 2020, Snow et al., 2021, Li et al., 2020b, Zhang et al., 2019a, Fathizadan et al., 2021, Westphal and Seitz, 2021, Ertay et al., 2021).

As an extension of the CNN model, deep CNN (DCNN) with a hierarchical structure that allows multilevel image features to be extracted to achieve accurate pattern discovery was employed by Caggiano et al. (Caggiano et al., 2019) for online defect recognition in the SLM process. Additionally, a modification of the CNN model developed by Scime and Beuth (Scime and Beuth, 2018), called multi-scale CNN (MsCNN), improves the flexibility and overall classification accuracy of the conventional CNN model in autonomous anomaly detection. The proposed MsCNN methodology has been demonstrated to be robust when analysing builds that were manufactured by different materials in the L-PBF systems. Lee et al. (Lee et al., 2020b) adopted 3D-CNN and CNN-LSTM for the classification of different statuses, including damaged, cured, and uncured, in the two-photon lithography process.

Some researchers have also explored image-based monitoring approaches with their corresponding control strategies (Wang et al., 2021b, Wang et al., 2018b). Wang et al. (Wang et al., 2018b) presented a closed-loop control framework by seamlessly integrating vision-based techniques and neural networks to detect droplet phenomena and accordingly implement control strategies in liquid metal jet printing processes. The complex relationship between droplet features and voltage level was modelled by a neural network model that enabled the conversion of real-time droplet features to voltage values. A proportional integral derivative process was used to adjust the drive voltage by comparing the output values of the model with target values for process control. Besides, Jin et al. (Jin et al., 2019) developed a real-time monitoring and

autonomous correction system for FDM processes. A CNN classification model was used for detecting defects and a feedback loop was used to modify processing parameters.

Apart from CNN-based models, SVM (Gobert et al., 2018, Scime and Beuth, 2019), Bayesian classification (Aminzadeh and Kurfess, 2019), deep belief networks (DBN) (Ye et al., 2018a), deep neural networks (DNN) (Siegel et al., 2020), *k*-means singular value decomposition (K-SVD) (Zhang et al., 2020c) have also been employed to analyse image data for quality inspection in AM systems. However, in Ref (Gobert et al., 2018, Aminzadeh and Kurfess, 2019, Scime and Beuth, 2019), key features of visual images need to be extracted before being fed into the ML models. In Ref (Ye et al., 2018a), Ye et al. proposed an in situ monitoring method based on analysing plume and spatter signatures during the SLM process. The plume and spatter images were obtained by a high-speed near-infrared (NIR) camera and normalized by zero mean and unit variance to capture the pair-wise interactions between pixel values. These processed data were then fed into the DBN structure with four-level hidden restricted Boltzmann machines for classifying 5 distinct melted states (i.e., over-melted, middle-over melted, normal melted, middle-under melted, and under melted).

- **Sensor Signal-based Approach**

Sensor signal-based approaches for system monitoring are widely applied in the manufacturing industry. In existing studies, different signals, including Acoustic emission (AE), optical emission, infrared signal, and multi-sensor signals are used for defect detection and monitoring in AM systems. A quality monitoring approach based on AE for PBF AM processes was proposed by S.A. Shevchik, et al. (Shevchik et al., 2018). In this paper, the AM machine was equipped with a fibre Bragg grating sensor to detect AE signals. The acoustic features, extracted from signals during the manufacturing process, were the relative energies of the narrow frequency bands of the wavelet packet transform. The spectrograms localized in the time-frequency domain were built from the acoustic features and used as input for spectral convolutional neural networks for classification. Similar methods using AE signals for

quality monitoring of PBF processes can be found in Ref (Shevchik et al., 2019, Wasmer et al., 2019).

In Ref (Wasmer et al., 2019), the reinforcement learning (RL) algorithm was adopted for training and classification. In addition, some other researchers have also developed monitoring strategies by analysing acoustic emission data based on various ML models, such as SVM (Wu et al., 2016), hidden semi-Markov model (HSMM) (Wu et al., 2017), Clustering by fast search and find of density peaks (Liu et al., 2018), and LSTM (Becker et al., 2020) for FDM processes, DBN (Ye et al., 2018b) for SLM processes and *k*-means (Gaja and Liou, 2017) for laser metal deposition (LMD) processes. For example, the methodology developed in Ref (Ye et al., 2018b) is capable of identifying five melted states, including balling, slight balling, overheating, slight overheating, and normal phenomena for the SLM process. Liu et al. (Liu et al., 2018) also developed a machine-state monitoring platform based on AE sensors for FDM machine-state identification using unsupervised learning.

Outputs from the visual and simulation-based porosity detection methods are possibly far from actual yields in some cases since they are often incapable of taking into account the uncertainty that results from material or process parameters (Khanzadeh et al., 2018a). Characteristics of a melt pool have been demonstrated to have a strong link with the formation of defects through existing studies(Pinkerton and Li, 2004, Song et al., 2012, Islam et al., 2013). Therefore, some researchers have explored methods for detecting and predicting porosity by capturing in situ melt pool morphologies using infrared sensors (Tian et al., 2021b, Khanzadeh et al., 2018a). The information about the melt pool can be obtained by using various instruments such as infrared sensors, pyrometers, or high-speed cameras.

Khanzadeh et al. (Khanzadeh et al., 2019) adopted self-organizing maps to analyse 2D melt pool images for detecting anomalies in additively manufactured thin walls in the DED process. As an extension of the work in Ref (Khanzadeh et al., 2019), a real-time porosity prediction method based on morphological characteristics of melt pool

boundaries was proposed by Khanzadeh et al. (Khanzadeh et al., 2018a). In the proposed method, features from melt pool boundaries were obtained through functional PCA and used as input in different supervised ML models, including *k*-NN, SVM, DT, and linear discriminant analysis (LDA), for predicting porosity.

Kim et al. (Kim et al., 2018) proposed a data-driven method based on SVM for monitoring and fault diagnosis of the FDM process states using two types of sensors, an accelerometer and an AE sensor. A heterogeneous sensor-based in situ monitoring approach was developed by Montazeri et al. (Montazeri et al., 2019) to detect the occurrence of lack-of-fusion defects in titanium alloy parts manufactured in the DED process. In this study, the data was collected from an optical emissions spectrometer and a CCD camera with a near-infrared (NIR) filter, aiming at capturing the dynamic phenomena around the melt pool region. The authors fused the data into a weighted network graph developed in Ref (Montazeri and Rao, 2018) and employed the graph Kronecker product approach to build a dictionary of graph-theoretic features related to the severity level of lack-of-fusion defects. These features were used as inputs to the SVM model for classification.

Similarly, strategies for using multi-sensor data for quality monitoring in AM systems are developed in (Bastani et al., 2016, Wu et al., 2019, Li et al., 2019). Photodiode data is considered closely correlated to the properties of the melt pool by Okaro (Okaro et al., 2019). In this paper, the authors used a semi-supervised ML model, Gaussian mixture model, trained by the key features extracted from photodiode data to classify ‘acceptable’ and ‘faulty’ AM builds regarding the tensile strength in the LPBF process. randomized SVD was employed as a feature extraction method to handle large datasets collected from photodiode sensors. Monitoring methods for AM systems based on vibration data and ML models were also developed by several researchers (Yen and Chuang, 2019, Stanisavljevic et al., 2019).

Various monitoring and defect detection methodologies have been developed, such as using pyrometer, AE, optical emission, infrared camera, and high-speed visual camera, to detect macroscale or mesoscale defects based on ML models. Typically, the 1D

(sensing signal-based) data can be processed faster but is normally less informative while the 2D (image-based) or 3D data is often incapable of taking into account the process and material uncertainties.

2.4.2.4 ML for Process Modelling and Control in AM

The properties and performances of additively manufactured parts have long been major concerns of the AM industry as a high degree of quality, performance, reliability, and repeatability is required in aerospace, automobile, defence, etc. (Bae et al., 2018). This urges the development of robust predicting tools to feedback on specific properties and performances under different AM conditions. With the development of in-process sensing systems and IoT technologies, researchers tend to model the process-structure (PS) (Popova et al., 2017, Özel et al., 2018, Li et al., 2020a, Lee et al., 2021, Nguyen et al., 2020, Han et al., 2020), process-structure-property (PSP) (Gan et al., 2019, Herriott and Spear, 2020, Yan et al., 2018a, Kouraytem et al., 2020), and process-property-performance (PPP) (Smith et al., 2016a) relationships directly by exploring the data and information acquired from the printing processes. This information includes processing parameters and processing resultant data during the printing process.

By building these models, further studies such as material design, process optimization, and quality improvement, can be explored. For instance, Gan et al. (Gan et al., 2019) introduced a data-driven method for modelling the PSP relationship in the DED process, where multi-physics modelling, experimental measurements, and data mining were integrated. In this method, simulations were carried out based on a computational thermal-fluid dynamics (CFD) model to obtain structure and property results (e.g., melt pool geometry, cooling rate, dilution, microhardness, etc.). These results were then validated by actual experiments and fed into the SOM (self-organizing map) model with process parameters (i.e., laser power, mass flow rate, and energy density) for investigating the PSP relationships. The following paragraph reviews and concludes the main areas that researchers apply ML technologies for process

modelling and control in AM, including the prediction for mechanical property and in-process signature.

- **Mechanical Property**

Masahiro et al. (Kusano et al., 2020) introduced a prediction model for tensile properties based on analysing the microstructural features of the fabricated parts with post-heat treatments. In this study, The microstructures on the cross-section of the specimens were observed using scanning electron microscopy (SEM), while the parallel-length part of the specimens was observed by using a micro-focus XCT. The averaged maximum and minimum Feret diameters and aspect ratios of each α and prior-β grains were extracted by using ML-based image analysis tools. In addition, the defect features (e.g., the volume fraction of pore) were also taken into consideration. Finally, these features were used for the prediction of tensile properties by multiple linear regression analysis. Process parameters are considered significant to determine the properties of the printed parts.

ANN is frequently adopted by researchers for modelling the complex relationships between process parameters and part properties such as the strain recovery rates and transformation temperatures (Mehrpouya et al., 2019) and compressive strength (Sood et al., 2012). Besides ANN, Nathan et al. (Hertlein et al., 2020) introduced a method that bridged the links between process parameters and part properties by using a BNN. In this study, laser power, scan speed, hatch spacing, and layer thickness were selected as the parent nodes with different parameter settings to govern the casual relationships with child nodes. The yield strength, ultimate tensile strength, surface roughness, hardness, and density were used as child nodes. By using this BNN model, the users can be provided with the probability distribution predictions of the remaining nodes when they enter a known value for one or more nodes.

Compared with previous studies that investigated the relationships between static factors and part properties, Zhang et al. (Zhang et al., 2019d) presented a method taking into account the in-process layer-wise information. The authors proposed a

predictive model based on deep learning to improve the quality control regarding the tensile strength of printed parts in the FDM process. In this model, a merged structure that combines an FCNN with an LSTM was constructed for tensile strength predictions. The LSTM network was employed to process sensing signals, temperature, and vibration. Other relevant factors, such as printing speed, layer height, extruder temperature, and material property, were combined with the output of the LSTM network and fed into the FCNN for the final part property prediction. Researchers have also investigated and studied the mechanical properties of fabricated parts in AM processes using ML technologies (Koeppe et al., 2018, Yan et al., 2018b, Zhou et al., 2019, Yan et al., 2018a, Baturynska, 2019, Zhan and Li, 2021b, Zhan and Li, 2021a, Demir et al., 2021, Hassanin et al., 2021, Herriott and Spear, 2020, Muhammad et al., 2021, Nasiri and Khosravani, 2021).

To explore substitute models for traditional numerical simulation methods, Koeppe et al. (Koeppe et al., 2018) introduced a strategy that combined experiments, FE simulations, and DL model, to predict the maximum von Mises and equivalent principal stresses of printed lattice-cell structures in AM. In this study, the FE simulations were validated by empirical experiments, and the datasets obtained from simulations were used to train the LSTM model for prediction. By taking design-related information into account, Baturynska, et al. (Baturynska, 2019) developed ML-based models for part property (e.g., tensile modulus, nominal stress, and elongation) prediction, where part location, orientation, and STL model properties were considered as the inputs. Using ANN for fatigue life predictions for aerospace alloy parts has been investigated by Zhan et al., (Zhan and Li, 2021b, Zhan and Li, 2021a).

The flexibility in design and unique production paradigm of AM make it suitable for manufacturing parts with highly complex geometries based on customized LS to meet specific functional requirements (Tao and Leu, 2016, Chen et al., 2021a). The mechanical properties of AM-produced LS are influenced by various factors in terms of design, material, and manufacturing process, making it challenging to predict. Understanding and optimizing these factors is crucial for producing high-quality and

reliable LS. The impact factors that affect the mechanical properties of LS in the literature (mainly focusing on the publications in the past 5 years) are summarized and presented in Table 2.3. The geometry of the unit cell of LS is considered one of the most important impact factors related to the mechanical properties of parts (Tang et al., 2017a). The lattice porosity, thickness, the number of unit cells in structures, and material properties are also identified as the impact factors on the mechanical properties of LS. In addition, the process type and parameter settings are also considered crucial factors since they influence the manufacturing of LS directly. Different parameter settings can lead to different quality of the produced parts. For example, excessive scanning speed or overly high laser power can both lead to severe defects in the LS especially intricate LS.

Conventional prediction or modelling methods for the mechanical properties of AM-produced LS are normally based on FEA or statistical analytical models (Borleffs, 2012, Maskery et al., 2018, McGregor et al., 2019, Zaharin et al., 2018). FEA, as a widely used method for mechanical property prediction, is able to simulate the mechanical responses of complex geometries under different boundary conditions (Azman and Nasir, 2019, Wang et al., 2020b). It offers high-fidelity physical-based models that allow for detailed simulations of complex LS geometries, capturing the intricate features of LS and simulating the mechanical responses under different constraints. However, it is highly time-consuming and computationally intensive to run the simulations, especially on fine meshes of complex LS with complicated conditions settings. Additionally, FEA often requires certain assumptions and simplifications about material behaviour, geometries, or loading conditions which might not always represent real-world scenarios. Using statistical-based analytical models for mechanical properties prediction requires fewer computation resources but they are normally limited by their non-linear modelling abilities.

Hassanin et al., (Hassanin et al., 2020) developed a DNN model for predicting the mechanical properties of the diamond-shaped LS made by the LPBF process using Ti-64 alloy. The strut length, strut diameter and strut orientation angle of LS were considered as the impact factors and used as input into the DNN model. By using the

information about the base material and porosity of the structure, Peloquin et al., (Peloquin et al., 2023) introduced a ML-based method for mechanical properties prediction of periodic gyroid LS manufactured by VP processes. The mechanical properties of the used material, including Young's modulus, ultimate strength, and fracture strain, were used as input features with structure porosity into the kernel ridge regression model for final mechanical properties prediction.

Table 2.3 Mechanical property-related factors of AM-produced LS in the literature

Existing studies	AM system	Mechanical property-related factors of LS	Method
(Borleffs, 2012)	EBM	Cell geometry, porosity	Statistical model, FEA
(Ahmadi et al., 2015)	SLM	Cell geometry, porosity	Experiment
(Zadpoor and Hedayati, 2016)	General AM	Cell geometry	Statistical model
(Maskery et al., 2018)	SLS	Cell geometry, number of unit cells	FEA
(Zaharin et al., 2018)	SLM	Cell geometry, pore size of porosity	FEA
(Yang et al., 2019a)	SLM	Cell geometry, number of cells, bulk size, thickness, aspect ratio	FEA
(McGregor et al., 2019)	VP	Cell geometry, material type, orientation	Statistical model
(Cao et al., 2020)	SLM	Geometric defects (Strut porosity, strut thickness variation, strut waviness)	FEA
(Peng et al., 2020)	Mental AM	Cell geometry, relative density	FEA
(Hassanin et al., 2020)	LPBF	Cell geometry	DNN
(Yang et al., 2021)	General AM	Geometry (material microstructure)	Conditional GAN
(Munford et al., 2021)	LPBF	Structure density and fabric	Multivariate LR
(Yang et al., 2022)	LPBF	Geometry	CNN, FEA
(Peloquin et al., 2023)	VP	Material properties, cell geometry	ML-based model

Munford et al., (Munford et al., 2021) used Multivariate LR for predicting anisotropic mechanical properties based on the density and fabric of LS. Apart from using hand-crafted or statistical features of cell geometry, the geometric images are explored to be analysed by DL-based algorithms. A conditional GAN-based model for bridging the link between material microstructures and physical performances was proposed by Yang et al., (Yang et al., 2021). In this work, the geometric images are fed into the generator of GAN to generate field images of interest with random noise. Then these images were evaluated by the discriminator by comparing them with the real field images obtained from FEA. The GAN was trained to predict strain and stress fields from geometry images.

The predicted mechanical properties of LS are higher than the experimental value due to the overestimated particle effect. Hence, a U-Net CNN model was employed to process μ-CT images of the LS printed by the LPBF process in the study (Yang et al., 2022). The original CT images were fed into U-net to obtain segmentation images after removing unmelted particles. Then the FEA analysis was adopted based on the U-Net processed image reconstruction models for mechanical properties prediction.

Previous studies have shown that predicting the mechanical properties of AM-manufactured LS is feasible either using FEA or ML-based models. Various factors in terms of design, material, and process have been explored for prediction based on different methods. The methods to be used should be selected based on the specific requirements or constraints of the real-world applications.

- **In-process Signature**

Meng and Zhang (Meng and Zhang, 2020) proposed a process modelling method for LPBF of stainless steel. In this work, a processing map of the re-melted depth of single tracks in terms of laser power and laser scan speed was developed by using the GP-based ML model. The GP regression model was trained using the datasets obtained from simulations of the CFD model. Tapia et al. (Tapia et al., 2018) also adopted the GP model for process modelling of LPBF. A GP-based surrogate modelling

framework was proposed in the paper, which was then used to predict the melt pool depth of single tracks in terms of laser power, scan speed, and laser beam size combination. ML models have also been applied to predict in-process signatures such as geometries of deposited metal trace using ANN (Caiazzo and Caggiano, 2018) in laser metal deposition (LMD), the stress distribution of cured layers using CNN (Khadilkar et al., 2019) in SLA, product magnetic characteristics using XGboost in SLM (Chang et al., 2021), connection status between printed lines using DNN in FDM (Jiang et al., 2020b), and printed line morphology using ANN (Chen et al., 2020b) in SLM and using GP (Zhang et al., 2020a) and SVM (Zhang et al., 2019c) in aerosol jet printing.

Melt-pool geometries or characteristics are closely related to the quality of the produced products in metal AM processes. The control and minimization of the melt-pool variation are crucial to the stability and reliability of the AM processes. A data-driven approach to predict melt-pool area for scan strategy improvement in the PBF process was developed by Yeung et al. (Yeung et al., 2020). The build time, laser power, scan speed, and neighbouring effect factors were considered as the input to the polynomial regression model for melt-pool area prediction. In addition, Mondal et al. (Mondal et al., 2020) also used the predictive melt-pool dimensions to obtain the optimal scan strategy based on the GP surrogate model. Other studies on the prediction of the characteristics of the melt-pool using ML models can be found in Ref (Kwon et al., 2020, Wang et al., 2020c, Lee et al., 2019, Kamath and Fan, 2018).

Thermal profiles are able to reflect the interaction between layers, resulting in residual stress and distortion distribution during the printing processes. This drives researchers to investigate the thermal profiles for the improvement of product quality. Mriganka and Olga (Roy and Wodo, 2020) introduced a data-driven method for the modelling of thermal history based on ANN in FDM. The authors proposed a geometry representation method that translated G-Code into a set of features. There were three types of features, including features related to the deposition time, features related to the distances from the cool surfaces and heat sources, that were used for predicting the

thermal profile. Other studies on the prediction of thermal histories in different AM processes can be found in Ref (Mozaffar et al., 2018, Ren et al., 2020, Ren et al., 2021, Zhou et al., 2021, Kumar et al., 2021, Nalajam and Varadarajan, 2021), where ML-based models were applied. For instance, Ren et al. (Ren et al., 2020) introduced a combined model called RNN-DNN to model the relationship between laser scanning strategies and their corresponding thermal history distributions in the DED process. From the studies above, it's apparent that ML technologies have made significant contributions to model complex AM processes, largely facilitating the development of control strategies and improving the reliability of manufacturing processes.

Integrating physical knowledge with ML models has great potential to provide more explainable results and reduce training samples. Hence, physical-informed ML techniques have risen in recent studies (Gaikwad et al., 2020, Kapusuzoglu and Mahadevan, 2020, Zhu et al., 2021, Liu et al., 2021). The bond formation and meso-structure have strong influences on the final mechanical properties of the FDM-produced products. Different from the studies that purely rely on data-driven or physical models, Berkcan et al., (Kapusuzoglu and Mahadevan, 2020) introduced a physical-informed ML approach to predict bond quality and porosity of the parts manufactured by the FDM process. In their study, two coupled multi-physics models, the thermal model and polymer sintering model, were first constructed to predict temperature evolution, bond formation, and meso-structure evolution. As the multi-physics models were built within certain assumptions that cannot fully represent the highly complex physical phenomenon, a DNN was adopted to improve the prediction performance.

2.4.2.5 ML on AM Sustainability

Over the past couple of decades, AM technologies have attracted extensive attention across the world. Compared with conventional manufacturing, AM shows higher efficiency and flexibility, leading to its increasing adoption in the industry. However, according to the Life Cycle Assessment (LCA), the energy consumption of AM systems tends to have a significant effect on the environment (Huang et al., 2016).

This drives AM sustainability to a crucial research topic as the number of AM systems being employed keeps growing. More specifically, cost and energy consumption are considered the key indicators to measure the sustainability of AM (Verma and Rai, 2017).

- **Cost Estimation**

Cost estimation is a crucial task before the manufacturing processes start. Reduction of costs (e.g., material and build time costs) is significant to AM sustainability in the industry. A data-driven cost estimation framework was introduced by Chan et al. (Chan et al., 2018) for AM systems based on big data analytics tools, aiming at reducing the subjectivity of the cost estimation process. In the framework, the automated cost estimation system is an online service provider where manufacturing jobs with 3D models and relevant information, such as material types, surface textures, and tolerances, were uploaded. Feature vectors of the submitted jobs were extracted and clustered which were then fed into ML models with their costs as output for training. A simulation-based cost prediction function was also presented in the framework to simulate the whole manufacturing process for cost estimation when there was a small number of relevant jobs in the database. The final cost prediction from the ML model combined the costs of similar jobs in the database and the prediction from the simulation.

- **Energy Consumption**

Mathematical models for estimating energy consumption have been explored and investigated in existing studies (Verma and Rai, 2017, Yang et al., 2017) of various AM systems. For instance, Verma and Rai (Verma and Rai, 2017), developed mathematical models for estimating energy consumption and material waste in the SLS system and optimized the AM processes. However, AM systems are complex of which the energy consumption is correlated with various subsystems and factors, showing a large difference in terms of different working principles and main material supplies. The influences of these factors are normally inconsistent due to different machines, processes, and materials. Thus, it is rather difficult to uncover and analyse

all the energy-related factors from a single study or experiment. The identified energy-related attributes with their energy consumption model in existing studies are summarized in Table 2.4.

Yang et al. (Yang et al., 2017) developed a mathematical model for estimating the energy consumption of the SLA system by calculating the power consumed from three sub-consumers. The authors analysed the influences of orientation, layer thickness, and the curing time of stable layers and transition rates on the power usage. Lv et al. (Lv et al., 2020) also introduced a physical-based prediction approach for estimating the energy consumed by a SLM system based on the machine subsystems, subprocesses, and working status. In this study, the power consumption of each subsystem was firstly calculated. Then, the temporal models for the subprocesses, including warming up, building, and cooling down, were developed by taking machine setting, product design, and process parameters as input parameters. This work provides solid physical insights that mainly focus on the investigation of the impacts of process parameters on energy consumption.

ML models have been increasingly adopted for analysing and modelling the energy consumption of AM systems. A linear regression (LR) model was adopted by Tian et al. (Tian et al., 2019) to capture the relationships between process parameters, part quality and energy consumption respectively in the FDM process. In the proposed method, the printing resolution, printing speed, and nozzle temperature were considered as the process parameters. The geometry accuracy features, including thickness deviation and average out-of-tolerance percentage, were selected as the indicators of part quality.

Qin et al. (Qin et al., 2018b) proposed a multi-source data analytics method for AM energy consumption modelling based on ANN. In this method, the data generation of an AM process was categorized into four sources, including design, process operation, working environment, and material condition. As an extension of the study, the authors (Qin et al., 2020) found that the design-relevant features, including part design and design optimization, had significant impacts on AM energy consumption based on the

weights of neurons in the ANN model. Thus, a design-relevant feature-based energy consumption prediction model was established and a particle swarm optimization (PSO) method was adopted to optimize the design-relevant features for reducing the energy consumption of the target AM system. Hu et al. (Hu et al., 2020) also analysed the impacts of design and working environment attributes on AM energy consumption based on the LGBM algorithm. In this work, information gain was used to evaluate the contribution of each attribute to the unit energy consumption in the SLS process.

Table 2.4 AM energy consumption-related factors in the literature

Existing studies	AM system	Identified energy consumption-related factors	Model
(Sreenivasan and Bourell, 2010)	SLS	The scan speed, layer thickness, laser power rate; road width size, material density	N/A
(Watson and Taminger, 2018)	Mental AM	Deposited material volume, part envelope volume, the transported distance of feedstock and recycling, build platform size	Mathematical model
(Baumers et al., 2011)	SLS	Manufacturing procedures, capacity utilization, Z-height, part geometry, build time	N/A
(Tian et al., 2019)	FDM	Process parameters (e.g., printing resolution, printing speed, nozzle temperature)	Linear regression
(Yang et al., 2017)	SLA	Part orientation, layer thickness, the curing time for stable layers, curing time transition rate	Mathematical model
(Lv et al., 2020)	SLM	Different machine subsystems, subprocesses, and working status	Physical-based model
(Qin et al., 2020)	SLS	Part geometry, process parameters (e.g., hatch width, hatch speed, hatch power, dispenser), in situ temperature, material conditions (e.g., temperature, humidity)	ANN
(Yang et al., 2020)	SLA	Part geometry	ML-based model
(Li et al., 2021b)	SLS	Part geometry, process parameters (e.g., hatch width, hatch speed, hatch power, recoater speed), in situ temperature, material types	ML-based model
(Wang et al., 2023)	FDM	Part geometry	DL-based model

Besides focusing on processing attributes and material-relevant information for power consumption modelling, the geometry characteristics of the products are also found significant influences on energy usage in several studies, such as build height (Telenko and Seepersad, 2010) and part envelop volume (Watson and Taminger, 2018). Geometry feature-based energy consumption estimation methods for mask image projection SLA systems using ML technologies were developed by Yang et al. (Yang et al., 2019b, Yang et al., 2020). In the Ref (Yang et al., 2020), three methods, including sensitivity analysis based on Pearson correlation coefficient (PCC) and Laplacian score, PCA, and stacked autoencoders (SAE), were applied to feature extraction and selection of layer-wise geometry-related indexes. These extracted features were fed into different ML models for predicting energy consumption. The main contribution of these studies (Yang et al., 2019b, Yang et al., 2020, Qin et al., 2018b, Qin et al., 2020, Hu et al., 2020) is presenting a design-based method to better manage the energy consumption of the target systems before the AM processes start for AM designers, which is an improvement for AM sustainability.

Several existing studies have demonstrated the effectiveness and superiority of using ML technologies for cost estimation, reducing cost, and improving energy management in different AM systems. However, the potential of applying ML for AM sustainability has not been fully achieved, where further studies of using ML for energy saving, reducing material waste, and improving manufacturing process efficiency need to be explored.

2.5 Summary

In summary, the implementation of advanced data analytics in the AM industry were reviewed in Section 2, concerning an overview of AM technologies, data fusion technologies and their applications in AM, and research of ML in AM. During the past decades, advanced data analytics has grown rapidly in popularity, allowing many industries to employ it to discover hidden patterns in their systems, enabling them to create new analytics models to improve production quality, productivity, optimum cost, and maintenance. As the most prevailing data analytics tools, ML technologies are

capable of fusing multi-source data with various modalities, modelling highly complex relationships, and supporting smart decisions. The most used ML technology is deep learning which was applied for over half of the reviewed research. It has been implemented as one of the most popular ML technologies for tackling AM issues. Benefiting from its high compatibility of input data, various types of data is collected and used for deep learning models, such as image, video, acoustic data, process parameters, CAD model, and other sensor data. Also, comparing ML technologies between deep learning and others, deep learning has generally shown merit.

Many researchers tend to compare deep learning with conventional ML algorithms which deep learning generally shows its merits, in terms of, high prediction accuracy, data adaptability and the capability of processing big data (Korotcov et al., 2017). However, deep learning algorithms are required a huge amount of training data to build the model. For many real issues, collecting high quality and large volume of data are challenging. Additionally, the majority of deep learning technologies require a high-performance computational platform to train the model which increases the research or development budget. What essential data to be collected for data analytics and how to select appropriate analytics models should be considered (Qi et al., 2019b)

In addition, about half of the reviewed research applied ML technologies to solve the issues in the research domain of defect detection and in-situ monitoring. However, for the work on defect detection and in-situ monitoring, multiple data processing and modelling are still crucial problems. While ML is a powerful tool for empirical modelling but it still highly depends on data. From the studies reviewed, various types of data are considered as the input of ML technologies, such as image data, video data, sensing data, and design data. How to integrate multi-source, multi-dimensional, and multi-modality data for ML is still an important research topic. Furthermore, researchers have moved their concentration from process to design and sustainability which ML technologies can also play a critical role.

Although ML technologies have been increasingly employed in digital manufacturing systems, there are still several challenges that remain to be tackled, as well as opportunities to be seized. For example, AM processes occur over a wide range of sizes and time scales. The wide ranges of spatial and temporal scales lead to significant challenges in AM process monitoring and control and, from an ML perspective, relate to the data fusion and latency issues. In what way and how to fuse the heterogeneous data for modelling and analysing becomes a critical challenge when applying ML for AM.

Chapter 3 Framework and Methodology of Task-driven Data Fusion for AM

3.1 Introduction

The integration of advanced data sensing and collection technologies in AM systems has enabled exponential growth of data, providing unprecedented opportunities for understanding the nature of AM processes and uncovering hidden knowledge (Khosravani et al., 2022). In recent years, with the rapid development of advanced data analytics tools (e.g., ML technologies), data-driven methods have increasingly played important roles in decision support for solving AM issues, as reviewed in section 2. Nonetheless, the majority of existing studies focus on the performance of using different data analytics models for tackling a few typical AM issues while what data to be considered in the models and how to deal with the data have not been extensively discussed and explored. This urges in-depth investigations of the guidelines for AM data management, integration, and analytics, especially in the increasingly data-rich environment of AM industries. The data generated during each phase of AM production can contain crucial information related to the process stability and part quality. It's essential to take the data from multiple sources or modalities into consideration. However, this multi-source data is normally heterogeneous (e.g., signals, images, geometries), multi-dimensional, and multi-hierarchical, leading to difficulties in integration, especially when high-speed and high-dimensional data is presented (Yin et al., 2020, Fernandez-Viagas and Framinan, 2022). Realizing the full

potential of data analytics for digging out critical knowledge from massive volumes of AM data with various modalities will significantly improve the process stability, repeatability, and product quality, and ultimately facilitate the development of AM industries (Seeger et al., 2022, Qin et al., 2022a). This section introduces a task-driven data fusion framework that provides guidelines when integrating heterogeneous data from various sources or modalities to support decision-making for AM.

3.2 Definition of Task-driven

In this thesis, the term “task-driven” refers to an approach, architecture, or system that is designed and developed to accomplish specific tasks to achieve predefined objectives. It focuses on achieving specific goals and is normally under particular constraints within the task. The term “task-driven” may have slight differences in interpretations under different application contexts, but they all share the common thread of focusing on specific tasks or objectives as a primary principle. Their designed approaches or frameworks are all driven by the tasks. For example, “task-driven dictionary learning” is defined as “the algorithms for learning dictionaries that are adapted to various tasks instead of dictionaries only adapted to data reconstruction” (Mairal et al., 2011, Bahrampour et al., 2015). “Task-driven colour coding” is described as “a colour coding approach that accounts for the different tasks users might pursue when analysing data” (Tominski et al., 2008). Other similar cases of using the term “task-driven” are widely shown in literature, such as “task-driven data augmentation” (Chaitanya et al., 2019, Chaitanya et al., 2021), “task-driven computing” (Wang and Garlan, 2000), “task-driven dynamic fusion" (Zhang et al., 2017b), and “task-driven generative modelling” (Zhang et al., 2018c).

As reviewed in Section 2, researchers and engineers adopted various data-fusion techniques and data analytics approaches for tackling different AM tasks in terms of DfAM, material analytics, monitoring, process modelling and control, and sustainability. However, for the same or similar tasks, the developed models are rarely comparable and compatible. The majority of these models are hard to generalise and they were developed without following a systematic way especially using data-driven-

based modelling and decision-making methods. It lacks a unified framework and guidelines on what essential data to be included in analytics and how to integrate multi-source information. Therefore, in the task-driven context, the developed data fusion models should focus on specific AM tasks with specific requirements, which have clear objectives and are easier to prioritize considerations. Meanwhile, the adopted techniques, developed models, and implemented strategies are more task-centric, making it more suitable to meet the specific demands of the tasks rather than employing a general strategy and method.

3.3 Categories of AM data

Previous studies have categorized AM data from different perspectives with different focuses, however, most of them aim for the ease of data storage and management, as reviewed in Section 2.2. To be closely linked to data analytics, this thesis classifies AM data into three major categories, process-input data, process-generated data, and validation data, based on the sequence of the stages (from part design to final part validation) in a standard AM process. Each category involves several stages of the whole process.

3.3.1 Process-input Data

Process-input data represents the data and information that are generated before the manufacturing process begins, including design-relevant data, process planning data, and parameter setting data. Examples of each sub-category are listed as follows.

- **Design-relevant data:** in design-relevant data, part geometries (CAD models) and material information (e.g., material density, material melting point, material chemistry, particle size distribution, etc.) are included. The materials used in AM production should consider the complexity of part geometries, the working principle of the AM process, and the requirements of final part quality. Hence, the material information is classified into design-relevant data.
- **Process planning data:** path planning, part orientation, location, adding support structures, etc.

- **Parameter setting data:** scan speed, voltage, scan width, etc.

3.3.2 Process-generated Data

Process-generated data consists of two parts, the data generated during the manufacturing process, and the data generated during the post-processing. During the manufacturing process, sensing and measuring technologies (e.g., multiple sensors, high-speed cameras, etc.) are employed for capturing in-process signatures (e.g., melt pool state, temperature, etc.). The in-process signatures are closely linked to the quality of the printed parts, process stability, and machine status. Most research focuses on this information to develop corresponding defect detection, monitoring, and process control strategies. Post-processing is essential in some AM processes in order to achieve quality requirements. Monitoring techniques can also be used during the post-processing to capture crucial information.

- **Process monitoring data:** voltage, current, temperature, gas rate, acoustic signals, optical emission, multi-sensor signals, melt pool images, etc.
- **Post-processing data:** support structure removal, near-net-shape (NNS) part properties, heat treatment, milling, etc.

3.3.3 Validation Data

The produced products are validated by various testing methods where testing data is generated (e.g., CT scan data, density, tensile strength, hardness, fatigue life, etc.). Besides, information such as material waste, time cost, and energy consumption, is collected. This data can be collected and calculated at the end of the whole AM production.

- **Quality-relevant Data:** density, tensile strength, surface roughness, part deformation, etc.
- **Cost-relevant Data:** material waste, total power consumption, time cost, etc.

The data generated in a standard AM process are classified into three categories in this section, process-input data, process-generated data, and validation data. In each category, sub-categories with detailed AM data and information are provided.

3.4 Task-driven Data Fusion Framework and Approaches

Challenges in the multi-source and heterogeneous data integration for data analytics in AM urge the development of systematic methods for guidance in terms of what data should be included and how to integrate it. This section introduces a task-driven data fusion approach that consists of 3 steps, including identification of task-driven data analytics, data required for tasks, acquisition, and characterization, and task-driven data fusion. The three-step approach provides guidelines for (1) the identification of data analytics activities and required data for the tasks, and (2) the fusion of multi-source data with different dimensions in data analytics for tackling different AM tasks. Figure 3.1 illustrates the proposed framework. In the framework, the general AM process falls into 4 main stages, part design, process planning and setting, part building and post-treatment, and part qualification, which constitutes the x-axis of the figure. The y-axis is constituted by different categories of AM data.

As described in section 3.2, the general AM data (i.e., design data, process planning data, process parameter setting data, process monitoring data, post-process data, and validation data) is classified into 3 main categories, process input data, process-generated data, and validation data. The maturity of the collected data and information increases vertically. Different AM tasks (e.g., design concept generation, defect detection, mechanical property prediction, etc) are assigned into different blocks (with dashed lines) according to the stages they belong to. With the increase in the maturity of the collected information, the tasks become more diverse. The collected data and information are processed by the task-driven data fusion methodology for data analytics to support the tasks. The detailed demonstrations of the proposed methodology are presented in Figure 3.2.

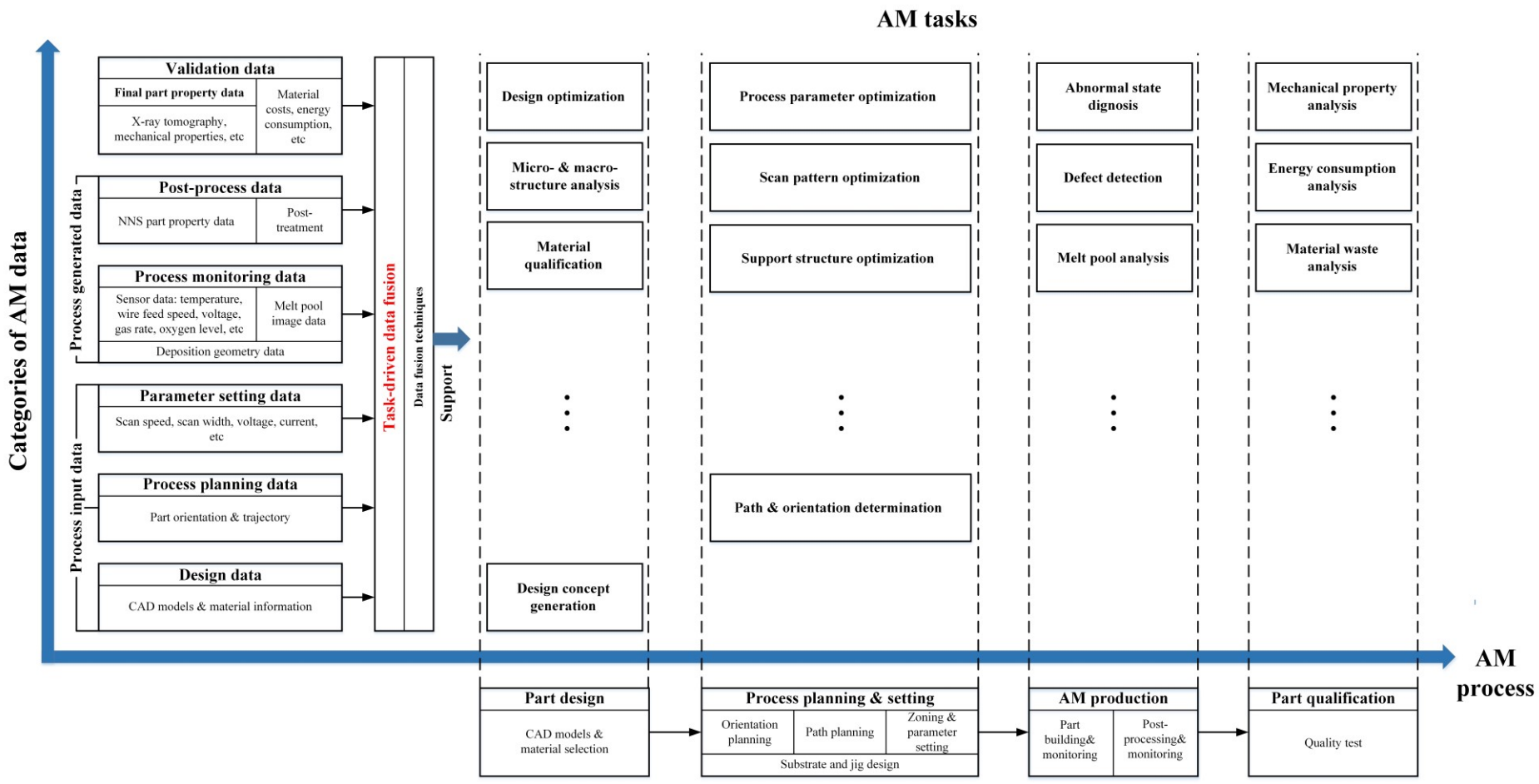

Figure 3.1 The proposed task-driven data fusion framework for AM

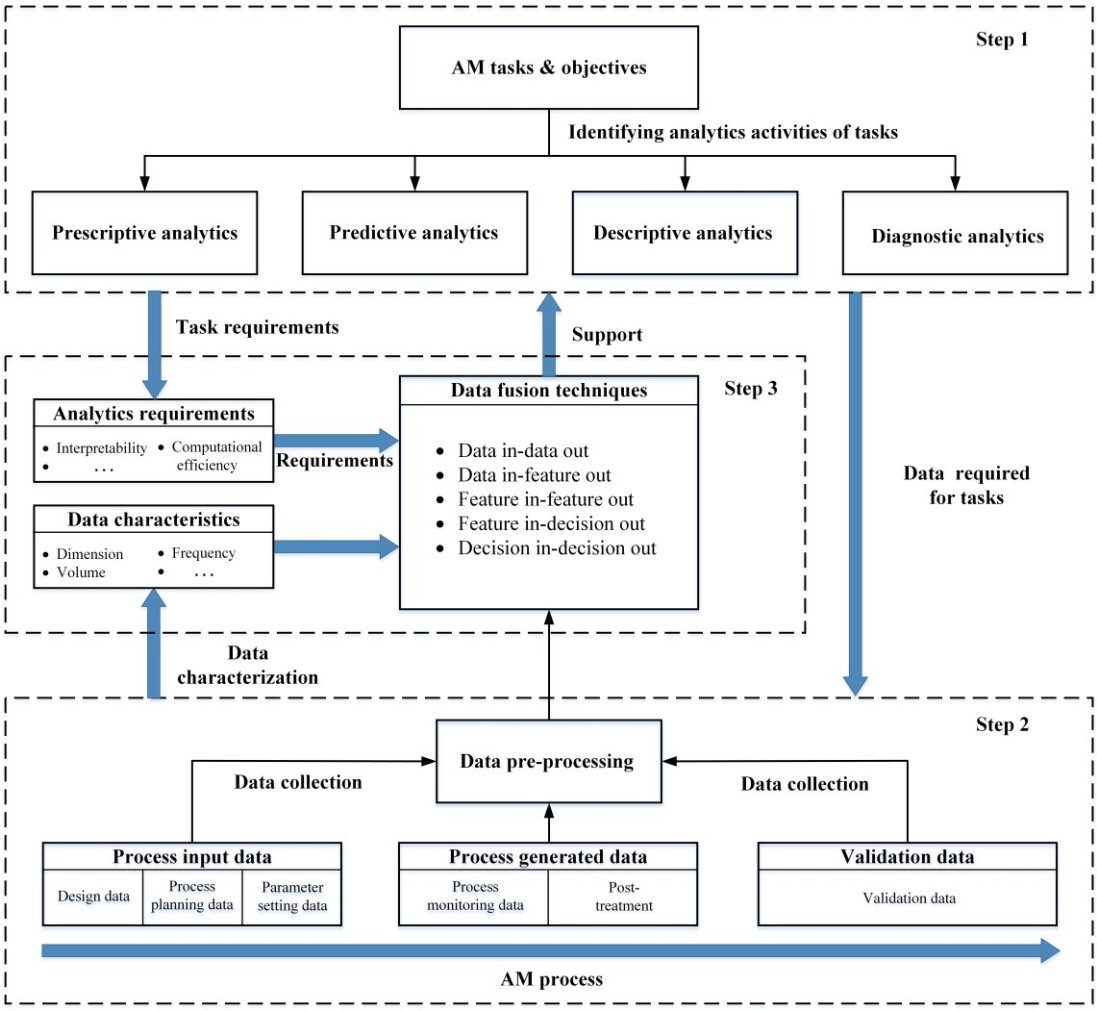

Figure 3.2 Illustration of the 3-step methodology for identifying, collecting, characterising, and fusing data for AM data analytics

3.4.1 Identification of Task-driven Data Analytics

In the first step, the method for identification of data analytics activities of AM tasks is inspired by the method developed in the study (Park et al., 2019). The AM task is firstly defined by AM researchers or engineers and its target value (V) is defined in terms of quality, cost, and delivery or their extensions (e.g., specific indicators of the quality). Decision activities involved in the task can be represented by a set of components using Input (I), Control (C), Output (O), and Mechanism (M) (Technology, 1993). Data, objects, or materials can be represented by inputs. They are transformed by the activity. Controls are the essential conditions to ensure that correct

outputs are produced by the activity. The output is generated through the activity. Mechanisms are tools (e.g., equipment, software) that help execute an activity. Based on the predefined target value (V) and identified decision-making activities, the decision objective can be stated as "Conducting [decision-making activities] for improving/ maximising [V]". Accordingly, the types of data analytics activities (i.e., descriptive, diagnostic, predictive, and prescriptive analytics) can be identified. The example statements of different types of data analytics are presented as follows.

- **Descriptive analytics:** characterizing [V], [I], [C], [O], and [M].
- **Diagnostic analytics:** identifying the relationship between [ICOM] and [V].
- **Predictive analytics:** predicting [V] based on [ICOM]
- **Prescriptive analytics:** prescribing [C] for maximising [V]

3.4.2 Data Required for Tasks, Acquisition, and Characterization

3.4.2.1 Data Required for Tasks

Once the data analytics activities and corresponding types are identified, the data required for the analytics can be identified, collected and characterized in the second step. The connections between different types of data analytics are illustrated in Figure 3.3. As shown in the figure, the lower-level data analytics supports the higher-level analytics while the higher-level analytics can reflect the results derived from the lower level. For example, descriptive analytics aims to describe or characterize the ICOM and V of which the analytics results are used to support the diagnostic analytics. Therefore, the data required for descriptive analytics is ICOM- and V-specific. Diagnostic analytics aims to analyse the relationship between ICOM and V, in other words, finding out their correlations or casual relations. Data required for this type of analytics should be the characterization data supported by descriptive analytics. The diagnostic analytics results can reflect whether the characterization data should be extended. The goal of predictive analytics is to accurately predict the target value V to support prescriptive analytics. Hence, supported by the diagnostic analytics, data required for predictive analytics is normally the characterization data of ICOM which has been identified to have correlations with V. Prescriptive analytics focuses on

developing strategies or providing possible solutions to achieve the decision-making objectives and is normally supported by the corresponding predictive analytics. The solutions or strategies generated from the prescriptive analytics aim to develop control C to obtain the desired target value V or obtain desired O based on I and M.

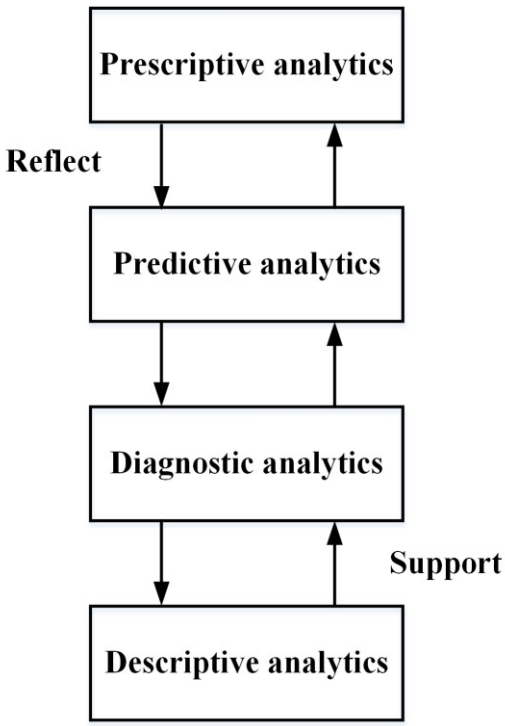

Figure 3.3 The connections between different types of data analytics

3.4.2.2 Data Acquisition and Characterisation

After the data required for the task is determined, it is crucial to ensure the quality of data during the acquisition. For example, sensors must be calibrated before data collection and the status of AM machines should be checked regularly. In some cases, due to the constraints or limitations of the equipment, some required data is hard to obtain. Considering this, optional data can be chosen for collection. This optional data needs to contain critical information that is relevant to the initially required data. Data sources for collecting the required data can be identified based on 4 main stages of an AM process. Some of the data is recorded by machine automatically while others need to be captured by specific devices.

Table 3.1 An example of the data generated during an AM process

Process stage	Data source	Measurement type	Data type	Device for Collection
Design (process stage 1)	Material	Chemistry	Multiple	Test equipment
		Properties		
	Part design	Part geometry	3D geometry	AM design software
Process planning & setting (process stage 2)	Process planning	Support detection & generation	3D geometry	AM software
		Part location & orientation	Multiple	AM software
	Parameter setting	Scan pattern, space, speed,	Numerical value	Machine log files
Part building & post-process treatment (process stage 3)	Process monitoring	Melt pool images	2D image	High-speed camera, infrared sensor
		Surface morphology	2D image	High-speed camera, spectral sensor
		Acoustic emission	Time-series signal	Acoustic sensor
		Optical emission		Spectral sensor
		Temperature		Infrared sensor
		Vibration		Acceleration sensor
		Chamber conditions or machine conditions		System-embedded sensor
		Power, voltage (laser, machine, etc.)		Power meter
		Material conditions		Multiple sensors
	Post-processing	Post-process type	Nominal information	Text record
		Process monitoring	Multiple	Multiple sensors
Part qualification (process stage 4)	Part test	Porosity	Multiple	XCT scan, acoustic sensor, etc.
		Mechanical properties	Multiple	Test equipment
		Surface roughness	3D geometry	XCT scan, profilometer, etc.
		Deformation	3D geometry	3D scan

Table 3 presents examples of the data generated during an AM process and the measurement types and devices are not limited to the information provided. The required data needs to be characterised after it is collected for better understanding and the development of corresponding processing strategies to meet the task requirements. Normally, data is characterised by the "3V" approach, volume, variety, and velocity, which has been used to characterise AM data in previous studies (Razvi et al., 2019). The volume represents the amount of data received during AM processes and is to be processed for further analytics where adequate storage capacity and computing power are necessary. Variety in data refers to the different types of data (e.g., sensor signals, images, videos, text, etc). Due to the heterogeneity, it is usually hard to simply combine the generated data for analytics. Velocity indicates how fast the data is being generated. It is crucial for developing appropriate data processing and analytics strategies for some particular AM tasks, for example, online monitoring.

3.4.3 Task-driven Data Fusion Techniques

Data fusion techniques have different categories due to various criteria in multi-disciplinary areas, such as the classification according to the relations between the data sources, the abstraction levels, and architectures. The data fusion defined in Dasarathy's architecture (Dasarathy, 1997) is adopted in this framework as it considers the nature of input data and output data that aligns with the framework and approach of this thesis. Data fusion techniques in Dasarathy's architecture fall into 5 categories:

- **Data In-Data Out Fusion** (DAI-DAO): The purpose of this type of fusion is to improve the accuracy or polish the input data and it is normally used to directly process the raw data captured from devices. The processing of signals and images is one of its typical applications.
- **Data In-Feature Out Fusion** (DAI-FEO): the raw data is integrated and extracted into a certain level of abstract information in this DAI-FEO fusion.
- **Feature In-Feature Out Fusion** (FEI-FEO): The majority of feature fusion algorithms fall into this category, which incorporates both feature inputs and feature outputs. Compared with raw data inputs, feature inputs are normally

refined and have initially extracted characteristics.

- **Feature In-Decision Out Fusion** (FEI-DEO): Most fusion models or algorithms are classified in this fusion type and they are typically used for classification or regression tasks to support predictive analytics. Decisions are acquired through FEI-DEO fusion based on feature inputs (e.g., pattern recognition, target identification, state estimation, etc).
- **Decision In-Decision Out Fusion** (DEI-DEO): DEI-DEO fusion involves the transfer of certain local or low-level decisions to a global decision, considering the information from the local or low-level decision-making nodes.

Figure 3.4 presents the flowchart of task-driven data fusion. The data required for AM tasks is first collected and characterized. Then the obtained data is judged if it is in the same dimensionality. If yes, the obtained data is pre-processed (e.g., dealing with missing data, abnormal data) and processed through data fusion techniques by considering data characteristics to support data analytics. If the obtained data is not in the same dimensionality, a dimensionality reduction process (e.g., feature extraction) is required to process the high dimensional data before using the data fusion techniques. The strategy for data fusion techniques follows Dasarathy's architecture. For example, Data In-Data out techniques are typically employed for processing in-process sensor signals. The evaluation process is conducted based on the task requirements to evaluate the analytics results and finally choose the fusion technique that best meets the requirements.

Different tasks have different evaluation metrics according to the types of data analytics and specific task requirements. In general, for regression tasks, the RMSE, R^2, and MAE are used to evaluate the performance of prediction models. These metrics are the most commonly used metrics for evaluating the regression. For classification tasks, accuracy and F1-score are the mostly commonly used metrics for evaluating classification results. Other metrics such as confusion matrix and sensitivity can also be adopted for classification evaluation. Additionally, based on specific task requirements or objectives, specific indicators or metrics can be used or designed for

results evaluation. For example, the number of trainable parameters and model size can be used to evaluate the complexity of the developed model.

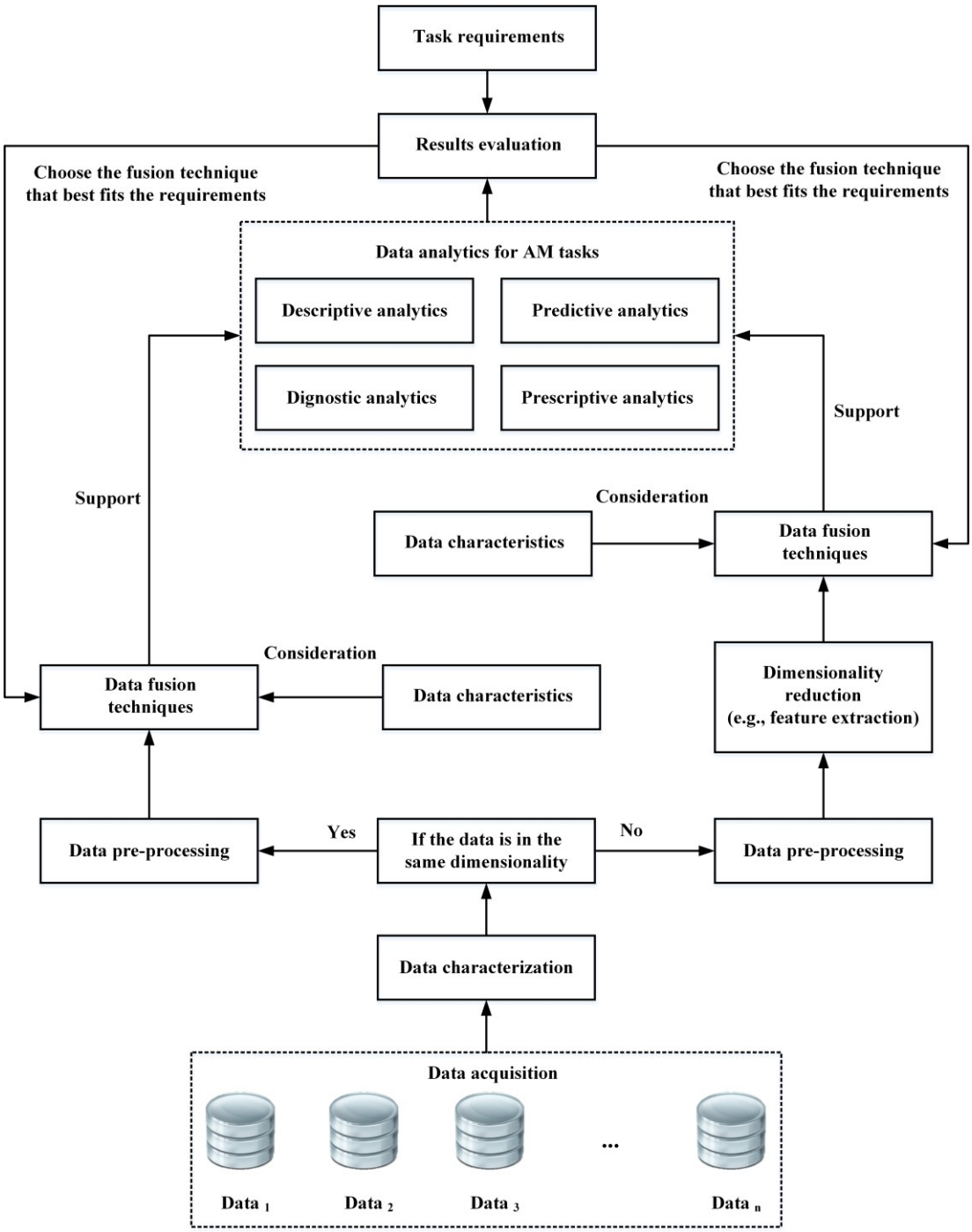

Figure 3.4 The flowchart of the task-driven data fusion

3.4.3.1 Multi-source and Multi-hierarchy Data Fusion

Typically, researchers and engineers focus on two levels of data and information collected from AM production for data analytics, layer level and build level. Layer-level data represents the data collected during the manufacturing process (e.g., sensor signals) and contains the information for each printed layer. The build-level data represents the information for the whole build. This data is normally obtained before the start of the process (e.g., CAD models, process parameters) or after the part is finished (e.g., part test). The target value of the data fusion driven by the AM task can be represented by the following equation (3.1).

$$V = F\left\{f_{li}[x_{li}(t), x_{li}(t-1), ..., x_{li}(t-k)], f_{bj}(x_{bj})\right\}, \qquad (i, j, k = 1, ..., n) \qquad (3.1)$$

In equation (3.1), t is the discrete-time, $x_{li}(t)$ represents the ith time-series measurement data at layer-level that is required by the task at time t, k represents the previous k^{th} discrete time, x_{bj} represents the jth build-level data, V is the target value, f_{li} and f_{bj} are the techniques used for processing the ith layer-level data and the jth build-level data (e.g., feature extraction, data refinement techniques) respectively, and F represents the data fusion techniques. The data fusion techniques follow Dasarathy's architecture and consider the characteristics of $x_{li}(t)$ and x_{bj}. The $f_{li}[x_{li}(t), x_{li}(t-1), ..., x_{li}(t-k)]$ and $f_{bj}(x_{bj})$ should be processed to the same dimension for fusion. Specifically, for the target value to be obtained at the layer-level (e.g., real-time defect detection), the target value of the next moment can be estimated based on the data collected at the current moment and previous measurement data. It can be represented by the following equation (3.2).

$$V_l(t+1) = F\left\{f_{li}[x_{li}(t), x_{li}(t-1), ..., x_{li}(t-k)], f_{bj}(x_{bj})\right\}, \qquad (i, j, k = 1, ..., n) \qquad (3.2)$$

In equation (3.2), V_l $(t+1)$ represent the estimated target value at $(t+1)$ discrete time. For the target value to be obtained at the build-level (e.g., mechanical properties prediction of printed parts), the layer-level data required by the task should be packed to the build-level and the fusion can be represented by the equation (3.3).

$$V_b = F\left\{f_{li}[x_{li}(t), x_{li}(t-1), ..., x_{li}(1)], f_{bj}(x_{bj})\right\}, \qquad (i, j = 1, ..., n) \quad (3.3)$$

In equation (3.3), $f_{li}[x_{li}(t), x_{li}(t-1), ..., x_{li}(1)]$ represents the time-series measurement data during the whole build, and V_b is the target value at the build-level. A typical f_{li} method is to extract time and frequency domain features.

3.4.3.2 Cloud-edge Fusion

Apart from multi-source and multi-hierarchy data fusion, researchers also explore how to implement data fusion from different system levels. Different from the concepts of traditional decentralized data fusion, Cloud-edge fusion is defined as a concept that integrates the capabilities of cloud computing with edge computing for data analytics, where data, knowledge, and analytics models can be analysed, shared, and transferred between different system levels. This fusion paradigm aims to meet some specific demands and requirements of AM tasks.

- **Cloud**

Data processing and analytics in Cloud platforms denote the data and applications are hosted on centralized servers or systems. Cloud computing provides powerful computation, large storage capacity, and advanced analytics services. It enables conducting computational-intensive tasks, such as training complex DL models on large datasets, large-scale data analytics, simulation on high-fidelity models, and so on.

- **Edge**

Data processing and analytics at edge devices refer to performing these operations closer to the source of data generation rather than in a centralized system (e.g., Cloud). Data analytics at edge is particularly beneficial for real-time applications or fast-inferencing required tasks where latency is the major concern. Edge computing architectures often use lightweight ML models and data streaming platforms to meet the demands of edge-based data processing and analytics.

Cloud-edge fusion paradigm leverages the strengths of both systems to deal with data analytics and their corresponding applications. It allows systems to scale as needed and efficiently manages where and how data should be processed. Given the sensing data collected from n sources $\boldsymbol{X} = [x_1, x_2, \ldots, x_n]$ with ground truth value $\boldsymbol{V}_A = [v_1, v_2, \ldots, v_n]$, data fusion techniques f_c, and the analytics model trained in the Cloud platform F_C, the estimated target value $\boldsymbol{V}_C$ in the Cloud can be represented by the following equation:

$$\boldsymbol{V}_C = F_C[f_c(x_1, x_2, ..., x_n)] \tag{3.4}$$

Since the analytics model trained in the Cloud is normally complicated and hard to make fast responses when new data is collected. Therefore, a lightweight analytics model used for estimating the target value at edge devices is needed. Given the initially designed target analytics model at edge F_E with parameter θ_E, the objective is to transfer the learned knowledge from the Cloud model while approximating the ground truth value, represented by the following equation:

$$\theta_E^{'} = \arg\min_{\theta_E} Loss\{(\boldsymbol{V}_A, \boldsymbol{V}_C), F_E[f_e(x_1, x_2, ..., x_n); \theta_E]\} \tag{3.5}$$

In equation (3.5), f_e is the data fusion technique employed to process the collected data $\boldsymbol{X}$, and the $\theta_E^{'}$ is the fine-tuned parameters by knowledge transfer from the Cloud model. The final analytics model at edge $F_E^{'}$ and its estimation $V_E^{'}$ can be represented by the equation (3.6).

$$V_E^{'} = F_E^{'}[\, f_e(x_1, x_2, ..., x_n); \theta_E^{'}] \tag{3.6}$$

It is worth noting that, the equations presented above show a general method to implement Cloud-edge fusion. For specific tasks, the detailed data fusion approaches, analytics models, and knowledge transfer paradigm can be specialised to meet the demands and requirements.

3.5 Summary

This chapter proposes a task-driven data fusion framework and methodology that provides a systematic way to identify, collect, characterise, and fuse the data to support data analytics for AM tasks. Data fusion techniques defined in Dasarathy's architecture are employed in the methodology to consider the nature of input data and output data in data analytics. Based on the levels (layer-level and build level) of the target value to be obtained, guidelines were introduced for integrating data with different sources, dimensions, and modalities. From the system level, methods for enabling the Cloud-edge fusion paradigm for data analytics are provided.

Chapter 4 Multi-source and Multi-hierarchy Data Fusion for AM Using Deep Learning

4.1 Introduction

An AM system is considered complex as it normally contains several subsystems with different sub-processes, of which the process stability, product quality, and system sustainability are influenced by numerous factors. These factors are rarely independent and affect the final target value jointly. The data generated of an AM system often covers a wide range of spatial and temporal scales and is normally from different sources, leading to critical challenges for joint analysis. As reviewed in Section 2.3, data fusion strategies and techniques have been increasingly employed in the AM industry in recent years. Appling data fusion strategies for tackling AM tasks not only considers the multiple measurements but also leverages the information from various modalities, aiming to improve the performance of the corresponding analytic models. Since AM data is normally heterogeneous and has different spatial and temporal scales, conventional data fusion techniques are hard to be applied to obtain desired outcomes. Hence, DL learning techniques have risen to play a crucial role in multi-source and multi-dimensional data fusion. Data fusion using DL techniques is also referred to as "deep fusion" in literature (Sun et al., 2020, Chen et al., 2017, Wagner et al., 2016, Chen et al., 2020a).

As a subset of ML techniques, DL is the algorithm based on artificial neural networks that is capable of learning hidden patterns from large amount of data automatically. The term “deep” in DL refers to the depth of hidden layers and is determined by the number of these layers. The number of hidden layers of conventional neural networks is normally less than three, making it less effective than deep neural networks when dealing with data with numerous variables for modelling highly complicated non-linear relationships. With the increasing number of hidden layers and neurons, the non-linear modelling ability is usually enhanced. However, it normally requires a significant amount of data and computational power to train such deep neural networks. Algorithms such as DCNN, RNN, CNN, and LSTM are the mainstream of DL techniques. Compared with conventional ML techniques, one of the crucial advantages of DL is the strong ability to learn hierarchical representations automatically while conventional ML techniques normally require feature engineering with domain knowledge in data processing. In AM, the final target values of data analytic models normally lie in the quality and cost aspects. Based on the nature of AM processes, the geometry features of CAD models are often considered critical factors related to the target values in various AM tasks (e.g., part deformation, mechanical property prediction, energy consumption estimation). Thus, essential geometric features need to be extracted for data analytics. In general, hand-crafted features, such as height, width, and area, are typical geometric features that are extracted in studies. However, these features are hard to describe highly complex geometries precisely. Meanwhile, these hand-crafted features usually cannot reflect the time-series patterns and they are difficult to fuse with other information of different hierarchies (e.g., sensory data). Additionally, how to integrate this multi-source and multi-hierarchy data for obtaining the target value of AM tasks is challenging.

To tackle the challenges stated above, this study aims to propose a multi-source and multi-hierarchy data fusion method for AM to obtain the target value of AM tasks based on the Merged CNN-LSTM (M-CNN-LSTM) model. The main contributions of this chapter are: (1) Different from the conventional hand-crafted feature extraction approach for AM CAD models, a layer-wise geometric feature extraction method based on CNN is developed. The developed method can extract highly representative

layer-wise geometric features of CAD models automatically. (2) Considering the layer-by-layer manufacturing nature of the AM process, an M-CNN-LSTM architecture is introduced to fuse the geometric features with other target value-related information where layer-level and build-level data is included. The rest of this chapter is organised as follows: Section 4.2 introduces the DL-based multi-source and multi-hierarchy data fusion method. A case study is demonstrated in Section 4.3 with detailed experimental setup and experimental results in Section 4.4. Finally, Section 4.5 presents the discussion of the experimental results, and Section 4.6 summarises this chapter.

4.2 Methodology

A multi-source and multi-hierarchy data fusion approach based on the M-CNN-LSTM architecture is proposed for predicting the target values of AM tasks in this section. This heterogeneous data contains information with different dimensions and hierarchies, such as 3D geometries, time-series data, layer-level information, and build-level information. The proposed method consists of three main parts, including convolutional feature extraction of CAD models based on CNN, layer-level and build-level data processing, and time-series modelling of layer-level information based on LSTM and merged with the neural networks of build-level information for predicting final target values of AM tasks. The approach is illustrated in Figure 4.1. As introduced in Section 3, the multi-source and multi-hierarchy data are first collected for further corresponding data analytics. This collected data contains 3D geometries or images that are essential information related to the final target value of the specific AM task (e.g., mechanical property prediction, power consumption estimation). Information such as process parameters, material information, or sensory measurement data can be involved. In the first place, the collected data is classified into CAD models, layer-level information, and build-level information for further processing respectively. Layer-level data represents the data collected during the manufacturing process (e.g., sensor signals) and contains the information for each printed layer. The build-level data represents the information for the whole build. This data is normally obtained before the start of the process (e.g., process parameters) or after the part is finished

(e.g., part test). In the layer-level and build-level data processing part, a data pre-processing step is employed to deal with the information. This step could involve a dimensionality reduction process to make sure the layer-level data is in the same dimension.

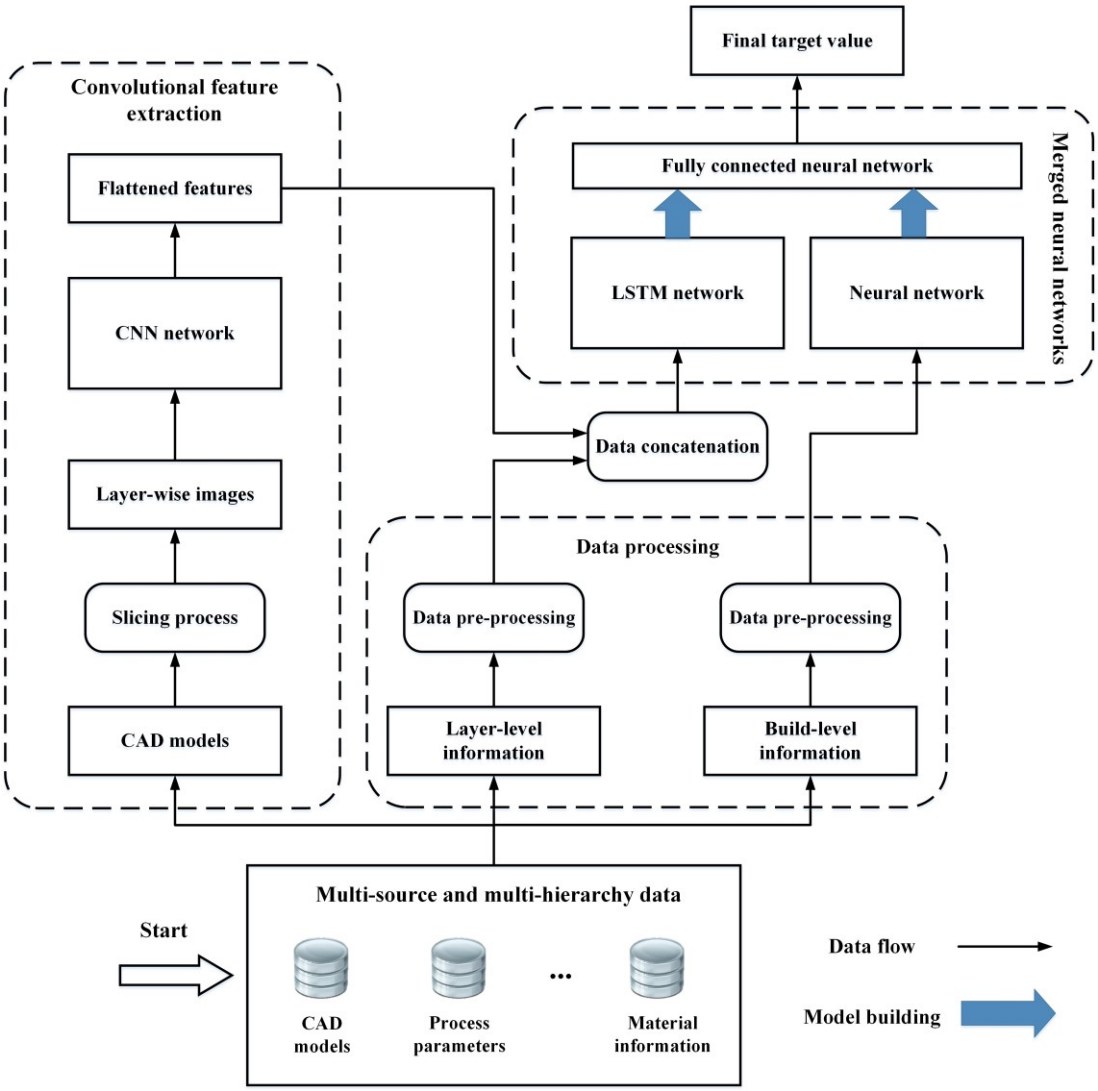

Figure 4.1 The flow chart of the proposed approach based on M-CNN-LSTM

The convolutional feature extraction part aims to reduce the dimension of 3D geometries while obtaining highly representative features automatically. Conventional geometric feature extraction is normally hand-crafted which focuses on the statistical domain of the geometry. However, hand-crafted features are useful in describing

simple geometries but are less effective in describing highly complicated geometries that inevitably lead to information loss. Therefore, the sliced CAD models are transformed into layer-wise images where highly representative convolutional features can be extracted by CNN. The CNN algorithm has been introduced in Section 2.4. During the transforming process, the precision of the images is determined by predefined pixels that can be adjusted according to different application scenarios. The number of convolution and pooling layers are also designed based on the performance of the models on the datasets. After several convolution and pooling operations in the CNN architecture, the extracted feature maps are flattened to obtain the one-dimensional convolutional features. In the time-series modelling part, the convolutional features of layer-wise images are concatenated with the processed layer-level information, which are used as input into the LSTM network. As the parts are created layer by layer, the LSTM network is capable of learning the sequential patterns within data and its detailed principles will be introduced in Section 4.2.2. The build-level information is used as the input into a neural network and merged with the output of the LSTM network in the FCNN to be trained for predicting the target value of the AM task by fusing the multi-source and multi-hierarchy data.

4.2.1 Convolutional Feature Extraction of CAD models

The CNN architecture used for CAD model feature extraction is illustrated in Figure 4.2. As introduced in Section 2.4, the layer-wise images are treated as arrays of numbers in CNN networks. A typical CNN architecture consists of the input layer, convolutional layer, activation function, pooling layer, and fully connected layer. However, in this CNN-LSTM architecture, the CNN part only consists of the input layer, convolutional layers, activation functions, pooling layers, and flatten layer. The fully connected layer is removed where the output feature maps at the last layer (flatten layer) are flattened to serve as the feature representation of the images.

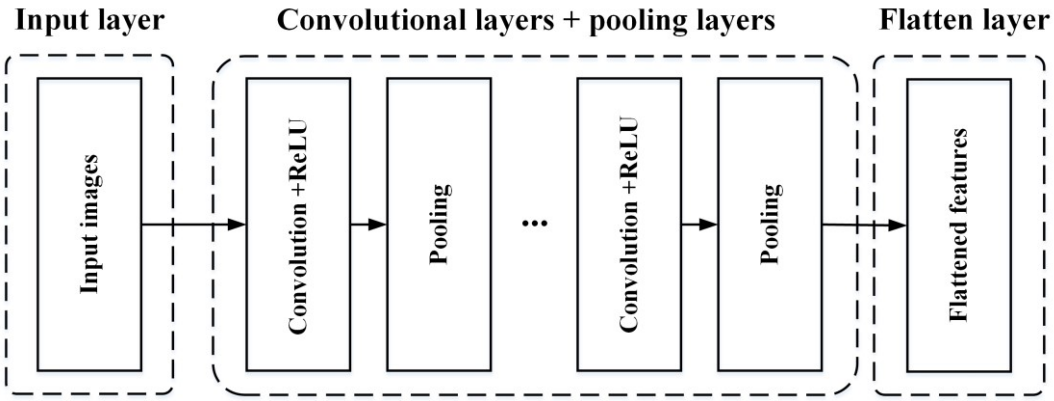

Figure 4.2 The illustration of the CNN architecture without the fully connected layer

In order to reduce the dimensionality of 3D geometries and consider the nature of AM processes at the same time, the CAD models were first sliced and transformed to binary layer-wise images with predefined layer thickness. The illustration of the convolutional feature extraction process is shown in Figure 4.3.

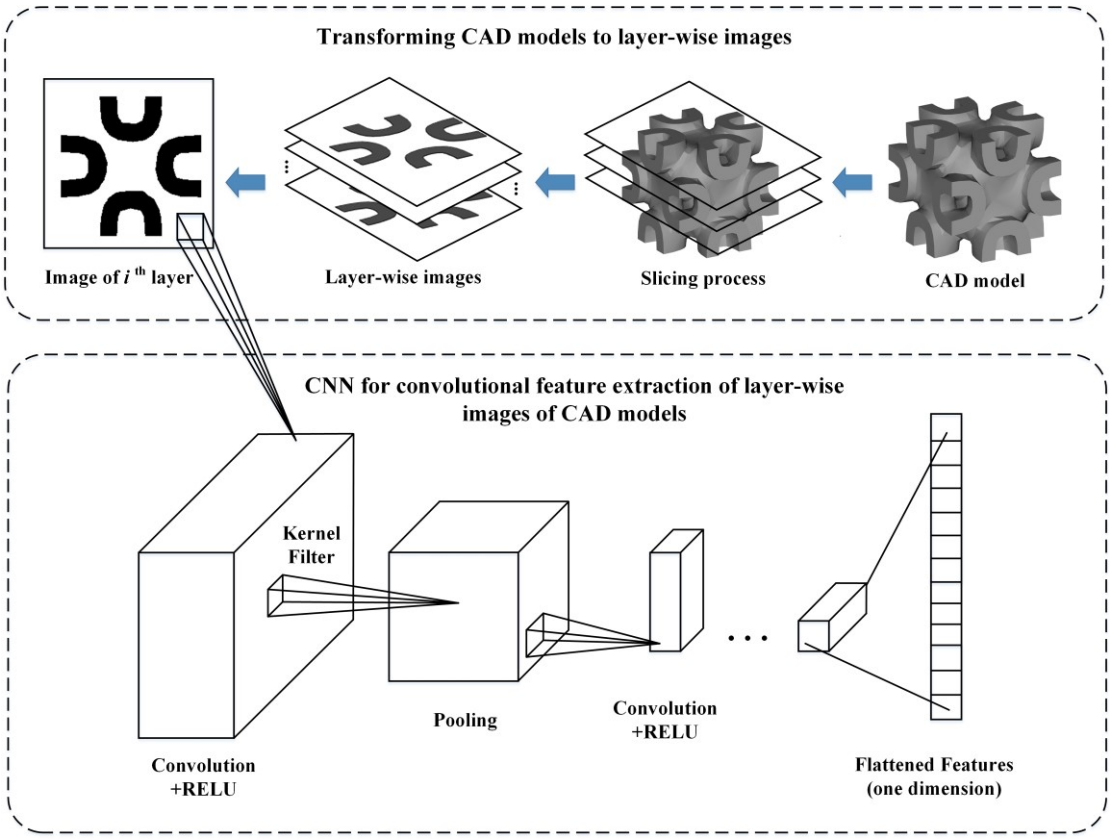

Figure 4.3 The illustration of the convolutional feature extraction process of CAD models

Choosing different planes to slice the parts to be printed can significantly influence the analysis and interpretation of their geometric features. For the part shown in Figure 4.3, due to its unique geometry, the same slicing results are obtained when slicing it along different planes (i.e., XY, XZ, and YZ planes). For general cases, to capture the geometric features of the parts' internal structures more accurately, the slicing plane should be perpendicular to the building direction. For instance, if the building direction is along the Z-axis, the slicing plane should be parallel to the XY plane.

- **Convolutional Layer**

In the convolutional layer, a kernel is employed to slide over the input matrix (image) where an element-wise product between each element of the kernel and the input matrix is calculated to obtain the output feature map. The convolution operation is expressed as:

$$Y(i,j) = \sum_m \sum_n K(i-m, j-n) * X(m,n) \tag{4.1}$$

In equation (4.1), $Y(i,j)$ is the output feature map of the next layer, (i,j) denotes the position of the output pixel, X is the input image, K is the kernel, (m, n) is the position of the kernel element, and * represents the convolution operation.

- **Activation Function (ReLU)**

The activation function is applied to the neurons after the convolution operation. The most commonly used activation function is the rectified linear unit (ReLU) that is expressed as:

$$f_{\mathrm{ReLU}}(x) = max(0,x) \tag{4.2}$$

The ReLU function aims to add non-linearity into the network. It returns x for all values of $x > 0$ and returns 0 for $x \leq 0$.

- **Pooling Layer**

The pooling layers offer down sampling functions such as max pooling and average pooling to reduce the dimensionalities of the feature map received from the previous convolution layer. The most commonly used pooling is max pooling which uses the maximum values from the given grids to serve as the output. The equation of max pooling is shown below.

$$y_n(i,j) = max(Y_n\{i,j\}) \tag{4.3}$$

In equation (4.3), $Y_n\{i,j\}$ are the elements in the neighbourhood of (i, j) in the extracted feature map at the nth layer and $y_n(i,j)$ is the output through the max pooling operation. The max pooling operation aims to replace the sub-region of feature maps with the maximum value in the region.

4.2.2 Time-series Modelling based on LSTM

After obtaining the flattened feature maps of each layer-wise image of the CAD models, the LSTM algorithm is adopted to treat the flattened features as time series data and fused with target value-related information (e.g., process parameter, material information). LSTM is a type of RNN in the field of DL techniques which consists of several cells that capture the temporal information of previous cells and are widely used for learning the sequential patterns within data. LSTM is composed of cells with the same structure where the data of the next moment is predicted each time by the previous data and historical data. In the LSTM cell, there are three gates, including the input gate, forget gate, and output gate, that are used to control memory in each cell. The schematic diagram of the LSTM structure and an LSTM cell are illustrated in Figure 4.4. As shown in the figure, the h_t represents the hidden state and LSTM maintains a memory cell c_t that stores the observed information up to the time step t. The behaviour of the memory cell is determined by the three gates of which the updating equations are expressed below.

$$i_t = sigmoid(U_i h_{t-1} + W_i x_t + b_i) \tag{4.4}$$

$$f_t = sigmoid(U_f h_{t-1} + W_f x_t + b_f) \tag{4.5}$$

$$o_t = sigmoid(U_o h_{t-1} + W_o x_t + b_o) \tag{4.6}$$

$$c_t = sigmoid(U_c h_{t-1} + W_c x_t + b_c) \tag{4.7}$$

$$c_t = f_t * c_{t-1} + i_t * \tilde{c}_t \tag{4.8}$$

$$h_t = o_t * \tanh(c_t) \tag{4.9}$$

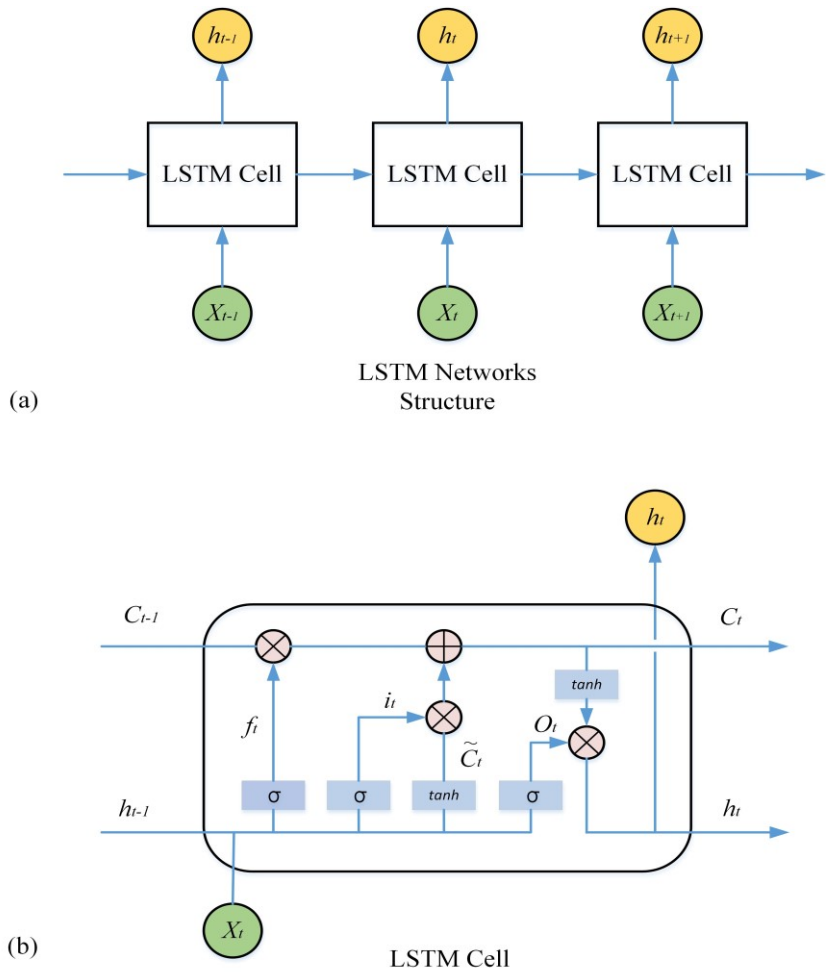

Figure 4.4 The schematic diagram of the LSTM structure and an LSTM cell

In equations (4.4) ~ (4.9), $\boldsymbol{U}$, $\boldsymbol{W}$, and $\boldsymbol{b}$ are learnable parameters. i_t, f_t, and o_t represents the input gate, forget gate, and output gate at time step t respectively. Firstly, the forget gate f_t is obtained by the function of the new input data x_t and previous hidden state h_{t-1}. The information from the last memory cell will remain if the value of forget gate is close to 1. The input gate i_t is formed by the function of the new input data and prior hidden state. Then, the memory cell c_t is obtained based on the input gate and forget gate. The new hidden state h_t is acquired through the equation (4.9) based on the output gate o_t.

4.2.3 Fusion of Multi-source and Multi-hierarchy Information based on M-CNN-LSTM

As described in Section 3, in AM systems, researchers and engineers focus on two levels of data and information for data analytics, layer level and build level. The build-level data represents the information for the whole build while layer-level data contains the information for each printed layer during the production. The collected AM data and information are normally from multi-source that may contain both layer-level and build-level information with different spatial and temporal scales, which are considered multi-hierarchy information. To fuse this information for final target value, the 3D geometries are transformed to layer-wise images where 1-D convolutional features are extracted based on CNN. These convolutional features are then concatenated with the processed layer-level data to serve as the input into the LSTM neural network. The build-level data is processed through the neural network and then merged with the output from the LSTM network in the FCNN for obtaining final target values, illustrated in Figure 4.5. In Figure 4.5, x_{ln} represents the concatenated feature vectors for n^{th} layer and the whole previous information used for LSTM prediction can be denoted as $\boldsymbol{X_l} = [x_{l1}, x_{l2}, x_{l3},\ldots, x_{ln}]$. The LSTM model can be represented as $f_{LSTM}(x_n)$ and the output of LSTM can be obtained by the following equation:

$$Y_l = f_{LSTM}(x_{l1}, x_{l2}, x_{l3}, \ldots, x_{ln}) \tag{4.10}$$

There are various parameters to be determined in the LSTM model during the training and test processes. Different parameter settings can lead to different model performances in terms of accuracy and are dependent on different application scenarios. $\boldsymbol{X_b} = [x_{b1}, x_{b2}, x_{b3}, \ldots, x_{bn}]$ represents the feature vectors of build-level information which are processed through the neural network where the output of neurons N_b can be obtained by the following equation:

$$N_b = (\sum_1^k w_b * X_b),\ y_b = f_b(N_b + b_b) \tag{4.11}$$

$$Y_b = [y_{b1}, y_{b2}, y_{b3}, \ldots, y_{bk}] \tag{4.12}$$

In the equation (4.11), w_b is the weight of each neuron in the neural network for build-level data processing, k is the number of neurons, b_b is the bias, f_b is the activation function, and y_b is the output of each neuron. The output of the neural network can be represented by equation (4.12), $\boldsymbol{Y}_b = [y_{b1}, y_{b2}, y_{b3}, \ldots, y_{bk}]$. In the concatenation layer, the vectors can be represented by $\boldsymbol{X}_{(l+b)} = [\boldsymbol{Y}_l, \boldsymbol{Y}_b]$ which are used as input into the FCNN for final target value prediction. The final output Y_{final} of the merged LSTM can be represented by the following equation:

$$Y_{final} = f_F(W_F * X_{(l+b)} + B_F) \tag{4.13}$$

In equation (4.13), f_F, $\boldsymbol{W}_F$, $\boldsymbol{B}_F$ are the activation function, the weight matrix, and the bias of the FCNN, respectively. In this section, a multi-source and multi-hierarchy data fusion approach based on the M-CNN-LSTM model was proposed for tackling the AM tasks which require taking into account the geometric features and other target-value-related information. This information could involve the layer-level data and build-level data which constitutes the multi-source and multi-hierarchy data.

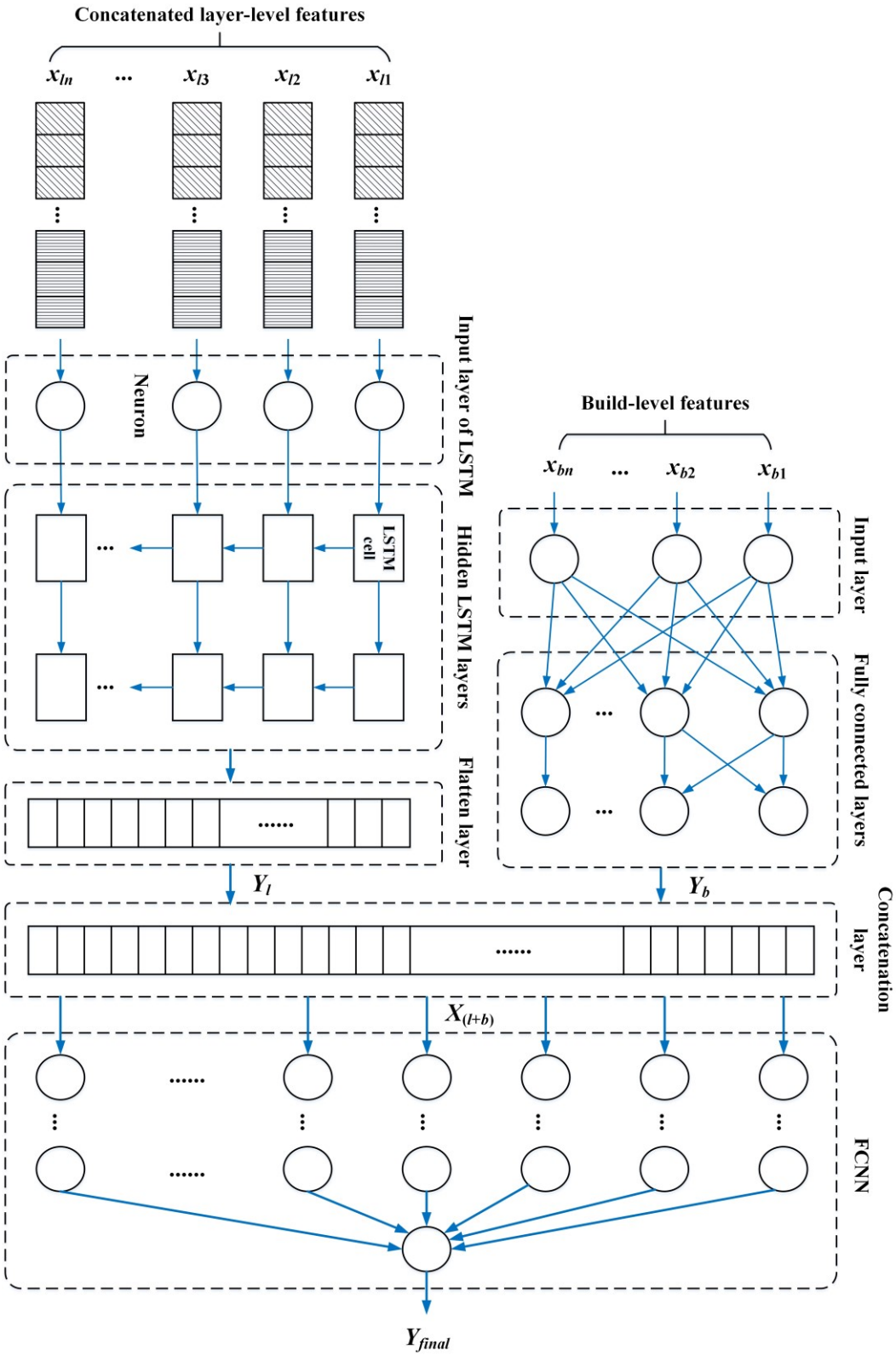

Figure 4.5 Fusion of the multi-source and multi-hierarchy information in the merged LSTM

4.3 Energy Consumption Prediction for AM

The energy efficiency of manufacturing processes is considered not only closely related to process parameters, but also other factors (e.g., processing time., material attributes, and auxiliary processes states) (Apostolos et al., 2013). For AM systems, existing studies (Telenko and Seepersad, 2010, Sreenivasan and Bourell, 2010, Watson and Taminger, 2018) have shown that energy usage has large variations due to different working principles and material types in different AM technologies. Several factors, such as the volume of part envelopes, part geometry, platform temperature, and process parameters, have been identified to have strong relationships with energy consumption in AM processes. Various approaches have been developed in previous research for modelling power usage. However, each of these methods has advantages and limitations. With the facilitation of IoT technologies and machine learning ML techniques, data-driven approaches have shown their merits and have been increasingly used for modelling complex systems, as well as uncovering hidden knowledge in digital manufacturing systems (e.g., AM systems).

Typically, in AM production, data is generated from the part design stage (i.e., CAD models) to the post-treatment stage. This data is heterogeneous and contains different formats, structures, and dimensions. It is rarely independent and hard to be jointly analysed. Moreover, CAD models normally contain highly complex geometries that are difficult to describe by simple hand-crafted features. Therefore, it is crucial to capture the information of part geometries more effectively and integrate the data collected from different sources for modelling AM energy consumption. Predicting energy consumption before AM production begins can provide opportunities for AM designers to optimize their design and process parameter settings. Also, based on the prediction results, the strategy for arranging the components in each build for energy saving can be developed. Therefore, in this case study, the task is to predict the AM energy consumption before the process begins.

4.4 Experimental Setup

As described in Section 4.3, the AM unit energy consumption prediction task requires that the prediction can be obtained before the manufacturing process begins. In other words, the task aims to leverage the essential information related to energy consumption that can be collected before the production (i.e., process-input data) to estimate the unit energy consumption. Hence, the data to be collected includes design CAD models, material information, process planning data, and process parameter setting data. Meanwhile, the ground-truth energy consumed during the manufacturing process should be collected by using a power meter.

4.4.1 Data Acquisition and Preparation

The target system in this case study is an SLS machine (EOS P700). The EOS P700 has a build envelope, maximum size is 740* 400* 590 mm (x, y, and z), and the effective build envelope size is 700* 380* 580 mm (x, y and z). This platform enables the production of multiple parts and components, sometimes even more than hundreds, at the same time. The collected datasets include data and information from more than a hundred production processes with thousands of produced parts. The produced products were designed by different AM designers and had a variety of shapes and geometries. Two examples of the builds manufactured by the SLS system are shown in Figure 4.6.

As shown in Figure 4.6, the SLS production covers a wide range of parts and components with various shapes and geometries. In production, the number of parts, part locations, and part orientations are determined by the experienced AM technicians. The information of process parameters, six attributes, was recorded in machine log files for each build, including hatch speed, hatch space, hatch power, recoater speed, and the values of the dispenser. The material used is polyamide PA2200. In an AM process, the total energy consumption largely depends on the building time for manufacturing parts. In other words, for the same process, the longer the build time is, the more energy is consumed.

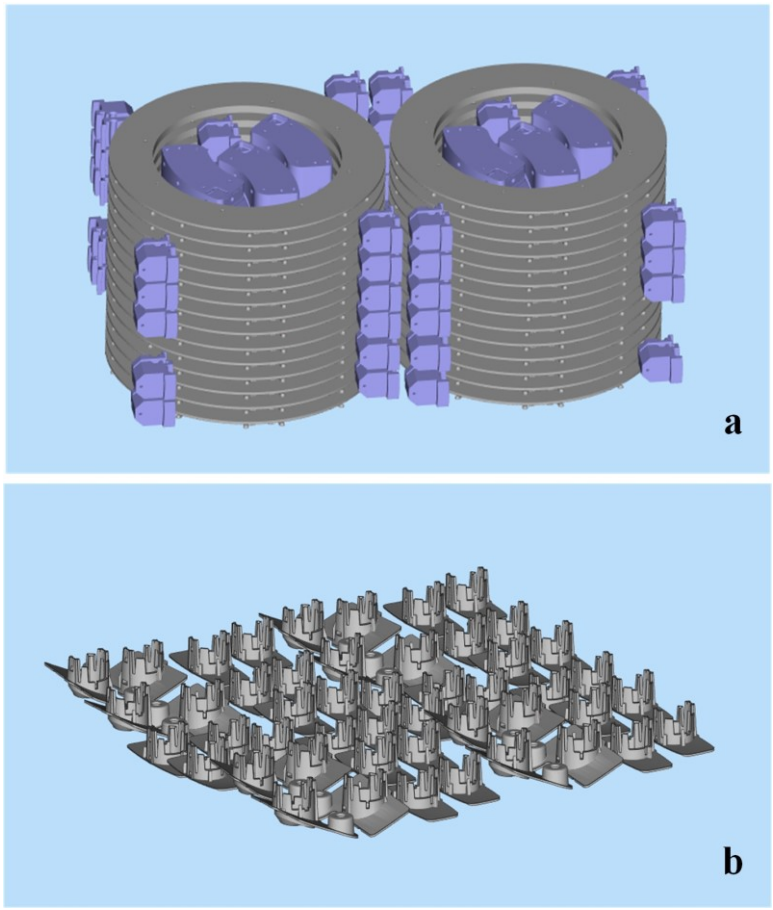

Figure 4.6 Examples of CAD models in the SLS production

Therefore, the unit energy consumption E_u (Wh/g) is used to evaluate the consumed energy level of printed layers and calculated by the following equation.

$$E_u = \frac{E_l}{M_l} = \frac{E_l}{A_l \times H_l \times D_m} \tag{4.14}$$

$$E_T = \sum_k (\int_0^t E_c) \tag{4.15}$$

$$E_{uT} = \frac{E_T}{M_T} = \frac{E_T}{\sum_n (A_l \times H_l \times D_m)} \tag{4.16}$$

In equation (4.14), E_l is the total energy consumed for each printed layer, and M_l represents the weight of each layer. The weight of each printed layer can be calculated

by the product of the area of the printed layer A_l and layer thickness H_l and material density D_m. In equation (4.15), E_T represents the total energy consumed for the whole build that equals to the sum of energy consumed of all energy consumers (e.g., sub-process), k and t represent the number of energy consumers and printing time respectively. The unit energy consumption of the whole printed build E_{uT} is calculated by the equation (4.16) where M_T represents the weight of the whole printed build and n represents the number of layers. The material properties and thermal properties of the used material, PA220, are collected from the support company material sheet which are presented in Table 4.1. The process parameters were recorded in the machine log files, including six attributes of which the detailed explanations are presented in Table 4.2.

Table 4.1 Material information collected from the support company material sheet

Material properties	**PA2200**
Average grain size	$56\mu m$
Bulk density	0.45g/cm^3
Density of the laser-sintered part	0.93g/cm^3
Melting point	172~180 ˚C
Vicat softening temperature B/50	163 ˚C
Vicat softening temperature A/50	181 ˚C

Table 4.2 Description of the process parameters recorded in the Job file

Attributes	**Description**
DispenserMax	The maximum value of the dispenser measured in '%'.
DispenserMin	The minimum value of the dispenser measured in '%'.
HatchPower	The power of the laser for sintering measured in '%'.
RecoaterSpeed	The recoater speed measured in 'mm/min'.
HatchSpeed	The scan speed of laser for sintering measured in 'mm/s'.
HatchWidth	The scan space of laser for sintering measured in 'mm'.

4.4.2 Evaluation Metrics

The evaluation metrics for the fusion models are the root mean squared error (RMSE) and the coefficient of determination (R^2). They are the most commonly used evaluation metrics for regression tasks. The evaluation metrics are calculated by the following equations.

$$RMSE=\sqrt{\frac{1}{s}\sum_{i=1}^{s}(y_i-\hat{y}_i)^2} \tag{4.17}$$

$$R^2=1-\frac{\sum_{i=1}^{s}(\hat{y}_i-y_i)^2}{\sum_{i=1}^{s}(\bar{y}-y_i)^2} \tag{4.18}$$

In equations (4.17) and (4.18), s represents the number of samples, y_i, $\hat{y}_i$, and $\bar{y}$ denote the actual, predicted, and mean value of the outputs, respectively.

4.4.3 Experiment 1: Analytics of the Impacts of Design Features on Energy Consumption

Design features of the parts to be manufactured by AM have been identified correlations with energy consumption. However, in existing studies, only a few hand-crafted statistical features of CAD models were extracted for modelling while their impacts on energy consumption have not been paid enough attention to. Investigating the relationship between design features and energy consumption will not only provide evidence for modelling energy consumption based on CAD models but also insights for AM designers to optimize their designs regarding power consumption reduction. The data used for analysing the impacts of design features on the unit energy consumption are primarily collected from the design models and the power meter. This collected data are generated from the AM process during different builds. The design feature data is collected from design models and analysed by using AM software where the information of features such as geometries, part locations, and part numbers can be obtained. To analyse the impact of design features on unit energy consumption, statistical correlation analysis based on the Pearson correlation coefficient (PCC)

combined with feature importance ranking based on information gain are adopted. The analytics method is illustrated in Figure 4.7.

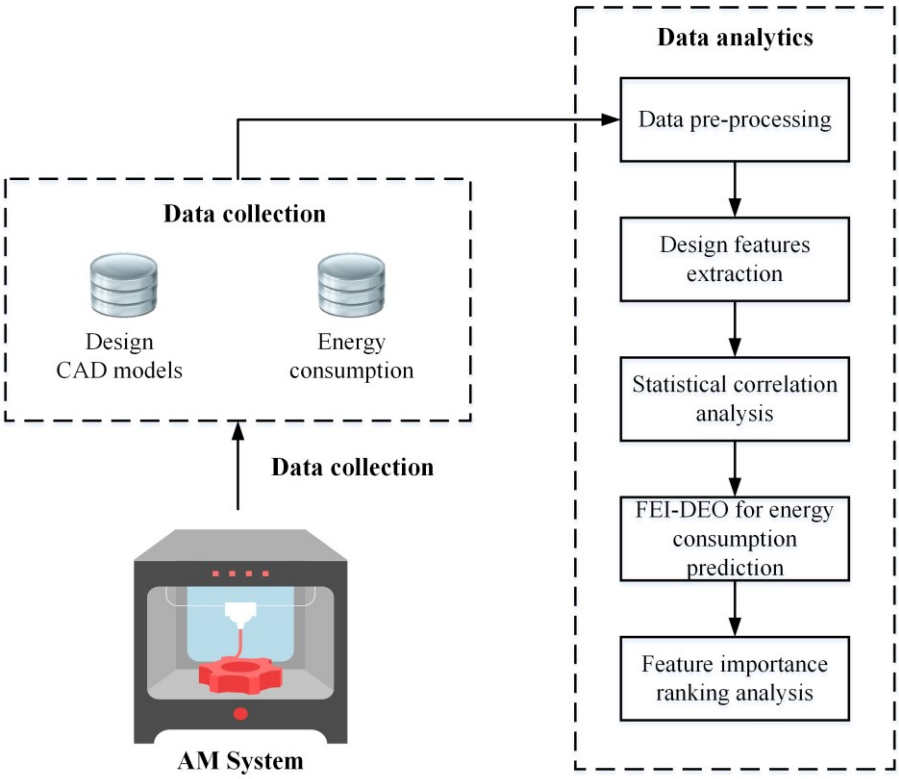

Figure 4.7 The flow chart for the analytics of the impacts of design features on energy consumption

The PCC is calculated by the following equation (4.19) where r_{XY} is the PCC between variables X and Y, $\bar{x}$ and $\bar{y}$ represent the mean values of X and Y respectively.

$$r_{XY} = \frac{\sum_{i=1}^{n}(x_i - \bar{x})(y_i - \bar{y})}{\sqrt{\sum_{i=1}^{n}(x_i - \bar{x})^2}\sqrt{\sum_{i=1}^{n}(y_i - \bar{y})^2}} \tag{4.19}$$

PCC analysis only measures the linear relationship between variables, therefore, feature importance ranking based on the information gain is employed for further investigation. Information gain measures the reduction in uncertainty about the target variable after splitting the dataset on a particular feature. The information gain of the tree-based algorithms is calculated by the following equations.

$$H(D) = \sum_{k=1}^{K} -p_i \log_2 p_i \tag{4.20}$$

$$H(D \mid A) = \sum_{i=1}^{n} \frac{|D_i|}{|D|} H(D_i) \tag{4.21}$$

$$Gain(D, A) = H(D) - H(D \mid A) \tag{4.22}$$

In equations (4.20) ~ (4.22), $H(D)$ is the entropy of dataset D relative to the K-wise classification, p_i denotes the proportion of D that belongs to class i. D_i denotes the subset of dataset D where feature A takes the value i. $|D_i|$ is the number of instances in Di, and $|D|$ is the total number of instances in D. $H(D \mid A)$ represents the entropy of D conditional on feature A, and Gain (D, A) represents the information gain of feature A relative to the dataset D. The FEI-DEO fusion strategy was adopted for design feature impact analytics. XGBoost was employed for unit energy consumption prediction which is an ensemble learning algorithm of decision trees. It provides a parallel tree boosting for classification, regression, and ranking tasks. The unit energy consumption of the whole build was used as the target value.

Table 4.3 The extracted design features of CAD models

Design feature	**Description**
Filling degree part	The average filling degree of the single printed part (%)
PartRate_wl	The average ratio of length to width of the printed parts (%)
PartRate_hl	The average ratio of length to height of the printed parts (%)
PartRate_wh	The average ratio of height to width of the printed parts (%)
Part height	The average height of the printed parts (mm)
Filling degree build	The filling degree of the whole printed build (%)
TotalRate_wl	The ratio of length to width of the whole printed build (%)
TotalRate_hl	The ratio of length to height of the whole printed build (%)
TotalRate_wh	The ratio of height to width of the whole printed build (%)
Height	The height of the whole build (mm)
Bottom_area	The area of the bottom of the whole build (mm^2)
NumPart	The number of printed parts

For design features extraction, twelve design features in terms of space utilization rate were extracted to describe the CAD models to be produced by the SLS machines. The features with their detailed explanations are presented in Table 4.3. For example, the feature "filling degree build" represents the filling degree of the whole printed build. It describes the whole space utilization rate of the SLS building platform. The feature "NumPart" represents the number of parts or components that are included in a build. The feature "PartRate_hl" represents the average ratio of length to height of the printed parts.

- **Results of Experiment 1**

The unit energy consumption of 102 builds was used in the analytics. The PCC between features and feature importance ranking are shown in Figure 4.8 and Figure 4.9 respectively. As shown in Figure 4.8, in general, the features "TotalRate_hl" and "Height" show relatively strong linear relationships (0.64) with the feature "Part height". This is because they all share dependencies on the dimensions of parts. The features "PartRate_wh" and "Filling degree build" show relatively strong linear relationships (0.56 and -0.32) with the unit energy consumption of the target SLS system. The filling degree of the whole printed build and the area of the bottom tend to have relatively strong negative linear relations (-0.32 and -0.29) with the power consumption which possibly indicates that the unit energy consumption tends to reduce if the spatial utilization rate of the building chamber increases. No strong linear relations are observed between the features " PartRate_wl", "PartRate_hl", "Part height", and energy consumption.

In Figure 4.9, the feature importance ranking is based on the average information gain of the XGBoost model in 5 trainings. The average ratio of height to width of the printed parts and the filling degree of the whole printed build have strong impacts on unit energy consumption. No strong impact is observed from other features. These results partially align with the result of the PCC analysis as the information gain reflects the non-linear aspect of the dataset. However, both results indicate that the utilization of the building platform space is crucial. The enhancement of the spatial utilization rate

of the whole build can improve the energy efficiency of the SLS system. This analytics result could provide AM designers and technicians with valuable insights to improve the sustainability of AM systems from the design perspective.

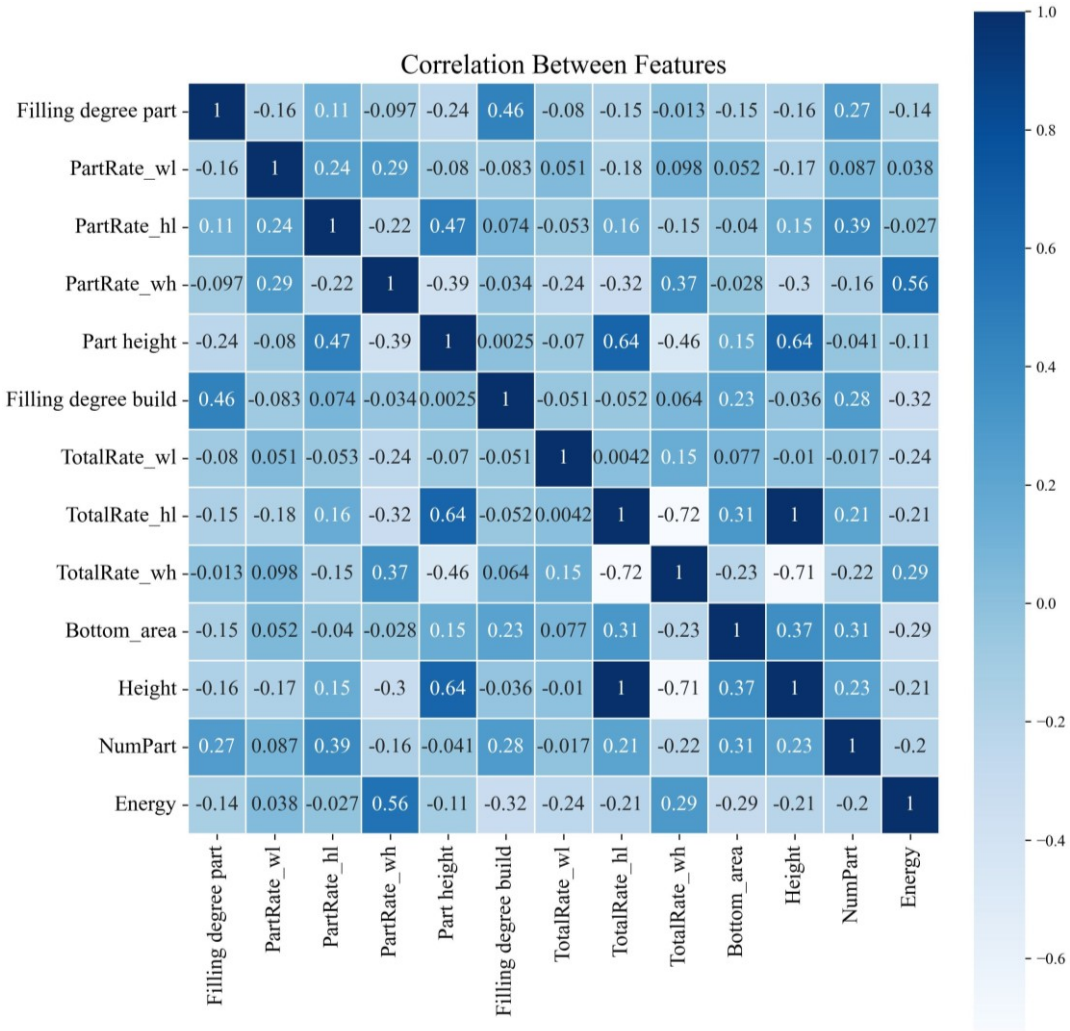

Figure 4.8 The PCC between design features and unit energy consumption

Conducting the analytics of the impacts of design features of CAD models on energy consumption helps to improve the understanding of energy consumption prediction based on geometry information and paves the way for energy reduction. The following sections demonstrate the method for energy consumption prediction by using multi-source and multi-hierarchy information.

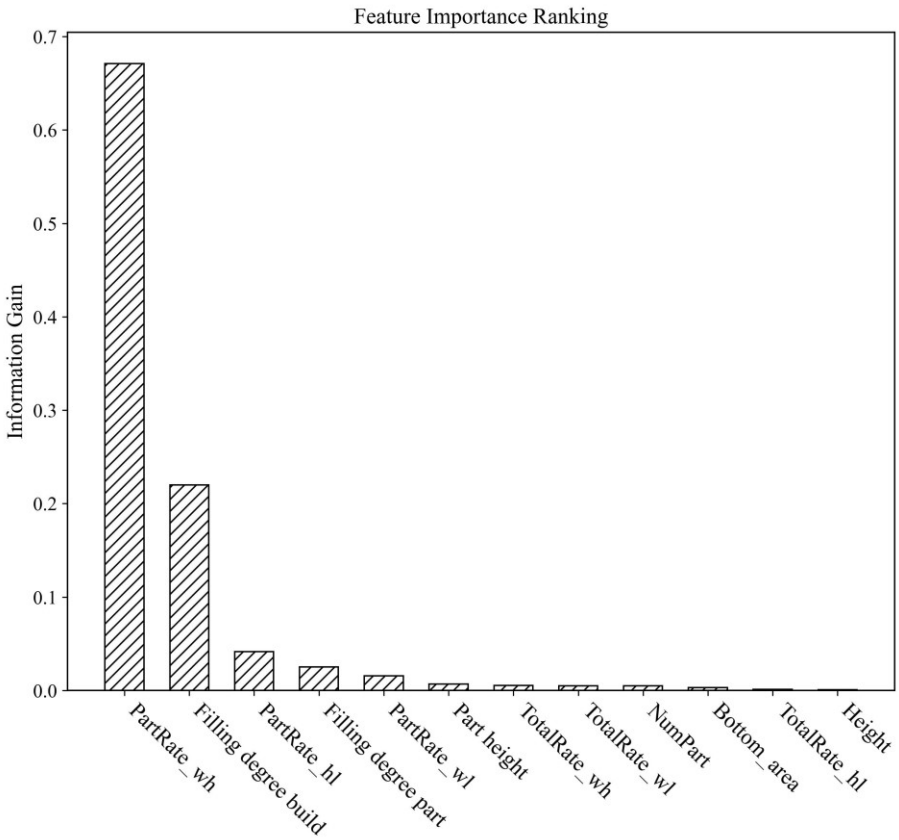

Figure 4.9 Feature importance ranking based on information gain

4.4.4 Experiment 2: Energy Consumption Prediction Based on M-CNN-LSTM

To implement the predictive analytics, different fusion strategies, including (1) FEI-DEO, and (2) FEI-FEO combined with FEI-DEO, are considered that directly use feature inputs for predicting the target energy consumption values. For the FEI-DEO fusion strategy, it is common for the 3D models of the products to have different shapes and geometries some of which are difficult to be described by hand-crafted features due to their complexity. In conventional feature extraction methods, such as statistical features or envelopes of geometries, the inner structures are inevitably neglected while the general information about geometries is extracted. 3D models in AM systems are sliced into layer-wise models with predefined layer thicknesses for layer-by-layer construction of physical objects. This facilitates the analysis of 3D geometries by

transforming the sliced models into layer-wise images (shown in Figure 4.10), which is consistent with the nature of AM processes.

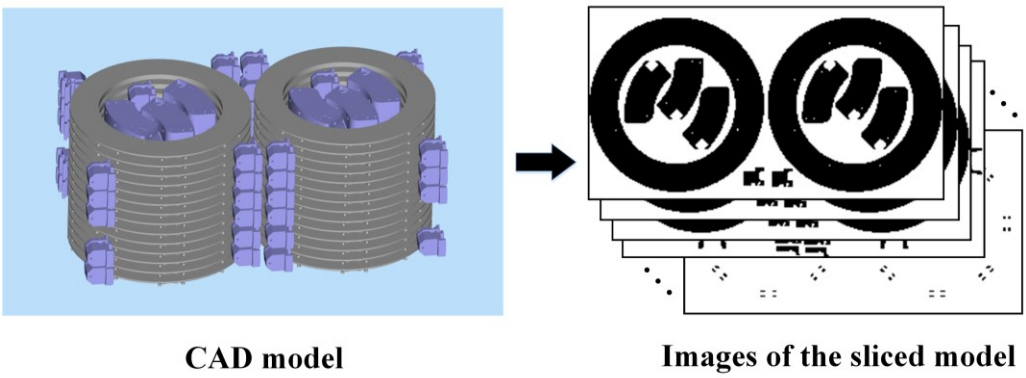

Figure 4.10 An example of transforming the CAD model to sliced layer-wise images for analysis

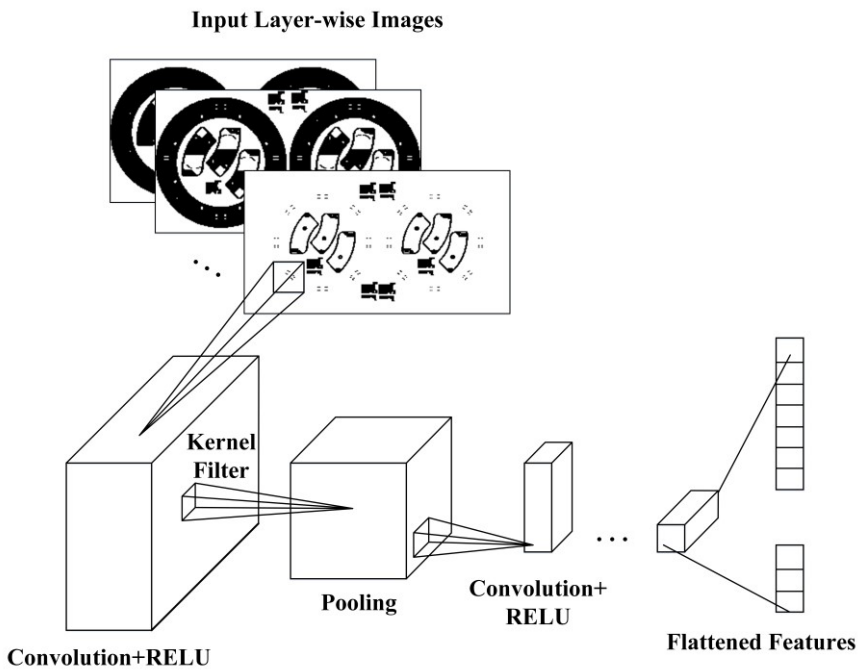

Figure 4.11 The illustration of the feature extraction process of layer-wise images of sliced CAD models

Figure 4.11 illustrates the convolutional feature-extracting process. The resolution of the images in this case study is 128*128. The extracted features of the layer-wise images are flattened into 1D feature vectors which are used as the input in the LSTM

and fused with the process parameters and material information in the FCNN for final energy consumption prediction of each printed layer. For comparison, different ML models, including LGBM, XGBoost, RFs, and ANN are adopted for energy consumption prediction where convolutional features from CNN are concatenated with process parameters and material information for being used as inputs.

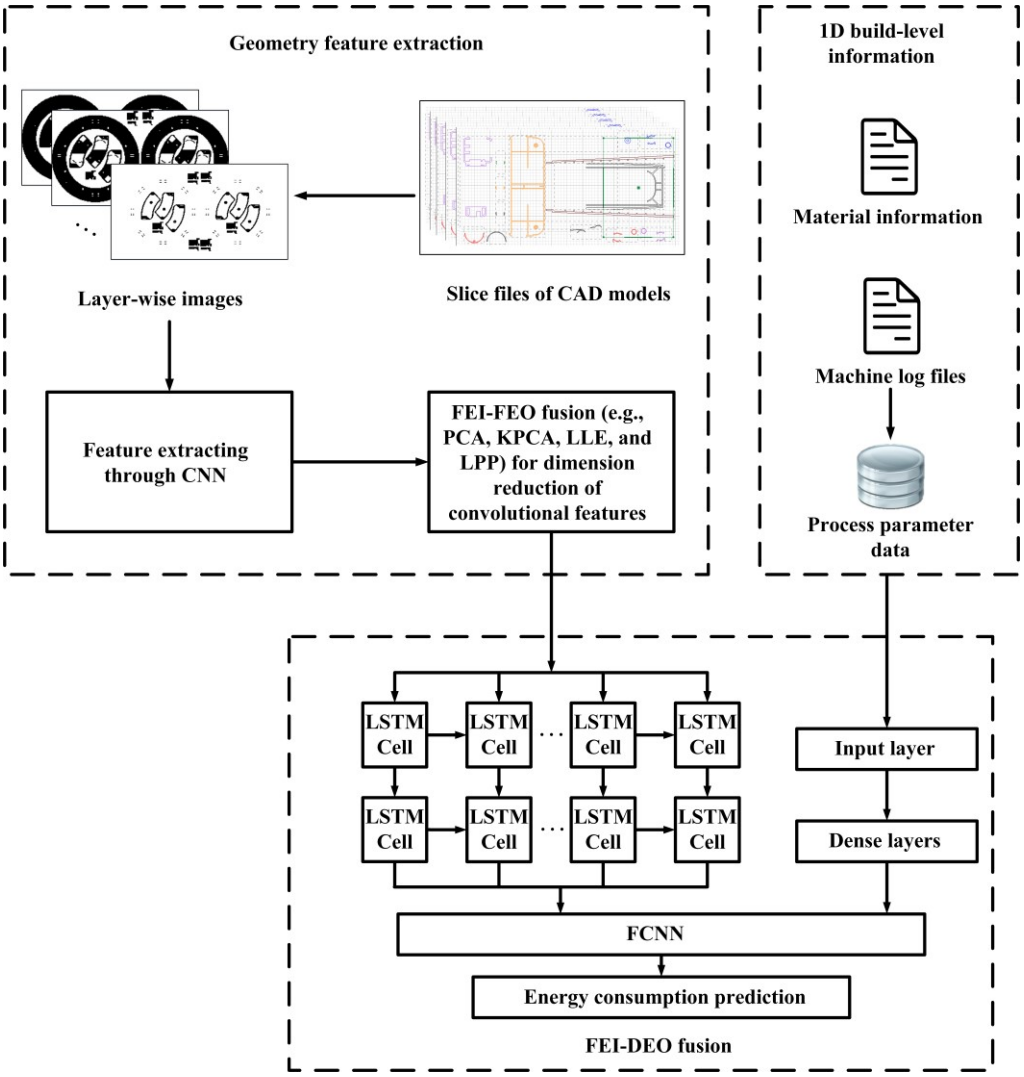

Figure 4.12 Energy consumption prediction based on the proposed M-CNN-LSTM model with different fusion strategies

For the FEI-FEO combined with the FEI-DEO fusion strategy, as the features (over thousands of feature vectors) extracted from layer-wise images through convolution operations are sparse and contain redundant features, the extracted features are refined

by typical fusion techniques before being used as inputs for FEI-DEO fusion in the LSTM model. PCA, kernel PCA (KPCA), LLE, and locality preserving projections (LPP) fusion techniques are applied to refine the features while simultaneously retaining essential information. The proposed approach is illustrated in Figure 4.12. The CNN architecture designed in the M-CNN-LSTM model in this case study consists of 4 convolution layers with kernel size 1*1 and 4 max-pooling layers with pool size 2*2. The activation function is ReLU. The number of neurons is 32, 64, 128, and 256 of the convolutional layers respectively. The FCNN has 2 dense layers.

- **Results of Experiment 2**

There were more than 10000 layer-wise images in the dataset used in this experiment. The values of the unit energy consumption of printed layers range from 2.84 to 301.63 Wh/g, with a mean value of 17.17 Wh/g. When the area utilization rate of the building platform is low, the unit energy consumption becomes very high due to the very small area of the parts being printed, such as at the beginning and end of the printing process. As a result, the range of unit energy consumption is relatively wide. So, outliers and unit energy consumption values on printing very small area were removed from the dataset.

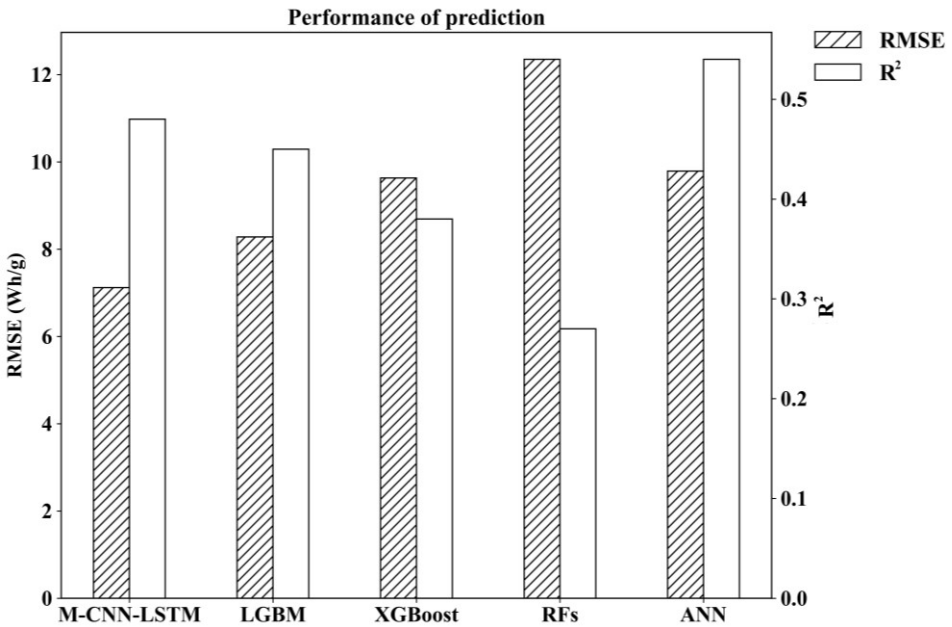

Figure 4.13 The performances of different prediction models

In the first FEI-DEO fusion strategy, the performances of different models are shown in Figure 4.13. In the figure, the proposed M-CNN-LSTM model had the best result with an RMSE of 7.12 while RFs performed the worst with an RMSE of 12.35. The experimental results of implementing the FEI-DEO strategy using the proposed M-CNN-LSTM model were demonstrated effective for learning the hidden patterns from the multisource and multi-hierarchy data while other employed ML algorithms are less effective. This is due to the strong ability of DL-based algorithms to model complex non-linear relationships through learning the hidden patterns from a large amount of data.

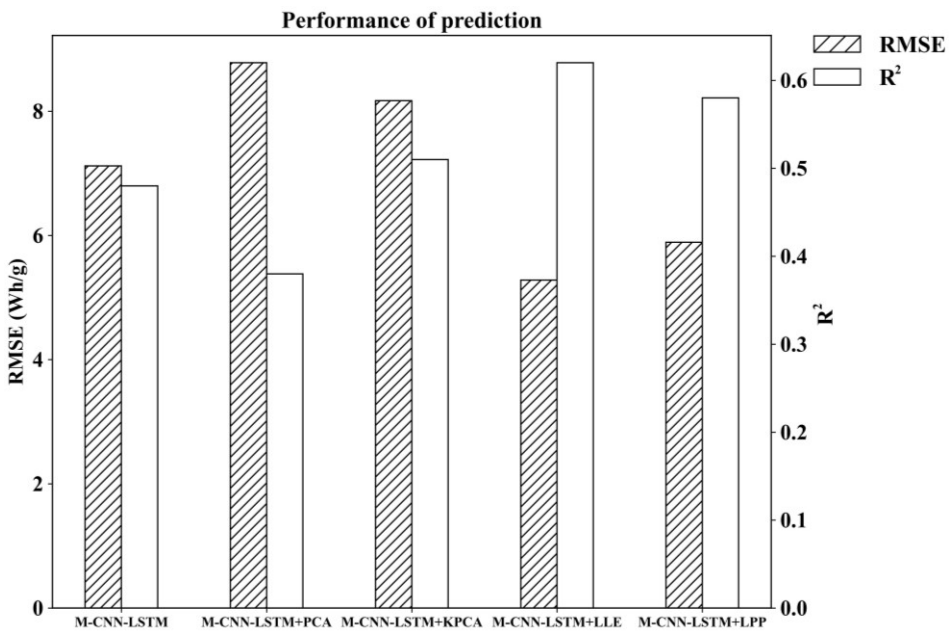

Figure 4.14 The comparisons of performances between different fusion techniques

Figure 4.14 shows the comparisons of the performances between the original M-CNN-LSTM model and the models with different fusion techniques. In this experiment, the fusion strategy was to combine FEI-DEO with FEI-FEO for energy consumption prediction. The M-CNN-LSTM model combined with the LLE fusion algorithm obtained the best results in terms of RMSE (5.28) and R^2 (0.62) while the M-CNN-LSTM combined with PCA had the largest error with an RMSE of 8.64. Also, the M-CNN-LSTM combined with PCA had the worst performance in R^2. Obviously, after

applying FEI-FEO strategies, the performances of most prediction models are improved. Although Information loss could occur during the FEI-FEO process, the fused features are normally more informative and less likely to lead to underfitting problems when the number of training samples is limited. The extracted features of layers-wise images contained thousands of feature vectors where some of these features are sparse. Using the FEI-FEO strategy properly to reduce the dimensionality of the extracted convolutional features is effective and can lead to better performance of the following FEI-DEO fusion. However, some FEI-FEO algorithms are less effective since their basic principles are not suitable for capturing hidden information inside the data. In this case, the evaluation method of the AM task is essential for selecting the most suitable algorithm for fitting the data.

4.5 Discussion

In this chapter, experiments on (1) impact factors analytics of AM energy consumption, and (2) multi-source and multi-hierarchy data fusion for predicting AM energy consumption based on M-CNN-LSTM were conducted. The results have demonstrated the feasibility and effectiveness of the proposed task-driven data fusion framework and detailed fusion approaches. In impact factors analytics, 13 geometric features of CAD models were extracted based on statistical and domain knowledge. The relationships between geometric features and energy consumption were analysed by PCC and the information gain derived from FEI-DEO results. The results of feature importance ranking based on information gain are partially aligned with the results of PCC. This is because only linear relationships were captured by PCC while non-linear relationships were analysed by information gain. This is why impact analytics in this case study employed two methods from different levels.

The PCC results measured the linear relationships between data points at a lower level while the feature importance ranking was calculated from a higher level by FEI-DEO. In addition, conducting control experiments can acquire more accurate and reliable results. However, considering the impact features are numerous, conducting control experiments to analyse the impacts of these features on energy consumption is almost

impossible due to constraints of time and expenses. Hence, to explore and analyse the relationships from observation data is more appropriate and efficient. However, in some cases, it is difficult to obtain insights into the causal relationships due to confounding variables that may influence the target value.

In the experiment of multi-source and multi-hierarchy data fusion for energy consumption prediction, the proposed M-CNN-LSTM model outperformed the prevailing ML algorithms based on the fusion of convolutional features, process parameters, and material information. This is largely due to the strong fitting ability for non-linear relationships of DL algorithms. Combined with the FEI-FEO and FEI-DEO fusion strategies, the proposed M-CNN-LSTM can effectively learn hidden knowledge of energy consumption from hierarchical information. This hidden knowledge refers to the complex patterns and dependencies within energy consumption data, including sequential patterns, geometric representations related to energy usage, and the joint influence of various features on energy consumption. It is worth noting that conducting the FEI-FEO fusion strategy on raw data can reduce the dimensionality, noise, and redundant information, leading to improved prediction results since the convolutional features extracted from CNN are normally sparse. However, significant information loss could occur during the FEI-FEO fusion if the input features are already selected, refined, and informative. Therefore, it is critical to implement the FEI-FEO strategy properly and evaluate the fusion from the prediction results.

Predicting energy consumption precisely based on convolutional features and other related information is challenging since the relationship is highly complex. The performance of the proposed model was improved by applying the fusion strategy, highlighting the value and effectiveness of the fusion strategy. Also, the model performances, especially DL-based models, are influenced by the model complexity and quantity of training data. There is potential to refine and improve the model by training with more data in the future. In addition, uncertainties will inevitably occur during the AM process where some latent factors can affect the energy consumed. Through experiments on training with available data, the obtained performances were

the best outcome of the current model, reflecting the unpredictable nature of the uncertainties within the underlying data. Another important thing should be mentioned that over 10000 images and corresponding energy consumption ground truth values were included in the dataset in experiment 2. If the data samples used for training are small, transfer learning and using other ML algorithms are better options.

Traditional statistical-based or physical-based methods for predicting energy consumption are generally easier to interpret than data-driven modelling methods. In scenarios where physical parameters and system dynamics of the AM process are well understood, traditional methods usually provide more accurate predictions. However, in cases where the underlying factors influencing the energy consumption of AM processes are unclear, data-driven methods are effective. These methods can learn hidden patterns and dependencies automatically from large datasets. The proposed method can predict unit energy usage based on the parts to be printed before the production begins, providing insights into the relationship between design models and energy consumption. It has great potential for AM engineers to reduce energy consumption from the design perspective.

4.6 Summary

As AM covers a wide range of spatial and temporal scales, it is often necessary and challenging to deal with data collected from different sources, with various types and modalities (referred to as multi-source and multi-hierarchy data) in data analytics. The contribution of this chapter is that a multi-source and multi-hierarchy data fusion method based on the M-CNN-LSTM model was proposed. This method is typically employed to address AM tasks that necessitate the combined analysis of geometric or image data with information across various hierarchical levels in sequential patterns. In this proposed method, the layer-level information and build-level information are processed separately and fused in the neural networks to obtain target values. A case study was carried out on an energy consumption prediction task since AM energy consumption prediction is a crucial and challenging issue in improving AM sustainability. Different from traditional statistical-based or physical-based energy

consumption modelling methods, the proposed energy consumption prediction methods take into account the geometric impacts and essential energy-related information of different levels, allowing the prediction can be implemented before the AM process begins and providing insights for AM designers to reduce energy usage from design perspectives. Considering the nature of the AM process that parts are manufactured layer-by-layer, the proposed method transforms CAD models into layer-wise images with a pre-defined layer thickness in sequential patterns, which aligns with the patterns of energy consumption during the AM process. The prediction results have demonstrated the rationality and effectiveness of the proposed fusion strategy and method.

Chapter 5 Cloud-edge Fusion for AM based on Knowledge Distillation-enabled Incremental Learning

5.1 Introduction

The costs of producing products using AM technologies tend to be relatively high (Frazier, 2014, Madhavadas et al., 2022, Prashar et al., 2022) when manufacturing parts with specific requirements in terms of material composition (e.g., Titanium alloys), process type, and part test method (e.g., XCT test) (Calignano and Mercurio, 2023). As a result, some AM tasks usually cannot provide a sufficient amount of data samples for analytics due to the constraints of time and expenses. According to the literature reviewed in Section 2, ML algorithms play an important role in the classification and regression of AM tasks. However, the performances of ML algorithms are influenced by the data available for training. For instance, in the topic of process monitoring, CNN is the prevailing algorithm to process image data for defect detection. It is capable of learning useful information from raw images directly and automatically. The convolutional layers and pooling layers in the CNN architecture can extract representative features and lower feature dimensions. In the meantime, its performance suffers from the data volume.

The CNN model often requires a sufficient amount of data for training processes and fine-tuning the parameters to yield high-accuracy results. Using XCT to detect defects (e.g., porosity, cracks, and lack of fusion) of the produced products for labelling data

is typically costly and time-consuming. Additionally, when using DL for mechanical property predictions, researchers need to conduct a series of experiments where different processing parameter combinations are considered. Testing the properties of the manufactured parts also requires considerable labour. Thus, it is always expensive and impractical to collect a large amount of training data from experiments.

Some researchers are investigating the use of process simulations for training, in addition to experimental results. Furthermore, the DL models are consequently applied to the real AM process and collaborate with some control algorithms, such as adaptive control. The limited data may lead to a high possibility of failure due to the lack of training. Even if the DL model is trained on large datasets, it is difficult to be robust and widely applied in the same AM process but for different machines where the uncertainties affect the model performance. Therefore, it is hard to obtain a robust and reliable DL model when dealing with AM tasks that only have a limited amount of training data. In addition, the developed DL model is hard to implement especially when tackling AM tasks where low latency is the major requirement (e.g., real-time defect detection) due to the model's complexity.

Using DL technologies for modelling and data analytics based on cloud computing often requires considerable computing power. For instance, DNN is a prevailing DL algorithm and DNN-based models are capable of performing high accuracy or generating reliable inferences in many different AM tasks. However, training a DNN-based model normally requires considerable time and computing resources. This is unlikely to be supported by local or edge devices due to the limited computing power. Thus, in the real-time monitoring and control scenario, the collected data normally needs to be sent to the Cloud for processing and analysis. Then the control instructions are sent back from the Cloud to the local system. This whole process normally causes latency for real-time defect detection and control. Moreover, the uncertainties of the network connection and the limitation of the network bandwidth also affect the reaction time.

To address the challenges above, combining knowledge distillation (KD) (Gou et al., 2021, Hinton et al., 2015) and incremental learning techniques (van de Ven et al., 2022) provides an effective way to transfer prior knowledge from a large and complex model to a smaller one and learn continuously to improve model performances when new data is collected. KD has attracted increasing attention in both industry and academia as it offers the perspectives of effective knowledge transfer and efficient computing. It is a representative knowledge transfer method for model compression and acceleration which employs a teacher-student scheme for the distillation of previously learned knowledge (Wang and Yoon, 2021). The term "knowledge" can be understood as a mapping from input vectors to output vectors. By mimicking the output class probabilities and feature representation of the teacher model, the prior learned knowledge can be transferred to the student model with a smaller network.

There are three typical schemes for KD, including online distillation, offline distillation, and self-distillation (Gou et al., 2023). Each scheme has its advantages and limitations which need to be selected based on application scenarios. Incremental learning refers to the ability of ML models to learn new information from newly collected data without forgetting previously learned information (Zhou et al., 2023). Compared with traditional ML models that are trained once on a static dataset, incremental learning retains previously learned knowledge and is trained continuously when new data arrives. It provides possibilities for improving model performances when the initial amount of training data is limited and adapting to new data distributions. Also, incremental learning techniques are memory-efficient and don’t need to store the whole dataset for training. In recent years, DL-based incremental learning techniques have become dominating (Xiang et al., 2019) in lifelong learning and AI systems which need to adapt to evolving environments.

This chapter proposed a Cloud-edge fusion paradigm based on transfer learning and the multi-stage KD-enabled incremental learning method that aims to address the issues (1) in the initial stage, building relatively accurate analytics models to tackle the AM tasks on a limited amount of training data, (2) fusion of previously learned

knowledge and new knowledge incrementally for the improvement of model performance, (3) towards implementation of the analytical model on the devices or platforms with constrained computational resources. A case study is carried out to demonstrate the feasibility and effectiveness of the proposed method, presented in the following sections.

The rest of this chapter is organised as follows: Section 5.2 introduces the transfer learning-based multi-stage KD-enabled incremental learning method. A case study on energy consumption prediction is demonstrated in Section 5.3 and 5.4, of which the results are presented. Finally, Section 5.5 discusses the experimental results, and Section 5.6 summarises this chapter.

5.2 Methodology

In this chapter, a multi-stage KD-enabled incremental learning method based on transfer learning was proposed for the fusion of knowledge from the Cloud system to edge devices for data analytics in AM. The proposed methodology is illustrated in Figure 5.1 and the Cloud-edge fusion process is explained in Figure 5.2. As illustrated in Figure 5.1, the proposed methodology consists of three main steps, including (1) transfer learning for feature extraction, (2) base model building via DML and fusion of base models, and (3) multi-stage KD-enabled incremental learning. In the first step, as the size of training data samples is small, a transfer learning approach is adopted for feature extraction of collected images. The model used for transfer learning needs to be pre-trained on related or similar tasks. For example, the model was pre-trained for object detection and it can be transferred to extract features of similar objects. The FEI-FEO fusion strategy is implemented on the extracted feature for dimensionality reduction. Other task-related information and data are pre-processed (e.g., remove outliers, dimensionality reduction, etc) and concatenated with the flattened convolutional features which are used as input features for the next step.

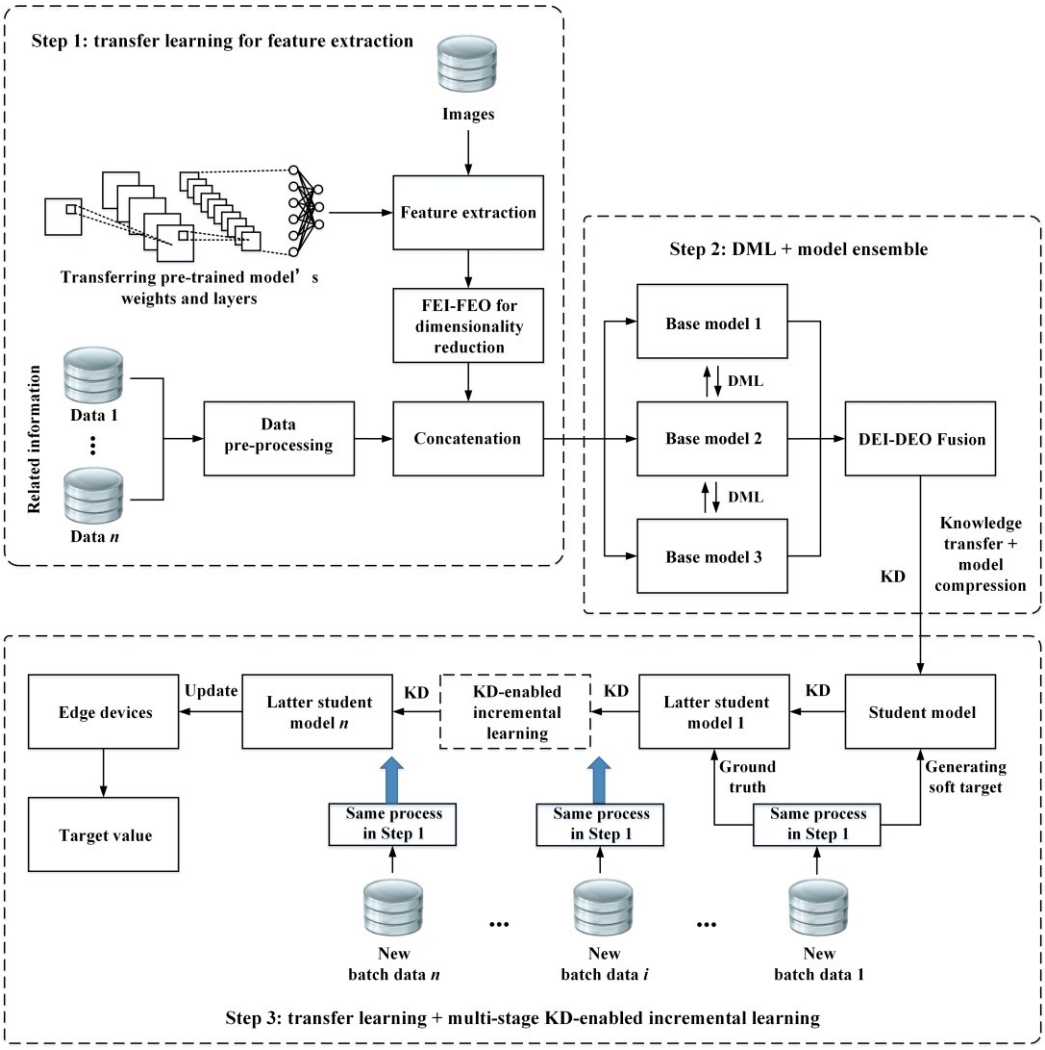

Figure 5.1 Illustration of the proposed methodology

In the second step, the features obtained from step 1 are used for base model training. DML strategy is adopted to train three neural network-based base models where the hidden knowledge learned by individual models can be shared during the training. The aim of employing DML is to improve the model performance. After the DML, a DEI-DEO model fusion strategy is applied to fuse the outputs of base models for building an ensemble model. The ensemble model is normally more robust and reliable, being less sensitive to outliers, noise, and bias. Then, a KD process is adopted to transfer the learned knowledge from the ensemble model to a student model with simplified structures.

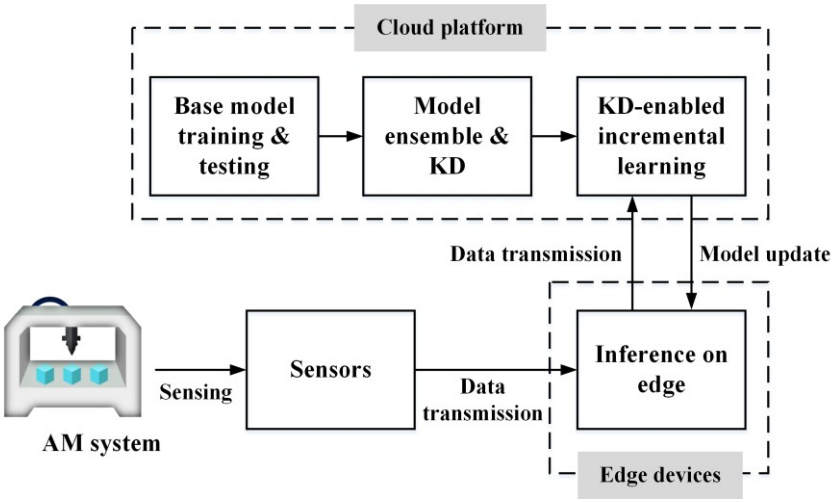

Figure 5.2 Illustration of the Cloud-edge fusion paradigm

Implementing KD aims to compress the ensemble model to the student model while simultaneously maintaining the performance of the student model by knowledge transfer. As the student model aims to be applied to edge devices for inferences, the structures of the student model should be simplified or less complicated than the ensemble model. In the third step, a multi-stage KD-enabled incremental learning approach is employed to improve the performance of the student model incrementally. In the multi-stage KD process, when the new batch data is collected, the previously trained student model acts as the teacher model for transferring learned knowledge to the latter student model with the same structures. In this incremental learning paradigm, the previously learned knowledge will be preserved in the latter student model while the knowledge inside new data will also be learned through training.

Figure 5.2 illustrates the Cloud-edge fusion process. At the initial stage, the data used for the tasks is collected by sensors from the AM system. Since no model is embedded on the edge devices at this stage, the data is directly sent to the Cloud platform. The base model training and testing, model fusion and knowledge transfer, and KD-enabled incremental learning processes are implemented on the Cloud platform due to their significant computing resource requirements. After KD on the ensemble model, the first student model is applied to edge devices to make inferences for the AM tasks.

When new data is coming, the embedded student model will make inferences on the edge devices while the new data is also sent to the Cloud platform for incremental learning. After KD-enabled incremental learning on the Cloud platform, the latter student model will be updated on the edge devices. The new data is also used for improving the base model. However, considering the computational resource efficiency, the base model is not retrained by using the whole dataset when every new data is collected. It is only retrained when the newly collected data accumulates to a certain volume. Through this paradigm, old knowledge and newly learned knowledge are fused incrementally from the Cloud to edge devices. The proposed methods and employed techniques in the three steps are described and explained in detail in the following sections.

5.2.1 Base Model Building via Transfer Learning and DML

- **Transfer Learning for Feature Extraction**

In real-world applications of AM, due to constraints of production cost and expenses, and the time-consuming of manual labelling, the collected data samples are usually insufficient to train a mature DL-based model for data analytics (e.g., CNN network for accurate image recognition and feature extraction). Even a well-trained DL model with complex structures is hard to be applied to fast-response scenarios, leading to the seeking of transfer learning approaches of pre-trained and well-trained models to leverage prior knowledge for saving costs and improved accuracy in some specific AM tasks. The purpose of transfer learning is to improve the performance of target learners by transferring knowledge from different but related source domains to target domains. Categorized by its solutions, transfer learning approaches can be classified into instance-based, feature-based, parameter-based, and relation-based approaches (Zhuang et al., 2020). Each approach has its pros and cons which need to be selected based on application scenarios.

Parameter-based approaches transfer knowledge at the model/parameter level while relational-based approaches mainly focus on the issues in relational domains. Feature-

based approaches use the features learned from one task to improve the performance on different but related tasks. They normally require fewer data samples to achieve faster convergence and better performance of the tasks. Therefore, in this study, feature-based transfer learning of DL is adopted and illustrated in Figure 5.3.

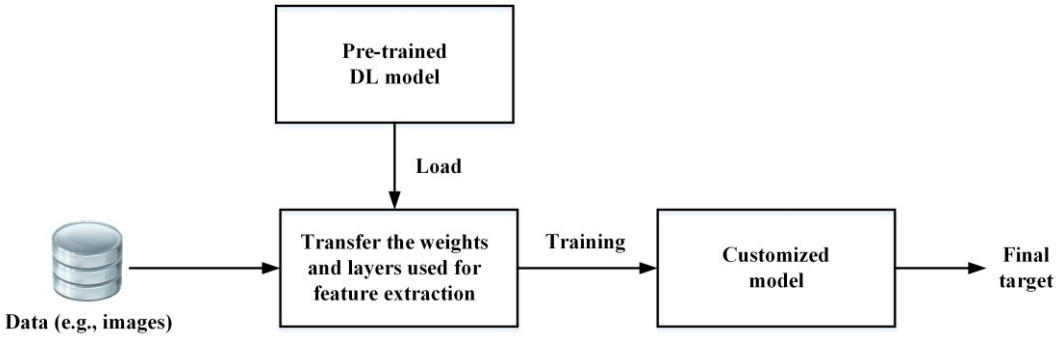

Figure 5.3 Illustration of the employed feature-based transfer learning approach for feature extraction

As shown in Figure 5.3, the pre-trained DL model should be trained on similar or related tasks (e.g., pre-trained CNN for image classification). The weights and layers used for feature extraction in the pre-trained model are transferred to process the data for training the customized model to obtain the final target of the task. In this study, the features extracted from the transferred model are used for base model training through DML.

- **DML for Base Model Training**

DML refers to a training and knowledge-sharing strategy between multiple neural network models and it was first proposed by Zhang et. al., (Zhang et al., 2018d) for multi-class classification tasks. The core concept of DML is to train the neural networks together so that each neural network can learn from the predictions of other models. This strategy was inspired by KD where the student model can learn from the teacher model. However, in real-world applications of AM, there are usually no well-trained or pre-trained teacher models for student models learning. In the DML, the base neural network models can learn from each other for knowledge sharing during training. The mutual learning paradigm makes the training more efficient and is capable of digging out hidden knowledge even from limited samples of data. In

addition, it normally leads to improved performance after DML than training individual models separately. Additionally, the DML strategy is flexible in training models with different architectures. The basic description of the original DML strategy for the muti-class classification task is presented as follows. Given n samples $\boldsymbol{X} = [x_1, x_2, \ldots, x_n]$ with M classes, and the ground truth label $\boldsymbol{Y} = [y_1, y_2, \ldots, y_n]$ with $y_i \in \{1,2,...,m\}$, for the neural network θ_1, the probability of class m for x_i can be calculated as:

$$p_1^m(x_i) = \frac{\exp(s_1^m)}{\sum_{m=1}^{M} \exp(s_1^m)} \tag{5.1}$$

In equation (5.1), s_i^m represents the output of the softmax layer in the neural network θ_1. For training the neural network θ_1, the cross-entropy error between the predicted classes and the ground truth labels is calculated as:

$$Loss_{CE_1} = -\sum_{i=1}^{n}\sum_{m=1}^{M} I(y_i, m)\log(p_1^m(x_i)) \tag{5.2}$$

In equation (5.2), $I(y_i, m) = 1$ if $y_i = m$, otherwise $I(y_i, m) = 0$. To improve the generalisation performance of the neural network θ_1, the training experience in the form of posterior probability of predictions is provided by another neural network θ_2 in the DML training. The Kullback Leibler (KL) Divergence is used to calculate the distance between the predictions of two neural networks. Then the overall loss function of neural networks θ_1 and θ_2 can be represented by the following equations:

$$D_{KL}(\boldsymbol{p}_2 \parallel \boldsymbol{p}_1) = \sum_{i=1}^{n}\sum_{m=1}^{M} p_2^m(x_i)\log\frac{p_2^m(x_i)}{p_1^m(x_i)} \tag{5.3}$$

$$Loss_{\theta_1} = Loss_{CE_1} + D_{KL}(\boldsymbol{p_2} \parallel \boldsymbol{p_1}) \tag{5.4}$$

$$Loss_{\theta_2} = Loss_{CE_2} + D_{KL}(\boldsymbol{p_1} \| \boldsymbol{p_2}) \tag{5.5}$$

In equations (5.3) ~ (5.5), the D_{KL} represents the KL distance between the predictions of neural networks and $Loss_\theta$ represents the overall loss function which combines the supervised loss function $Loss_{\mathrm{CE}}$ and the probability estimate of its peer neural network D_{KL} loss.

In this study, the DML strategy is extended to regression tasks on three base neural network models. The illustration of the extended DML on the regression task is shown in Figure 5.4. Given k input variables $\boldsymbol{Z} = [z_1, z_2, \ldots, z_k]$, and the ground truth values $\boldsymbol{V} = [v_1, v_2, \ldots, v_n]$, the mean squared error (MSE) is employed to calculate the error between the predicted and the ground-truth values for the regression. Hence, the loss function of MSE for the neural network θ is calculated as:

$$Loss_{MSE}(\theta) = \frac{1}{n}\sum_{i=1}^{n}(v_i - \hat{v}_i)^2, \ \hat{v}_i = \theta(\boldsymbol{Z})_i \tag{5.6}$$

In equation (5.6), $\hat{v}_i$ is the ith predicted values of the neural network θ on given variables $\boldsymbol{Z}$, and v_i is the ith ground truth value. The distance between the predictions of neural networks θ_1 and θ_2 for regression is calculated as:

$$D_{MSE}(\boldsymbol{y_2} \| \boldsymbol{y_1}) = \frac{1}{n}\sum_{i=1}^{n}(\hat{y}_{\theta_2,i} - \hat{y}_{\theta_1,i})^2 \tag{5.7}$$

In equation (5.7), $\boldsymbol{y}_2$ and $\boldsymbol{y}_1$ are the predictions of neural networks θ_1 and θ_2 respectively, $\hat{y}_{\theta,i}$ represents the ith predicted value of the neural network for sample i. Based on the equations (5.6) and (5.7), the overall loss function for DML on three neural networks can be denoted as the following equations:

$$Loss(\theta_1) = \alpha Loss_{MSE}(\theta_1) + \beta D_{MSE}(\boldsymbol{y}_2 \| \boldsymbol{y}_1) + \gamma D_{MSE}(\boldsymbol{y}_3 \| \boldsymbol{y}_1) \tag{5.8}$$

$$Loss(\theta_2) = \alpha Loss_{MSE}(\theta_2) + \beta D_{MSE}(\boldsymbol{y}_3 \parallel \boldsymbol{y}_2) + \gamma D_{MSE}(\boldsymbol{y}_1 \parallel \boldsymbol{y}_2) \tag{5.9}$$

$$Loss(\theta_3) = \alpha Loss_{MSE}(\theta_3) + \beta D_{MSE}(\boldsymbol{y}_1 \parallel \boldsymbol{y}_3) + \gamma D_{MSE}(\boldsymbol{y}_2 \parallel \boldsymbol{y}_3) \tag{5.10}$$

$$\alpha + \beta + \gamma = 1 \tag{5.11}$$

In equations (5.8) ~ (5.11), the α, β, and γ are the weights for the training loss, normally, the value of weight is equal to each other if no prior knowledge of the training neural networks is given. During the training, the objective is to minimize the loss function (5.8) ~ (5.10) by stochastic gradient descent. The following Table 5.1 shows the Pseudo-code of the DML process. A common criterion for convergence is no improvement of the model's performance that has been observed for a certain number of epochs during training.

Table 5.1 The Pseudo-code of the DML on three base models for regression tasks

Algorithm 1: DML on three base models for regression tasks
Input: Training data set X of the task, ground truth value Y, learning rate λ_t
Initialise: Initialise base models θ_1, θ_2, and θ_3; $t = 0$
Repeat:
$t = t + 1$
Sample data x from X
Compute predictions y_1, y_2, and y_3 by $\theta_1(x)$, $\theta_2(x)$, and $\theta_3(x)$ respectively
1: Based on loss function (5.8), compute the stochastic gradient and update θ_1 : $\theta_1 \leftarrow \theta_1 + \lambda_t \frac{\partial Loss(\theta_1)}{\partial \theta_1}$
2: Update the predictions y_1 of x by $\theta_1(x)$.
3: Based on loss function (5.9), compute the stochastic gradient and update θ_2 : $\theta_2 \leftarrow \theta_2 + \lambda_t \frac{\partial Loss(\theta_2)}{\partial \theta_2}$
4: Update the predictions y_2 of x by $\theta_2(x)$.
5: Based on loss function (5.10), compute the stochastic gradient and update θ_3 : $\theta_3 \leftarrow \theta_3 + \lambda_t \frac{\partial Loss(\theta_3)}{\partial \theta_3}$
6: Update the predictions y_3 of x by $\theta_3(x)$.
Until: convergence

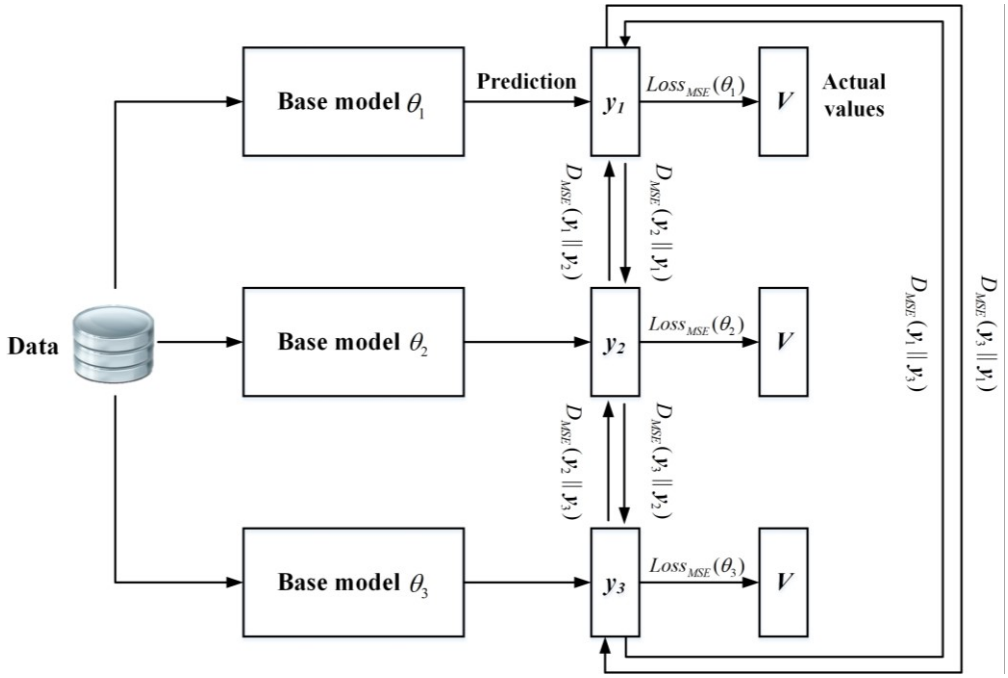

Figure 5.4 The illustration of DML for regression tasks on three base models

- **Fusion of Base Models**

The main objective of the model fusion is to improve the performance of the final model by combining the outputs of each base model. By integrating decision outputs from multiple sources to reduce overall uncertainty, the final prediction result is less sensitive to training data and is normally more reliable and robust. The ensemble method used for fusing the outputs of DML-trained base models is weighted averaging. The weighted averaging method is widely used in regression tasks where predictions from multiple models are averaged to obtain the final prediction. It can be denoted as:

$$\theta_{EN}(\boldsymbol{Z}) = \frac{\sum_{i=1}^{b} w_i \theta_i(\boldsymbol{Z})}{\sum_{i=1}^{b} w_i} \tag{5.12}$$

In equation (5.12), $\boldsymbol{Z} = [z_1, z_2, \ldots, z_k]$ is the given input with k variables, $\theta_i(\boldsymbol{Z})$ denotes the prediction of the ith base model, w_i denotes the weight assigned to the ith base model, and θ_{EN} is the final ensemble model. By weighted averaging the predictions of base

models, the ensemble model is normally more robust with improved performance, which can reduce bias and uncertainties from individual models.

5.2.2 Knowledge Transfer and Model Compression based on KD

Typically, the learning schemes of KD can be divided into three main categories, online distillation, offline distillation, and self-distillation. In online distillation, both the teacher and student models are updated simultaneously while offline distillation transfers the knowledge from a pre-trained teacher model to the student model. Self-distillation represents the student model of learning knowledge by itself. The teacher model in online distillation is updated with the most recent knowledge but is normally computationally intensive which is not suitable for edge devices with low computation ability. Hence, in the first stage of the proposed method, an offline distillation process is adopted to transfer prior knowledge from a pre-trained larger model to a smaller one to make the latter model more computationally efficient in deployment while retaining as much of the performance as possible.

- **Offline Distillation**

The offline distillation procedure includes two main steps: 1) a complex teacher model is first trained based on the collected datasets, and 2) leveraging the previously trained teacher model to provide extracted information, such as logits or intermediate features, to assist the student model through the distillation process. Offline distillation is efficient during the student's model training when the computational resources are limited in an online platform. However, as there is usually a capacity gap between teachers and students, students highly rely on their teachers.

Therefore, in this study, 3 base models are trained via DML strategies with limited training samples and a model fusion strategy is employed to ensemble the output of each base model. The final ensemble model is treated as the teacher model for KD. As training base models through DML require considerable computing resources, the

training process of the teacher model and the corresponding KD process are implemented offline.

- **Teacher-student Architecture**

The classic KD architecture employs a teacher-student paradigm for knowledge transfer where three major components are included, a teacher network, a student network, and the distillation operator, as shown in Figure 5.5.

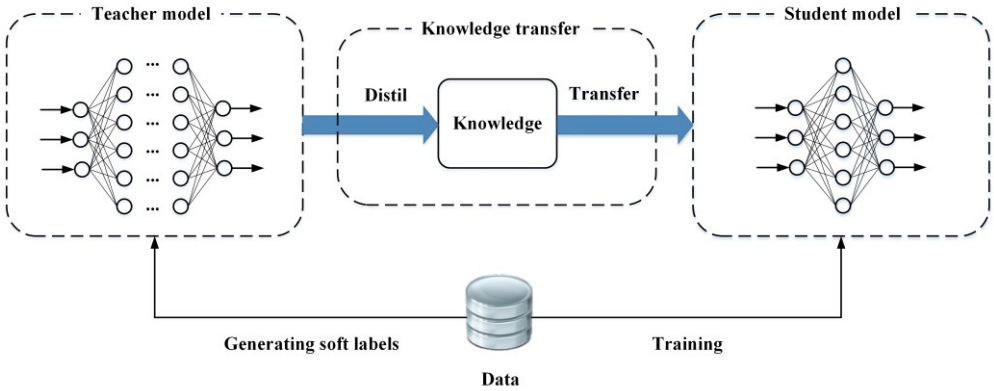

Figure 5.5 The schematic diagram of KD in the classic teacher-student architecture

In classification tasks, the soft labels are the probability distributions generated by the softmax function of the teacher model. In regression tasks, the soft labels are the predicted values of the teacher model. In KD, the softmax function is often modified with a temperature parameter *T*, shown as follows.

$$\text{softmax}_T(l_i) = \frac{\exp(l_i / T)}{\sum_j \exp(l_j / T)} \tag{5.13}$$

In equation (5.13), $\text{softmax}_T(l_i)$ represents the estimated probabilities by the softmax function for the given input that belongs to the class, l_i is the logit that passes through the softmax function. *T* represents the hyperparameter, called temperature, to control the importance of each soft target.

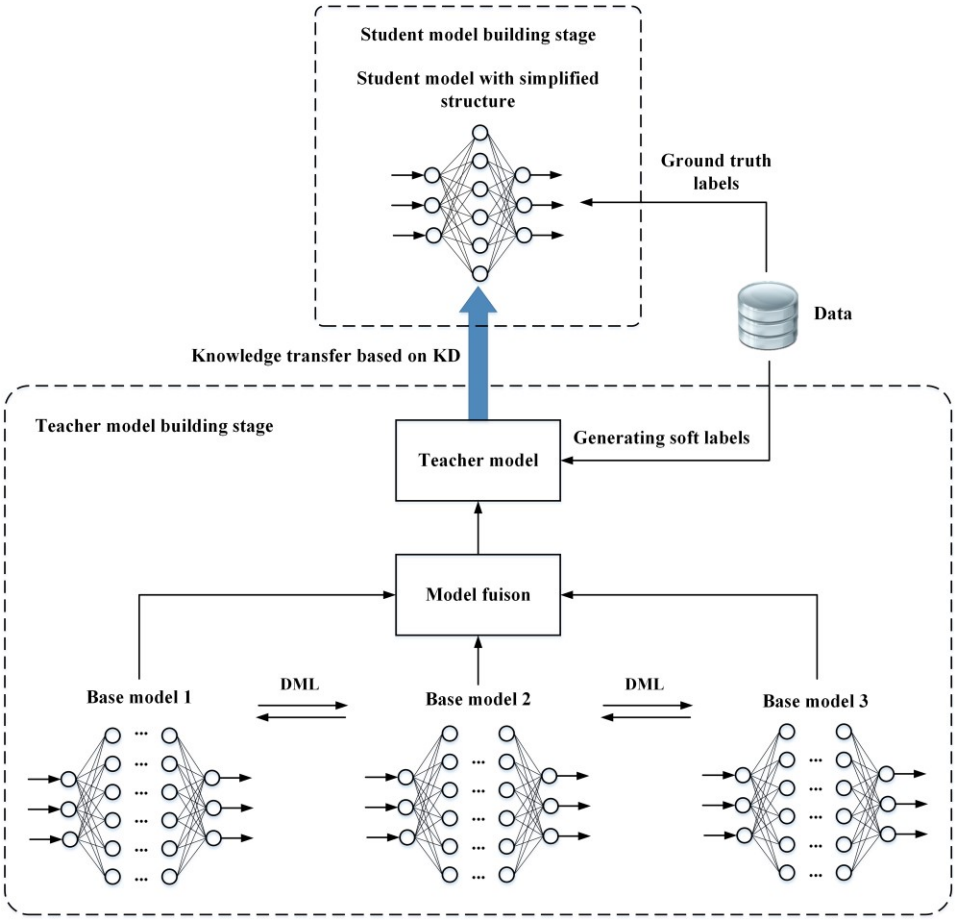

Figure 5.6 The schematic diagram of KD between the ensemble teacher model and student model

In the KD process, the teacher model is used to generate soft labels for student model training, and the student model is trained on both soft labels and ground truth labels. In this study, the teacher model is built based on the ensemble of three base models with complex structures which are trained through the DML strategy. The student model is designed to have a simplified structure. The KD process between the ensembled teacher model and student model is illustrated in Figure 5.6. In KD from the ensemble teacher model to the student model, the loss function for classification tasks is defined as:

$$Loss_{student} = \alpha Loss_{soft} + \beta Loss_{hard}, \ \alpha + \beta = 1 \tag{5.14}$$

$$Loss_{soft} = \sum_{i=1}^{n} q_i^T \log(\frac{q_i^T}{q_{si}^T}),\ q_i = \frac{\sum_j w_i q_{ij}}{\sum_j w_i} \tag{5.15}$$

In equations (5.14) ~ (5.15), T denotes the hyperparameter temperature in the softmax function, $\boldsymbol{q}_i$ is the weighted averaging soft label generated from the teacher ensemble, q_{si} is the soft label generated from student model, and w_i is the weight assigned to the base model in the teacher ensemble. $Loss_{soft}$ measures the difference between the student model's predictions and the teacher model's predictions while $Loss_{hard}$ measures the difference between the student model's predictions and ground truth labels. For regression tasks, the loss function for the student model is calculated as:

$$Loss_{student} = \alpha Loss_{distill} + \beta Loss_A,\ \alpha + \beta = 1 \tag{5.16}$$

$$Loss_{distill} = \frac{1}{n}\sum_{i=1}^{n}(\hat{v}_{Ei} - \hat{v}_{si})^2,\ \hat{v}_{Ei} = \frac{\sum_j w_i \hat{v}_{bij}}{\sum_j w_i} \tag{5.17}$$

$$Loss_A = \frac{1}{n}\sum_{i=1}^{n}(v_i - v_{si})^2 \tag{5.18}$$

In equations (5.16) ~ (5.18), v_i denotes the actual value, $\hat{v}_{Ei}$ is the predicted value of the teacher ensemble, and $\hat{v}_{si}$ is the predicted value of the student model. Through the KD from the teacher ensemble model with strong learning ability and complex structure to the simplified student model, the hidden knowledge of the teacher model is transferred to the student model during training. The learning capacity of the student model is inevitably lower than the teacher ensemble model, however, the student with simplified structures is more computationally efficient and normally performs better than the one training without a teacher model.

5.2.3 Cloud-edge Fusion through KD-enabled Incremental Learning

The capability of incremental learning is to continuously process the flow of information, digging out the hidden knowledge from the new data and absorbing it

while retaining, integrating, and optimizing old knowledge. Instead of training on static datasets, incremental learning techniques enable the model to learn incrementally from incoming data and are particularly effective in scenarios where the pre-trained model needs updating, the storage capacity of computing platforms is limited, the computational efficiency is a major concern, and the task requires real-time responses. As a result of learning new data, ML models tend to forget what they have learned previously, making catastrophic forgetting the main challenge in incremental learning.

KD-enabled incremental learning methods have been explored by several studies (Kang et al., 2022, Shi et al., 2022, Michieli et al., 2021, Zhang et al., 2020b, Hou et al., 2019) and have proven to be effective in preserving the old knowledge and absorbing new knowledge during the incremental learning process. To achieve fast responses and implement KD-enabled incremental learning on edge devices with limited computing resources, transfer learning of pre-trained models with similar tasks or related tasks is used to process data for feature extraction and for incremental learning on the edge side. The developed approach is shown in Figure 5.7.

As shown in Figure 5.7, the KD process from teacher ensemble to compressed student model is implemented on the Cloud platform (central server). Then the compressed model is loaded and treated as a previously trained model where KD is implemented for transferring learned hidden knowledge. In this KD process, the structures of the previous student model and the latter student model remain the same. Hence, the latter student model is not compressed but learns knowledge from the previous student model and incoming data. The KD process is repeated with the arrival of each batch of new data from edge devices to continuously improve the performance of models. By this incremental learning paradigm, the knowledge is transferred from the Cloud model to the final model that is embedded on the edge devices where the fusion of knowledge occurs during the multi-stage KD-enabled incremental learning process in the form of the weights update of neurons in the neural networks.

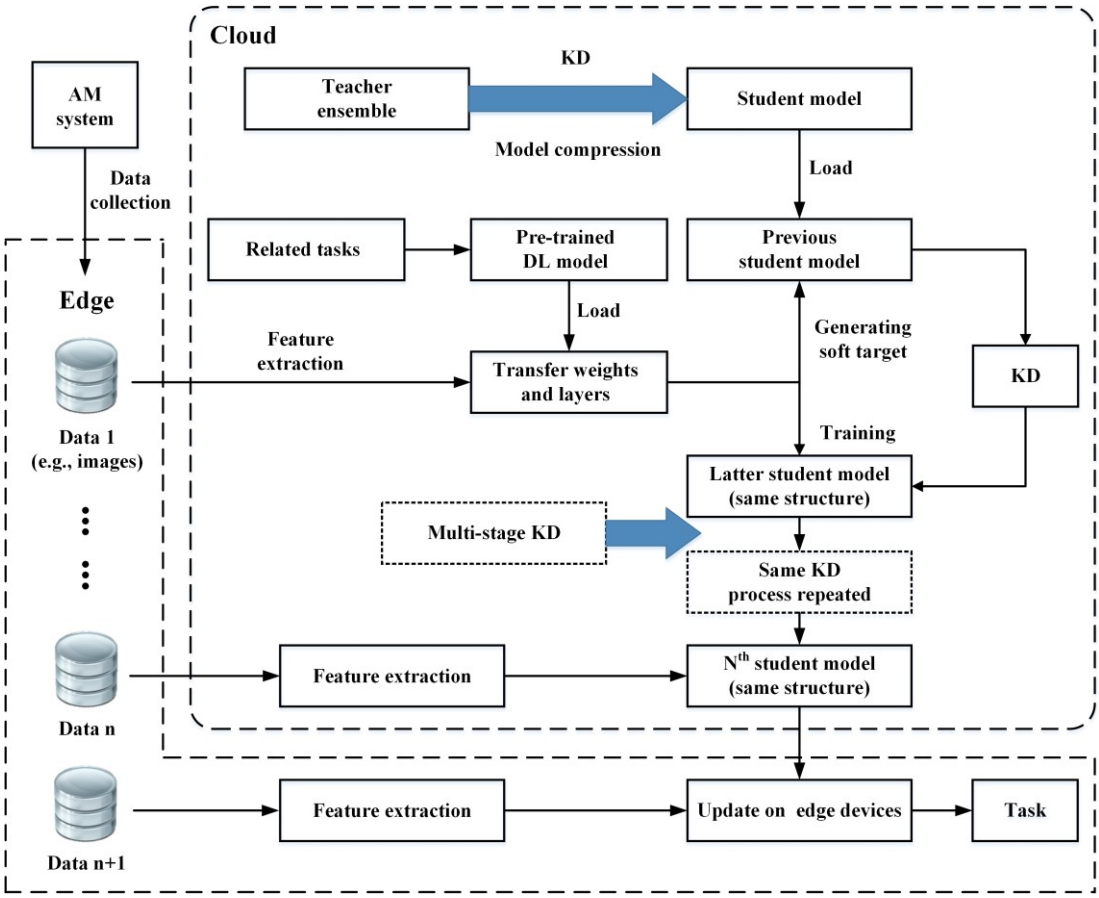

Figure 5.7 The proposed Cloud-edge fusion approach through multi-stage KD-enabled incremental learning

Take two-stage KD-enabled incremental learning for regression tasks as an example, given the training batch dataset X^P and ground truth value Y^P, load the pre-trained network θ_p and initialise the latter network θ_l. The structures of networks θ_p and θ_l are the same. The loss function for the KD process can be defined as:

$$Loss_{distill}(\theta_l) = \frac{1}{n}\sum_{i=1}^{n}(\boldsymbol{y}_{pi} - \boldsymbol{y}_{li})^2,\ \ \boldsymbol{y}_{pi} = \theta_l(x^p)_i,\ \boldsymbol{y}_{li} = \theta_l(x^p)_i \tag{5.19}$$

$$Loss_{true}(\theta_l) = \frac{1}{n}\sum_{i=1}^{n}(\boldsymbol{y}^p - \boldsymbol{y}_{li})^2 \tag{5.20}$$

$$Loss_{latter} = \alpha Loss_{distill} + \beta Loss_{true},\ \alpha + \beta = 1 \tag{5.21}$$

In equations (5.19) ~ (5.21), the $Loss_{distill}(\theta_l)$ represents the MSE of predictions between the pre-trained network θ_p and the latter network θ_l, and $Loss_{true}(\theta_l)$ represents the MSE between the predictions of the latter network θ_l and the ground truth values. Then the overall loss function is denoted as $Loss_{latter}$. In the second stage, the latter network θ_l will be treated as the teacher model for KD where the process is repeated as the same as it is in the first stage. The Pseudo-code for the whole process described above is presented in Table 5.2.

Table 5.2 The Pseudo-code of the two-stage KD-enabled incremental learning

Algorithm 2: Two-stage KD-enabled incremental learning for regression tasks

Input: Training batch dataset X^p of the task, ground truth value Y^p, learning rate λ_l

Initialise: Load pre-trained network θ_p, Initialise latter network θ_l; $t_p = 0$, $t_l = 0$

Step 1: KD from network θ_p to latter network θ_l

Repeat:

$t_p = t_p + 1$

Sample sub-batch data (x^p, y^p) from (X^p, Y^p)

Compute predictions y_p and y_l by networks $\theta_p(x^p)$ and $\theta_l(x^p)$ respectively

Based on loss function (5.20), compute the stochastic gradient and update θ_l :

$$\theta_l \leftarrow \theta_l + \lambda_l \frac{\partial Loss(\theta_l)}{\partial \theta_l}$$

Until: convergence

Step 2: Collecting batch dataset X^l of the task, ground truth value Y^l, Treat network θ_l as the teacher network, KD from θ_l to latter network θ_{l2}

Initialise: Initialise the second latter network θ_{l2}

Repeat:

$t_l = t_l + 1$

Sample sub-batch data (x^l, y^l) from (X^l, Y^l)

Compute predictions y_{l1} and y_{l2} by networks $\theta_l(x^l)$ and $\theta_{l2}(x^l)$ respectively

Based on loss function (5.20), compute the stochastic gradient and update θ_{l2} :

$$\theta_{l2} \leftarrow \theta_{l2} + \lambda_l \frac{\partial Loss(\theta_{l2})}{\partial \theta_{l2}}$$

Until: convergence

Output: The second latter network θ_{l2}

The proposed Cloud-edge fusion paradigm and approaches in this chapter aim to deal with (1) building analytics models to tackle the AM tasks with a limited amount of training data in the initial stage, (2) fusion of previously learned knowledge and new knowledge incrementally for the improvement of model performance, (3) towards implementation of the analytics model on the devices or platforms with constrained computational resources. A case study is carried out to demonstrate the feasibility and effectiveness of the proposed method, presented in the following sections.

5.3 Multi-stage KD-enabled Incremental Learning for AM Energy Consumption Prediction

In Chapter 4, the datasets collected for AM energy consumption prediction have sufficient samples to train a DL-based model with relatively complicated structures. However, as discussed in previous chapters, in real-world applications of AM, the collected data is usually with a limited number of samples due to the constraints of time and expenses. Some AM material powders are expensive and testing the quality of the products can be time-consuming which leads to the insufficient amount of training samples to build robust and reliable analytics models for some specific AM tasks. Additionally, some AM tasks require fast responses of models and the analytics models built for the tasks are not suitable to be applied in devices with limited computing resources. To address these challenges, this case study demonstrates the application of the proposed Cloud-edge fusion method through multi-stage KD-enabled incremental learning for energy consumption prediction.

5.4 Experimental Setup

The detailed description of the AM energy consumption data collection and preparation can refer to Section 4.4.1. According to the task scenario, the data samples of AM energy consumption collected at the initial stage are limited, the strategy is to leverage the proposed transfer learning and KD-enabled incremental learning method

to tackle the task. Three experiments were designed to demonstrate the feasibility and effectiveness of the proposed method.

5.4.1 Evaluation Metrics

As energy consumption prediction is a regression task, RMSE and mean absolute error (MAE) are adopted. R^2 was adopted for evaluation of the previous regression task, however, the increase of R^2 doesn't necessarily reflect the improvement of the model's non-linear relationship fitting ability. Hence, RMSE and MAE are used to reflect the improvement of the models after DML and KD-enabled incremental learning. Besides, as the developed model aims to be applied in edge devices with constrained computing resources, the model size and inference time also need to be considered. The MAE is calculated by the following equations:

$$MAE = \frac{\sum_{i=1}^{n} | y_i - \hat{y}_i |}{n} \tag{5.22}$$

In the equation, y_i, and $\hat{y}_i$ are actual values and predicted values respectively. MAE calculates the average of the absolute errors between the predicted values and the actual values. It is robust to outliners so that large errors don't disproportionately affect the metric.

5.4.2 Experiment 1: Transfer Learning Combined with FEI-FEO Strategy

Since the training samples of energy consumption data are limited at the initial stage, it is hard and almost impossible to train an entirely customized DL-based model (e.g., M-CNN-LSTM) with reliable and robust performances. Therefore, based on the proposed method in Section 5.2.1, transfer learning combined with the FEI-FEO fusion strategy is applied in this experiment. To obtain relatively accurate representations of layer-wise images of CAD models, the weights and layers used for feature extraction of pre-trained CNN models with (similar tasks or related tasks) can

be transferred for extracting convolutional features. These extracted convolutional features are then concatenated with essential energy consumption-related features to be fed into three DL-based models for energy consumption prediction via DML. Considering the extracted convolutional features are normally sparse and contain a large number of feature vectors while the volume of training samples is small, the FEI-FEO strategy is adopted to reduce the dimensionality of the extracted convolutional features. The overall method is illustrated in Figure 5.8.

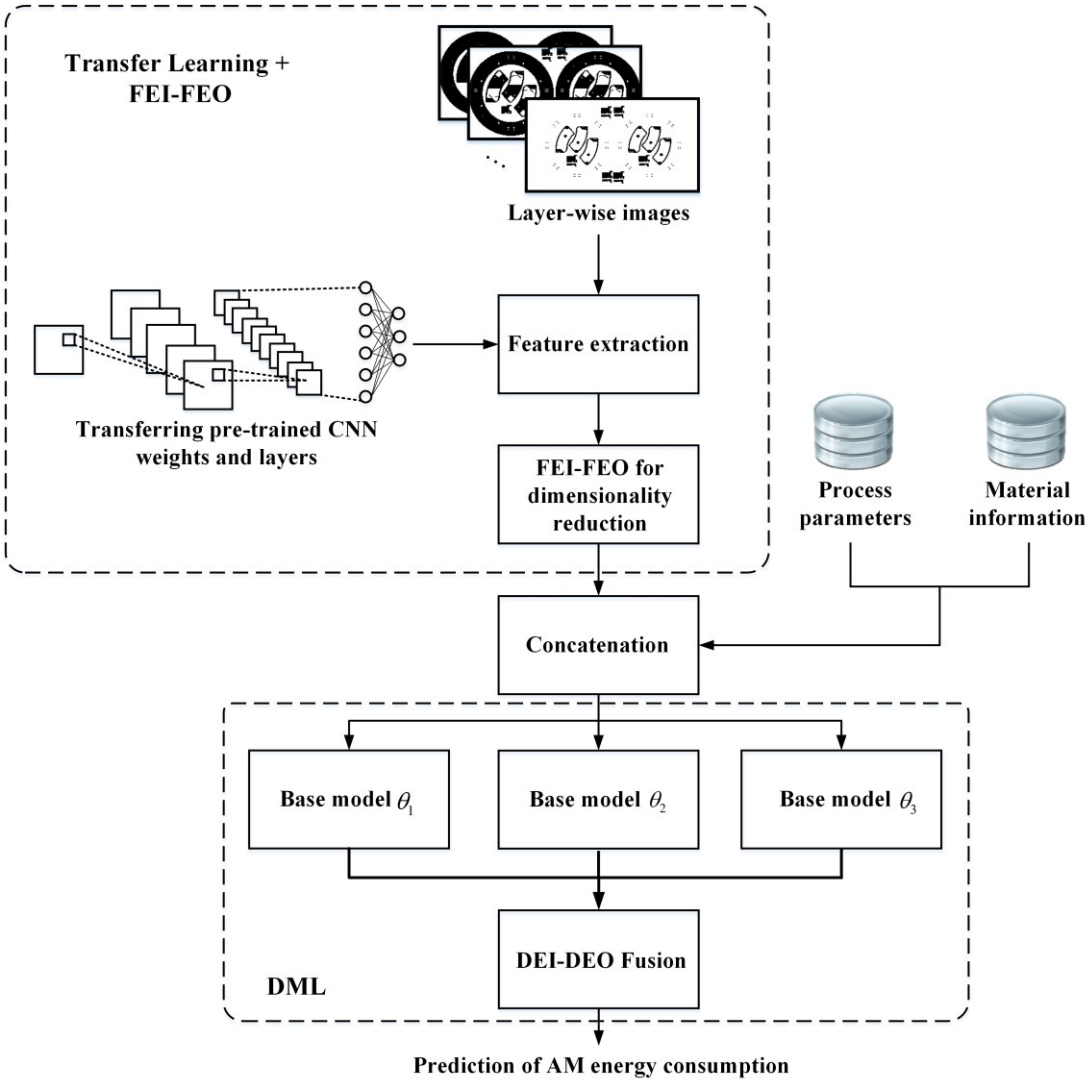

Figure 5.8 The transfer learning combined with FEI-FEO strategy for energy consumption prediction via DML

The pre-trained CNN model adopted in this study is MobileNet V3 (Howard et al., 2019) which is an efficient CNN model for multi-class classification tasks. It was trained on the ImageNet dataset (with more than a million image samples) and had the best performances in the MobileNet series. It is typically applied in resource-constrained environments or devices due to its efficiency, small size of model, and adaptability.

The FEI-FEO technique used in this study is LLE, which performed the best for fitting the layer-wise image dimensionality reduction (Section 4.4). In DML, for using the features extracted by MobileNet V3 as the input, three DNN models with different numbers of dense layers and neurons were used as the base models (DNN1 has one dense layer with 32 neurons and an output layer, DNN2 has one dense layer with 64 neurons and an output layer, and DNN3 has one dense layer with 128 neurons and an output layer). For comparison, three different CNN architectures, but their dense layers and the number of neurons are the same as the previous DNN networks respectively. The layer-wise images of CAD models are directly used as input into these CNN models. A DEI-DEO model fusion strategy (weighted averaging) is adopted to fuse the outputs from the three base models for the final prediction of energy consumption. As the experiment assumes that the collected data is limited at the initial stage, the training samples for base model training only use 100 sample images.

- **Results of Experiment 1**

Table 5.3 presents the experimental results from experiment 1. As is shown, comparing the performances of ensemble models, the best prediction results in terms of RMSE and MAE (7.65 and 4.65) were obtained from the ensemble model with the strategy that transferred MobileNet V3 for feature extraction and employed LLE for feature fusion and dimensionality reduction. The ensemble model combined with features extracted from MobileNet V3 but without dimensionality reduction achieved 10.42 and 9.48 for RMSE and MAE respectively, which was slightly better than the performance (12.17 and 10.69) of the ensemble model from three CNN base networks.

These results show that employing a pre-trained model from related tasks or similar tasks for feature extraction contributes to the improvement of the final model.

Table 5.3 Performances of models in experiment 1

Models	RMSE (Wh/g)	MAE (Wh/g)
CNN 1	14.10	12.56
CNN 2	14.12	12.58
CNN 3	7.81	6.82
Ensemble 1	**12.17**	**10.69**
DNN 1 + MobileNet V3	2.54	1.46
DNN 2 + MobileNet V3	14.92	13.57
DNN 3 + MobileNet V3	14.91	13.56
Ensemble 2 + MobileNet V3	**10.42**	**9.48**
DNN 1 + MobileNet V3 + LLE	7.56	4.56
DNN 2 + MobileNet V3 + LLE	7.88	4.82
DNN 3 + MobileNet V3 + LLE	7.46	4.57
Ensemble 2 + MobileNet V3 + LLE	**7.65**	**4.65**

However, due to the limited data samples used for training, the ensemble model either used or did not use the transfer learning strategy performed almost the same. This was largely due to the number of feature vectors far exceeding the number of training samples, leading to underfitting problems. It can be seen from these results that employing proper FEI-FEO techniques can reduce redundant information and help avoid underfitting problems. The worst results were obtained by the DNN2 combined with the transfer learning strategy, having an RMSE of 14.92 and MAE of 13.57. This showed that directly using extracted features without fusion for training on small data samples can lead to underfitting problems. In addition, some base models achieved relatively good performances (e.g., CNN3, DNN1+MobileNet V3) even without transfer learning, feature fusion, or ensemble. This could result from the randomness, bias, and overfitting problems.

5.4.3 Experiment 2: With DML or Without DML

In experiment 2, the training of models is implemented on two strategies, with DML or without DML. This experiment is conducted to compare the performances of base models trained with different strategies to show whether DML is effective or not. The base models designed in this experiment contain different algorithms and structures. As the core concept of DML is to learn from other models during the training process, the base model can learn different hierarchies of hidden information from different algorithms. Therefore, 1D-CNN and DNNs with different structures are used as the base models. The 1D-CNN has 3 convolutional layers with kernel size 3 and 2 max-pooling layers. The neurons of convolutional layers are 16, 32, and 64 respectively. The first DNN base model has 4 dense layers with neurons 128, 64, 32, and 16 respectively. The other DNN base model has 3 dense layers with neurons 256, 128, and 64 respectively. For capture the features more accurately, VGG16 is adopted in this experiment as the pre-trained model for transfer learning. The method used for the fusion of the base models is weighted averaging which assigns lower weights to the models with significant differences in prediction to avoid bias. The data used in experiment 2 for training are 100 samples (same as experiment 1).

- **Results of Experiment 2**

The results of experiment 2 are presented in Figure 5.9 and Figure 5.10. Overall, from both figures, the performances of models trained via DML were better than the models trained without DML. It's apparent that DML helped improve the learning ability and knowledge-sharing process between peer models. Figure 5.9 shows the RMSE of predictions of models with and without DML. The best RMSE result (3.62) was achieved by the base CNN model trained via DML. The worst performance of RMSE (8.02) was achieved by the base DNN3 model trained without DML.

In Figure 5.10, the best MAE (2.65) was obtained by the base CNN model trained via DML while the worst result was achieved by the base DNN3 model without DML. The ensemble model assigned a lower weight to the base CNN model to avoid bias. It

is worth noting that although the student model obtained by the KD process performed slightly worse than the teacher ensemble model, it still outperformed most of the base models which had relatively more complex structures.

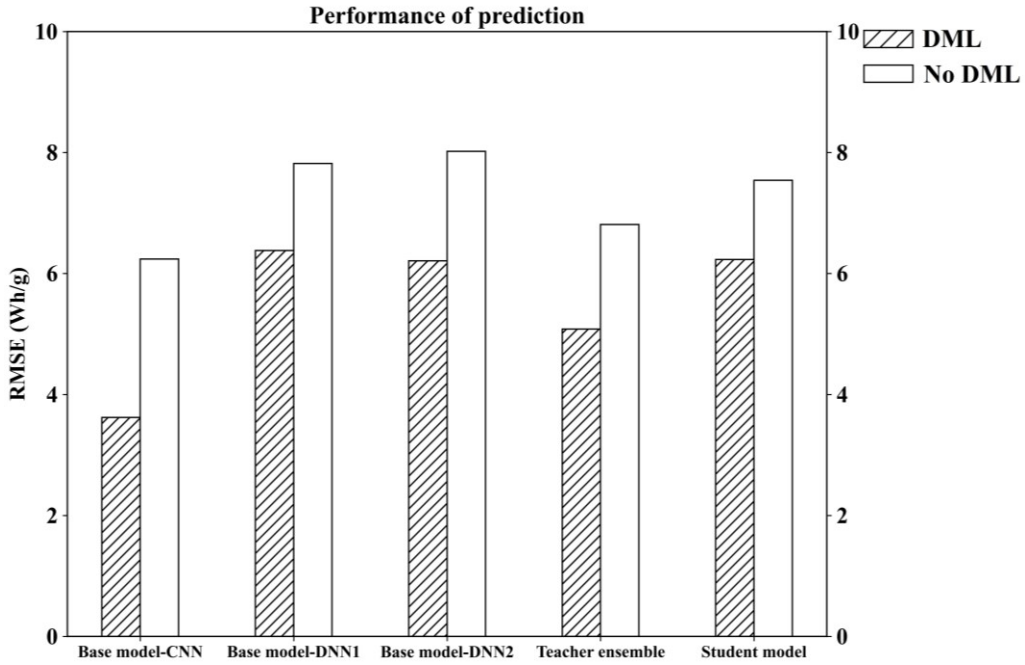

Figure 5.9 The RMSE results of models trained via different strategies

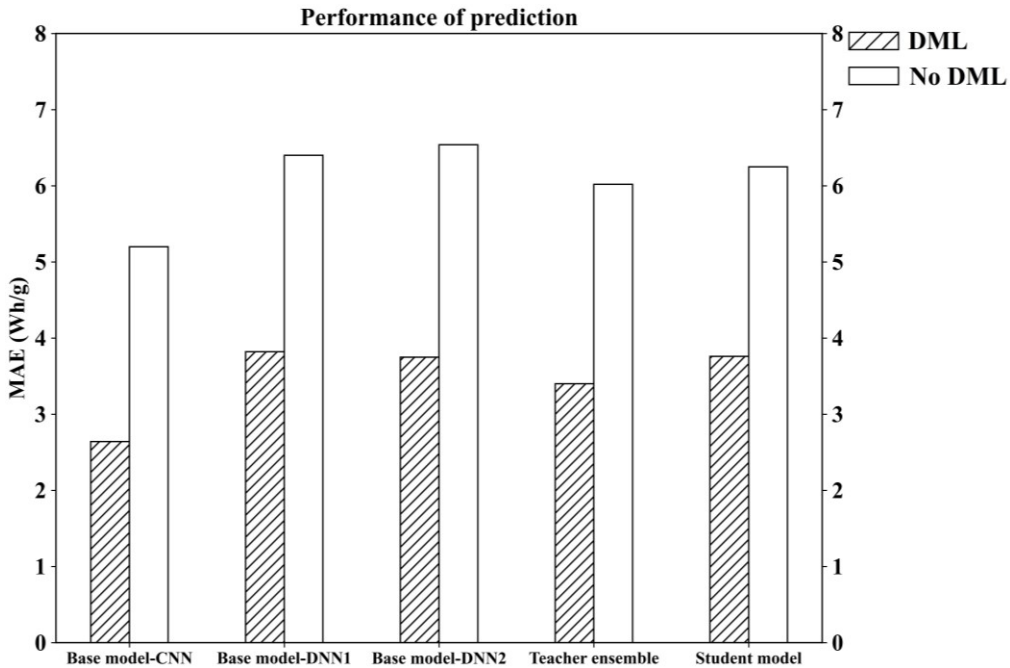

Figure 5.10 The MAE results of models trained via different strategies

It can be seen from the results that implementing the DML training strategy can improve the performance of peer models even on small samples of training data. In addition, the learned knowledge can be transferred effectively from the teacher ensemble model to the student model by the KD process.

5.4.4 Experiment 3: Multi-stage KD-enabled Incremental Learning

In this experiment, the multi-stage KD-enabled incremental learning method is adopted to learn and predict AM energy consumption, illustrated in Figure 5.11.

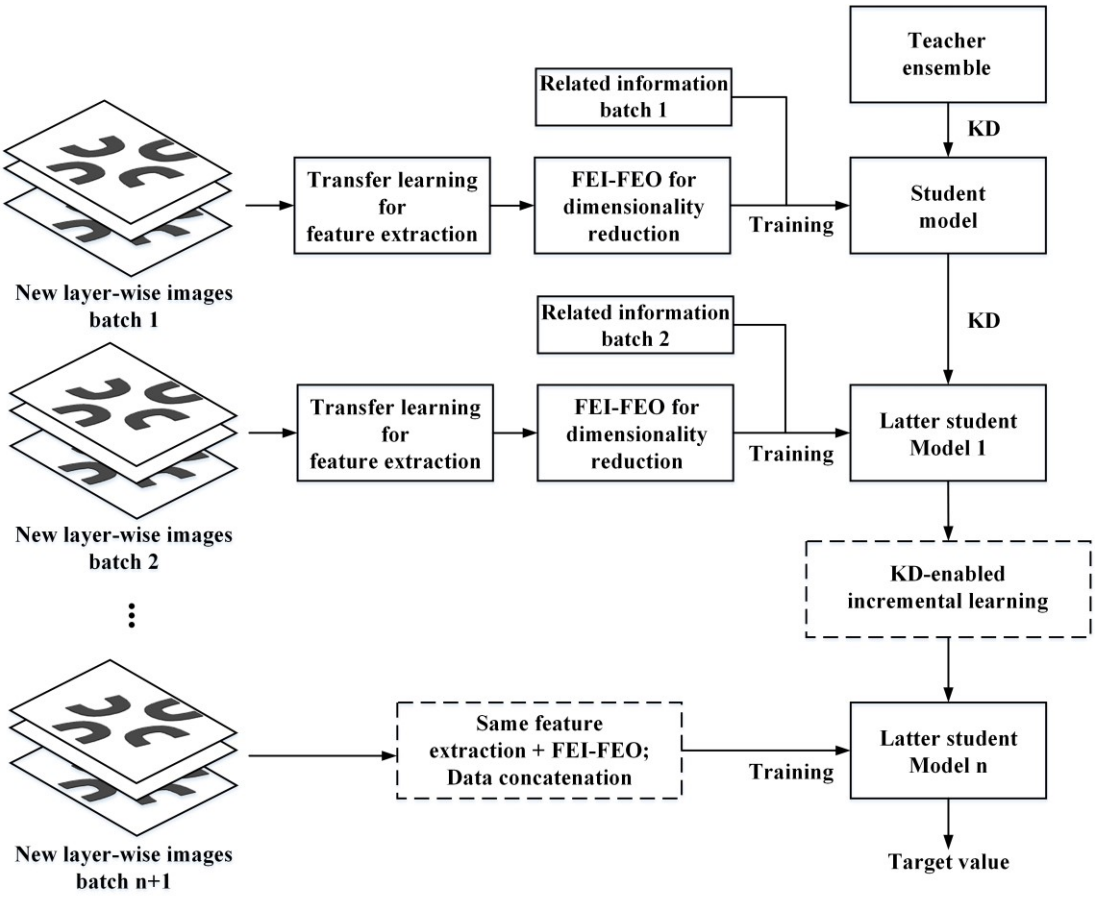

Figure 5.11 Multi-stage KD-enabled incremental learning for AM energy consumption prediction

The teacher ensemble model is obtained through experiment 2, where 1D-CNN and two DNN networks are used as base models. For knowledge transfer and model compression, the first KD is implemented between the teacher ensemble model and

the first student model. To simplify the structures of the student model, the student model only uses 1D-CNN with 2 convolutional layers with kernel size 3 and 2 max-pooling layers. The neurons are 32 and 16 for the convolutional layers respectively. In KD-enabled incremental learning, the structures of the previous student model and the latter student model retain the same so that the old knowledge can be transferred to the new student model smoothly. During the training, the test samples are obtained randomly from the whole dataset (5085 samples in total) and the data used for training contains 50 samples for each batch. Each batch of data is used for implementing one KD process. For comparison, another model is designed to have the same structures as the student model, but it is trained on the batch data continuously without KD.

- **Results of Experiment 3**

The experimental results are shown in Figures 5.12 and 5.13 where the RMSE and MAE of student models trained with and without KD-enabled incremental learning are presented. As is shown in Figure 5.12, the solid line in red represents the RMSE of the student model trained with the KD-enabled incremental learning strategy (KD_IL) for each batch and the dotted line in black shows the RMSE of the student model trained without the strategy (Without KD_IL). It can be seen from the red line that the trend of RMSE declined apparently during the batch training while the dotted line in black fluctuated severely.

The RMSE of the student model trained with the KD_IL showed fewer fluctuations during training which was largely due to the model learning both knowledge from the previous model and new data. It needed to fit both data distributions (previous and new) rather than to fit new data only. Large differences between peak values and valley values are observed in the dotted line for almost every 10 batches of training. This is because the student model trained without the KD_IL strategy was easily affected by the changes in data distributions. In addition, even after 80 batches of training, a clear decline trend is not observed in the dotted line. For the solid line in red, not only a clear decline trend is observed but also a relatively more stable performance during training with the changes in data distributions can be seen.

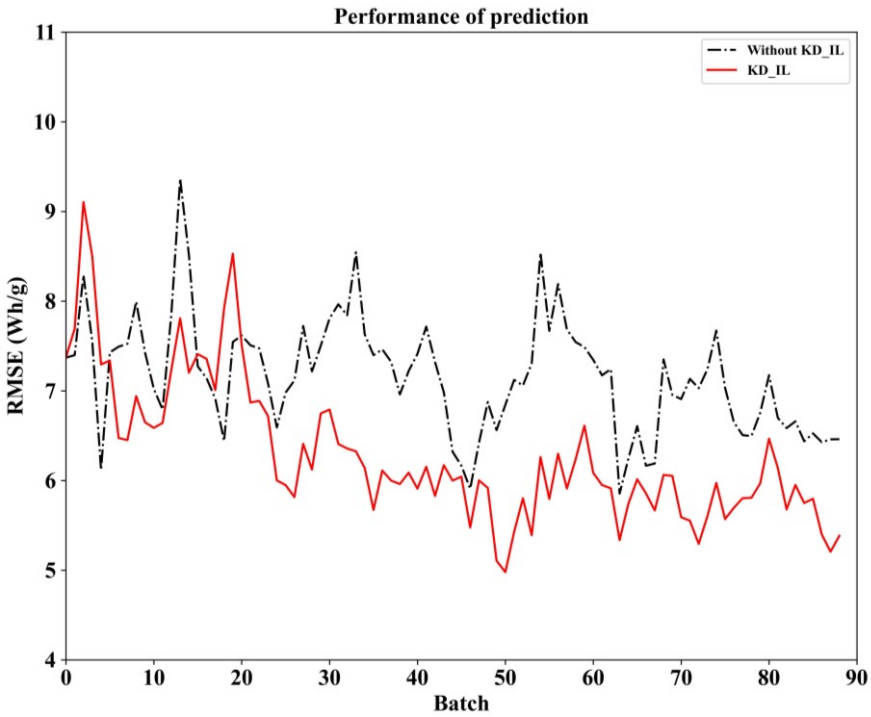

Figure 5.12 The RMSE of student models trained with and without KD_IL strategy

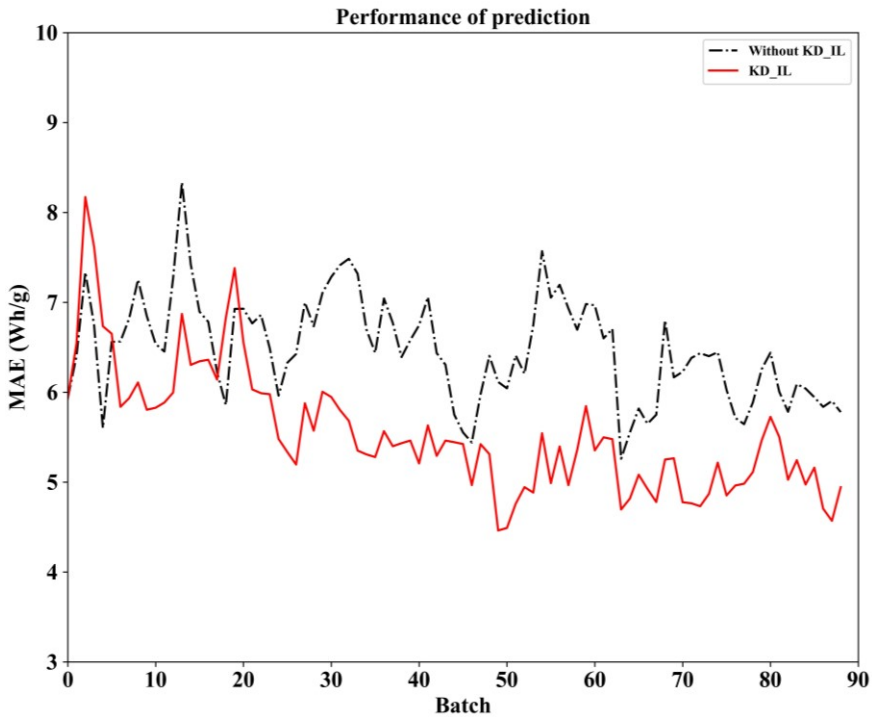

Figure 5.13 The MAE of student models trained with and without KD_IL strategy

In Figure 5.13, for both the solid line and dotted line, similar trends to that observed in Figure 5.12 can be seen. The MAE of the student model trained with the KD_IL strategy was declined stably. From both figures, the student model trained with the KD_IL showed better performance than the model trained without the KD_IL. It learned hidden knowledge not only from the previous model but also from new data. The old knowledge can be preserved in the latter student model in the form of KD. As the trained student model aims to be deployed in devices or platforms with constrained computing resources, detailed information of the models is presented in Table 5.4.

Table 5.4 Detailed information of the models

Model	Model size (MB)	Trainable parameters	Average training time/ epoch (ms)	Average prediction time/ batch (ms)
Teacher ensemble	9.77	844067	N/A	88
Student_KD_IL	2.09	543233	131	56

As shown in Table 5.4, the model size of the student model (2.09MB) is much smaller than that of the teacher ensemble model (9.77MB). Since the teacher ensemble model adopted DML strategy for training, the training times of teacher and student models were not comparable. Also, the student model using the KD_IL strategy required 131 ms for training per epoch and only took 56 ms to make inferences on each batch of data (50 samples). It is easy to apply on the edge devices for quick responses. In addition, it didn't need much training time for incremental learning which could reduce the time of updating the model from the Cloud server to edge devices.

5.5 Discussion

In this chapter, a case study was carried out on the energy consumption prediction task. The task assumed that the data samples collected from AM production at the initial stage were small. Three experiments were conducted that aimed to demonstrate the feasibility and effectiveness of the proposed transfer learning-based multi-stage KD-enabled incremental learning method for AM energy consumption prediction. In

experiment 1, the model trained with transfer learning combined with the FEI-FEO strategy had the best prediction performances in terms of RMSE and MAE. The weights and layers of pre-trained CNN models (MobileNet V3 and VGG16) were transferred to extract representative features from layer-wise images of CAD models. Although the prediction results showed that the extracted features are informative and contain critical information about CAD models, the model trained on original features without the processing with FEI-FEO fusion had bad performances in terms of RMSE and MAE. This was largely due to the sparsity of features and the number of feature vectors far exceeded the number of training data samples.

Also, it still recommends transferring the model that has been trained on more related tasks. For example, if the task requires predicting the tensile strength of the AM-produced parts, the pre-trained CNN model used for transfer learning is better trained for porosity detection or porosity prediction tasks since the extracted features can be more accurate and task-related. As these kinds of pre-trained models are barely shared in AM communities, choosing public pre-trained DL models with relatively similar tasks is also an acceptable alternative option. This is because the customized model for your tasks also needs to be trained where the weights can be fine-tuned to fit the specific task value. The reason for choosing MobileNet V3 for transfer learning in experiment 1 is that it not only maintains accuracy but also efficiency, which makes it suitable to apply in edge devices.

In experiment 2, the improved performance of models trained via the DML strategy was observed. The DML enabled the base models to learn from each other where some hidden information learnt by individual models could be shared during the training. This hidden information includes several aspects, such as feature representation and bias correction. The models adjust their neuron weights based on the feedback from the loss function during training, learning more diverse feature representations for better prediction accuracy. Though three base models with different algorithms and structures were employed in this case study, it could be extended to more than three models with more complex structures and diverse algorithms. However, this will

require large computational resources and training times. Additionally, since it is trained on small data samples, the performance of models won't be improved significantly with the growth of base models and their complexity. On the contrary, underfitting problems may occur. Using the DEI-DEO strategy to fuse the outputs from base models can improve stability and robustness, making the ensemble model less sensitive to outliers and bias.

In experiment 3, the proposed transfer-learning-based KD-enabled incremental learning method was proven to be effective. The model with the KD_IL strategy was observed to be more stable and effective in learning new knowledge while still preserving old knowledge transferred from the previous model. The student model had a much smaller size (only 2.09 MB) than the teacher ensemble model with a much faster response time for inferences. According to the computing capabilities of edge devices in the current market, the developed student model is easy to apply for fast responses. Also, this Cloud-edge fusion paradigm doesn't require re-training teacher ensemble models with the whole datasets when the new data comes. This considerably reduces computing costs and improves resource efficiency. As mentioned in previous sections, this experiment was used to demonstrate the feasibility and effectiveness of the proposed method in the case of AM energy consumption prediction. For specific edge devices, customized models can be designed to tackle specific tasks. In the future work, the complex teacher model and compressed student model can be embedded in different edge devices for performance testing.

5.6 Summary

The scarcity of large-scale datasets presents a significant bottleneck for leveraging ML and DL to tackle critical challenges in AM. The demand for large-scale, diverse, and high-fidelity data is critical to move from empirical, trial-and-error methods to data-ML-based driven approaches that can unlock the full potential of AM technologies. In addition to the scarcity of data issues at an initial stage, some AM tasks often require fast responses or near real-time responses that lead to the analytical model becoming more computationally efficient. The contribution of this chapter is that a transfer

learning and multi-stage KD-enabled incremental learning method was proposed to tackle the issues. To tackle the issue of the limited amount of data samples, the transfer learning approach combined with the DML training strategy was proposed which has been demonstrated effective in improving the performance for energy consumption prediction in the experiments. Then, to implement the prediction model on the devices with constrained computing resources for fast responses, a transfer learning-based multi-stage KD-enabled incremental learning method was proposed to transfer the knowledge from the pre-trained teacher ensemble model to the compressed student model to learn new knowledge incrementally. The student model can be trained and learned from the Cloud server and updated to edge devices when new data samples is collected. This Cloud-edge fusion paradigm has potential to be implemented in real-world AM applications.

Chapter 6 Case Studies

6.1 Introduction

To demonstrate the feasibility and effectiveness of the proposed task-driven data fusion framework and methodology, three case studies on different AM tasks were carried out, including mechanical property prediction of additively manufactured LS, porosity defect classification, and investigating the effect of the remelting process on part density. (1) In case study 1, the task is to predict the mechanical properties of AM-produced LS with the requirement that the prediction model can be applied to different materials and LS. Considering the requirement, the data and information to be collected should be relevant to the mechanical properties of AM-produced parts, such as the used material density, LS types, process parameter settings, etc. The mechanical property data of printed LS need to be collected from the part qualification stage (process stage 4) by using specific test equipment. As the LS is complex, the fusion strategies should consider the complexity of LS for the prediction model. (2) In case study 2, the AM task is to classify different porosity defects of AM-produced parts Therefore, it is predictive analytics involving porosity defect classification. In order to obtain different porosity defects of parts, different combinations of process parameters for production should be employed. For acquiring detailed information of defects, cross-section micrograph images of AM-produced parts need to be collected. The fusion strategy should be evaluated by the classification performances. (3) In case study 3, the AM task aims to investigate the joint effect of different remelting process parameters on printed part density.

Table 6.1 The details of applying the proposed task-driven data fusion framework and methodology for the case studies

Step	Sub-items		Case study 1	Case study 2	Case study 3
Step 1	AM task		Mechanical property prediction of LS	Porosity defect classification of parts	Investigation of the joint effect of remelting processes on part density
	Task requirements		Applicable to different materials	Classification of different defect patterns resulting from different parameter settings	Identifying the relationship between remelt process and part density
	Type of the target value		Quality	Quality	Quality
	Involved decision-making activities		Predicting mechanical properties of LS manufactured by using different materials	Classification of the porosity defects of parts based on the micrograph images of cross-sections	Predicting part density level
	Type of data analytics		Predictive analytics	Predictive analytics	Diagnostic analytics
Step 2	Data required for the task		Design CAD models, material information, parameter setting data, the mechanical property of final printed parts	Parameter setting data, micrograph images of cross-sections of printed parts	Parameter setting data, remelting strategy, the density of final printed parts
	Data acquisition	Process stage 1	AM design software, material test equipment	N/A	N/A
		Process stage 2	Machine log file	Machine log file	Machine log file, manual records

		Process stage 3	N/A		N/A		N/A	
		Process stage 4	Mechanical property test equipment		XCT equipment		Density test equipment	
	Data characterization		Volume	5MB (total)	Volume	780 MB (total)	Volume	>1GB (total)
			Velocity	N/A	Velocity	N/A	Velocity	N/A
			Variety	3D models, 1D numerical data	Variety	2D images, 1D numerical data	Variety	1D numerical data (porosity is calculated based on the 3D reconstruction)
Step 3	Data dimensionality		Multi-dimensional data		Multi-dimensional data		Data in the same dimension	
	Data fusion strategy		FEI-DEO		FEI-FEO + FEI-DEO		FEI-DEO	
	Data fusion techniques consideration		The fusion technique should consider the complexity of 3D geometry features, and the sample size		The fusion technique should consider the complexity of porosity images and extracted features of images		Combined with statistical analysis, leveraging feature importance ranking based on information entropy in predictive models for density prediction	
	Evaluation method		Prediction accuracy		Prediction accuracy		Prediction accuracy	

Hence, it is diagnostic analytics involving statistical correlation analysis. As predictive analytics can provide reflections to its corresponding diagnostic analytics, predictive analytics is also adopted in this case study. Data required for the task is different combinations of remelting process parameters and corresponding part densities of printed parts. Combined with statistical analysis, the importance of each remelting process parameter is analysed based on the predictive model for density prediction. Table 6.1 presents the details of applying the proposed task-driven data fusion methods for the case studies. The specific fusion techniques adopted for the case studies are demonstrated in the following sub-sections.

6.2 Case Study 1: Mechanical Property Prediction of AM Produced LS

6.2.1 Background

This LS is a porous structure formed by repeating unit cells in a 3D grid (Seharing et al., 2020). It is a complex geometric design where its patterns influence the mechanical performance of the structures. LS has attracted tremendous attention from academia and industry as it offers opportunities for multifunctional design and great potential for lightweight applications (e.g., aerospace and automotive) (Wang et al., 2018c). Compared with non-lattice or solid structures, one of the main advantages of LS is to reduce the weight of the produced parts while still maintaining the mechanical property. Additionally, apart from weight reduction, it can reduce the cost of material since LS normally uses less material than solid structures. Another main advantage of LS is that it can customize the mechanical properties (e.g., strength) of the parts by changing the design of its unit cells, size, or porosity of the lattice. The complexity of designed LS is largely restricted by traditional manufacturing processes. AM greatly enlarges the design space of LS. The mechanical properties of LS fabricated by AM are influenced by numerous factors, making it challenging to predict. Traditional prediction methods, such as FEA, are usually time-consuming and computationally intensive. Also, simplifications and assumptions can lead to discrepancies between simulation results and real-world behaviour. Therefore, using data-driven approaches based on ML

techniques for mechanical property prediction of LS has become a critical research issue.

6.2.2 Data Description

This case study is conducted via research collaboration with the 3D printing research group of Chongqing University where the AM data used in this case study includes 57 samples in total. The parts were fabricated by SLM machines using Ti6Al4 V and 316L stainless steel powders. Different LS, strut structures and strut-based and sheet-based TPMS structures, are included in the samples. The final printed parts are composed of LS units. The examples of LS are shown in Figure 6.1. The mechanical properties of produced LS were tested through compressive experiments and indicated by the elastic modulus and yield strength. Elastic modulus and yield strength are widely used and the most essential indicators for mechanical properties. The tested elastic modulus of the final printed LS ranges from 37.5 to 9309 MPa, with a mean value of 3299 MPa. The tested yield strength of the final LS ranges from 1.9 MPa to 590.3 MPa, with a mean value of 154.88 MPa. The test was conducted in accordance with the standard "ISO 6892-1:2019(en) Metallic materials — Tensile testing — Part 1: Method of test at room temperature" (ISO, 2019).

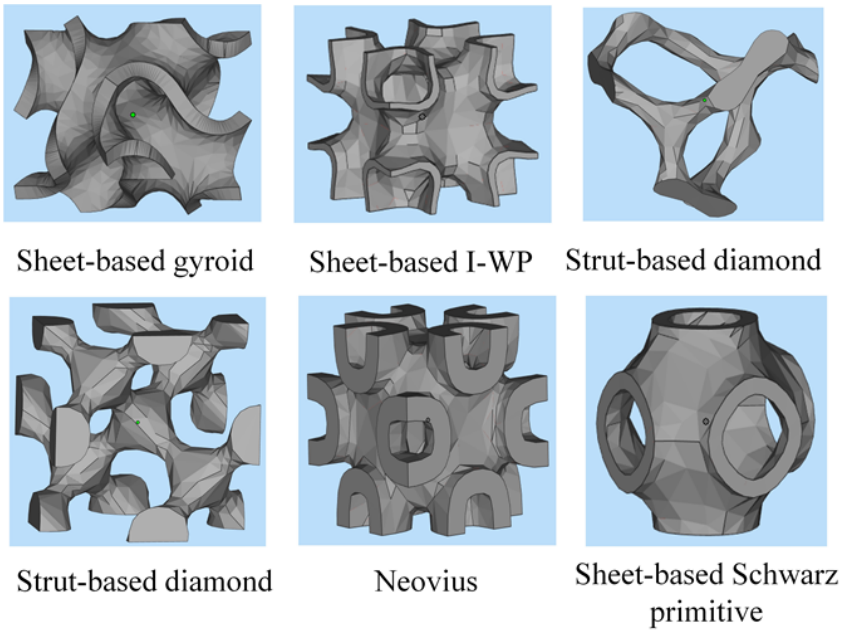

Figure 6.1 The examples of LS in the case study

6.2.3 Data Fusion for Mechanical Properties Prediction based on ML Models

LS produced by AM has been increasingly adopted in industries, such as the aerospace industry, due to its adjustable mechanical properties and light weights. LS are normally complex and their geometric features are hard to be extracted and analysed. Methods such as point clouds and feature curves are typically employed for analysing LS geometries. However, there are also drawbacks when applying these methods, such as too much data generated through point clouds, and hard to represent the internal shapes and structures of LS. The proposed geometry analysis method in Section 4 is effective and feasible for geometric feature learning and extraction, especially for AM CAD models. However, the prediction performance based on convolutional features using DL is largely affected by the volume of data samples. Since DL models are normally "data-hungry", it usually needs a considerable amount of labelled data to train a DL model. The data collected in this case study only includes 57 samples as the experiments are time-consuming and expensive. Therefore, considering the mechanical properties of printed parted are affected by the solid proportion of LS units, the geometric features of LS can be extracted and represented by the entropy of their voxelized 3D models (Ma et al., 2022).

As described in Section 6.1, the AM task requires the prediction model can be applied to different materials and LS types. The common attributes of materials and LS units should be considered. The geometric features of LS can be represented by the entropy vector of the unit, the unit length, and the porosity of the unit. The density and elastic modulus of used materials and the machine process parameters are closely related to the mechanical properties of the final printed parts. Thus, the geometry of different LS units, the porosity of LS units, the length of LS units, process parameters of AM production, material density, and the elastic modulus of materials are used as input features in ML models for mechanical properties prediction. The descriptions of input features are presented in Table 6.2 and the proposed method is illustrated in Figure 6.2.

Table 6.2 The input features for mechanical properties prediction

Input feature	Data dimension	Description
Entropy of LS unit	3D	The entropy is calculated based on the voxelized CAD model
Porosity of LS unit	1D	The porosity of the LS unit (%)
Length of LS unit	1D	The length of the LS unit (mm)
Material density	1D	The density of the used material (kg/m^3)
Material elastic modulus	1D	The elastic modulus of the used material (MPa)
Process parameter	1D	The process parameter settings in the AM production

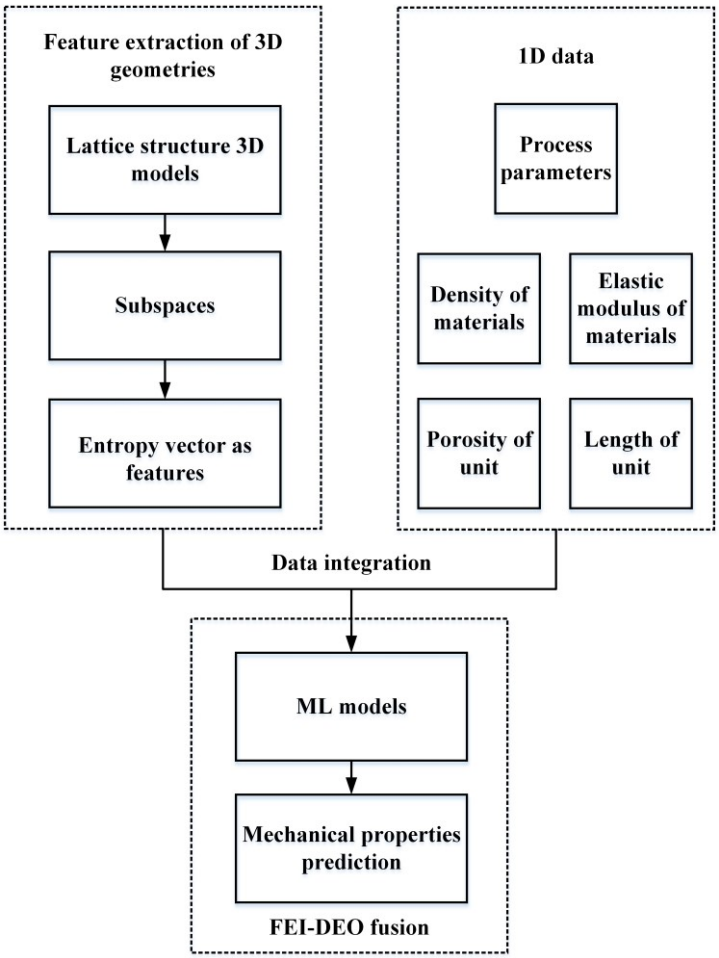

Figure 6.2 The proposed fusion method for mechanical properties prediction of LS

The model with the best performance of prediction should be selected as the final prediction model. The proposed method fuses multi-source and multi-dimensional data where the geometry of the LS cell is 3D data and other input features are 1D data.

- **Geometric Feature Extraction based on Entropy of Voxelized 3D models**

Voxelization refers to the process of converting 3D models into a volumetric representation using voxels. Similar to the grid patterns of 2D images, a voxel stands for the volume pixel and voxelization divides a 3D space into a grid of small voxels. Voxelization can simplify complex geometries into a uniform grid, making certain computations more straightforward. Also, the 3D models can be voxelized at different resolutions according to different precision requirements of applications. By voxelization of a 3D model, a new model consisting of pixels of a specified size is created and positioned in a space with an R^3 resolution. This space contains empty and solid pixels to represent the geometries of LS. In this case study, 100 × 100 × 100 resolution was used. The LS units were first voxelized into 3D voxels of which the porosities can be calculated. Examples of the voxelization of LS unit is presented in Figure 6.3.

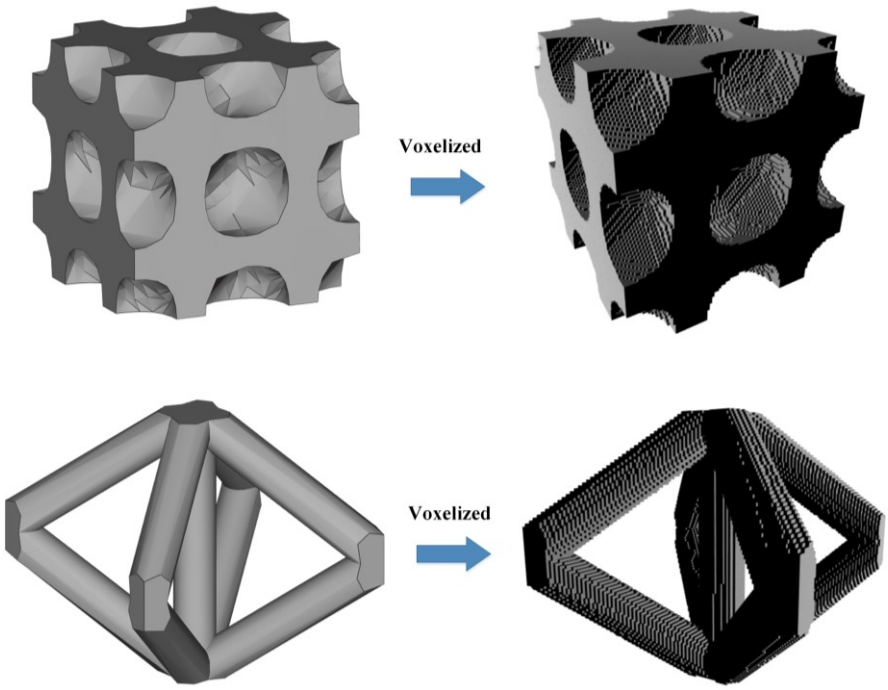

Figure 6.3 Examples of voxelization of LS with 100*100*100 resolution

The following equations are used to calculate the entropy of the geometry (Liu and He, 2008). In equations (6.1) ~ (6.2), E_g is the entropy of the given geometry, and P_1 and P_2 represent the proportions of solid and empty voxels respectively.

$$E_g = -P_1 \log_2 P_1 - P_2 \log_2 P_2 \tag{6.1}$$

$$P_1 + P_2 = 1 \tag{6.2}$$

Using entropy to describe geometries integrates concepts from information theory into geometry representation. It is a quantitative measure to describe the complexity or structural information of 3D models for understanding and analysing shapes and structures. As described in the equations, the entropy of different LS units can be the same if the proportions of solid and empty voxels are the same. Since it is hard to distinguish different LS unit models with the same entropy but have completely different geometries, the units were divided into subspaces and the entropy of each subspace was calculated.

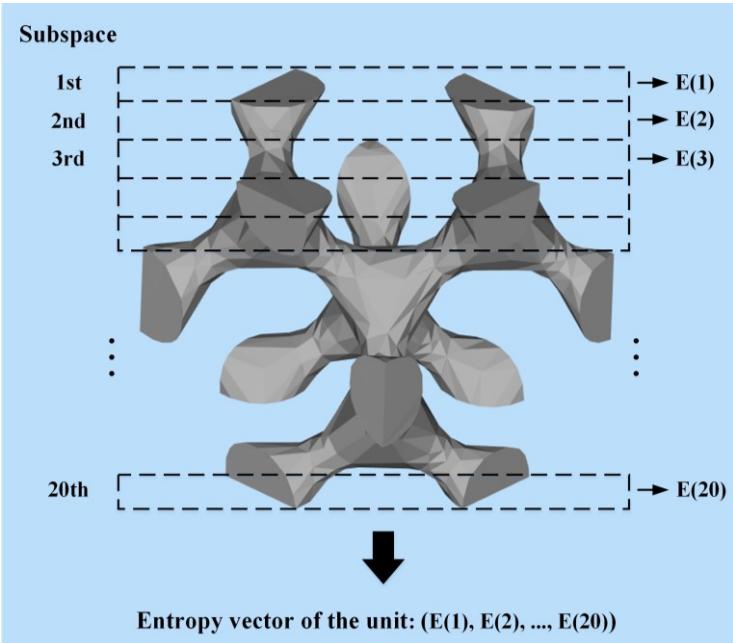

Figure 6.4 Obtaining the entropy vector of LS units based on the entropy of 20 subspaces

The direction for dividing the LS units aligns with the fabrication direction Z-axis. Then the entropy of an LS unit is represented by the entropy vector that consists of the

entropy of subspaces. To better distinguish the LS units while not making the features redundant, 20 subspaces were used, illustrated in Figure 6.4. The LS unit was divided into 100×100×5 voxels for each subspace. Therefore, the geometric features of an LS unit can be represented by the entropy of its 20 subspaces, denoted by the following equation.

$$E_g(X_{whole}) = [E_g(x_{sub1}), E_g(x_{sub2}), ..., E_g(x_{sub20})] \tag{6.3}$$

In equation (6.3), X_{whole} is the whole geometry of an LS unit, x_{subn} represents the nth subspace of the unit.

6.2.4 Evaluation Metrics

The evaluation metrics for the fusion models are RMSE and R^2. They are the most commonly used evaluation metrics for regression tasks. The evaluation metrics are calculated by the equations (4.17) and (4.18) which have been explained in Section 4.4.

6.2.5 Experimental Results

The elastic modulus and yield strength are used as indicators of part mechanical properties. Figure 6.5 and Figure 6.6 show the prediction results for elastic modulus and yield strength respectively. The RMSE and R^2 were used to evaluate the model's accuracy. As shown in the figures, the RFs achieved the best results in RMSE (556.80 MPa) for elastic modulus prediction with an R^2 of 0.76. Also, it had an RMSE of 28.28 MPa with an R^2 of 0.78 for yield strength prediction. The k-NN algorithm had the worst performance with an RMSE of 1417.96 MPa for elastic modulus prediction and an RMSE of 81.31 MPa for yield strength prediction. The SVM had the best performance in R^2 (0.91) for elastic modulus prediction while ANN had the best performance in R^2 (0.96) for yield strength prediction. Since R^2 measures the linear relationship between independent variables and the dependent variable, models with a lower RMSE are given priority. Thus, the RFs model was chosen as the final model

for the mechanical properties prediction task as it had the lowest RMSE with a relatively high R^2 among prevailing ML algorithms.

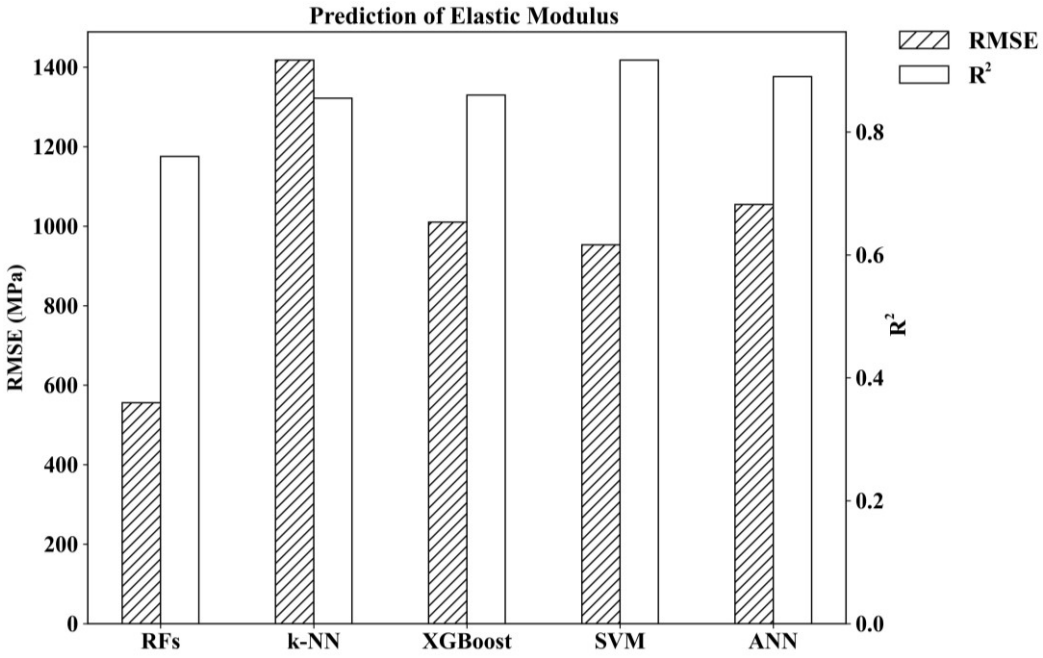

Figure 6.5 The performances of different prediction models for elastic modulus prediction

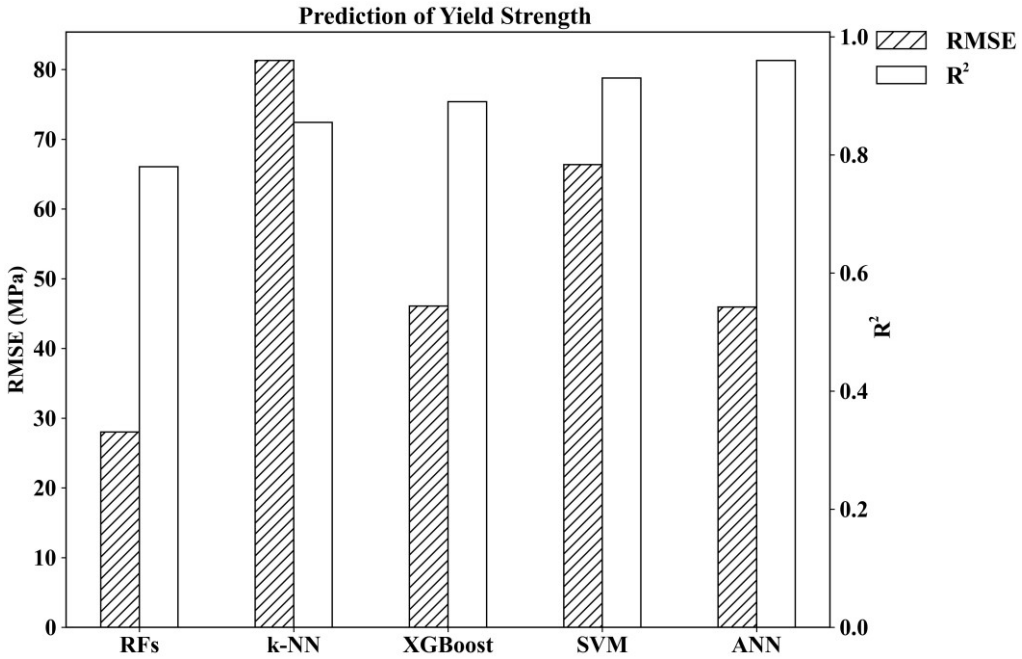

Figure 6.6 The performances of different prediction models for yield strength prediction

Normally, the more subspaces the LS unit is divided into, the more detailed geometric information can be obtained, leading to better prediction performance theoretically. However, it usually causes underfitting problems when the dimensionality of features is high and the training samples are insufficient. Additionally, the computational costs will increase significantly when the dimensionality of features increases. Therefore, the adopted approaches and strategies should be determined based on specific AM tasks and conditions.

6.3 Case Study 2: Porosity Defects Classification of Parts

6.3.1 Background

Ensuring and improving part quality of AM-produced products have always been the major concerns in the AM industry. Owing to the diversity in material supplies and the working principles of various AM processes, the defects or quality issues of produced components can be various. For example, in powder-based AM processes, porosity defects are the most common and concerning issues. Porosity defects can be classified into different types, including lack-of-fusion, balling, and cracking. These defects can significantly impact the mechanical properties and overall quality of the printed parts. They are particularly prevalent due to the challenges associated with managing powder materials and the specific melting and solidification dynamics inherent in these AM processes. Porosity defects are influenced by a variety of factors, such as powder material properties, process parameters, process stability, and part geometry and orientation. Classification of the porosity defects of printed parts helps in understanding the root causes of these defects, which can be linked to different impact factors for process optimization, reducing material waste, and quality enhancement. It also helps to reduce huge labour costs for manual checking and classification, largely improving efficiency.

Hence, this case study aims to classify the porosity defects of parts that are manufactured by different process parameter settings based on the proposed task-driven data fusion framework and methodology. It offers methods to reduce the labour

costs involved in manual categorization and labelling, and to provide assistance for further root cause analysis.

6.3.2 Data Description

The data used in this case study is a public dataset (Ackermann, 2023) which was published in 2023. The dataset is based on 81 printed cubes of high manganese steel with different process parameters (varied laser speed and power) through the LPBF process. In this dataset, 1135 light optical microscopy (LOM) images of different cross-sections of the printed cubes are collected. Cubes were prepared by metallography (grinding and polishing to one micron as surface finish). The examples of raw LOM images are shown in Figure 6.7.

Figure 6.7 Examples of LOM images for porosity detection in the dataset

The raw LOM images were processed to ignore scratches, uneven lighting, and stains from metallography by using various data pre-processing techniques (e.g., binarization, thresholding, blurring, etc.). The images used for porosity detection are the binary images after pre-processing, shown in Figure 6.8.

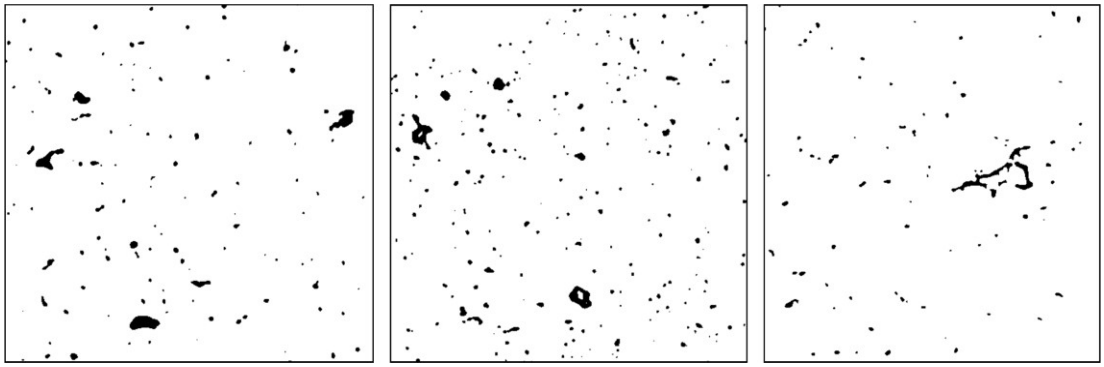

Figure 6.8 Examples of binarized LOM images in the dataset

Binary images are less sensitive to noise and suitable for fast processing since they contain less information per pixel compared to colour images. Also, it requires significantly less storage space and memory, which is ideal for devices with low storage capacity.

6.3.3 Data Fusion for Porosity Defects Classification based on ML Models

Classification of porosity is crucial for quality assurance, as it helps in determining whether a part meets the required strength and density specifications. Also, advanced data analytics (e.g., ML models) are increasingly applied to automate the detection and classification of porosity, enabling more efficient quality control in additive manufacturing processes. The following figure shows the proposed approach for classifying porosity defects of the cross-section of cubes.

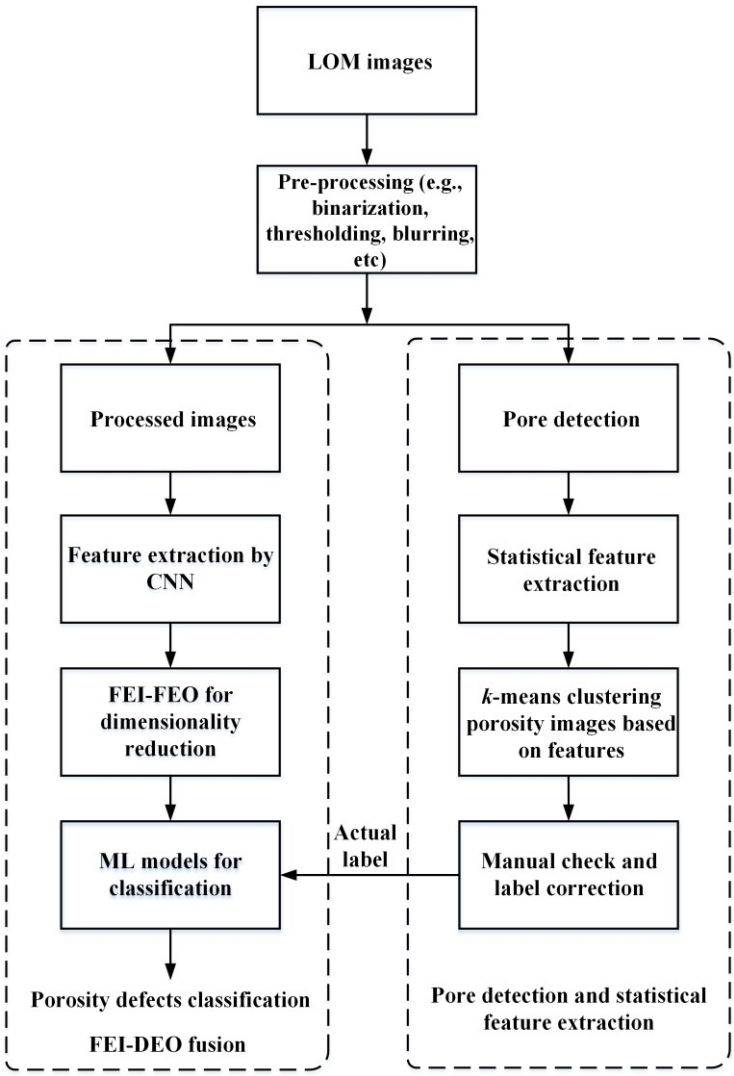

Figure 6.9 Illustration of the proposed approach for classifying porosity defects of the cross-section of cubes

In the proposed approach, the LOM images are pre-processed by different pre-processing techniques to improve the quality of images by removing noise, enhancing contrast, and making the images more suitable for the algorithms to work with. Also, the empty and corrupted images are removed from the dataset. After pre-processing of the LOM images, the processed images are processed through two different workflows. The first workflow is used for pore detection and statistical feature extraction, aiming to categorize the images by *k*-Means clustering on the statistical features of pores (FEI-FEO). The statistical features of detected pores are clustered into different clusters for

initially labelling different images. The labels of clustered images are then processed by manual checking and correction. For the other workflow, the pre-processed images are used for classification by ML models where convolutional features are extracted by pre-trained CNN models. FEI-FEO fusion strategy is adopted for dimensionality reduction of the extracted convolutional features and the FEI-DEO fusion strategy is applied to obtain the final target value.

6.3.4 Evaluation Metrics

Accuracy and F1-score are commonly used evaluation metrics for classification tasks. Accuracy is one of the most intuitive performance measures and it is simply a ratio of correctly predicted observation to the total observations. It is the most straightforward metric to assess the performance of a classification model. The accuracy for binary classification can be calculated by the following equation:

$$Accuracy = \frac{TP + TN}{TP + TN + FP + FN} \tag{6.4}$$

In equation (6.4), positive samples refer to the samples that belong to the class of interest or the target class. Conversely, negative samples are the samples that do not belong to the class of interest. *TP* represents the number of correctly predicted positive samples, *FP* represents the number of incorrectly predicted positive samples, *TN* is the number of correctly predicted negative samples, and *FN* is the number of incorrectly predicted negative samples. For multi-class classification problems, the accuracy is calculated as the ratio of correctly predicted samples to the total number of samples. The F1-score is a measure of a model's accuracy that considers both precision and recall to compute the score. Precision is the number of correct positive results divided by the number of all positive results, including those not identified correctly, and recall is the number of correct positive results divided by the number of positives that should have been identified. F1-score can be calculated by the following equation:

$$\text{F1-Score} = \frac{2TP}{2TP + FP + FN} \tag{6.5}$$

The F1-score is the harmonic mean of precision and recall, taking both false positives and false negatives into account.

6.3.5 Experimental Results

The statistical features extracted of pores in each cross-section image are the average area of pores, the max area of pores, the standard deviation of pores, and the ratio of pores area to normal area. The *k*-means clustering was performed on these statistical features for assigning images to different clusters. To determine the optimal *k*, the elbow method and silhouette score were used. The elbow method is in determining the number of clusters in a dataset. The method consists of plotting the explained variation as a function of the number of clusters and picking the elbow of the curve as the number of clusters to use. The silhouette score is a measure of how similar an object is to its cluster compared to other clusters. The silhouette score ranges from -1 to 1, where a high value indicates that the object is well-matched to its cluster and poorly matched to neighbouring clusters. The clustering results with different *k* are presented in Figure 6.10 and Figure 6.11. As shown in Figure 6.10, the sum of squared errors (SSE) of different *k* of clusters was calculated where the downward trend slowed down when the number of *k*=3. Also, in Figure 6.11, the highest silhouette score was obtained when the number of *k*=2. However, in these clusters, the images are merely categorized into those with pores or a small number of pores and those with a large number of pores. Hence, in this experiment, the *k*=3 was adopted for clustering the images.

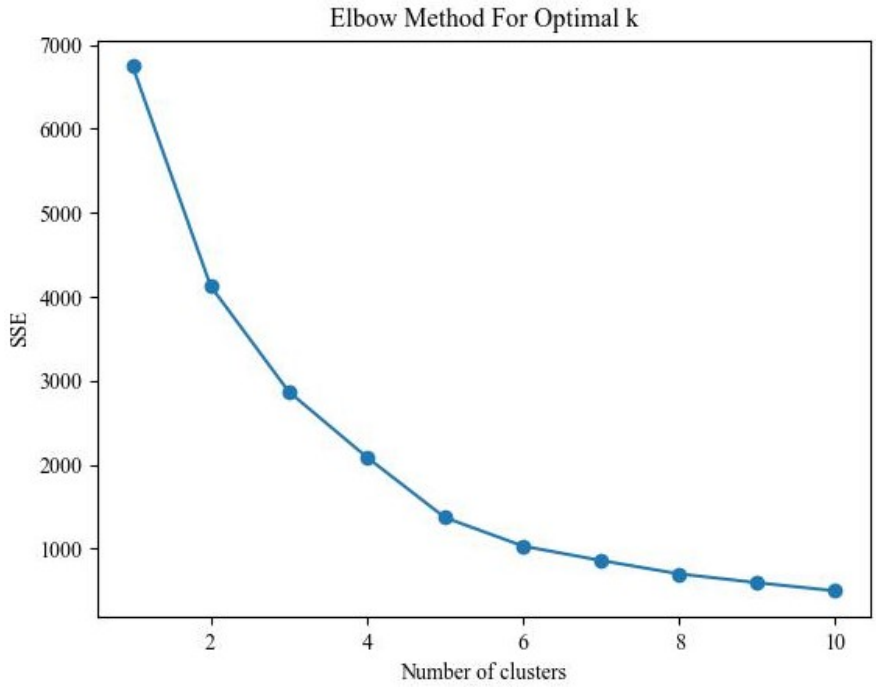

Figure 6.10 The SSE of different numbers of clusters

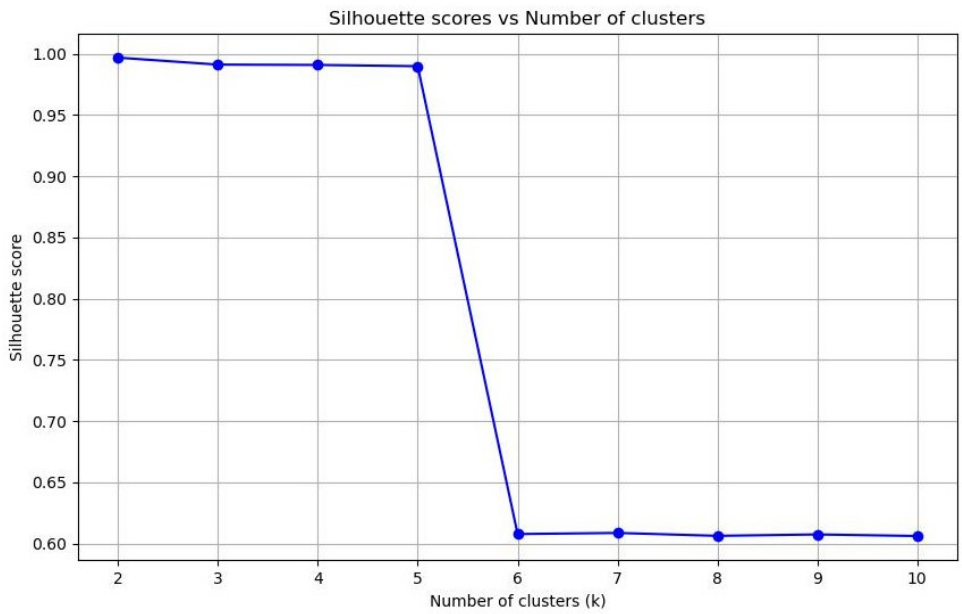

Figure 6.11 The silhouette scores of different numbers of clusters

After clustering images based on k=3, manual checks and corrections were conducted in the clusters to improve the clustering results. Figure 6.12 shows the typical porosity defect images for each cluster.

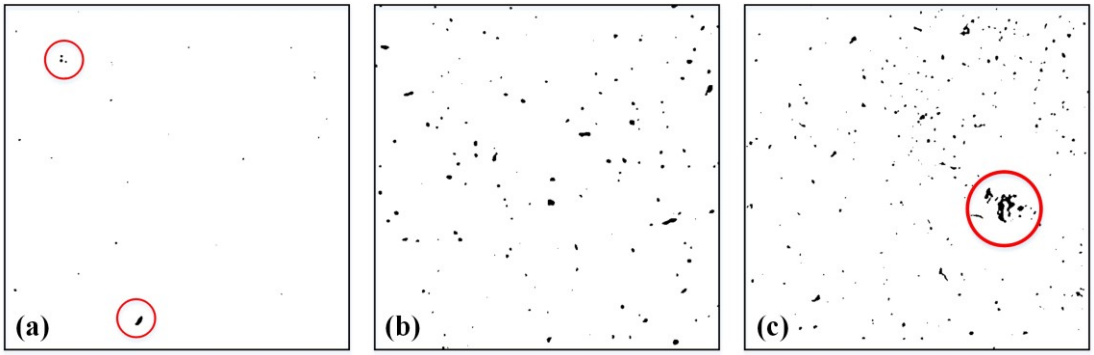

Figure 6.12 Typical porosity defect images for each cluster

In Figure 6.12, (a) represents the images in cluster 1 with a small number of tiny pores, (b) shows the images in cluster 2 with a large number of pores and distributed in the cross-section, and (c) shows the images in cluster 3 with large pores (the standard deviation of pore areas in the cross-section is large). Then, the pre-trained CNN was used to extract features from processed images for further classification by ML models. The pre-trained model used in this experiment is VGG16 and a CNN model is designed to use the processed images directly as inputs. The technique adopted for FEI-FEO fusion strategy is LLE. The performance of classification in terms of accuracy and F1-score of different ML algorithms are presented in Figure 6.13 and Figure 6.14. Figure 6.13 shows the performance of classification of ML models where non-FEI-FEO technique was applied to the extracted features for dimensionality reduction. The SVM model had the best results with an accuracy of 69.75 % and F1-score of 57.32%, while the CNN performed the worst with an accuracy of 61.21% and F1-score of 60.57%. Figure 6.14 shows the results of classification after implementing the FEI-FEO strategy. The performances of models were slightly improved while the SVM also achieved the best results, followed by the LGBM model. The accuracy of LGBM was improved from 65.48% to 69.03% with the F1-score from 61.57% to 61.96%. The accuracy of XGBoost was also improved from 63.34% to 66.90%.

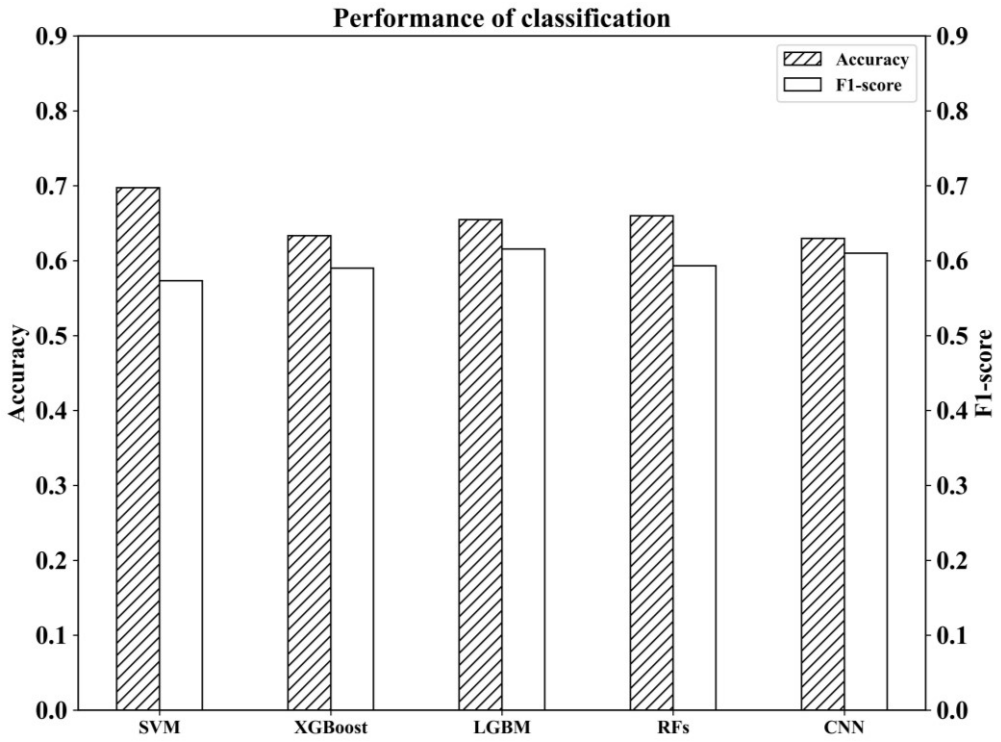

Figure 6.13 The classification results of different ML algorithms

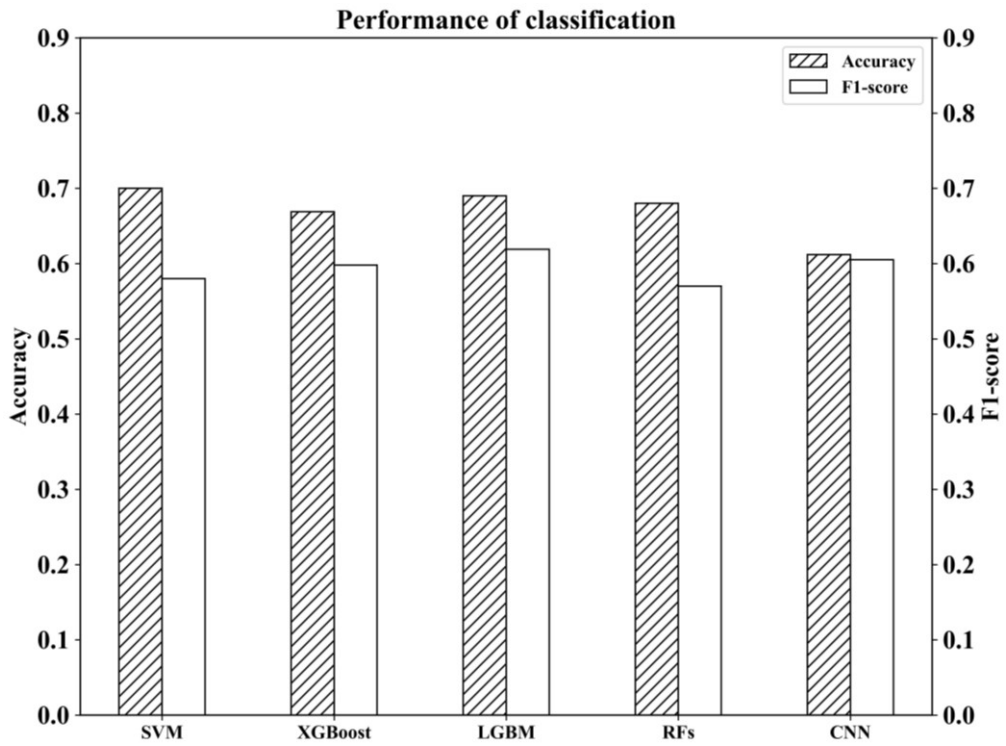

Figure 6.14 The classification results of different ML algorithms after implementing FEI-FEO strategy on extracted features

From the results presented above, implementing FEI-FEO strategy helped improve the model performances. Due to the relatively small sample size of the data samples, the CNN didn't achieve decent results in terms of accuracy and F1-score. CNN is supposed to achieve better results if the training samples increases.

6.4 Case Study 3: Investigating the Effect of the Remelting Process on Part Density

6.4.1 Background

The density of AM-produced components significantly influences their mechanical properties and functional performance. It is crucial to ensure the part density in a desired level in various industries, particularly where the strength, durability, and reliability of components are critical. For example, in the aerospace industry, parts with optimal density are crucial for withstanding the rigors of high-altitude and space environments, including extreme pressures and temperatures, while also contributing to fuel efficiency through weight optimization. Several industries and sectors require improved part density to meet their specific operational demands and performance criteria. Enhancing part density normally leads to better product quality, increased safety, and higher efficiency.

A promising approach to improve part density is laser remelting, which is a process that scans the same layer and remelts it (twice or multiple times) with the same laser source before spreading a new powder layer (Song et al., 2022). Therefore, this case study aims to present a exploration study on investigation of the effects of the remelting process on part density based on statistical correlation analysis and information gain analysis obtained from FEI-DEO fusion.

6.4.2 Data Description

In this experimental study, both AM and remelting processes were conducted on an SLM machine (EP-M250) where the used material was 18Ni-300 maraging steel. The schematic diagram of the remelting process is shown in Figure 6.15 where the arrows

in red represent the remelt scan paths. The remelt angle in Figure 6.15 is 90°. Different process parameters combined with remelting strategies were used to investigate the relationship between the remelting process and part density. The parts were manufactured in a cube shape with dimensions of 8 × 8 × 8 mm^3.

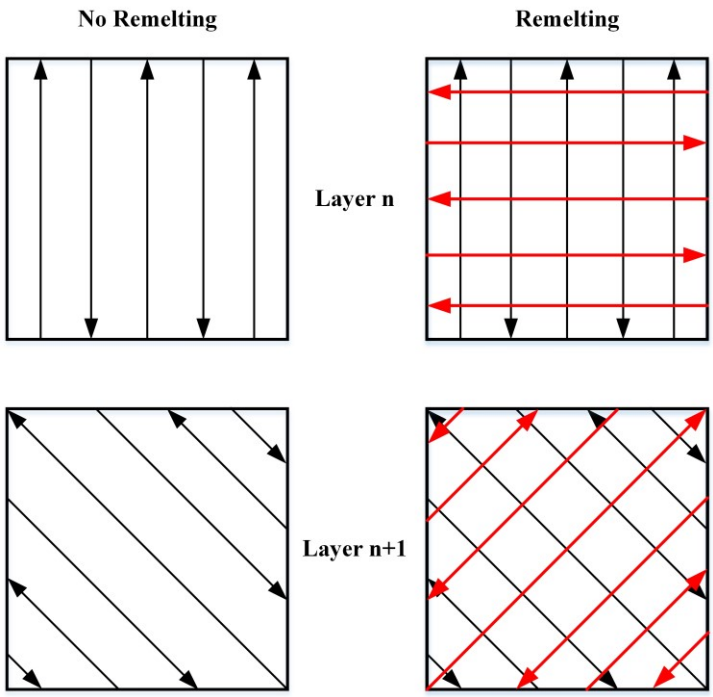

Figure 6.15 Schematic diagram of the remelting process

6.4.3 Data Fusion for Identifying the Relationship between Remelt Process and Part Density

To investigate the effect of the remelting process on part density, the statistical correlation between remelt process settings and relative density was first analysed based on the PCC. The PCC is calculated by the following equations (6.6) where r_{XY} is the PCC between variables X and Y, $\bar{x}$ and $\bar{y}$ represent the mean values of X and Y respectively.

$$r_{XY} = \frac{\sum_{i=1}^{n}(x_i - \bar{x})(y_i - \bar{y})}{\sqrt{\sum_{i=1}^{n}(x_i - \bar{x})^2}\sqrt{\sum_{i=1}^{n}(y_i - \bar{y})^2}} \tag{6.6}$$

PCC analysis only measures the linear relationship between variables, therefore, feature importance ranking based on the information gain is employed for further investigation. Information gain measures the reduction in uncertainty about the target variable after splitting the dataset on a particular feature. The information gain of the tree-based algorithms is calculated by the following equations. The detailed explanations of the information gain have been presented in Section 4.4.2.

$$H(D) = \sum_{k=1}^{K} -p_i \log_2 p_i \tag{6.7}$$

$$H(D \mid A) = \sum_{i=1}^{n} \frac{|D_i|}{|D|} H(D_i) \tag{6.8}$$

$$Gain(D, A) = H(D) - H(D \mid A) \tag{6.9}$$

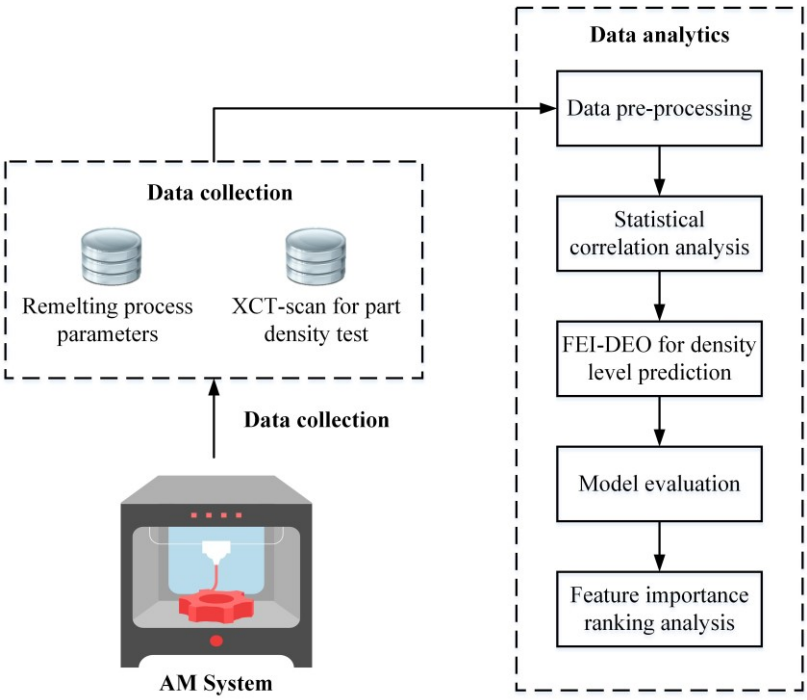

Figure 6.16 Data fusion for identifying the relationship between the remelting process and part density level

For the quality of the part density, based on the XCT-scan results, the porosity level was classified into three quality levels by AM experts: low, medium, and high. The

FEI-DEO fusion strategy is adopted where the remelting process setting data is used for part density level prediction. Based on the prediction result, the importance of features is analysed through information gain. The approach is illustrated in Figure 6.16. The prediction model used in this case study is XGBoost which is an ensemble learning algorithm of decision trees. It provides a parallel tree boosting for classification, regression, and ranking tasks.

6.4.4 Analytics Results

As shown in Figure 6.17, the PCC between each feature is calculated and presented. From the results, the laser power and scan speed tend to have negative correlations with part density while the remelt angle and hatch space tend to have positive correlations. However, there is no strong linear relationship between the remelting process parameters and part density that has been observed.

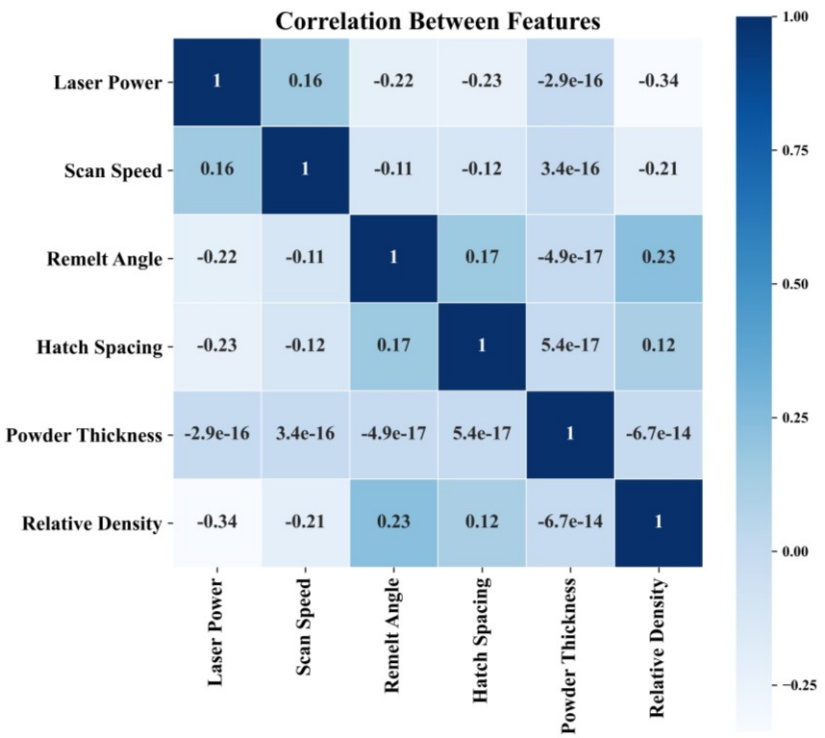

Figure 6.17 PCC between remelting process parameters and part density

For further investigation, the feature importance ranking through predictive analytics was conducted. Different tree-based algorithms, RFs, XGBoost, LGBM, and Adaptive

Boosting (AdaBoost), were trained for part density level classification based on the given remelting process parameters. Besides tree-based algorithms, *k*-NN was also adopted for comparison. The performances of different models are shown in Figure 6.18.

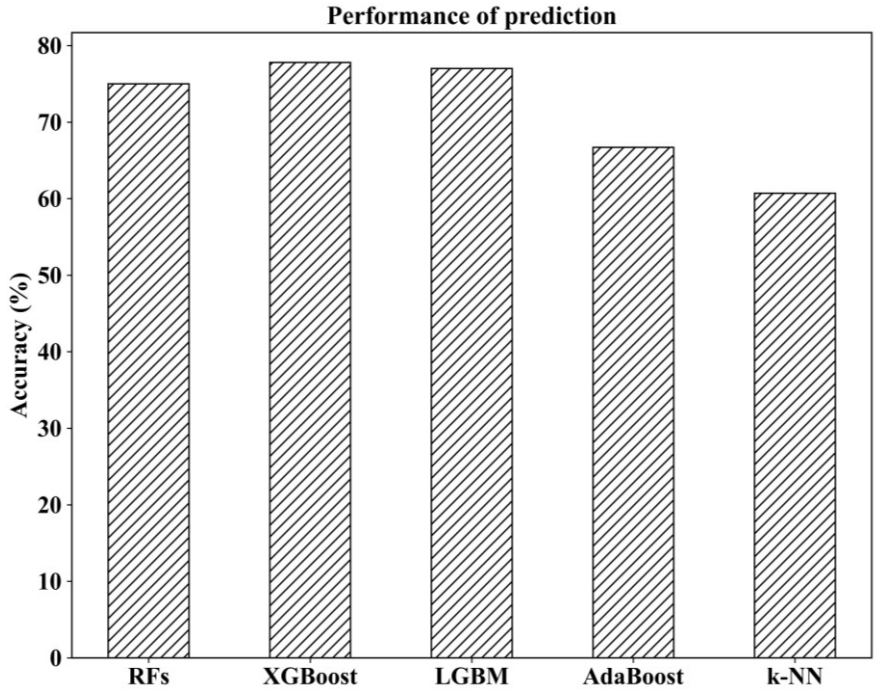

Figure 6.18 The accuracy for classifying part density levels of different models

As shown in the figure, XGBoost achieved the best classification accuracy (77.8%) while the *k*-NN had the worst accuracy (60.7%). Based on the XGBoost model, the feature importance ranking of remelting process parameters on part density level is shown in Figure 6.19 by calculating the information gain. It can be seen from the results that the scan speed has the most significant impact on part density level, followed by the hatch space. However, there is no strong relationship observed between laser power and part density level. The information gain of layer thickness on the prediction model is zero as the value of layer thickness in this experimental study remains the same. More experiments need to be carried out for further investigation.

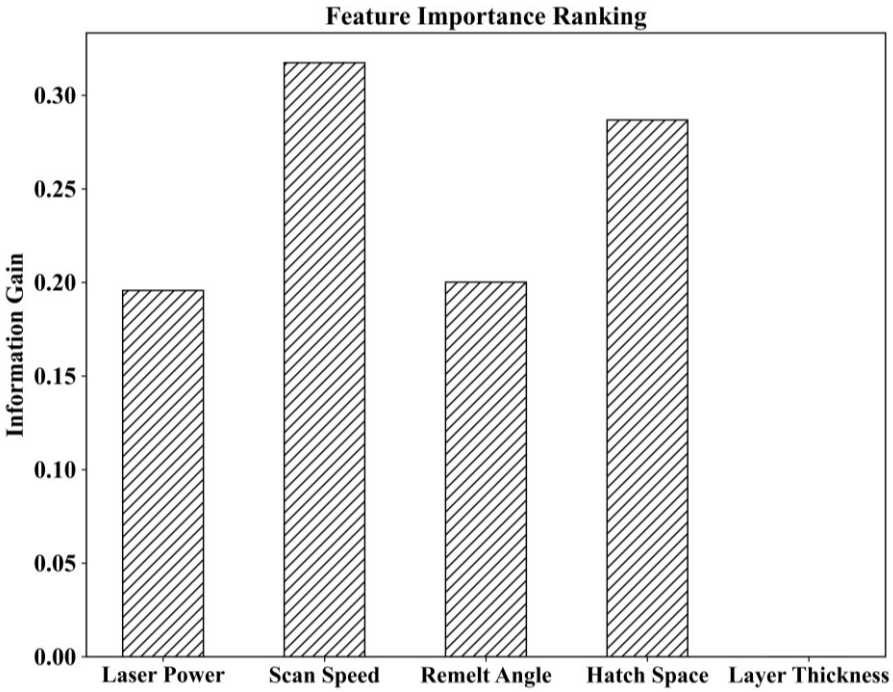

Figure 6.19 The feature importance ranking of remelting process parameters

6.5 Discussion

6.5.1 Data Considered in Analytics

AM data used in analytics vary in terms of type, volume, and dimension. The variety and heterogeneity of data lead to challenges when jointly analysed. Given that the characteristics of the generated data normally depend on the nature of AM processes and the collection devices, essential data pre-processing and dimensionality reduction processes are required for data alignment before analysing. During data analytics, the performances of different analytics models vary due to the differences in their capabilities when dealing with different kinds of data. It is crucial to employ the analytics models that best fit the data structures. For example, in case study 1 and the previous energy consumption prediction task in Section 4.3, 3D CAD models were both involved in predictive analytics. However, different feature extraction processes and fusion models were considered. The layer-level energy consumption prediction in energy consumption should consider the time-series patterns while case study 2 should consider how the LS of parts can be precisely represented. Also, too many data points

generated after feature extraction or data fusion process should be avoided in some cases as it normally requires considerable computational capabilities for further data analytics. In addition, the data consideration in analytics needs to take the task requirements into account. For example, implementing an X-ray CT scan for part density calculation is accurate but fairly time-consuming. Thus, using acoustic emission and Archimedes' principle for density tests are preferable alternatives in some cases.

6.5.2 With Fusion and Without Fusion

Large amounts of AM data are generated from labs and industries nowadays, offering huge opportunities for data analytics to improve the understanding of AM processes and support decision-making activities. However, some of this data can contain crucial information related to the decision-making activities while some data is redundant. The inclusion of redundant data or irrelevant data for data analytics not only affects the performances of analytics models where conflicts may occur but also causes resource inefficiency. Therefore, when comes to data fusion of multi-sourced data, the sources to be included should be the most relevant to the decision-making activities. Additionally, some data fusion techniques provide a refining process of data where noise data, outliers, or redundant data can be reduced. However, the refining process can also lead to considerable information loss that ultimately jeopardizes the performance of data analytics models. Considering this, evaluations are essential for the assessment of fusion processes on whether the data should be included or whether the refining processes are appropriate. Evaluation criteria from different perspectives should be developed in future research. In the case studies, this thesis adopted RMSE for evaluating the regression performances of different models, as RMSE is the most effective and widely employed indicator for assessing regressions. With the task requirements becoming more complex and diverse, other evaluation metrics should be employed.

6.5.3 Optimization between Performance and Task Requirements

When evaluating the performances of analytics models supported by data fusion techniques, the results derived from the analytics models should best fit the AM task requirements. However, in some cases, for example, real-time process monitoring requires the time for inference of the analytical model to be as short as possible. This leads to the pursuit of a fast reaction of models while the data and information to be involved are inevitably reduced. Some essential information may be lost during the shrinking or refining process of the data, which ultimately affects the model's performance. As described in Section 5.3, the energy consumption prediction task aims to be conducted on edge devices where the computing resources are limited. Therefore, the trade-off between model performances and computing constraints should be made. The prediction accuracy of the developed student model is inevitably worse than the complex ensemble model while it had a much smaller model size and faster inferencing time for being applied to edge devices. In addition, apart from the data and information to be considered, the complexity of the analytical model also needs to be reduced to avoid extra computing time. Therefore, the optimization between model performance and task requirements is critical and challenging. Establishing evaluation models for specific AM tasks to find optimized solutions between analytical model performance and task requirements is a promising strategy.

6.6 Summary

Three case studies on different AM tasks were carried out to demonstrate the feasibility and effectiveness of the proposed framework and approaches, including mechanical property prediction of additively manufactured LS, porosity defects classification of parts, and investigation of the joint effect of remelting process on part density. The experimental results show that the applied data fusion strategies and techniques can effectively integrate the data with different dimensions, structures, and types for data analytics to support decision-making activities. Due to the strong capability in learning hidden information within data and modelling complex nonlinear relationships, ML has been widely used for fusing data to obtain desired target values. Therefore, in the

FEI-DEO fusion, ML algorithms prevail. Besides, in case study 1, as the task requirement is accurate prediction, RMSE and R^2 were adopted as indicators to evaluate the fusion in regression tasks. Accuracy and F1-score were used as the indicators for the classification task. The fusion model with the best performance was used to obtain the target value. In different AM tasks, different requirements can be attached, thus, different evaluation methods should be applied. Compared with traditional single-dimensional and single-modality data analytics, the proposed task-driven data fusion framework and approach not only systematically identifies and collects the data required for the AM task but effectively leverages the information from multiple sources, measurements, and modalities to support decision-making activities. It has great potential to be applied in the AM industry to help improve AM production.

Chapter 7 Achievements and Conclusions

7.1 Achievements

This research aims to provide task-driven data fusion methodology and approaches to support decision-making activities for AM. This motivation was explored at the beginning of this thesis and is underpinned by the discussion of the background of AM and emerging technologies. The analytics of heterogeneous AM data and information enables the improvement of AM production, such as design optimisation, quality control, predictive maintenance, and adaptive manufacturing processes. It is crucial for the advanced AM ecosystems envisioned in Industry 4.0. In this thesis, there are three research questions proposed in Chapter 1. Based on the work achieved, the answers to the research questions are obtained.

To determine the state-of-the-art research, the literature review was provided with the related technologies and relevant research. Firstly, AM processes and the data generation process of AM systems were reviewed to give an overview of AM technologies. Secondly, the concepts and prevailing techniques of data fusion were reviewed, followed by their applications in the AM industry. As the collected AM data has become more diverse in recent years, researchers have increasingly employed data fusion strategies for dealing with challenging AM issues. Critical information and signatures can be captured in the form of multi-source and multi-modal data by advanced sensing technologies. Each source offers a unique perspective or type of

information that, when integrated, can provide a comprehensive understanding of the target value of the tasks. Thirdly, as the most prevailing data fusion technologies, the studies and applications of ML for tackling different AM tasks were reviewed. The tasks within different AM domains were categorized and detailed techniques used for tackling the tasks were reviewed and discussed. This would be significantly helpful in determining how to effectively leverage the collected data and advanced data analytical methods when addressing various AM tasks.

The first research question is: what is an appropriate data fusion framework for AM with the full exploitation of the data and information resources to support decision-making activities? Following the understanding of the state-of-the-art relevant research in AM, a task-driven data fusion framework and its corresponding methodology were proposed. In the framework, based on the sequence of the stages in a standard AM process, the data generated during an AM process is categorized into three major categories, process-input data, process-generated data, and validation data. Each category involves several stages of the whole process. The proposed methodology consists of three steps, including (1) identification of task-driven data analytics, (2) data required for tasks, acquisition, and characterization, and (3) task-driven data fusion techniques. Driven by AM tasks, the proposed methodology helps AM engineers and decision-makers systematically identify the decision-making activities involved in the tasks, the data and information required for tackling the tasks, and the implementation of data fusion techniques based on the data characteristics to best fit the task requirements. It provides a methodological way to collect, fuse, analyse, and evaluate the multi-source and multi-dimensional data and information in data analytics for AM.

The second research question is: how to analyse and integrate geometric features with other related information of different hierarchies to obtain target values of AM tasks? To deal with the critical challenges in this research question, an M-CNN-LSTM model was proposed. In contrast to the traditional approach of manually extracting features for CAD models, the work introduces a method based on CNN that automates the extraction of geometric features on a layer-wise basis. This method is capable of

autonomously learning and extracting geometric features of CAD models that are highly indicative of each layer's characteristics. Furthermore, to align with the AM process's sequential manufacturing patterns, the M-CNN-LSTM architecture is designed. This architecture integrates the geometric features with additional information pertinent to the target values, encompassing both layer-level and build-level data. A case study was carried out on an energy consumption prediction task. Experimental studies have investigated the impacts of geometric features on AM energy consumption, demonstrating the importance of the inclusion of geometric features in the prediction of AM energy consumption. Also, compared to conventional ML algorithms, the experimental results showed the merits of the proposed M-CNN-LSTM model.

After addressing the second research question, the third research question is: how to leverage the new incoming AM data of the tasks and enable the analytics model to make fast inferences? The formulation of this research question was motivated by the crucial issues encountered in applying DL-based models to data analytics for AM tasks, as clarified in previous chapters. To address these critical issues, a Cloud-edge fusion strategy and method based on transfer learning and multi-stage KD-enabled incremental learning was proposed. The proposed method consists of three main steps, including (1) transfer learning for feature extraction, (2) base model building via DML and model ensemble, and (3) multi-stage KD-enabled incremental learning. As part of the base model training, employing transfer learning for feature extraction of images is driven by the limited AM data samples. A pre-trained CNN model (on similar or related tasks) is transferred to extract features from images and concatenates them with task-related information. DML strategy is adopted to train three neural network-based base models, which are then fused into an ensemble model to obtain a more reliable and robust prediction result. By implementing the multi-stage KD-enabled incremental learning method, knowledge is transferred from the ensemble model to the compressed student model while new knowledge is acquired incrementally when new AM data is collected. In the case study, the prediction of the AM energy consumption task was focused but with a different task scenario. From the experimental results, by applying the transfer learning and DML strategy, the model performances were improved even

with a small number of training samples. When new energy consumption data was collected, the compressed student could learn both knowledge from the previous student model with old knowledge and new incoming data. Meanwhile, its model size was much smaller than the ensemble model and had a very short inference time, which could be easily applied to edge devices.

The proposed methods driven by AM tasks in Chapters 4 and 5 are demonstrated as feasible and effective in an energy consumption prediction task. Given the diverse considerations and requirements of AM tasks, the proposed task-driven data fusion methodology was applied to different AM tasks for demonstration. Chapter 6 presents three case studies, including mechanical property prediction of additively manufactured LS, porosity defect classification, and investigating the effect of the remelting process on part density. The details of employing the task-driven data fusion methodology and specific fusion techniques adopted for the case studies were presented where the experimental results have shown the effectiveness of the proposed methods.

7.2 Limitations

The data fusion architecture in the framework is based on Dasarathy's architecture which focuses on the nature of input data and output data. This architecture does not prescribe specific algorithms or processes, offering flexibility in terms of the techniques that can be used for fusion at different levels. Also, the hierarchical nature of the architecture provides a structured approach that can be scaled up or down depending on the complexity and requirements of the task. Limited by the type of fusion architecture, the proposed methodology particularly focuses on leveraging the AM data for supporting decision-making while the fusion of the distributed AM nodes, networks, and systems is not considered. Though a Cloud-edge fusion strategy and corresponding approach were developed in this thesis, it mainly targeted the AM tasks with specific requirements rather than a universal architecture for AM data fusion with distributed networks or systems. The fusion for the system level of AM will be explored in future studies.

In addition, most data fusion strategies employed in this thesis were FEI-FEO and FEI-DEO while DAI-DAO and DAI-FEO were not implemented and demonstrated. This is due to the nature of the collected datasets. Also, the FEI-DEO strategy was accomplished by ML algorithms due to their strong learning and fitting abilities. Besides, when adopting data-driven methods to tackle AM issues, the quality of data should be ensured. Sensors must be calibrated and the status of AM machines should be checked regularly to avoid errors when collecting data. However, the performance of developed models will inevitably be affected by uncertainties. Process stability and repeatability might also influence the accuracy of predictions of the developed models. In some cases, environment variations could affect the target value and they should be treated as variables in data analytics.

7.3 Future Works

For the specific models developed in the thesis, their performances can be further improved by further exploring different architectures, fine-tuning hyperparameters, and acquiring more diverse data to improve their reliability and robustness. Due to the limitations of the collected data, the proposed M-CNN-LSTM model and the transfer learning-based KD-enabled incremental learning method were applied to tackle the AM energy consumption task. In future studies, these methods will be applied to tackle different AM tasks, such as tensile strength prediction of parts, porosity prediction based on in-situ melt pool characteristics or thermal profiles, and so on. For the energy consumption prediction task, future studies can be explored to investigate how to reduce energy usage from the design perspective. The model can be adjusted to only rely on the geometric features for prediction, and the interpretation of convolutional features that link to energy consumption can be explored. For the KD-enabled incremental learning, as the incremental learning is performed in the centralized system (e.g., PC, Cloud), a more lightweight and efficient model can be explored to enable fast training and learning in edge devices. Additionally, as stated in the previous section, the data fusion framework for distributed AM networks or systems was not developed in this thesis. In future works, the fusion for distributed AM networks and systems will be investigated since the data sharing, transmission, fusion, and

estimation can be accomplished by local servers. How to fuse this information effectively and efficiently from different local servers with centralized servers is worth studying.

Another important work for future study is the knowledge fusion for AM. As the knowledge of AM can be derived from data analytics, domain experts, and existing literature, how to effectively extract, collect, store, and leverage the knowledge becomes a crucial challenge in both academia and industry. The AM knowledge can be leveraged to guide decision-making for AM tasks, optimize production, enhance the quality and performance of AM parts, and improve process reliability and stability. The knowledge graph (KG) is a promising method for storing and organising data that allows for the interconnection and integration of information in AM, allowing both humans and computers to process the complex relationships between the information. By establishing relationships between different data points, the KG can reveal connections that might not be immediately apparent, aiding in the discovery of new insights and relationships. Also, the rich contextual information available within a KG can improve the decision-making process, supporting more informed and accurate decisions in the AM workflow. Moreover, the KG can improve the interpretability of different AM data and information, and help organize and manage knowledge efficiently. The KG can serve as a backbone for advanced data analytics and decision-making, providing a structured approach for managing the vast amounts of data and information generated by AM processes.

7.4 Conclusions

In conclusion, the proposed task-driven data fusion framework and methodology presented in this thesis mark an advancement over conventional data analytics that rely on single-dimensional, single-modality techniques. This framework not only methodically identifies and collects the necessary data for AM tasks but also proficiently leverages information from diverse sources, measurements, and modalities to enhance decision-making processes. Detailed methods and approaches for multi-source and multi-hierarchy data fusion and Cloud-edge fusion are proposed

and demonstrated in the thesis. The proposed framework and methodology aim to bridge the gap between the complex manufacturing process of AM systems and the resultant outcomes for the enhancement of process reliability, stability, and efficiency. To the best of our knowledge, the proposed multi-source and multi-hierarchy data fusion strategy was the first study that predicted AM energy consumption by transforming 3D models to layer-wise images and fusing them with other related information. Also, based on the experimental results, the KD-enabled incremental learning combined with the transfer learning strategy effectively improved the model performance, providing a promising strategy to address the challenge in AM that lacks sufficient training samples at the initial stage. Moreover, the compressed student model not only improved model performance, but also demonstrated a faster inference speed compared to the complex ensemble model. The proposed task-driven data fusion framework and methodology, and different fusion strategies and methods, have great potential to be applied in the AM industry to help improve AM production.

References

ACKERMANN, M. 2023. Porosity Detection In Metal Additive Manufacturing. https://github.com/mrc989crm/PorosityDetectionInMetalAdditiveManufacturing.

AHMADI, S. M., AMIN YAVARI, S., WAUTHLE, R., POURAN, B., SCHROOTEN, J., WEINANS, H. & ZADPOOR, A. A. 2015. Additively manufactured open-cell porous biomaterials made from six different space-filling unit cells: The mechanical and morphological properties. *Materials,* 8**,** 1871-1896.

AHN, D., KWEON, J.-H., KWON, S., SONG, J. & LEE, S. 2009. Representation of surface roughness in fused deposition modeling. *Journal of Materials Processing Technology,* 209**,** 5593-5600.

AHSAN, N., HABIB, A. & KHODA, B. J. P. M. 2016. Geometric Analysis for Concurrent Process Optimization of AM. *Procedia Manufacturing,* 5**,** 974-988.

ALEJANDRINO, J. D., CONCEPCION II, R. S., LAUGUICO, S. C., TOBIAS, R. R., VENANCIO, L., MACASAET, D., BANDALA, A. A. & DADIOS, E. P. 2020. A machine learning approach of lattice infill pattern for increasing material efficiency in additive manufacturing processes. *Int. J. Mech. Eng. Robot. Res.,* 9**,** 1253-1263.

AMINZADEH, M. & KURFESS, T. R. 2019. Online quality inspection using Bayesian classification in powder-bed additive manufacturing from high-resolution visual camera images. *Journal of Intelligent Manufacturing,* 30**,** 2505-2523.

ANGELONE, R., CAGGIANO, A., TETI, R., SPIERINGS, A., STAUB, A. & WEGENER, K. 2020. Bio-Intelligent Selective Laser Melting System based on Convolutional Neural Networks for In-Process Fault Identification. *Procedia CIRP,* 88**,** 612-617.

APOSTOLOS, F., ALEXIOS, P., GEORGIOS, P., PANAGIOTIS, S. & GEORGE, C. 2013. Energy efficiency of manufacturing processes: a critical review. *Procedia Cirp,* 7**,** 628-633.

ARRIETA, A. B., DíAZ-RODRíGUEZ, N., DEL SER, J., BENNETOT, A., TABIK, S., BARBADO, A., GARCíA, S., GIL-LóPEZ, S., MOLINA, D. & BENJAMINS, R. 2020. Explainable Artificial Intelligence (XAI): Concepts, taxonomies, opportunities and challenges toward responsible AI. *Information fusion,* 58**,** 82-115.

AZMAN, A. H. & NASIR, A. R. M. 2019. Lattice Structure Design Optimisation For Additive Manufacturing Using Finite Element Analysis. *Perintis eJournal,* 9**,** 37-47.

BAE, C.-J., DIGGS, A. B. & RAMACHANDRAN, A. 2018. Quantification and certification of additive manufacturing materials and processes. *Additive Manufacturing.* Elsevier.

BAHRAMPOUR, S., NASRABADI, N. M., RAY, A. & JENKINS, W. K. 2015. Multimodal task-driven dictionary learning for image classification. *IEEE transactions on Image Processing,* 25**,** 24-38.

BASTANI, K., RAO, P. K. & KONG, Z. 2016. An online sparse estimation-based classification approach for real-time monitoring in advanced manufacturing processes from heterogeneous sensor data. *IIE Transactions,* 48**,** 579-598.

BATURYNSKA, I. J. A. S. 2019. Application of Machine Learning Techniques to Predict the Mechanical Properties of Polyamide 2200 (PA12) in Additive Manufacturing. *Applied Sciences,* 9**,** 1060.

BAUMERS, M., TUCK, C., BOURELL, D., SREENIVASAN, R. & HAGUE, R. 2011. Sustainability of additive manufacturing: measuring the energy consumption of the laser sintering process. *Proceedings of the Institution of Mechanical Engineers, Part B: Journal of Engineering Manufacture,* 225**,** 2228-2239.

BAUMGARTL, H., TOMAS, J., BUETTNER, R. & MERKEL, M. 2020. A deep learning-based model for defect detection in laser-powder bed fusion using in-situ thermographic monitoring. *Progress in Additive Manufacturing***,** 1-9.

BECKER, P., ROTH, C., ROENNAU, A. & DILLMANN, R. Acoustic Anomaly Detection in Additive Manufacturing with Long Short-Term Memory Neural Networks. 2020 IEEE 7th International Conference on Industrial Engineering and Applications (ICIEA), 2020. IEEE, 921-926.

BHATT, P. M., KABIR, A. M., PERALTA, M., BRUCK, H. A. & GUPTA, S. K. 2019. A robotic cell for performing sheet lamination-based additive manufacturing. *Additive Manufacturing,* 27**,** 278-289.

BISHEH, M. N., CHANG, S. I. & LEI, S. 2021. A layer-by-layer quality monitoring framework for 3D printing. *Computers Industrial Engineering,* 157**,** 107314.

BORLEFFS, M. 2012. Finite element modeling to predict bulk mechanical properties of 3D printed metal foams.

BUGATTI, M. & COLOSIMO, B. M. 2021. Towards real-time in-situ monitoring of hot-spot defects in L-PBF: a new classification-based method for fast video-imaging data analysis. *Journal of Intelligent Manufacturing***,** 1-17.

CAGGIANO, A., ZHANG, J., ALFIERI, V., CAIAZZO, F., GAO, R. & TETI, R. 2019. Machine learning-based image processing for on-line defect recognition in additive manufacturing. *CIRP Annals,* 68**,** 451-454.

CAI, Y., STARLY, B., COHEN, P. & LEE, Y.-S. 2017. Sensor data and information fusion to construct digital-twins virtual machine tools for cyber-physical manufacturing. *Procedia manufacturing,* 10**,** 1031-1042.

CAIAZZO, F. & CAGGIANO, A. 2018. Laser Direct Metal Deposition of 2024 Al alloy: Trace geometry prediction via machine learning. *Materials,* 11**,** 444.

CALIGNANO, F. & MERCURIO, V. 2023. An overview of the impact of additive manufacturing on supply chain, reshoring, and sustainability. *Cleaner Logistics Supply Chain,* 7**,** 100103.

CAO, X., JIANG, Y., ZHAO, T., WANG, P., WANG, Y., CHEN, Z., LI, Y., XIAO, D. & FANG, D. 2020. Compression experiment and numerical evaluation on mechanical responses of the lattice structures with stochastic geometric defects originated from additive-manufacturing. *Composites Part B: Engineering,* 194**,** 108030.

CASTANEDO, F. 2013. A review of data fusion techniques. *The scientific world journal,* 2013.

CHAITANYA, K., KARANI, N., BAUMGARTNER, C. F., BECKER, A., DONATI, O. & KONUKOGLU, E. Semi-supervised and task-driven data augmentation. Information Processing in Medical Imaging: 26th International Conference, IPMI 2019, Hong Kong, China, June 2–7, 2019, Proceedings 26, 2019. Springer, 29-41.

CHAITANYA, K., KARANI, N., BAUMGARTNER, C. F., ERDIL, E., BECKER, A., DONATI, O. & KONUKOGLU, E. 2021. Semi-supervised task-driven data augmentation for medical image segmentation. *Medical Image Analysis,* 68**,** 101934.

CHAN, S. L., LU, Y. & WANG, Y. 2018. Data-driven cost estimation for additive manufacturing in cybermanufacturing. *Journal of manufacturing systems,* 46**,** 115-126.

CHANG, T.-W., LIAO, K.-W., LIN, C.-C., TSAI, M.-C. & CHENG, C.-W. 2021. Predicting magnetic characteristics of additive manufactured soft magnetic composites by machine learning. *The International Journal of Advanced Manufacturing Technology,* 114**,** 3177-3184.

CHARTRAIN, N. A., WILLIAMS, C. B. & WHITTINGTON, A. R. 2018. A review on fabricating tissue scaffolds using vat photopolymerization. *Acta biomaterialia,* 74**,** 90-111.

CHEN, C., LIU, Y., WANG, S., SUN, X., DI CAIRANO-GILFEDDER, C., TITMUS, S. & SYNTETOS, A. A. 2020a. Predictive maintenance using cox proportional hazard deep learning. *Advanced Engineering Informatics,* 44**,** 101054.

CHEN, L.-Y., LIANG, S.-X., LIU, Y. & ZHANG, L.-C. 2021a. Additive manufacturing of metallic lattice structures: Unconstrained design, accurate fabrication, fascinated performances, and challenges. *Materials Science Engineering: R: Reports,* 146**,** 100648.

CHEN, L., YAO, X., XU, P., MOON, S. K. & BI, G. 2021b. Rapid surface defect identification for additive manufacturing with in-situ point cloud processing and machine learning. *Virtual Physical Prototyping,* 16**,** 50-67.

CHEN, Y., LI, C., GHAMISI, P., JIA, X. & GU, Y. 2017. Deep fusion of remote sensing data for accurate classification. *IEEE Geoscience Remote Sensing Letters,* 14**,** 1253-1257.

CHEN, Y., WANG, H., WU, Y. & WANG, H. 2020b. Predicting the Printability in Selective Laser Melting with a Supervised Machine Learning Method. *Materials,* 13**,** 5063.

CHEN, Z., HAN, C., GAO, M., KANDUKURI, S. Y. & ZHOU, K. 2022. A review on qualification and certification for metal additive manufacturing. *Virtual Physical Prototyping,* 17**,** 382-405.

COCCHI, M. 2019. *Data Fusion Methodology and Applications*, Elsevier.

CORTES, C. & VAPNIK, V. 1995. Support-vector networks. *Machine learning,* 20**,** 273-297.

DAFFLON, B., MOALLA, N. & OUZROUT, Y. 2021. The challenges, approaches, and used techniques of CPS for manufacturing in Industry 4.0: A literature review. *The International Journal of Advanced Manufacturing Technology,* 113**,** 2395-2412.

DASARATHY, B. V. 1997. Sensor fusion potential exploitation-innovative architectures and illustrative applications. *Proceedings of the IEEE,* 85**,** 24-38.

DAVTALAB, O., KAZEMIAN, A., YUAN, X. & KHOSHNEVIS, B. 2020. Automated inspection in robotic additive manufacturing using deep learning for layer deformation detection. *Journal of Intelligent Manufacturing***,** 1-14.

DECOST, B. L. & HOLM, E. A. 2017. Characterizing powder materials using keypoint-based computer vision methods. *Computational Materials Science,* 126**,** 438-445.

DECOST, B. L., JAIN, H., ROLLETT, A. D. & HOLM, E. A. 2017. Computer vision and machine learning for autonomous characterization of am powder feedstocks. *Jom,* 69**,** 456-465.

DEMIR, K., ZHANG, Z., BEN-ARTZY, A., HOSEMANN, P. & GU, G. X. 2021. Laser scan strategy descriptor for defect prognosis in metal additive manufacturing using neural networks. *Journal of Manufacturing Processes,* 67**,** 628-634.

DESPRéS, N., CYR, E., SETOODEH, P., MOHAMMADI, M. J. J.-J. O. T. M., METALS & SOCIETY, M. 2020. Deep Learning and Design for Additive Manufacturing: A Framework for Microlattice Architecture. *JOM-Journal of the Minerals, Metals Materials Society,* 72**,** 2408-2418.

DIEZ-OLIVAN, A., DEL SER, J., GALAR, D. & SIERRA, B. 2019. Data fusion and machine learning for industrial prognosis: Trends and perspectives towards Industry 4.0. *Information Fusion,* 50**,** 92-111.

DING, D., HE, F., YUAN, L., PAN, Z., WANG, L. & ROS, M. 2021. The first step towards intelligent wire arc additive manufacturing: An automatic bead modelling system using machine

learning through industrial information integration. *Journal of Industrial Information Integration,* 23**,** 100218.

ERTAY, D. S., KAMYAB, S., VLASEA, M., AZIMIFAR, Z., MA, T., ROGALSKY, A. D. & FIEGUTH, P. 2021. Toward Sub-Surface Pore Prediction Capabilities for Laser Powder Bed Fusion Using Data Science. *Journal of Manufacturing Science Engineering,* 143**,** 071016.

ERTEL, W. 2018. *Introduction to artificial intelligence*, Springer.

EVERTON, S. K., HIRSCH, M., STRAVROULAKIS, P., LEACH, R. K. & CLARE, A. T. 2016. Review of in-situ process monitoring and in-situ metrology for metal additive manufacturing. *Materials Design,* 95**,** 431-445.

FATHIZADAN, S., JU, F. & LU, Y. 2021. Deep representation learning for process variation management in laser powder bed fusion. *Additive Manufacturing,* 42**,** 101961.

FERNANDEZ-VIAGAS, V. & FRAMINAN, J. M. 2022. Exploring the benefits of scheduling with advanced and real-time information integration in Industry 4.0: A computational study. *Journal of Industrial Information Integration,* 27**,** 100281.

FERREIRA, I. A., GODINA, R. & CARVALHO, H. 2021. Waste valorization through additive manufacturing in an industrial symbiosis setting. *Sustainability,* 13**,** 234.

FERREIRA, R. D. S. B., SABBAGHI, A. & HUANG, Q. 2019. Automated geometric shape deviation modeling for additive manufacturing systems via Bayesian neural networks. *IEEE Transactions on Automation Science Engineering,* 17**,** 584-598.

FRAZIER, W. E. 2014. Metal additive manufacturing: a review. *Journal of Materials Engineering performance,* 23**,** 1917-1928.

GAIKWAD, A., GIERA, B., GUSS, G. M., FORIEN, J.-B., MATTHEWS, M. J. & RAO, P. 2020. Heterogeneous sensing and scientific machine learning for quality assurance in laser powder bed fusion–A single-track study. *Additive Manufacturing,* 36**,** 101659.

GAIKWAD, A., WILLIAMS, R. J., DE WINTON, H., BEVANS, B. D., SMOQI, Z., RAO, P. & HOOPER, P. A. 2022. Multi Phenomena Melt Pool Sensor Data Fusion for Enhanced Process Monitoring of Laser Powder Bed Fusion Additive Manufacturing. *Materials Design***,** 110919.

GAJA, H. & LIOU, F. 2017. Defects monitoring of laser metal deposition using acoustic emission sensor. *The International Journal of Advanced Manufacturing Technology,* 90**,** 561-574.

GAN, Z., LI, H., WOLFF, S. J., BENNETT, J. L., HYATT, G., WAGNER, G. J., CAO, J. & LIU, W. K. 2019. Data-Driven Microstructure and Microhardness Design in Additive Manufacturing Using a Self-Organizing Map. *Engineering,* 5**,** 730-735.

GERDES, N., HOFF, C., HERMSDORF, J., KAIERLE, S. & OVERMEYER, L. 2021. Hyperspectral imaging for prediction of surface roughness in laser powder bed fusion. *The International Journal of Advanced Manufacturing Technology***,** 1-10.

GIBSON, I., ROSEN, D., STUCKER, B. & KHORASANI, M. 2021a. *Additive manufacturing technologies*, Springer.

GIBSON, I., ROSEN, D. W., STUCKER, B., KHORASANI, M., ROSEN, D., STUCKER, B. & KHORASANI, M. 2021b. *Additive manufacturing technologies*, Springer.

GOBERT, C., REUTZEL, E. W., PETRICH, J., NASSAR, A. R. & PHOHA, S. J. A. M. 2018. Application of supervised machine learning for defect detection during metallic powder bed fusion additive manufacturing using high resolution imaging. *Additive Manufacturing,* 21**,** 517-528.

GOKULDOSS, P. K., KOLLA, S. & ECKERT, J. 2017. Additive manufacturing processes: Selective laser melting, electron beam melting and binder jetting—Selection guidelines. *Materials,* 10**,** 672.

GOU, J., XIONG, X., YU, B., DU, L., ZHAN, Y. & TAO, D. 2023. Multi-target knowledge distillation via student self-reflection. *International Journal of Computer Vision***,** 1-18.

GOU, J., YU, B., MAYBANK, S. J. & TAO, D. 2021. Knowledge distillation: A survey. *International Journal of Computer Vision,* 129**,** 1789-1819.

GRANDVIEWRESEARCH. 2022. *Additive Manufacturing Market Size, Share & Trends Analysis Report By Component, By Printer Type, By Technology, By Software, By Application, By Vertical, By Material, By Region, And Segment Forecasts, 2022 - 2030* [Online]. GrandViewResearch. Available: https://www.grandviewresearch.com/industry-analysis/additive-manufacturing-market [Accessed 23/06 2023].

GRASSO, M., GALLINA, F. & COLOSIMO, B. M. 2018. Data fusion methods for statistical process monitoring and quality characterization in metal additive manufacturing. *Procedia CIRP,* 75**,** 103-107.

GUO, S., AGARWAL, M., COOPER, C., TIAN, Q., GAO, R. X., GRACE, W. G. & GUO, Y. 2022. Machine learning for metal additive manufacturing: Towards a physics-informed data-driven paradigm. *Journal of Manufacturing Systems,* 62**,** 145-163.

GUPTA, N., TIWARI, A., BUKKAPATNAM, S. T. & KARRI, R. 2020. Additive manufacturing cyber-physical system: Supply chain cybersecurity and risks. *IEEE Access,* 8**,** 47322-47333.

HAN, Y., GRIFFITHS, R. J., HANG, Z. Y. & ZHU, Y. 2020. Quantitative microstructure analysis for solid-state metal additive manufacturing via deep learning. *Journal of Materials Research,* 35**,** 1936-1948.

HARBIG, J., WENZLER, D. L., BAEHR, S., KICK, M. K., MERSCHROTH, H., WIMMER, A., WEIGOLD, M. & ZAEH, M. F. 2022. Methodology to Determine Melt Pool Anomalies in Powder Bed Fusion of Metals Using a Laser Beam by Means of Process Monitoring and Sensor Data Fusion. *Materials,* 15**,** 1265.

HASSANIN, H., ALKENDI, Y., ELSAYED, M., ESSA, K. & ZWEIRI, Y. 2020. Controlling the properties of additively manufactured cellular structures using machine learning approaches. *Advanced Engineering Materials,* 22**,** 1901338.

HASSANIN, H., ZWEIRI, Y., FINET, L., ESSA, K., QIU, C. & ATTALLAH, M. 2021. Laser powder bed fusion of Ti-6Al-2Sn-4Zr-6Mo alloy and properties prediction using deep learning approaches. *Materials,* 14**,** 2056.

HERRIOTT, C. & SPEAR, A. D. 2020. Predicting microstructure-dependent mechanical properties in additively manufactured metals with machine-and deep-learning methods. *Computational Materials Science,* 175**,** 109599.

HERTLEIN, N., DESHPANDE, S., VENUGOPAL, V., KUMAR, M. & ANAND, S. 2020. Prediction of selective laser melting part quality using hybrid Bayesian network. *Additive Manufacturing,* 32**,** 101089.

HIMEUR, Y., RIMAL, B., TIWARY, A. & AMIRA, A. 2022. Using artificial intelligence and data fusion for environmental monitoring: A review and future perspectives. *Information Fusion,* 86**,** 44-75.

HINTON, G., VINYALS, O. & DEAN, J. 2015. Distilling the knowledge in a neural network. *arXiv preprint arXiv:.02531*.

HOU, S., PAN, X., LOY, C. C., WANG, Z. & LIN, D. Learning a unified classifier incrementally via rebalancing. Proceedings of the IEEE/CVF conference on computer vision and pattern recognition, 2019. 831-839.

HOWARD, A., SANDLER, M., CHU, G., CHEN, L.-C., CHEN, B., TAN, M., WANG, W., ZHU, Y., PANG, R. & VASUDEVAN, V. Searching for mobilenetv3. Proceedings of the IEEE/CVF international conference on computer vision, 2019. 1314-1324.

HSIAO, S.-W. & TSAI, H.-C. 2005. Applying a hybrid approach based on fuzzy neural network and genetic algorithm to product form design. *International Journal of Industrial Ergonomics,* 35**,** 411-428.

HU, F., LIU, Y., QIN, J., SUN, X. & WITHERELL, P. Feature-level Data Fusion for Energy Consumption Analytics in Additive Manufacturing. 2020 IEEE 16th International Conference on Automation Science and Engineering (CASE), 2020. IEEE, 612-617.

HU, F., QIN, J., LI, Y., LIU, Y. & SUN, X. 2021. Deep fusion for energy consumption prediction in additive manufacturing. *Procedia CIRP,* 104**,** 1878-1883.

HUANG, J., KWOK, T.-H., ZHOU, C. & XU, W. 2019. Surfel convolutional neural network for support detection in additive manufacturing. *The International Journal of Advanced Manufacturing Technology,* 105**,** 3593-3604.

HUANG, Q., WANG, Y., LYU, M. & LIN, W. 2020. Shape Deviation Generator--A Convolution Framework for Learning and Predicting 3-D Printing Shape Accuracy. *IEEE Transactions on Automation Science Engineering*.

HUANG, R., RIDDLE, M., GRAZIANO, D., WARREN, J., DAS, S., NIMBALKAR, S., CRESKO, J. & MASANET, E. 2016. Energy and emissions saving potential of additive manufacturing: the case of lightweight aircraft components. *Journal of Cleaner Production,* 135**,** 1559-1570.

ISLAM, M., PURTONEN, T., PIILI, H., SALMINEN, A. & NYRHILä, O. 2013. Temperature profile and imaging analysis of laser additive manufacturing of stainless steel. *Physics Procedia,* 41**,** 835-842.

ISO/ASTM 2016. Standard Terminology for Additive Manufacturing–General Principles–Terminology.

ISO 2019. Metallic Materials — Tensile Testing — Part 1: Method of Test at Room Temperature. ISO 6892-1:2019(en).

JHA, A. V., APPASANI, B., GHAZALI, A. N., PATTANAYAK, P., GURJAR, D. S., KABALCI, E. & MOHANTA, D. 2021. Smart grid cyber-physical systems: Communication technologies, standards and challenges. *Wireless Networks,* 27**,** 2595-2613.

JIANG, J. 2023. A survey of machine learning in additive manufacturing technologies. *International Journal of Computer Integrated Manufacturin***,** 1-23.

JIANG, J., XIONG, Y., ZHANG, Z. & ROSEN, D. W. 2020a. Machine learning integrated design for additive manufacturing. *Journal of Intelligent Manufacturin***,** 1-14.

JIANG, J., YU, C., XU, X., MA, Y. & LIU, J. 2020b. Achieving better connections between deposited lines in additive manufacturing via machine learning. *Math. Biosci. Eng,* 17.

JIN, Z., ZHANG, Z. & GU, G. X. 2019. Autonomous in-situ correction of fused deposition modeling printers using computer vision and deep learning. *Manufacturing Letters,* 22**,** 11-15.

KALMAN, R. E. 1960. A new approach to linear filtering and prediction problems.

KAMAL, M. & RIZZA, G. 2019. Design for metal additive manufacturing for aerospace applications. *Additive manufacturing for the aerospace industry.* Elsevier.

KAMATH, C. & FAN, Y. J. 2018. Regression with small data sets: a case study using code surrogates in additive manufacturing. *Knowledge Information Systems,* 57**,** 475-493.

KANG, M., PARK, J. & HAN, B. Class-incremental learning by knowledge distillation with adaptive feature consolidation. Proceedings of the IEEE/CVF conference on computer vision and pattern recognition, 2022. 16071-16080.

KAPUSUZOGLU, B. & MAHADEVAN, S. 2020. Physics-informed and hybrid machine learning in additive manufacturing: Application to fused filament fabrication. *JOM,* 72**,** 4695-4705.

KARNIADAKIS, G. E., KEVREKIDIS, I. G., LU, L., PERDIKARIS, P., WANG, S. & YANG, L. 2021. Physics-informed machine learning. *Nature Reviews Physics,* 3**,** 422-440.

KE, G., MENG, Q., FINLEY, T., WANG, T., CHEN, W., MA, W., YE, Q. & LIU, T.-Y. Lightgbm: A highly efficient gradient boosting decision tree. Advances in neural information processing systems, 2017. 3146-3154.

KELEŞ, Ö., BLEVINS, C. W. & BOWMAN, K. J. 2017. Effect of build orientation on the mechanical reliability of 3D printed ABS. *Rapid Prototyping Journal,* 23**,** 320-328.

KHADILKAR, A., WANG, J. & RAI, R. 2019. Deep learning–based stress prediction for bottom-up sla 3d printing process. *The International Journal of Advanced Manufacturing Technology,* 102**,** 2555-2569.

KHAN, M. F., ALAM, A., SIDDIQUI, M. A., ALAM, M. S., RAFAT, Y., SALIK, N. & AL-SAIDAN, I. 2021. Real-time defect detection in 3D printing using machine learning. *Materials Today: Proceedings,* 42**,** 521-528.

KHANZADEH, M., CHOWDHURY, S., MARUFUZZAMAN, M., TSCHOPP, M. A. & BIAN, L. 2018a. Porosity prediction: Supervised-learning of thermal history for direct laser deposition. *Journal of manufacturing systems,* 47**,** 69-82.

KHANZADEH, M., CHOWDHURY, S., TSCHOPP, M. A., DOUDE, H. R., MARUFUZZAMAN, M. & BIAN, L. 2019. In-situ monitoring of melt pool images for porosity prediction in directed energy deposition processes. *IISE Transactions,* 51**,** 437-455.

KHANZADEH, M., RAO, P., JAFARI-MARANDI, R., SMITH, B. K., TSCHOPP, M. A. & BIAN, L. 2018b. Quantifying geometric accuracy with unsupervised machine learning: Using self-organizing map on fused filament fabrication additive manufacturing parts. *Journal of Manufacturing Science Engineering,* 140.

KHOSRAVANI, M. R., NASIRI, S. & REINICKE, T. 2022. Intelligent knowledge-based system to improve injection molding process. *Journal of industrial information Integration,* 25**,** 100275.

KIM, D. B., WITHERELL, P., LIPMAN, R. & FENG, S. C. J. A. M. 2015. Streamlining the additive manufacturing digital spectrum: A systems approach. 5**,** 20-30.

KIM, J. S., LEE, C. S., KIM, S.-M. & LEE, S. W. 2018. Development of data-driven in-situ monitoring and diagnosis system of fused deposition modeling (FDM) process based on support vector machine algorithm. *International Journal of Precision Engineering Manufacturing-Green Technology,* 5**,** 479-486.

KO, H., WITHERELL, P., LU, Y., KIM, S. & ROSEN, D. W. 2021. Machine learning and knowledge graph based design rule construction for additive manufacturing. *Additive Manufacturing,* 37**,** 101620.

KOEPPE, A., PADILLA, C. A. H., VOSHAGE, M., SCHLEIFENBAUM, J. H. & MARKERT, B. 2018. Efficient numerical modeling of 3D-printed lattice-cell structures using neural networks. *Manufacturing Letters,* 15**,** 147-150.

KONG, L., PENG, X., CHEN, Y., WANG, P. & XU, M. 2020. Multi-sensor measurement and data fusion technology for manufacturing process monitoring: a literature review. *International journal of extreme manufacturing,* 2**,** 022001.

KOROTCOV, A., TKACHENKO, V., RUSSO, D. P. & EKINS, S. 2017. Comparison of deep learning with multiple machine learning methods and metrics using diverse drug discovery data sets. *Molecular pharmaceutics,* 14**,** 4462-4475.

KOURAYTEM, N., LI, X., TAN, W., KAPPES, B. & SPEAR, A. 2020. Modeling process-structure-property relationships in metal additive manufacturing: A review on physics-driven versus data-driven approaches. *Journal of Physics: Materials*.

KüHN, A., JOPPEN, R., REINHART, F., RöLTGEN, D., VON ENZBERG, S. & DUMITRESCU, R. J. P. C. 2018. Analytics canvas–a framework for the design and specification of data analytics projects. 70**,** 162-167.

KUMAR, H. A., KUMARAGURU, S., PAUL, C. & BINDRA, K. 2021. Faster temperature prediction in the powder bed fusion process through the development of a surrogate model. *Optics Laser Technology,* 141**,** 107122.

KUMAR, S. & TRIPATHI, B. K. 2018. High-dimensional information processing through resilient propagation in quaternionic domain. *Journal of Industrial Information Integration,* 11**,** 41-49.

KUMKE, M., WATSCHKE, H. & VIETOR, T. 2016. A new methodological framework for design for additive manufacturing. *Virtual Physical Prototyping,* 11**,** 3-19.

KUSANO, M., MIYAZAKI, S., WATANABE, M., KISHIMOTO, S., BULGAREVICH, D. S., ONO, Y. & YUMOTO, A. 2020. Tensile properties prediction by multiple linear regression analysis for selective laser melted and post heat-treated Ti-6Al-4V with microstructural quantification. *Materials Science Engineering: A***,** 139549.

KWON, O., KIM, H. G., KIM, W., KIM, G.-H. & KIM, K. 2020. A Convolutional Neural Network for Prediction of Laser Power Using Melt-Pool Images in Laser Powder Bed Fusion. *IEEE Access,* 8**,** 23255-23263.

LAMSELLAK, O., BENLGHAZI, A., CHETOUANI, A. & BENALI, A. Human body action recognition with machine learning for bionic applications: a Sensor Data Fusion Approach. 2022 International Conference on Electrical, Computer and Energy Technologies (ICECET), 2022. IEEE, 1-5.

LEE, C. H., KüHN, U., LEE, S. C., PARK, S. J., SCHWAB, H., SCUDINO, S. & KOSIBA, K. 2021. Optimizing laser powder bed fusion of Ti-5Al-5V-5Mo-3Cr by artificial intelligence. *Journal of Alloysn Compounds,* 862**,** 158018.

LEE, J., AZAMFAR, M., SINGH, J. & SIAHPOUR, S. 2020a. Integration of digital twin and deep learning in cyber‐physical systems: towards smart manufacturing. *IET Collaborative Intelligent Manufacturing,* 2**,** 34-36.

LEE, S., PARK, W., CHO, H., ZHANG, W. & LEU, M.-C. 2001. A neural network approach to the modelling and analysis of stereolithography processes. *Proceedings of the Institution of Mechanical Engineers, Part B: Journal of Engineering Manufacture,* 215**,** 1719-1733.

LEE, S., PENG, J., SHIN, D., CHOI, Y. S. J. S. & MATERIALS, T. O. A. 2019. Data analytics approach for melt-pool geometries in metal additive manufacturing. *Science and Technology of Advanced Materials,* 20**,** 972-978.

LEE, W.-C., WEI, C.-C. & CHUNG, S.-C. 2014. Development of a hybrid rapid prototyping system using low-cost fused deposition modeling and five-axis machining. *Journal of Materials Processing Technology,* 214**,** 2366-2374.

LEE, X. Y., SAHA, S. K., SARKAR, S. & GIERA, B. 2020b. Automated Detection of Part Quality During Two Photon Lithography via Deep Learning. *Additive Manufacturing***,** 101444.

LEW, A. J. & BUEHLER, M. J. 2021. Encoding and exploring latent design space of optimal material structures via a VAE-LSTM model. *Forces in Mechanics,* 5**,** 100054.

LI, J., SAGE, M., GUAN, X., BROCHU, M. & ZHAO, Y. F. 2020a. Machine Learning-Enabled Competitive Grain Growth Behavior Study in Directed Energy Deposition Fabricated Ti6Al4V. *JOM,* 72**,** 458-464.

LI, R., JIN, M. & PAQUIT, V. C. 2021a. Geometrical defect detection for additive manufacturing with machine learning models. *Materials Design,* 206**,** 109726.

LI, X., JIA, X., YANG, Q. & LEE, J. 2020b. Quality analysis in metal additive manufacturing with deep learning. *Journal of Intelligent Manufacturing,* 31**,** 2003-2017.

LI, Y., HU, F., QIN, J., RYAN, M., WANG, R. & LIU, Y. 2021b. A hybrid machine learning approach for energy consumption prediction in additive manufacturing. *25th International Conference on Pattern Recognition (ICPR 2020), Virtual***,** 622-636.

LI, Y., POLDEN, J., PAN, Z., CUI, J., XIA, C., HE, F., MU, H., LI, H. & WANG, L. 2022. A defect detection system for wire arc additive manufacturing using incremental learning. *Journal of Industrial Information Integration,* 27**,** 100291.

LI, Y., SUN, Y., HAN, Q., ZHANG, G. & HORVáTH, I. 2018. Enhanced beads overlapping model for wire and arc additive manufacturing of multi-layer multi-bead metallic parts. *Journal of Materials Processing Technology,* 252**,** 838-848.

LI, Z., ZHANG, Z., SHI, J. & WU, D. 2019. Prediction of surface roughness in extrusion-based additive manufacturing with machine learning. *Robotics Computer-Integrated Manufacturing,* 57**,** 488-495.

LIN, W., SHEN, H., FU, J. & WU, S. 2019. Online quality monitoring in material extrusion additive manufacturing processes based on laser scanning technology. *Precision Engineering,* 60**,** 76-84.

LIU, W. & HE, Y. 2008. Representation and retrieval of 3D CAD models in parts library. *The International Journal of Advanced Manufacturing Technology*, 36, 950-958.

LIU, J., HU, Y., WU, B. & WANG, Y. 2018. An improved fault diagnosis approach for FDM process with acoustic emission. *Journal of Manufacturing Processes,* 35**,** 570-579.

LIU, R., LIU, S. & ZHANG, X. 2021. A physics-informed machine learning model for porosity analysis in laser powder bed fusion additive manufacturing. *The International Journal of Advanced Manufacturing Technology,* 113**,** 1943-1958.

LUN, Y. Z., D'INNOCENZO, A., SMARRA, F., MALAVOLTA, I. & DI BENEDETTO, M. D. 2019. State of the art of cyber-physical systems security: An automatic control perspective. *Journal of Systems Software,* 149**,** 174-216.

LV, J., PENG, T., ZHANG, Y. & WANG, Y. 2020. A novel method to forecast energy consumption of selective laser melting processes. *International Journal of Production Research***,** 1-17.

MA, S., TANG, Q., LIU, Y. & FENG, Q. 2022. Prediction of Mechanical Properties of Three-Dimensional Printed Lattice Structures Through Machine Learning. *Journal of Computing Information Science in Engineering,* 22**,** 031008.

MADHAVADAS, V., SRIVASTAVA, D., CHADHA, U., RAJ, S. A., SULTAN, M. T. H., SHAHAR, F. S. & SHAH, A. U. M. 2022. A review on metal additive manufacturing for intricately shaped aerospace components. *CIRP Journal of Manufacturing Science Technology,* 39**,** 18-36.

MAIRAL, J., BACH, F. & PONCE, J. 2011. Task-driven dictionary learning. *IEEE transactions on pattern analysis machine intelligence,* 34**,** 791-804.

MALIK, A., LHACHEMI, H. & SHORTEN, R. 2023. A cyber-physical system to design 3D models using mixed reality technologies and deep learning for additive manufacturing. *Plos one,* 18**,** e0289207.

MALIK, P. K., SHARMA, R., SINGH, R., GEHLOT, A., SATAPATHY, S. C., ALNUMAY, W. S., PELUSI, D., GHOSH, U. & NAYAK, J. 2021. Industrial Internet of Things and its applications in industry 4.0: State of the art. *Computer Communications,* 166**,** 125-139.

MASKERY, I., STURM, L., AREMU, A. O., PANESAR, A., WILLIAMS, C. B., TUCK, C. J., WILDMAN, R. D., ASHCROFT, I. A. & HAGUE, R. J. 2018. Insights into the mechanical properties of several triply periodic minimal surface lattice structures made by polymer additive manufacturing. *Polymer,* 152**,** 62-71.

MCGREGOR, D. J., TAWFICK, S. & KING, W. P. 2019. Mechanical properties of hexagonal lattice structures fabricated using continuous liquid interface production additive manufacturing. *Additive Manufacturing,* 25**,** 10-18.

MEHRPOUYA, M., GISARIO, A., RAHIMZADEH, A., NEMATOLLAHI, M., BAGHBADERANI, K. S. & ELAHINIA, M. 2019. A prediction model for finding the optimal laser parameters in additive manufacturing of NiTi shape memory alloy. *The International Journal of Advanced Manufacturing Technology,* 105**,** 4691-4699.

MENG, L. & ZHANG, J. 2020. Process Design of Laser Powder Bed Fusion of Stainless Steel Using a Gaussian Process-Based Machine Learning Model. *JOM,* 72**,** 420-428.

MICHIELI, U., ZANUTTIGH, P. J. C. V. & UNDERSTANDING, I. 2021. Knowledge distillation for incremental learning in semantic segmentation. *Computer Vision Image Understanding,* 205**,** 103167.

MONDAL, S., GWYNN, D., RAY, A. & BASAK, A. 2020. Investigation of Melt Pool Geometry Control in Additive Manufacturing Using Hybrid Modeling. *Metals,* 10**,** 683.

MONTAZERI, M., NASSAR, A. R., STUTZMAN, C. B. & RAO, P. 2019. Heterogeneous sensor-based condition monitoring in directed energy deposition. *Additive Manufacturing,* 30**,** 100916.

MONTAZERI, M. & RAO, P. 2018. Sensor-based build condition monitoring in laser powder bed fusion additive manufacturing process using a spectral graph theoretic approach. *Journal of Manufacturing Science Engineering,* 140.

MOZAFFAR, M., PAUL, A., AL-BAHRANI, R., WOLFF, S., CHOUDHARY, A., AGRAWAL, A., EHMANN, K. & CAO, J. 2018. Data-driven prediction of the high-dimensional thermal history in directed energy deposition processes via recurrent neural networks. *Manufacturing letters,* 18**,** 35-39.

MUHAMMAD, W., BRAHME, A. P., IBRAGIMOVA, O., KANG, J. & INAL, K. 2021. A machine learning framework to predict local strain distribution and the evolution of plastic anisotropy & fracture in additively manufactured alloys. *International Journal of Plasticity,* 136**,** 102867.

MUNEESWARAN, V., NAGARAJ, P., DHANNUSHREE, U., ISHWARYA LAKSHMI, S., AISHWARYA, R. & SUNETHRA, B. 2021. A Framework for Data Analytics-Based Healthcare Systems. *Innovative Data Communication Technologies and Application.* Springer.

MUNFORD, M., HOSSAIN, U., GHOUSE, S. & JEFFERS, J. R. 2021. Prediction of anisotropic mechanical properties for lattice structures. *Additive Manufacturing,* 32**,** 101041.

NALAJAM, P. K. & VARADARAJAN, R. 2021. A Hybrid Deep Learning Model for Layer-Wise Melt Pool Temperature Forecasting in Wire-Arc Additive Manufacturing Process. *IEEE Access*.

NASIRI, S. & KHOSRAVANI, M. R. 2021. Machine learning in predicting mechanical behavior of additively manufactured parts. *Journal of Materials Research Technology*.

NGO, T. D., KASHANI, A., IMBALZANO, G., NGUYEN, K. T. & HUI, D. 2018. Additive manufacturing (3D printing): A review of materials, methods, applications and challenges. *Composites Part B: Engineering,* 143**,** 172-196.

NGUYEN, L., BUHL, J. & BAMBACH, M. 2020. Continuous Eulerian tool path strategies for wire-arc additive manufacturing of rib-web structures with machine-learning-based adaptive void filling. *Additive Manufacturing,* 35**,** 101265.

OKARO, I. A., JAYASINGHE, S., SUTCLIFFE, C., BLACK, K., PAOLETTI, P. & GREEN, P. L. 2019. Automatic fault detection for laser powder-bed fusion using semi-supervised machine learning. *Additive Manufacturing,* 27**,** 42-53.

ÖZEL, T., ALTAY, A., DONMEZ, A. & LEACH, R. J. T. I. J. O. A. M. T. 2018. Surface topography investigations on nickel alloy 625 fabricated via laser powder bed fusion. 94**,** 4451-4458.

PAOLINI, A., KOLLMANNSBERGER, S. & RANK, E. 2019. Additive manufacturing in construction: A review on processes, applications, and digital planning methods. *Additive manufacturing,* 30**,** 100894.

PARK, H., KO, H., LEE, Y.-T. T., CHO, H. & WITHERELL, P. A framework for identifying and prioritizing data analytics opportunities in additive manufacturing. 2019 IEEE International Conference on Big Data (Big Data), 2019. IEEE, 3458-3467.

PARK, H., KO, H., LEE, Y.-T. T., FENG, S., WITHERELL, P. & CHO, H. 2021. Collaborative knowledge management to identify data analytics opportunities in additive manufacturing. *Journal of Intelligent Manufacturing***,** 1-24.

PARK, S.-I., ROSEN, D. W., CHOI, S.-K. & DUTY, C. E. 2014. Effective mechanical properties of lattice material fabricated by material extrusion additive manufacturing. *Additive Manufacturing,* 1**,** 12-23.

PELOQUIN, J., KIRILLOVA, A., RUDIN, C., BRINSON, L. & GALL, K. 2023. Prediction of tensile performance for 3D printed photopolymer gyroid lattices using structural porosity, base material properties, and machine learning. *Materials Design,* 232**,** 112126.

PENG, C., TRAN, P., NGUYEN-XUAN, H. & FERREIRA, A. 2020. Mechanical performance and fatigue life prediction of lattice structures: Parametric computational approach. *Composite Structures,* 235**,** 111821.

PINKERTON, A. J. & LI, L. J. J. O. P. D. A. P. 2004. Modelling the geometry of a moving laser melt pool and deposition track via energy and mass balances. *Journal of Physics D: Applied Physics,* 37**,** 1885.

POORGANJI, B., OTT, E., KELKAR, R., WESSMAN, A. & JAMSHIDINIA, M. 2020. Materials Ecosystem for Additive Manufacturing Powder Bed Fusion Processes. *JOM,* 72**,** 561-576.

POPOVA, E., RODGERS, T. M., GONG, X., CECEN, A., MADISON, J. D. & KALIDINDI, S. R. 2017. Process-structure linkages using a data science approach: application to simulated additive manufacturing data. *Integrating Materials Manufacturing Innovation,* 6**,** 54-68.

PRASHAR, G., VASUDEV, H. & BHUDDHI, D. 2022. Additive manufacturing: expanding 3D printing horizon in industry 4.0. *International Journal on Interactive Design Manufacturing***,** 1-15.

QI, X., CHEN, G., LI, Y., CHENG, X. & LI, C. 2019a. Applying Neural-Network-Based Machine Learning to Additive Manufacturing: Current Applications, Challenges, and Future Perspectives. *Engineering*.

QI, X., CHEN, G., LI, Y., CHENG, X. & LI, C. 2019b. Applying neural-network-based machine learning to additive manufacturing: current applications, challenges, and future perspectives. *Engineering,* 5**,** 721-729.

QIN, J., HU, F., LIU, Y., WITHERELL, P., WANG, C. C., ROSEN, D. W., SIMPSON, T., LU, Y. & TANG, Q. 2022a. Research and application of machine learning for additive manufacturing. *Additive Manufacturing***,** 102691.

QIN, J., HU, F., LIU, Y., WITHERELL, P., WANG, C. C., ROSEN, D. W., SIMPSON, T. W., LU, Y. & TANG, Q. 2022b. Research and application of machine learning for additive manufacturing. *Additive Manufacturing,* 52**,** 102691.

QIN, J., LI, Z., WANG, R., LI, L., YU, Z., HE, X. & LIU, Y. 2021. Industrial Internet of Learning (IIoL): IIoT based pervasive knowledge network for LPWAN—concept, framework and case studies. *CCF Transactions on Pervasive Computing Interaction,* 3**,** 25-39.

QIN, J., LIU, Y. & GROSVENOR, R. 2018a. Multi-source data analytics for AM energy consumption prediction. *Advanced Engineering Informatics,* 38**,** 840-850.

QIN, J., LIU, Y. & GROSVENOR, R. 2018b. Multi-source data analytics for AM energy consumption prediction. *Advanced Engineering Informatics,* 38**,** 840-850.

QIN, J., LIU, Y., GROSVENOR, R., LACAN, F. & JIANG, Z. 2020. Deep learning-driven particle swarm optimisation for additive manufacturing energy optimisation. *Journal of Cleaner Production,* 245**,** 118702.

QUAN, Z., WU, A., KEEFE, M., QIN, X., YU, J., SUHR, J., BYUN, J.-H., KIM, B.-S. & CHOU, T.-W. 2015. Additive manufacturing of multi-directional preforms for composites: opportunities and challenges. *Materials Today,* 18**,** 503-512.

RAZVI, S. S., FENG, S., NARAYANAN, A., LEE, Y.-T. T. & WITHERELL, P. A review of machine learning applications in additive manufacturing. International Design Engineering Technical Conferences and Computers and Information in Engineering Conference, 2019. American Society of Mechanical Engineers, V001T02A040.

REN, K., CHEW, Y., LIU, N., ZHANG, Y., FUH, J. & BI, G. 2021. Integrated numerical modelling and deep learning for multi-layer cube deposition planning in laser aided additive manufacturing. *Virtual Physical Prototyping***,** 1-15.

REN, K., CHEW, Y., ZHANG, Y., FUH, J. & BI, G. 2020. Thermal field prediction for laser scanning paths in laser aided additive manufacturing by physics-based machine learning. *Computer Methods in Applied Mechanics Engineering,* 362**,** 112734.

RONG-JI, W., XIN-HUA, L., QING-DING, W. & LINGLING, W. 2009. Optimizing process parameters for selective laser sintering based on neural network and genetic algorithm. *The International Journal of Advanced Manufacturing Technology,* 42**,** 1035-1042.

ROY, M. & WODO, O. 2020. Data-driven modeling of thermal history in additive manufacturing. *Additive Manufacturing,* 32**,** 101017.

SALCEDO-SANZ, S., GHAMISI, P., PILES, M., WERNER, M., CUADRA, L., MORENO-MARTíNEZ, A., IZQUIERDO-VERDIGUIER, E., MUñOZ-MARí, J., MOSAVI, A. & CAMPS-VALLS, G. 2020. Machine learning information fusion in Earth observation: A comprehensive review of methods, applications and data sources. *Information Fusion,* 63**,** 256-272.

SAMIE TOOTOONI, M., DSOUZA, A., DONOVAN, R., RAO, P. K., KONG, Z. J. & BORGESEN, P. 2017. Classifying the dimensional variation in additive manufactured parts from laser-scanned three-dimensional point cloud data using machine learning approaches. *Journal of Manufacturing Science Engineering,* 139.

SARVANKAR, S. G. & YEWALE, S. N. 2019. Additive manufacturing in automobile industry. *Int. J. Res. Aeronaut. Mech. Eng,* 7**,** 1-10.

SBARGOUD, F., DJEHA, M., GUIATNI, M. & ABABOU, N. 2019. WPT-ANN and Belief Theory Based EEG/EMG Data Fusion for Movement Identification. *Traitement du Signal,* 36**,** 383-391.

SCHROFF, F., KALENICHENKO, D. & PHILBIN, J. Facenet: A unified embedding for face recognition and clustering. Proceedings of the IEEE conference on computer vision and pattern recognition, 2015. 815-823.

SCIME, L. & BEUTH, J. 2018. A multi-scale convolutional neural network for autonomous anomaly detection and classification in a laser powder bed fusion additive manufacturing process. *Additive Manufacturing,* 24**,** 273-286.

SCIME, L. & BEUTH, J. 2019. Using machine learning to identify in-situ melt pool signatures indicative of flaw formation in a laser powder bed fusion additive manufacturing process. *Additive Manufacturing,* 25**,** 151-165.

SEEGER, P. M., YAHOUNI, Z. & ALPAN, G. 2022. Literature review on using data mining in production planning and scheduling within the context of cyber physical systems. *Journal of Industrial Information Integration***,** 100371.

SEHARING, A., AZMAN, A. H. & ABDULLAH, S. 2020. A review on integration of lightweight gradient lattice structures in additive manufacturing parts. *Advances in Mechanical Engineering,* 12**,** 1687814020916951.

SHAHRUBUDIN, N., LEE, T. C. & RAMLAN, R. 2019. An overview on 3D printing technology: Technological, materials, and applications. *Procedia Manufacturing,* 35**,** 1286-1296.

SHEN, Z., SHANG, X., ZHAO, M., DONG, X., XIONG, G. & WANG, F.-Y. 2019. A learning-based framework for error compensation in 3D printing. *IEEE TRANSACTIONS ON CYBERNETICS,* 49**,** 4042-4050.

SHEVCHIK, S. A., KENEL, C., LEINENBACH, C. & WASMER, K. 2018. Acoustic emission for in situ quality monitoring in additive manufacturing using spectral convolutional neural networks. *Additive Manufacturing,* 21**,** 598-604.

SHEVCHIK, S. A., MASINELLI, G., KENEL, C., LEINENBACH, C. & WASMER, K. 2019. Deep learning for in situ and real-time quality monitoring in additive manufacturing using acoustic emission. *IEEE TRANSACTIONS ON INDUSTRIAL INFORMATICS,* 15**,** 5194-5203.

SHI, Z., LI, Y. & LIU, C. Knowledge Distillation-enabled Multi-stage Incremental Learning for Online Process Monitoring in Advanced Manufacturing. 2022 IEEE International Conference on Data Mining Workshops (ICDMW), 2022. IEEE, 860-867.

SHIM, D.-S., BAEK, G.-Y., SEO, J.-S., SHIN, G.-Y., KIM, K.-P., LEE, K.-Y. J. O. & TECHNOLOGY, L. 2016. Effect of layer thickness setting on deposition characteristics in direct energy deposition (DED) process. *Optics Laser Technology,* 86**,** 69-78.

SIEGEL, J. E., BEEMER, M. F. & SHEPARD, S. M. 2020. Automated Non-Destructive Inspection of Fused Filament Fabrication Components Using Thermographic Signal Reconstruction. *Additive Manufacturing,* 31**,** 100923.

SIMONYAN, K. & ZISSERMAN, A. 2014. Very deep convolutional networks for large-scale image recognition. *arXiv preprint*

SINGH, S., RAMAKRISHNA, S. & SINGH, R. 2017. Material issues in additive manufacturing: A review. *Journal of Manufacturing Processes,* 25**,** 185-200.

SMITH, J., XIONG, W., YAN, W., LIN, S., CHENG, P., KAFKA, O. L., WAGNER, G. J., CAO, J. & LIU, W. K. 2016a. Linking process, structure, property, and performance for metal-based additive manufacturing: computational approaches with experimental support. *Computational Mechanics,* 57**,** 583-610.

SMITH, J., XIONG, W., YAN, W., LIN, S., CHENG, P., KAFKA, O. L., WAGNER, G. J., CAO, J. & LIU, W. K. 2016b. Linking process, structure, property, and performance for metal-based additive manufacturing: computational approaches with experimental support. *Computational Mechanics,* 57**,** 583-610.

SNOW, Z., DIEHL, B., REUTZEL, E. W. & NASSAR, A. 2021. Toward in-situ flaw detection in laser powder bed fusion additive manufacturing through layerwise imagery and machine learning. *Journal of Manufacturing Systems,* 59**,** 12-26.

SONG, L., BAGAVATH-SINGH, V., DUTTA, B. & MAZUMDER, J. J. T. I. J. O. A. M. T. 2012. Control of melt pool temperature and deposition height during direct metal deposition process. *The International Journal of Advanced Manufacturing Technology,* 58**,** 247-256.

SOOD, A. K., OHDAR, R. K. & MAHAPATRA, S. S. 2012. Experimental investigation and empirical modelling of FDM process for compressive strength improvement. *Journal of Advanced Research,* 3**,** 81-90.

SREENIVASAN, R. & BOURELL, D. 2010. Sustainability Study in Selective Laser Sintering- An Energy Perspective. Minerals, Metals and Materials Society/AIME, 420 Commonwealth Dr., P. O. Box ….

STANISAVLJEVIC, D., CEMERNEK, D., GURSCH, H., URAK, G. & LECHNER, G. 2019. Detection of interferences in an additive manufacturing process: an experimental study integrating methods of feature selection and machine learning. *International Journal of Production Research***,** 1-23.

SUN, G., ZHANG, X., JIA, X., REN, J., ZHANG, A., YAO, Y. & ZHAO, H. 2020. Deep Fusion of Localized Spectral Features and Multi-scale Spatial Features for Effective Classification of Hyperspectral Images. *nternational Journal of Applied Earth Observation Geoinformation,* 91**,** 102157.

TAHERI, H., SHOAIB, M., KOESTER, L. W., BIGELOW, T. A., COLLINS, P. C. & BOND, L. J. 2017. Powder based additive manufacturing-A review of types of defects, generation mechanisms, detection, property evaluation and metrology. *Electrical and Computer Engineering,* 1**,** 172-209.

TANG, Y., DONG, G., ZHOU, Q. & ZHAO, Y. F. 2017a. Lattice structure design and optimization with additive manufacturing constraints. *Additive Manufacturing,* 15**,** 1546-1562.

TANG, Y., DONG, G., ZHOU, Q. & ZHAO, Y. F. 2017b. Lattice structure design and optimization with additive manufacturing constraints. *IEEE Transactions on Automation Science Engineering,* 15**,** 1546-1562.

TAO, W. & LEU, M. C. Design of lattice structure for additive manufacturing. 2016 International Symposium on Flexible Automation (ISFA), 2016. IEEE, 325-332.

TAPIA, G., KHAIRALLAH, S., MATTHEWS, M., KING, W. E. & ELWANY, A. 2018. Gaussian process-based surrogate modeling framework for process planning in laser powder-bed fusion additive manufacturing of 316L stainless steel. *The International Journal of Advanced Manufacturing Technology,* 94**,** 3591-3603.

TECHNOLOGY, N. I. O. S. A. 1993. Integration Definition for Function Modeling (IDEF0). Federal Information Processing Standard Publication.

TELENKO, C. & SEEPERSAD, C. C. Assessing energy requirements and material flows of selective laser sintering of Nylon parts. Proceedings of the Solid Freeform Fabrication Symposium, 2010. 8-10.08.

THOMPSON, M. K., MORONI, G., VANEKER, T., FADEL, G., CAMPBELL, R. I., GIBSON, I., BERNARD, A., SCHULZ, J., GRAF, P. & AHUJA, B. 2016. Design for Additive Manufacturing: Trends, opportunities, considerations, and constraints. *CIRP annals,* 65**,** 737-760.

TIAN, Q., GUO, S., MELDER, E., BIAN, L. & GUO, W. 2021a. Deep learning-based data fusion method for in situ porosity detection in laser-based additive manufacturing. *Journal of Manufacturing Science Engineering,* 143.

TIAN, Q., GUO, S., MELDER, E., BIAN, L. & GUO, W. G. 2021b. Deep learning-based data fusion method for in situ porosity detection in laser-based additive manufacturing. *Journal of Manufacturing Science Engineering,* 143**,** 041011.

TIAN, W., MA, J. & ALIZADEH, M. 2019. Energy consumption optimization with geometric accuracy consideration for fused filament fabrication processes. *The International Journal of Advanced Manufacturing Technology,* 103**,** 3223-3233.

TOMINSKI, C., FUCHS, G. & SCHUMANN, H. Task-driven color coding. 2008 12th International Conference Information Visualisation, 2008. IEEE, 373-380.

UDROIU, R., BRAGA, I. C. & NEDELCU, A. 2019. Evaluating the quality surface performance of additive manufacturing systems: Methodology and a material jetting case study. *Materials,* 12**,** 995.

VAFADAR, A., GUZZOMI, F., RASSAU, A. & HAYWARD, K. 2021. Advances in metal additive manufacturing: a review of common processes, industrial applications, and current challenges. *Applied Sciences,* 11**,** 1213.

VALENTE, R., OSTAPENKO, A., SOUSA, B. C., GRUBBS, J., MASSAR, C. J., COTE, D. L. & NEAMTU, R. Classifying Powder Flowability for Cold Spray Additive Manufacturing Using Machine Learning. 2020 IEEE International Conference on Big Data (Big Data), 2020. IEEE, 2919-2928.

VAN DE VEN, G. M., TUYTELAARS, T. & TOLIAS, A. S. 2022. Three types of incremental learning. *Nature Machine Intelligence,* 4**,** 1185-1197.

VANDONE, A., BARALDO, S. & VALENTE, A. 2018. Multisensor data fusion for additive manufacturing process control. *IEEE Robotics Automation Letters,* 3**,** 3279-3284.

VERMA, A. & RAI, R. 2017. Sustainability-induced dual-level optimization of additive manufacturing process. *The International Journal of Advanced Manufacturing Technology,* 88**,** 1945-1959.

VOSNIAKOS, G., MAROULIS, T. & PANTELIS, D. 2007. A method for optimizing process parameters in layer-based rapid prototyping. *Proceedings of the Institution of Mechanical Engineers, Part B: Journal of Engineering Manufacture,* 221**,** 1329-1340.

VRáBEL, J., POŘíZKA, P., KLUS, J., PROCHAZKA, D., NOVOTNý, J., KOUTNý, D., PALOUŠEK, D. & KAISER, J. 2019. Classification of materials for selective laser melting by laser-induced breakdown spectroscopy. *Chemical Papers,* 73**,** 2897-2905.

WACKER, C., KöHLER, M., DAVID, M., ASCHERSLEBEN, F., GABRIEL, F., HENSEL, J., DILGER, K. & DRöDER, K. 2021. Geometry and Distortion Prediction of Multiple Layers for Wire Arc Additive Manufacturing with Artificial Neural Networks. *Applied Sciences,* 11**,** 4694.

WAGNER, J., FISCHER, V., HERMAN, M. & BEHNKE, S. Multispectral Pedestrian Detection using Deep Fusion Convolutional Neural Networks. ESANN, 2016.

WANG, A., SONG, S., HUANG, Q. & TSUNG, F. 2016. In-plane shape-deviation modeling and compensation for fused deposition modeling processes. *IEEE Transactions on Automation Science,* 14**,** 968-976.

WANG, C., TAN, X., TOR, S. B. & LIM, C. 2020a. Machine learning in additive manufacturing: State-of-the-art and perspectives. *Additive Manufacturing,* 36**,** 101538.

WANG, C. C., LEUNG, Y.-S. & CHEN, Y. 2010. Solid modeling of polyhedral objects by layered depth-normal images on the GPU. *Computer-Aided Design,* 42**,** 535-544.

WANG, J., MA, Y., ZHANG, L., GAO, R. X. & WU, D. 2018a. Deep learning for smart manufacturing: Methods and applications. *Journal of manufacturing systems,* 48**,** 144-156.

WANG, K., XU, J., ZHANG, S. & TAN, J. 2023. Economically evaluating energy efficiency performance in fused filament fabrication using a multi-scale hierarchical transformer. *The International Journal of Advanced Manufacturing Technology,* 128**,** 329-343.

WANG, L. & ALEXANDER, C. A. 2016. Additive manufacturing and big data. *International Journal of Mathematical, Engineering and Management Sciences,* 1**,** 107-121.

WANG, L. & YOON, K.-J. 2021. Knowledge distillation and student-teacher learning for visual intelligence: A review and new outlooks. *IEEE transactions on pattern analysis machine intelligence,* 44**,** 3048-3068.

WANG, T., KWOK, T.-H., ZHOU, C. & VADER, S. 2018b. In-situ droplet inspection and closed-loop control system using machine learning for liquid metal jet printing. *Journal of manufacturing systems,* 47**,** 83-92.

WANG, X., MAO, D. & LI, X. 2021a. Bearing fault diagnosis based on vibro-acoustic data fusion and 1D-CNN network. *Measurement,* 173**,** 108518.

WANG, Y., LI, S., YU, Y., XIN, Y., ZHANG, X., ZHANG, Q. & WANG, S. 2020b. Lattice structure design optimization coupling anisotropy and constraints of additive manufacturing. *Materials Design,* 196**,** 109089.

WANG, Y., LU, J., ZHAO, Z., DENG, W., HAN, J., BAI, L., YANG, X. & YAO, J. 2021b. Active disturbance rejection control of layer width in wire arc additive manufacturing based on deep learning. *Journal of Manufacturing Processes,* 67**,** 364-375.

WANG, Y., ZHANG, C., LU, J., BAI, L., ZHAO, Z. & HAN, J. 2020c. Weld Reinforcement Analysis Based on Long-Term Prediction of Molten Pool Image in Additive Manufacturing. *IEEE Access,* 8**,** 69908-69918.

WANG, Y., ZHANG, L., DAYNES, S., ZHANG, H., FEIH, S. & WANG, M. Y. 2018c. Design of graded lattice structure with optimized mesostructures for additive manufacturing. *Materials Design,* 142**,** 114-123.

WANG, Z. & GARLAN, D. 2000. *Task-driven computing*, School of Computer Science, Carnegie Mellon University.

WANG, Z., YANG, W., LIU, Q., ZHAO, Y., LIU, P., WU, D., BANU, M. & CHEN, L. 2022. Data-driven modeling of process, structure and property in additive manufacturing: A review and future directions. *Journal of Manufacturing Processes,* 77**,** 13-31.

WASMER, K., LE-QUANG, T., MEYLAN, B., SHEVCHIK, S. & PERFORMANCE 2019. In situ quality monitoring in AM using acoustic emission: A reinforcement learning approach. *Journal of Materials Engineering,* 28**,** 666-672.

WATSON, J. & TAMINGER, K. 2018. A decision-support model for selecting additive manufacturing versus subtractive manufacturing based on energy consumption. *Journal of Cleaner Production,* 176**,** 1316-1322.

WESTPHAL, E. & SEITZ, H. 2021. A machine learning method for defect detection and visualization in selective laser sintering based on convolutional neural networks. *Additive Manufacturing,* 41**,** 101965.

WHITE, F. E. 1991. Data fusion lexicon. *Joint Directors of Laboratories, Technical Panel for C*.

WITHERELL, P. Emerging Datasets and Analytics Opportunities in Metals Additive Manufacturing. Direct Digital manufacturing Conference, 2018.

WOHLERS, T. 2022. Wohlers Report 2022: Analysis. Trends. Forecasts. 3D Printing and Additive Manufacturing State of the Industry. Wohlers Associates: Wohlers Associates.

WOHLERS, T. 2023. Wohlers Report 2023: 3D printing and additive manufacturing global state of the industry. Wohlers Associates: Wohlers Associates.

WOHLERS, T. & GORNET, T. 2014. History of additive manufacturing. *Wohlers report,* 24**,** 118.

WU, D., WEI, Y. & TERPENNY, J. 2019. Predictive modelling of surface roughness in fused deposition modelling using data fusion. *International Journal of Production Research,* 57**,** 3992-4006.

WU, H., WANG, Y. & YU, Z. 2016. In situ monitoring of FDM machine condition via acoustic emission. *The International Journal of Advanced Manufacturing Technology,* 84**,** 1483-1495.

WU, H., YU, Z. & WANG, Y. 2017. Real-time FDM machine condition monitoring and diagnosis based on acoustic emission and hidden semi-Markov model. *The International Journal of Advanced Manufacturing Technology,* 90**,** 2027-2036.

XIA, C., PAN, Z., POLDEN, J., LI, H., XU, Y. & CHEN, S. 2021. Modelling and prediction of surface roughness in wire arc additive manufacturing using machine learning. *Journal of Intelligent Manufacturing***,** 1-16.

XIANG, Y., FU, Y., JI, P. & HUANG, H. Incremental learning using conditional adversarial networks. Proceedings of the IEEE/CVF International Conference on Computer Vision, 2019. 6619-6628.

XIE, S., GIRSHICK, R., DOLLáR, P., TU, Z. & HE, K. Aggregated residual transformations for deep neural networks. Proceedings of the IEEE conference on computer vision and pattern recognition, 2017. 1492-1500.

XU, K., LYU, J. & MANOOCHEHRI, S. 2022. In situ process monitoring using acoustic emission and laser scanning techniques based on machine learning models. *Journal of Manufacturing Processes,* 84**,** 357-374.

YAMASHITA, R., NISHIO, M., DO, R. K. G. & TOGASHI, K. 2018. Convolutional neural networks: an overview and application in radiology. *Insights into imaging,* 9**,** 611-629.

YAN, F., CHAN, Y.-C., SABOO, A., SHAH, J., OLSON, G. B. & CHEN, W. 2018a. Data-driven prediction of mechanical properties in support of rapid certification of additively manufactured alloys. *Computer Modeling in Engineering Sciences,* 117**,** 343-366.

YAN, W., LIN, S., KAFKA, O. L., LIAN, Y., YU, C., LIU, Z., YAN, J., WOLFF, S., WU, H. & NDIP-AGBOR, E. 2018b. Data-driven multi-scale multi-physics models to derive process–structure–property relationships for additive manufacturing. *Computational Mechanics,* 61**,** 521-541.

YANAMANDRA, K., CHEN, G. L., XU, X., MAC, G. & GUPTA, N. 2020. Reverse engineering of additive manufactured composite part by toolpath reconstruction using imaging and machine learning. *Composites Science Technology***,** 108318.

YANG, E., LEARY, M., LOZANOVSKI, B., DOWNING, D., MAZUR, M., SARKER, A., KHORASANI, A., JONES, A., MACONACHIE, T. & BATEMAN, S. 2019a. Effect of geometry on the mechanical properties of Ti-6Al-4V Gyroid structures fabricated via SLM: A numerical study. *Materials Design,* 184**,** 108165.

YANG, H., WANG, W., LI, C., QI, J., WANG, P., LEI, H. & FANG, D. 2022. Deep learning-based X-ray computed tomography image reconstruction and prediction of compression behavior of 3D printed lattice structures. *Additive Manufacturing,* 54**,** 102774.

YANG, Y., HE, M. & LI, L. 2019b. A new machine learning based geometry feature extraction approach for energy consumption estimation in mask image projection stereolithography. *Procedia CIRP,* 80**,** 741-745.

YANG, Y., HE, M. & LI, L. 2020. Power consumption estimation for mask image projection stereolithography additive manufacturing using machine learning based approach. *Journal of Cleaner Production,* 251**,** 119710.

YANG, Y., LI, L., PAN, Y. & SUN, Z. 2017. Energy consumption modeling of stereolithography - based additive manufacturing toward environmental sustainability. *Journal of Industrial Ecology,* 21**,** S168-S178.

YANG, Z., YU, C.-H. & BUEHLER, M. J. 2021. Deep learning model to predict complex stress and strain fields in hierarchical composites. *Science Advances,* 7**,** eabd7416.

YAO, X., MOON, S. K. & BI, G. 2017. A hybrid machine learning approach for additive manufacturing design feature recommendation. *Rapid Prototyping Journal*.

YE, D., FUH, J. Y. H., ZHANG, Y., HONG, G. S. & ZHU, K. 2018a. In situ monitoring of selective laser melting using plume and spatter signatures by deep belief networks. *ISA Transactions,* 81**,** 96-104.

YE, D., HONG, G. S., ZHANG, Y., ZHU, K. & FUH, J. Y. H. 2018b. Defect detection in selective laser melting technology by acoustic signals with deep belief networks. *The International Journal of Advanced Manufacturing Technology,* 96**,** 2791-2801.

YEN, C.-T. & CHUANG, P.-C. 2019. Application of a neural network integrated with the internet of things sensing technology for 3D printer fault diagnosis. *Microsystem Technologies***,** 1-11.

YEUNG, H., YANG, Z. & YAN, L. 2020. A Meltpool Prediction Based Scan Strategy for Powder Bed Fusion Additive Manufacturing. *Additive Manufacturing***,** 101383.

YIN, Y., XU, B., CAI, H. & YU, H. 2020. A novel temporal and spatial panorama stream processing engine on IoT applications. *Journal of Industrial Information Integration,* 18**,** 100143.

ZADPOOR, A. A. & HEDAYATI, R. 2016. Analytical relationships for prediction of the mechanical properties of additively manufactured porous biomaterials. *Journal of Biomedical Materials Research Part A,* 104**,** 3164-3174.

ZAHARIN, H. A., ABDUL RANI, A. M., AZAM, F. I., GINTA, T. L., SALLIH, N., AHMAD, A., YUNUS, N. A. & ZULKIFLI, T. Z. A. 2018. Effect of unit cell type and pore size on porosity and mechanical behavior of additively manufactured Ti6Al4V scaffolds. *Materials,* 11**,** 2402.

ZHAN, Z. & LI, H. 2021a. Machine learning based fatigue life prediction with effects of additive manufacturing process parameters for printed SS 316L. *International Journal of Fatigue,* 142**,** 105941.

ZHAN, Z. & LI, H. 2021b. A novel approach based on the elastoplastic fatigue damage and machine learning models for life prediction of aerospace alloy parts fabricated by additive manufacturing. *International Journal of Fatigue,* 145**,** 106089.

ZHANG, B., JAISWAL, P., RAI, R., GUERRIER, P. & BAGGS, G. 2019a. Convolutional neural network-based inspection of metal additive manufacturing parts. *Rapid Prototyping Journal*.

ZHANG, B., LI, Y. & BAI, Q. 2017a. Defect formation mechanisms in selective laser melting: a review. *Chinese Journal of Mechanical Engineering,* 30**,** 515-527.

ZHANG, B., LIU, S. & SHIN, Y. C. 2019b. In-Process monitoring of porosity during laser additive manufacturing process. *Additive Manufacturing,* 28**,** 497-505.

ZHANG, H., MOON, S. K. & NGO, T. H. 2019c. Hybrid Machine Learning Method to Determine the Optimal Operating Process Window in Aerosol Jet 3D Printing. *ACS applied materials interfaces,* 11**,** 17994-18003.

ZHANG, H., MOON, S. K., NGO, T. H., TOU, J. & YUSOFF, M. A. B. M. 2020a. Rapid Process Modeling of the Aerosol Jet Printing Based on Gaussian Process Regression with Latin Hypercube Sampling. *International Journal of Precision Engineering Manufacturing,* 21**,** 127-136.

ZHANG, H., VALLABH, C. K. P. & ZHAO, X. 2022a. Registration and fusion of large-scale melt pool temperature and morphology monitoring data demonstrated for surface topography prediction in LPBF. *Additive Manufacturing***,** 103075.

ZHANG, J., WANG, P. & GAO, R. X. 2019d. Deep learning-based tensile strength prediction in fused deposition modeling. *Computers in Industry,* 107**,** 11-21.

ZHANG, J., ZHANG, J., GHOSH, S., LI, D., TASCI, S., HECK, L., ZHANG, H. & KUO, C.-C. J. Class-incremental learning via deep model consolidation. Proceedings of the IEEE/CVF Winter Conference on Applications of Computer Vision, 2020b. 1131-1140.

ZHANG, S., SUN, Z., LONG, J., LI, C. & BAI, Y. 2019e. Dynamic condition monitoring for 3D printers by using error fusion of multiple sparse auto-encoders. *Computers in Industry,* 105**,** 164-176.

ZHANG, X., GAO, K., ZHANG, Y., ZHANG, D., LI, J. & TIAN, Q. Task-driven dynamic fusion: Reducing ambiguity in video description. Proceedings of the IEEE Conference on Computer Vision and Pattern Recognition, 2017b. 3713-3721.

ZHANG, X., LE, X., PANOTOPOULOU, A., WHITING, E. & WANG, C. C. J. A. T. O. G. 2015. Perceptual models of preference in 3D printing direction. *ACM Transactions on Graphics,* 34**,** 1-12.

ZHANG, X., SANIIE, J. & HEIFETZ, A. 2020c. Detection of Defects in Additively Manufactured Stainless Steel 316L with Compact Infrared Camera and Machine Learning Algorithms. *JOM,* 72**,** 4244-4253.

ZHANG, X., ZHOU, X., LIN, M. & SUN, J. Shufflenet: An extremely efficient convolutional neural network for mobile devices. Proceedings of the IEEE conference on computer vision and pattern recognition, 2018a. 6848-6856.

ZHANG, Y., HARIK, R., FADEL, G. & BERNARD, A. 2019f. A statistical method for build orientation determination in additive manufacturing. *Rapid Prototyping Journal*.

ZHANG, Y., HONG, G. S., YE, D., ZHU, K., FUH, J. Y. J. M. & DESIGN 2018b. Extraction and evaluation of melt pool, plume and spatter information for powder-bed fusion AM process monitoring. *Materials and Design,* 156**,** 458-469.

ZHANG, Y., MIAO, S., MANSI, T. & LIAO, R. Task driven generative modeling for unsupervised domain adaptation: Application to x-ray image segmentation. International Conference on Medical Image Computing and Computer-Assisted Intervention, 2018c. Springer, 599-607.

ZHANG, Y., SAFDAR, M., XIE, J., LI, J., SAGE, M. & ZHAO, Y. F. 2022b. A systematic review on data of additive manufacturing for machine learning applications: the data quality, type, preprocessing, and management. *Journal of Intelligent Manufacturing***,** 1-36.

ZHANG, Y., SOON, H. G., YE, D., FUH, J. Y. H. & ZHU, K. 2019g. Powder-Bed Fusion Process Monitoring by Machine Vision With Hybrid Convolutional Neural Networks. *IEEE Transactions on Industrial Informatics,* 16**,** 5769-5779.

ZHANG, Y., XIANG, T., HOSPEDALES, T. M. & LU, H. Deep mutual learning. Proceedings of the IEEE conference on computer vision and pattern recognition, 2018d. 4320-4328.

ZHOU, D.-W., WANG, Q.-W., QI, Z.-H., YE, H.-J., ZHAN, D.-C. & LIU, Z. 2023. Deep class-incremental learning: A survey. *arXiv preprint arXiv:.03648*.

ZHOU, X., HSIEH, S.-J. & WANG, J.-C. 2019. Accelerating extrusion-based additive manufacturing optimization processes with surrogate-based multi-fidelity models. *The International Journal of Advanced Manufacturing Technology,* 103**,** 4071-4083.

ZHOU, Z., SHEN, H., LIU, B., DU, W. & JIN, J. 2021. Thermal field prediction for welding paths in multi-layer gas metal arc welding-based additive manufacturing: A machine learning approach. *Journal of Manufacturing Processes,* 64**,** 960-971.

ZHU, Q., LIU, Z. & YAN, J. 2021. Machine learning for metal additive manufacturing: predicting temperature and melt pool fluid dynamics using physics-informed neural networks. *Computational Mechanics,* 67**,** 619-635.

ZHU, Z., ANWER, N., HUANG, Q. & MATHIEU, L. 2018. Machine learning in tolerancing for additive manufacturing. *CIRP Annals,* 67**,** 157-160.

ZHUANG, F., QI, Z., DUAN, K., XI, D., ZHU, Y., ZHU, H., XIONG, H. & HE, Q. 2020. A comprehensive survey on transfer learning. *Proceedings of the IEEE,* 109**,** 43-76.

ZOU, Y., LI, J. & JU, Y. 2022. Surface topography data fusion of additive manufacturing based on confocal and focus variation microscopy. *Optics Express,* 30**,** 23878-23895.

Appendix A.Advanced Data Analytics Technologies

A1 Machine learning

With the growing availability of data in manufacturing industries, advanced data analytics is increasingly employed for decision-making in place of conventional data analytics methods. The past decade has witnessed the rise of the adoption of ML technologies for smart manufacturing. ML technologies have proven to be powerful data analytics tools as they are capable of processing, interpreting, and leveraging big data to support decision-making. Two prevailing tree-based algorithms which are XGBoost and RFs have not been detailed in the thesis. In this subsection, the algorithm details of both algorithms are introduced.

- **XGBoost**

XGBoost (Chen et al., 2016) is a scalable, distributed gradient-boosted decision tree (GBDT). The core idea of XGBoost is to build a series of decision trees, where each tree is constructed to correct the errors made by the previous ones. XGBoost optimizes a loss function that is a combination of a differentiable convex loss function and a regularization term to control model complexity. The objective function and loss function can be expressed as:

$$Obj(\theta_{tree}) = Loss(\theta_{tree}) + \Omega(\theta_{tree}) \tag{A1}$$

$$Loss^{(m)} = \sum_{i=1}^{n} l(y_i, \hat{y}_i^{(m-1)} + f_m(x_i)) \tag{A2}$$

In equation (A1), the objective function of XGBoost $Obj(\theta_{tree})$ is the combination of the loss function $Loss(\theta_{tree})$ and the regularization term $\Omega(\theta_{tree})$, where θ_{tree} is the parameter to be optimised. In equation (A2), $Loss^{(m)}$ represents the loss function at the mth iteration, $f_m(x_i)$ is the prediction of the mth tree, $l(\ )$ is the differentiable convex loss function, and y_i and $\hat{y}_i^{(m-1)}$ are the actual label and predicted value respectively. The regularization term penalises the complexity of the model and can be calculated by the following equation:

$$\Omega(f_m) = \gamma_{tree} N_{leaf} + \frac{1}{2}\lambda_{leaf} \| w_{leaf} \|^2 \tag{A3}$$

In equation (A3), N_{leaf} is the number of leaves in the tree, w_{leaf} is the vector of scores on the leaves, γ_{tree} represents the parameter penalising the number of leaves, and λ_{leaf} is the parameter penalising the leaf scores. Then, the final prediction model is an ensemble of trees and can be expressed as:

$$\hat{y}_i = \sum_{m=1}^{M} f_m(x_i) \tag{A4}$$

- **RFs**

is a prevailing and effective ML algorithm that falls under the category of ensemble learning methods. It consists of multiple decision trees and leverages the collective output of these trees to enhance prediction accuracy and control overfitting. To add diversity and thereby reduce the variance of the model, RFs introduces randomness when constructing each decision tree, through random selection of data subsets and features. Each decision tree in the RFs is constructed using a subset of the training data, typically chosen through bootstrapping (sampling with replacement). The decision at

each node of the tree is based on a subset of features and is determined by measures like Gini impurity or information gain for classification, and variance reduction for regression. For classification tasks, the Gini impurity of a node is calculated as:

$$Gini(p) = 1 - \sum (p_i)^2 \tag{A5}$$

In equation (A5), p_i is the proportion of samples belonging to class i at a given node. The entropy can be used as an alternative measure for classification tasks:

$$H(D) = -\sum p_i \log_2(p_i) \tag{A6}$$

In equation (A6), D is the given dataset of samples, and p_i is the proportion of samples belonging to class i. For regression tasks, the trees often use variance reduction as a criterion, which is computed as the difference in variance before and after the split. The RFs aggregates the predictions of multiple base decision trees. For the classification tasks, the final prediction is made by majority voting while the final prediction is typically the average of all the individual tree predictions for regression tasks.

Appendix B. Datasets used in this Thesis

B1 Extracted build-level design features dataset

Filling degree part	PartRate_ wl	PartRate_ hl	PartRate_ wh	Part height	Filling degree build	TotalRate_ wl	TotalRate_ hl	TotalRate_ wh	Bottom_ area	Height	NumPart	Energy
8.996	0.100	0.079	1.267	48.395	8.280	0.541	0.450	1.202	2585.639	311.000	45.000	211.068
20.317	1.294	0.673	1.923	59.242	17.022	0.553	0.264	2.096	2480.893	176.700	59.000	339.947
25.118	1.211	0.366	3.310	35.281	15.891	0.538	0.428	1.258	2581.136	296.418	115.000	358.247
9.129	1.211	0.436	2.779	82.302	6.892	0.528	0.528	1.000	2508.800	363.744	41.000	504.633
10.079	0.835	0.279	2.989	29.148	10.541	0.536	0.113	4.753	2477.000	76.686	27.000	348.880
9.344	0.681	0.355	1.920	93.241	10.613	0.492	0.339	1.450	2018.679	217.267	5.000	388.765
24.622	0.330	0.547	0.603	89.987	10.765	0.544	0.570	0.954	2434.704	381.410	34.000	342.025

Continue to next page

(Continued)

21.650	0.926	0.557	1.662	83.079	4.868	0.520	0.691	0.752	2238.271	453.543	13.000	257.990
14.106	0.974	0.475	2.051	29.331	2.342	0.564	0.257	2.193	2518.024	171.905	38.000	769.808
9.183	0.473	0.392	1.206	51.016	2.143	0.488	0.175	2.782	1821.576	107.179	12.000	2750.399
17.745	0.947	0.317	2.985	27.331	6.602	0.627	0.064	9.801	1953.420	35.714	4.000	320.235
5.746	0.607	0.197	3.087	30.375	5.344	0.541	0.443	1.220	2577.383	305.988	90.000	384.983
5.458	0.981	0.176	5.571	44.035	4.914	0.540	0.639	0.845	2613.217	444.475	33.000	632.454
11.235	0.334	0.157	2.127	63.719	5.059	0.540	0.466	1.159	2587.446	322.400	16.000	332.399
7.814	1.036	0.222	4.676	46.106	7.477	0.536	0.106	5.066	2553.330	73.043	10.000	416.412
11.252	2.949	1.658	1.778	90.741	9.125	0.515	0.187	2.748	2294.050	125.099	20.000	1299.784
13.598	0.901	0.032	28.193	16.550	7.335	0.472	0.073	6.486	2023.008	47.625	4.000	3468.426
6.032	1.408	0.179	7.859	36.426	4.678	0.543	0.212	2.556	2476.450	143.491	11.000	534.899
9.768	0.969	1.511	0.641	73.530	3.724	0.534	0.225	2.371	1748.363	128.816	26.000	625.278
7.118	1.948	0.722	2.699	68.395	4.722	0.537	0.458	1.173	2566.860	316.443	32.000	476.520
31.040	1.009	0.386	2.612	54.211	21.154	0.543	0.227	2.397	2485.550	153.303	15.000	166.504
23.177	1.108	0.147	7.549	26.208	22.731	0.541	0.094	5.776	2498.567	63.645	9.000	144.948
30.754	0.434	0.083	5.216	40.082	10.414	0.538	0.241	2.234	2544.425	165.581	5.000	589.716
18.261	0.954	0.786	1.213	89.551	13.822	0.530	0.208	2.554	2512.897	142.922	38.000	352.242
5.176	5.483	0.919	5.964	45.653	4.301	0.542	0.106	5.110	2547.612	72.707	28.000	617.075
18.086	0.378	0.057	6.690	40.955	2.356	0.518	0.179	2.899	2369.075	120.888	7.000	548.612

Continue to next page

(Continued)

27.745	0.762	0.595	1.281	41.925	12.206	0.534	0.124	4.326	2428.042	83.262	43.000	341.423
23.317	0.573	0.268	2.141	58.791	4.177	0.514	0.164	3.138	2200.487	107.200	19.000	503.092
11.772	0.803	0.196	4.092	32.609	11.196	0.540	0.081	6.685	2557.011	55.584	13.000	387.952
10.538	1.084	0.062	17.510	19.210	6.553	0.483	0.046	10.455	1976.620	29.543	2.000	2850.952
13.663	1.070	0.407	2.630	45.537	12.720	0.524	0.072	7.249	2473.824	49.676	21.000	377.072
16.026	0.791	0.425	1.862	72.216	11.349	0.550	0.254	2.163	2602.279	174.966	33.000	347.655
22.227	0.742	0.405	1.830	26.186	6.265	0.528	0.140	3.766	2532.076	97.146	73.000	421.597
9.824	0.786	0.248	3.162	76.304	5.617	0.537	0.369	1.453	2549.203	254.567	16.000	454.497
26.159	2.295	0.783	2.930	56.990	14.096	0.545	0.122	4.448	2069.423	75.467	11.000	148.652
34.795	0.829	0.257	3.225	24.324	8.280	0.532	0.166	3.198	2417.187	112.104	23.000	804.062
8.862	0.379	0.352	1.075	128.041	6.999	0.542	0.426	1.270	2622.473	296.657	16.000	390.784
16.123	1.009	0.384	2.631	22.042	7.929	0.510	0.056	9.032	1968.721	35.067	25.000	609.844
13.800	0.839	0.988	0.849	192.074	5.041	0.530	0.649	0.817	2562.885	451.200	17.000	249.889
11.751	3.001	0.467	6.421	52.093	7.428	0.543	0.320	1.695	2655.043	224.033	28.000	411.778
23.028	0.424	0.593	0.715	51.030	10.175	0.551	0.164	3.358	1547.433	86.933	16.000	210.564
30.653	1.165	0.754	1.544	42.746	8.883	0.501	0.178	2.821	2146.171	116.267	24.000	403.005
4.708	0.495	0.201	2.464	68.249	2.824	0.575	0.326	1.761	2384.846	210.187	12.000	419.332
21.372	1.180	0.415	2.840	42.666	13.951	0.539	0.182	2.966	2590.797	125.964	32.000	137.779
17.662	1.831	0.852	2.149	58.131	11.510	0.553	0.237	2.338	2413.347	156.267	43.000	142.196

Continue to next page

(Continued)

10.035	0.690	1.936	0.357	321.096	14.442	0.544	0.788	0.691	2612.598	545.873	20.000	307.520
8.050	0.460	0.560	0.822	220.490	13.563	0.518	0.486	1.064	2501.766	338.105	12.000	380.012
10.184	1.828	0.931	1.964	76.592	7.236	0.540	0.156	3.462	2603.404	108.267	18.000	397.032
23.773	0.838	0.601	1.394	72.623	8.526	0.524	0.343	1.528	2461.853	235.067	51.000	394.465
14.673	0.981	0.644	1.524	42.967	7.565	0.543	0.240	2.259	2587.914	165.833	55.000	184.814
6.987	1.116	0.244	4.580	34.718	7.706	0.543	0.339	1.604	2593.979	234.033	51.000	200.332
12.034	1.057	0.610	1.734	106.513	11.172	0.550	0.541	1.016	2585.512	371.020	24.000	376.662
17.588	1.315	1.684	0.781	188.497	9.346	0.532	0.825	0.645	2546.881	570.685	54.000	365.603
11.313	0.877	0.271	3.236	40.084	10.435	0.540	0.377	1.434	2582.768	260.513	47.000	415.443
20.027	0.895	0.512	1.750	80.049	4.545	0.502	0.318	1.576	2279.717	214.667	12.000	348.133
23.104	1.234	0.441	2.796	40.828	4.693	0.492	0.171	2.871	1917.705	107.000	10.000	287.687
5.572	4.003	0.330	12.132	28.436	4.908	0.554	0.171	3.234	2530.330	115.751	28.000	599.061
8.833	1.019	0.508	2.005	90.382	4.994	0.549	0.690	0.796	2620.010	476.553	35.000	302.582
7.633	2.773	0.312	8.897	42.339	7.732	0.534	0.181	2.957	2595.734	125.913	15.000	504.998
9.830	1.867	0.462	4.044	27.080	5.758	0.623	0.061	10.172	2241.628	36.751	9.000	485.864
37.750	1.234	1.045	1.181	76.988	18.498	0.531	0.248	2.144	2434.868	167.710	41.000	107.283
30.645	0.496	0.212	2.337	54.480	20.965	0.546	0.341	1.600	2433.545	227.864	31.000	128.262

Continue to next page

(Continued)

4.840	0.770	0.301	2.558	125.028	3.820	0.471	0.276	1.706	2219.167	189.500	2.000	401.058
13.422	1.517	0.813	1.867	63.136	4.659	0.510	0.220	2.320	2038.235	139.046	12.000	583.060
13.207	1.104	0.493	2.237	43.060	4.211	0.524	0.148	3.548	2491.805	101.867	10.000	389.751
14.717	0.965	0.109	8.891	27.880	12.748	0.494	0.118	4.189	2355.213	81.394	14.000	262.942
17.374	0.544	0.102	5.323	27.938	4.852	0.604	0.305	1.983	2361.819	190.533	13.000	531.358
9.317	0.940	0.532	1.765	81.886	2.741	0.490	0.265	1.847	1705.939	156.559	5.000	610.875
11.877	0.703	0.334	2.103	38.109	13.949	0.560	0.217	2.582	2571.963	146.960	22.000	509.976
31.685	0.425	0.283	1.500	50.227	13.918	0.556	0.225	2.470	2582.399	153.333	21.000	135.271
31.869	0.395	0.326	1.213	55.269	6.025	0.478	0.242	1.975	1919.449	153.333	11.000	315.057
16.748	0.919	0.616	1.492	49.947	3.776	0.653	0.109	5.984	2195.976	63.281	5.000	583.596
7.147	0.453	0.335	1.350	106.278	10.923	0.525	0.299	1.755	2435.601	203.836	12.000	406.084
4.232	0.604	0.473	1.276	150.794	3.037	0.541	0.419	1.292	2644.929	292.946	11.000	558.866
41.401	0.938	0.266	3.524	21.115	5.226	0.527	0.119	4.428	2476.983	81.600	26.000	1514.601
10.135	0.997	0.438	2.275	49.123	3.538	0.596	0.131	4.552	1630.554	68.505	6.000	857.648
24.692	2.709	1.056	2.566	28.954	3.657	0.574	0.166	3.465	1228.415	76.667	20.000	841.331
4.303	1.107	0.315	3.511	70.744	6.468	0.541	0.223	2.432	2632.619	155.188	16.000	194.757
6.220	0.554	0.253	2.188	82.425	5.786	0.536	0.151	3.542	2442.111	102.133	5.000	239.639
10.378	0.366	0.150	2.437	47.562	6.882	0.466	0.222	2.097	1603.289	130.400	9.000	283.463

Continue to next page

(Continued)

13.217	0.071	0.236	0.302	105.840	12.974	0.560	0.460	1.216	2304.188	295.420	44.000	385.211
17.135	0.688	0.151	4.560	31.109	6.628	0.542	0.218	2.488	2466.396	146.937	30.000	427.197
20.108	1.924	1.210	1.590	66.160	11.101	0.588	0.323	1.822	2185.567	196.667	20.000	376.421
5.797	7.809	0.756	10.324	35.916	4.989	0.536	0.174	3.085	2567.034	120.202	42.000	425.749
4.576	1.216	0.401	3.034	136.646	3.942	0.547	0.312	1.751	2350.640	204.800	3.000	663.626
19.163	2.929	1.253	2.338	107.565	16.239	0.525	0.218	2.407	2260.758	143.037	11.000	330.169
25.288	1.224	0.948	1.292	76.483	12.691	0.536	0.312	1.720	2558.357	215.276	27.000	111.353
10.872	0.799	0.524	1.523	91.184	5.118	0.541	0.362	1.495	2622.536	251.943	19.000	254.984
11.523	0.949	0.293	3.244	61.684	9.214	0.519	0.145	3.579	2356.059	97.657	9.000	166.374
19.438	0.332	0.251	1.322	47.645	5.034	0.609	0.164	3.713	1427.107	79.383	7.000	417.795
13.798	1.900	0.291	6.528	20.796	9.437	0.546	0.106	5.173	2559.432	72.291	50.000	291.811
23.254	0.654	0.163	4.009	38.505	13.181	0.540	0.306	1.766	2362.726	202.235	39.000	127.592
7.056	0.383	0.270	1.416	106.029	6.422	0.545	0.329	1.656	2634.065	228.861	11.000	401.613
16.072	1.009	0.148	6.821	25.693	10.067	0.524	0.104	5.048	2514.660	71.943	13.000	241.378
2.124	1.583	0.914	1.732	171.712	1.490	0.547	0.293	1.863	2194.927	185.943	3.000	1030.601
26.043	2.212	8.390	0.264	197.676	11.413	0.506	0.324	1.563	2332.575	219.765	114.000	505.535
24.305	0.361	0.378	0.956	43.829	9.464	0.537	0.219	2.446	2579.023	152.079	34.000	191.640

Continue to next page

(Continued)

5.452	0.389	0.185	2.103	26.738	16.888	0.536	0.049	10.888	2586.627	34.208	38.000	331.994
37.607	0.322	0.504	0.638	52.552	8.368	0.528	0.296	1.783	2512.167	204.203	81.000	411.162
36.458	1.312	0.099	13.298	15.496	15.658	0.482	0.193	2.495	2110.806	127.809	38.000	151.522
28.504	1.161	0.318	3.651	27.250	15.157	0.517	0.153	3.386	2316.880	102.267	46.000	137.428
28.567	1.211	0.511	2.372	27.992	13.368	0.530	0.118	4.490	2102.161	74.367	67.000	363.883

B2 Statistical features of detected pores (Selected region)

Image_name	Area_avg	Area_max	Area_std	Ratio of Pores
4_1_1	66.993	449.018	79.834	0.085
4_1_2	44.134	85.198	30.415	0.013
4_2_1	55.264	283.227	70.037	0.078
4_2_2	104.175	693.1	154.974	0.110
4_2_3	77.907	246.384	67.568	0.056
4_3_1	50.576	198.029	47.116	0.061
4_3_2	67.106	225.66	58.886	0.037
4_3_3	64.244	181.91	53.046	0.028
4_3_4	58.613	156.581	47.102	0.026
4_4_1	82.961	310.859	72.815	0.119
4_4_2	81.744	269.411	67.945	0.050
4_4_3	56.991	181.91	49.307	0.030
4_4_4	57.055	198.029	47.808	0.045
5_1_1	54.112	232.568	71.029	0.019
5_1_2	78.619	292.438	71.968	0.041
5_1_3	147.893	499.677	108.995	0.235
5_2_1	116.284	373.031	100.494	0.100
5_2_2	82.187	227.963	72.521	0.042
5_2_3	111.679	200.331	57.332	0.037
5_2_4	172.412	803.628	133.73	0.304
5_3_1	96.637	343.096	87.24	0.118
5_3_2	114.406	338.491	82.237	0.159
5_3_3	157.016	557.243	142.366	0.206
5_3_4	176.025	458.229	119.283	0.109
5_4_1	62.172	92.106	22.166	0.015
5_4_2	88.443	419.084	89.148	0.072
5_4_3	123.925	216.45	50.979	0.052
5_4_4	153.291	373.031	107.349	0.039
6_1_1	90.306	347.701	77.484	0.185
6_1_2	64.968	230.266	54.838	0.073

6_1_3	61.185	290.135	68.073	0.052
6_1_4	79.86	274.016	71.542	0.068

Continue to next page

(Continued)

6_2_1	108.129	237.174	67.64	0.099
6_2_2	116.434	600.994	122.614	0.099
6_2_3	63.662	147.37	42.882	0.043
6_2_4	176.647	665.468	210.452	0.044
6_3_1	98.842	414.478	89.818	0.149
6_3_2	90.955	354.609	87.427	0.071
6_3_3	64.265	241.779	55.233	0.058
6_3_4	173.686	257.898	52.463	0.044
6_4_1	88.507	472.045	86.868	0.297
6_4_2	98.356	495.071	86.991	0.157
6_4_3	78.027	460.532	81.628	0.108
6_4_4	66.448	225.66	51.19	0.060
7_1_1	74.261	241.779	55.502	0.086
7_1_2	106.055	472.045	92.961	0.200
7_1_3	146.828	280.924	70.299	0.088
7_1_4	90.571	276.319	72.199	0.062
7_2_1	74.782	326.977	73.66	0.064